An Examination of the Arkoma Foreland Basin and its Petroleum System through Burial and Thermal History Modeling

---

A Thesis Presented to

the Faculty of the Department of Earth and Atmospheric Sciences

University of Houston

In Partial Fulfillment

of the Requirements for the Degree

Master of Science

By

Julianne Lamb

May 2014

An Examination of the Arkoma Foreland Basin and its Petroleum System through Burial and Thermal History Modeling

Julianne Lamb

APPROVED:

Dr. Michael Murphy

Dr. Joel Saylor

Dr. Jolante Van Wijk

Dan E. Wells, Dean, College of Natural Sciences and Mathematics

ACKNOWLEDGEMENTS

I dedicate this thesis to everyone who has given me their enduring support and faith throughout this tremendous journey towards completing my degree. Without your inspiration, the vision of this thesis would have not become a reality. I am forever grateful to all of you.

My heartfelt thanks goes to the support I received from Southwestern Energy (SWN) and the countless individuals within the organization. Through SWN, a rare and unsurpassable opportunity to further my education could not have been made any more graciously. The bounds and ideas for my thesis topic were limitless due to the amount of data and resources available. I want to thank the management team for their long, continuous assistance throughout my years as a graduate student. I also must thank the numerous geoscientists who would unhesitatingly let me sit in their offices and pick their brains for hours upon hours. Your guidance, opinions, and most importantly, your patience, were truly needed and acknowledged in order for this thesis to be successful. I would also like to thank The University of Texas at Austin for providing the strong foundation of learning that led me to achieve my goals with SWN and the University of Houston.

I am extremely appreciative of those who served on my thesis committee. Firstly, I would like to recognize my advisor, Dr. Michael Murphy. Thank you for unhesitatingly taking me in as your student and understanding that the project would require a tremendous amount of work outside the campus environment. You provided exceptional ideas and feedback and gave me the guidance I needed to successfully complete the degree. Likewise, my deepest gratitude goes to my committee members: Dr. Joel Saylor

at the University of Houston, and Dr. Jolante Van Wijk at the University of Houston and New Mexico Tech. Your wholehearted support and excitement for the project has been greatly recognized and I give many thanks to you. Thank you all for your patience throughout this process.

This thesis marks the end of a journey for my friends and most importantly, for my family. At many points, my thesis became a long-distance personal experience for each and every one of them. I praise them for remaining steady-minded and for shedding their hope and support onto me. To my parents, Connie and Jon, and my sister, Haley: you are the most loving and supportive family on this Earth. Thank you from the bottom of my heart.

An Examination of the Arkoma Foreland Basin and its Petroleum System through Burial and Thermal History Modeling

---

An Abstract of a Thesis

Presented to

the Faculty of the Department of Earth and Atmospheric Sciences

University of Houston

In Partial Fulfillment

of the Requirements for the Degree

Master of Science

By

Julianne Lamb

May 2014

ABSTRACT

The Arkoma Basin is a Carboniferous arcuate foreland basin that spans across west-central Arkansas into southeastern Oklahoma along the northern side of the Ouachita orogenic belt. High levels of thermal maturity are observed in the basin; however, the existence of an extensive post-Pennsylvanian/Permian surface unconformity has complicated the interpretation and correlation between basin sedimentation, subsidence, and exhumation. Through the calibration against maturity data provided by Southwestern Energy (SWN), 50 1D models are generated in a geologically coherent basin modeling study in the Arkansas portion of the Arkoma Basin. In each well, the synthesis of vitrinite reflectance and apatite fission track analysis (AFTA) data are used to estimate erosion and heat-flow variations in burial and thermal history reconstructions. To aid the estimation of heat flow in areas lacking data, a regional geothermal gradient map was generated from the corrected bottom-hole temperatures of 229 wells. Structure and isochore maps invoking depocenter migration and fault configurations were produced from formation tops picked at tectonically significant stratigraphic levels (foreland and pre-foreland basin settings). Within this study area, the calibrated burial and thermal history models indicate that nearly 9,000 to 19,000 feet of section have been removed. The estimated amount of eroded overburden is in agreement with a geologically realistic framework of previously established stratigraphic thicknesses. To avoid an unrealistic amount of eroded section, all models required a paleo-heat flow higher than the present-day value, with such differences increasing from south to north. A regional picture of the thermal maturity in the central-eastern Arkoma Basin is rendered upon combination of all reconstructed elements. Results are consistent with those suggested from previous

authors in that patterns of increasing thermal maturity generally reflect those of increasing depth and erosion. In addition, this study indicates that there are no pronounced reoccurring patterns between anomalous thermal values and proximity to faulting. Possible reasons for anomalous data points can be attributed to vitrinite reflectance measurement error and variations in localized heat flow. However, most lateral variations in thermal maturity can be explained by estimates of erosion and a spatially reasonable change in heat flow.

CONTENTS

CHAPTER 1: Introduction

The Arkoma Basin is a mature and productive gas-bearing Carboniferous peripheral foreland basin that spans west-central Arkansas into southeastern Oklahoma (Figure 1). Early exploration of the eastern Arkoma Basin in Arkansas was discouraged due to the presence of high thermal-maturity values located in strata at the present-day surface. Previous studies have generated burial and thermal history models from comprehensive public vitrinite reflectance data sets to evaluate the impacts of varying estimates of eroded overburden on thermal maturity. However, basin reconstruction has proven to be problematic because of the existence of an extensive post-Pennsylvanian/Permian surface unconformity.

The purpose of this study is to perform a basin analysis for the Arkoma foreland basin. This study investigates thermal-maturity patterns through the construction of burial and thermal history models for 50 wells (Figure 2). Large lateral changes in vitrinite reflectance versus depth profiles along an east to west transect have been reported by Houseknecht et al. (1992). The subsurface data presented by Houseknecht et al. (1992) suggest lower-than-expected thermal maturities in the eastern part of the basin that can neither be adequately explained by the presence of faults, unconformities, or igneous intrusions. Byrnes and Lawyer (1999) attribute the variation in thermal maturity simply to an increase in overburden and subsequent surface erosion. Recent exploitation of natural gas production across the Arkoma Basin has provided a growing repository of well log and geochemical data to aid the enigma of burial reconstruction and observed thermal anomalies. Abundant well log, seismic, and geochemical data provided by

Southwestern Energy (SWN) and from public records are utilized in the analysis. The burial and thermal reconstructions that are generated in this study incorporate existing and new thermal maturation data, such as apatite fission track analysis (AFTA) and vitrinite reflectance. Several structure and isochore maps illustrating depocenter migration and fault configurations were produced from formation tops picked at tectonically significant stratigraphic levels (foreland and pre-foreland basin settings). Reconstructions and subsequent geological maps are compared with existing interpretations to gain a better understanding of the thermal maturity patterns observed in the evolving Arkoma foreland basin.

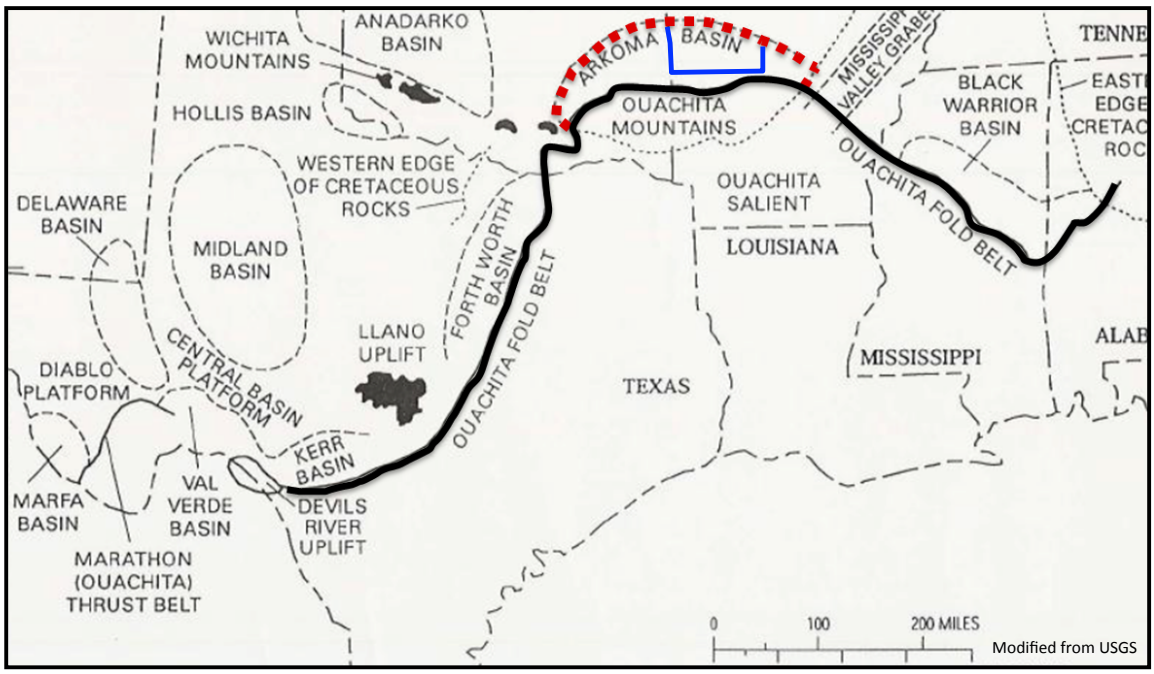

Figure 1: Regional map of the foreland basins associated with the Ouachita orogeny. The Arkoma Basin is delimited by the red stippled lineament and the Ouachita fold belt. Blue area denotes the location of interest (Modified from USGS).

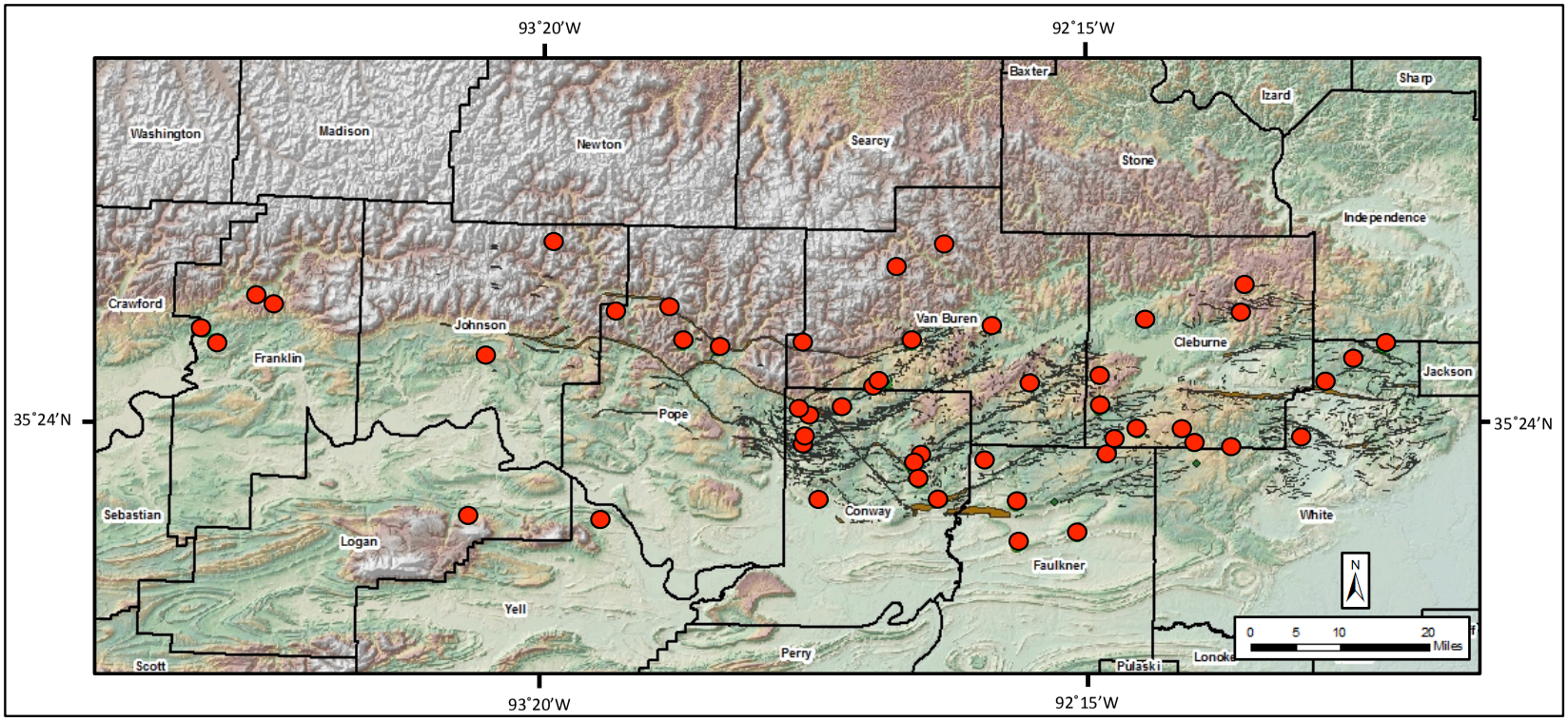

Figure 2: Key structural features that delineate the Arkoma Basin. The locations of the 50 wells for which basin models were generated are represented by the red circles. Well names are listed in Appendix A-1.

CHAPTER 2: Geologic Overview

2.1 Location of the Arkoma Basin

The Arkoma Basin is an arcuate foreland basin that extends from the Gulf coastal plain in central Arkansas westward 400 km to the Arbuckle Mountains in south-central Oklahoma. The basin ranges from 32 to 80 km wide (Sutherland, 1988) and is bounded to the north by the Ozark Uplift, to the northwest by the central Oklahoma platform, and to the east by the Mississippi Embayment. The Ross Creek and Choctaw faults on the southern edge of the basin separate the Arkoma Basin from the Ouachita orogenic belt (Lee et al., 1996). This study is confined to the central and eastern portion of the Arkoma Basin in Arkansas.

2.2 Regional Tectonic Setting

The Ouachita orogeny records the collision and stitching of Pangaea along the southern margin of the North American craton during the late Paleozoic time (Figure 3 Corrigan, 1998). Figure 4 illustrates the Wilson Cycle as it pertains to the Arkoma Basin area. Predating the Ouachita orogeny, rifting of Rodinia during the latest Precambrian or earliest Paleozoic (~750-500 Ma) resulted in the opening of a proto-Atlantic Ocean basin along the southern margin of North America. This vast and stable passive continental margin existed from the Cambrian through the middle Paleozoic (Lee et al., 1996). Closing of the ocean basin and the formation of Pangaea from the Marathon-Ouachita-Appalachian orogeny was underway in the Devonian or early Mississippian with southward subduction of Laurussia (North America) under the Afro-South American

plate of Gondwana, otherwise known as Llanoria in the Arkoma area (Byrnes and Lawyer, 1999; Houseknecht and Matthews, 1985). The Arkoma Basin is one in a series of basins that formed as a result of tectonic loading in front of the approaching Ouachita orogeny (Meckel et al., 1992). Presently, most of the orogenic belt is buried beneath Mesozoic and Cenozoic strata of the Gulf coastal plain (Houseknecht, 1986). The Ouachita Mountains, located south of the Arkoma Basin, represent the largest exposure of this Carboniferous orogenic belt (Houseknecht, 1986). The convergent margin setting around the Arkoma area continued throughout the Mississippian and into the Pennsylvanian before culminating in the Atokan when the subduction complex became consumed by the rifted continental margin (Houseknecht and Matthews, 1985). Erosion from flexural-isostatic rebound from crustal unloading of the foreland basin has been the main tectonic activity since the formation of the Arkoma Basin in the Atokan (310 Ma), removing several kilometers of sediment (Beaumont, 1981; Jamieson and Beaumont, 1988; Corrigan, 1998; Lee et al., 1996).

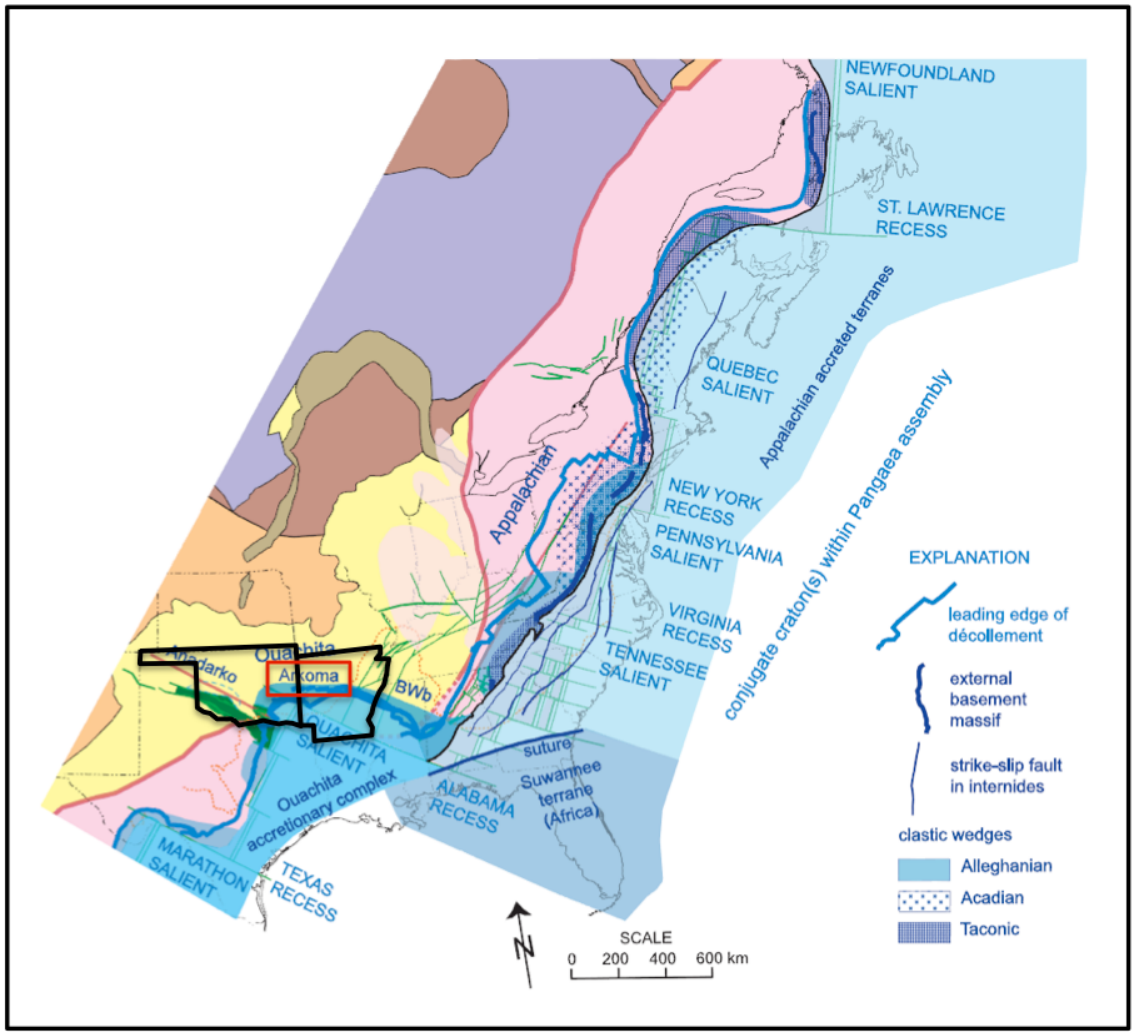

Figure 3: Location of the Appalachian-Ouachita orogeny during the formation of Pangaea. Arkoma Basin is denoted by the red box. The study area is in the Arkansas portion of the Arkoma Basin. Modified from Thomas, 2006.

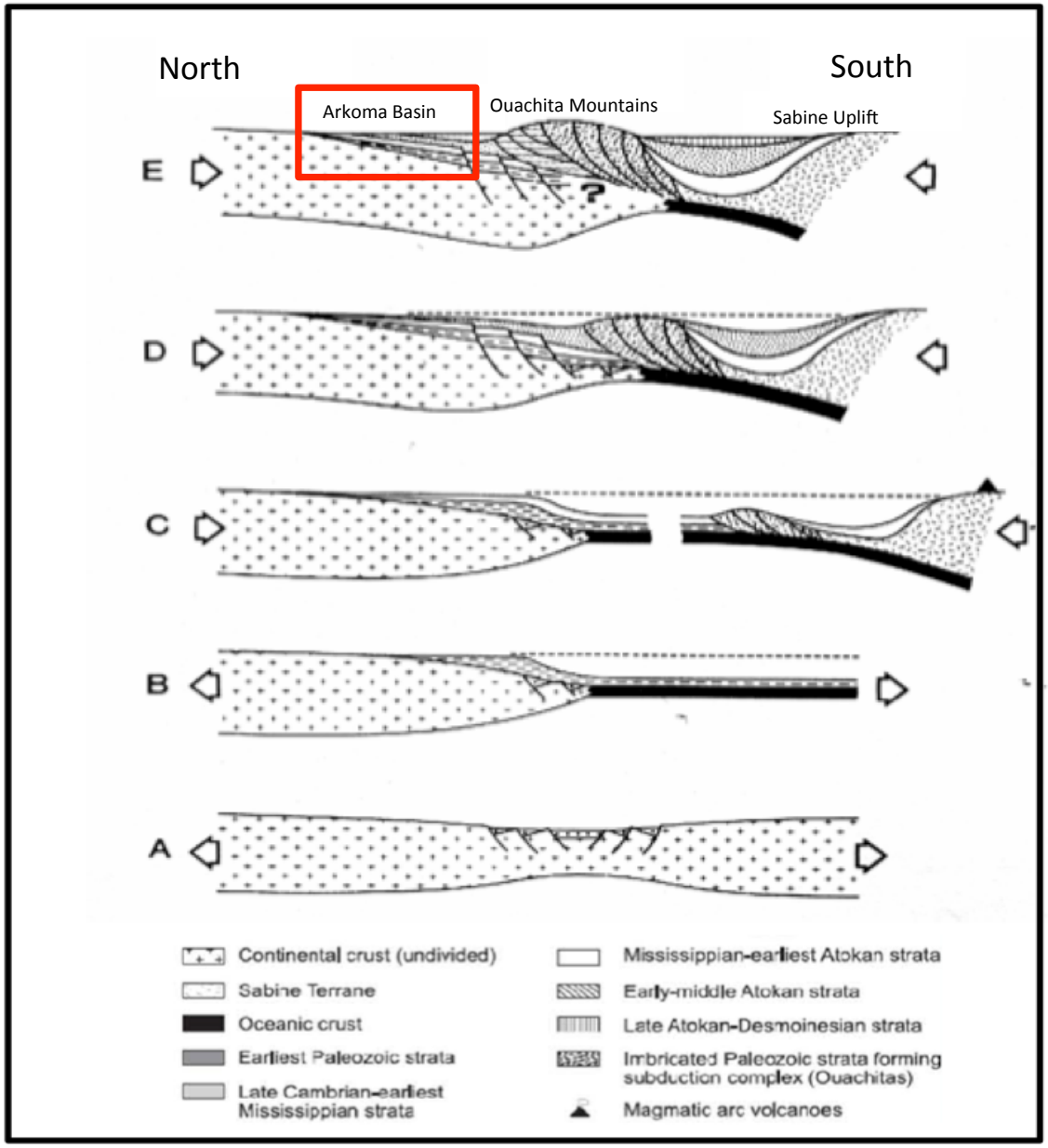

Figure 4. Cross-section illustrating the Wilson Cycle and tectonic evolution of the Arkoma Basin and Ouachita orogenic belt (A) rifting of the North American continent: late Precambrian – early Paleozoic, (B) oceanic crust formation: late Cambrian – earliest Mississippian, (C) subduction from convergent plate motion between North America and Gondwana: early Mississippian – early Atokan, (D) plate collision: early – middle Atokan, and (E) uplift of the Ouachita Mountains and formation of the Arkoma Basin: late Atokan – Desmoinesian. Modified from Houseknecht (1986).

2.3 Tectonic History and Associated Stratigraphy of the Arkoma Basin

Bounded below by Precambrian igneous rock and above by a major Paleozoic unconformity, which exists at the present-day surface, a stratigraphic section from the Arkoma Basin can generally be characterized as consisting of Paleozoic carbonates and organic-rich shale overlain by a thick section of alternating Pennsylvanian basin-fill sandstones and shales, all of which are extensively faulted (Byrnes and Lawyer, 1999). Post-dating late Proterozoic or early Cambrian rifting, deposition occurred on a shelf setting along a passive continental margin that post-dated late Proterozoic or early Cambrian rifting (Van Arsdale, 1990). With exception to an influx of terrigenous sediment during the Ordovician and erosional events in the middle and late Devonian, deposition on the shelf generally consisted of southward-thickening shallow water carbonates, and black shales and cherts deposited in thin beds in the deeper waters of the basin (Byrnes and Lawyer, 1999).

At the beginning of the middle Mississippian, the effects of far-field continental convergence from Ouachita thrust loading initiated subsidence on the stable shelf (Byrnes and Lawyer, 1999). Down-to-the-south normal faulting and footwall anticline formation occurred by the latest Mississippian and into the earliest Pennsylvanian (Frezon and Glick, 1959; Houseknecht, 1986). Rapid changes took place in the Arkoma Basin during the Atokan epoch as a result of the closure of the Ouachita trough and continental collision. Rapid deposition initiated in the deep, remnant ocean basin and sedimentation on the cratonward Arkoma shelf remained relatively slow with terrigenous sediments sourcing from the Illinois Basin region to the northeast (Byrnes and Lawyer, 1999). By the middle Atokan, stratigraphically shallower, very active down-to-the-south

syndepositional listric growth faults from flexural downwarping of the southern margin transformed the shelf into an incipient foreland basin (Byrnes and Lawyer, 1999). Major movement of the syndepositional faults ceased and rapid deposition and filling closed the basin by the beginning of the late Atokan (Houseknecht, 1986; Sutherland, 1988). With the development of a fully formed foreland basin, evidence of continued compressional deformation throughout the late Atokan and early Desmoinesian is represented by the persistent subsidence and downwarping of the basin, and further northward migration of the axis of deposition (Sutherland, 1988). Deposition in the late Atokan and Desmoinesian was characterized by shallow-marine, deltaic, fluvial, and coal-bearing sediments that were transported westward along the axis of the basin before deposition concluded by the end of the Desmoinesian (Sutherland, 1988). In general, tectonic subsidence of the basin was time-transgressive as a result of oblique plate convergence from east to west. The east to west stratigraphy of the basin is indicative of a thoroughgoing change in the age of the transition from pre-collisional shelf deposition to foreland basin clastic deposition.

2.4 Structural Controls

The structural framework of the Arkoma Basin is controlled by the residual basement geometry of a Precambrian to early Paleozoic rift margin. Around the Cambrian time (550 Ma), passive rifting and strike-slip faulting resulted in the creation of a triple junction that formed in the corner of a rifted block in southwestern Arkansas (Hendricks, 1988). The triple junction left two failed arms extending at high angles on the North American continental margin, the Reelfoot Rift and the Oklahoma Aulacogen

(Figure 5). The Reelfoot Rift is a northeast-trending 70 km wide feature that extends from east-central Arkansas to western Kentucky. The rift arm consists of northeast-southwest striking horst and graben linear features. The southeast-trending Arkansas transform fault abruptly terminates the Reelfoot Rift at its southwestern end, however, the Reelfoot Rift may have once extended further southwest (Hildenbrand and Hendricks, 1995). The southwestward structures were obliterated by the thrusting and sedimentation associated with the Mississippian Ouachita orogeny.

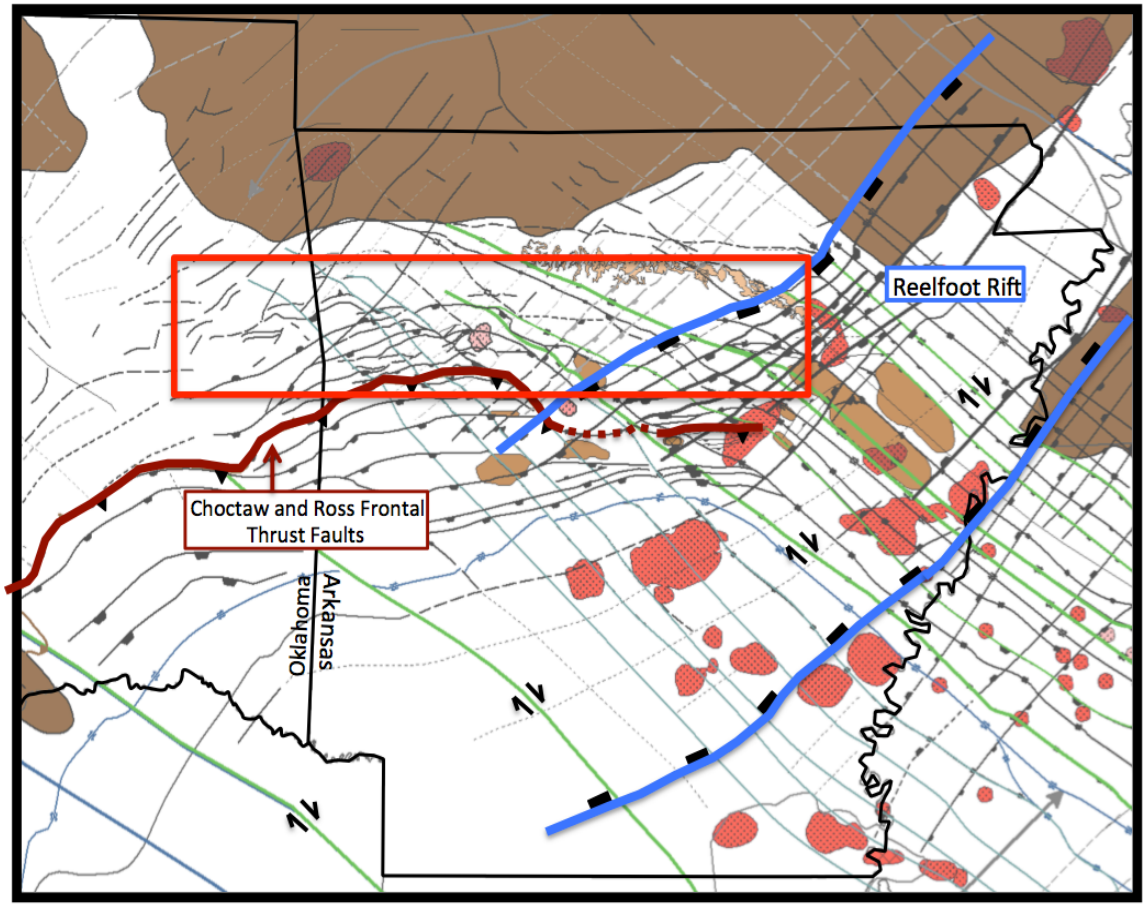

Figure 5: Generalized map of the structural architecture of the Arkoma Basin. The Arkansas portion of the red box denotes the study area; blue lines and area within: northwest trending horst and graben sets of the Reelfoot Rift; maroon line: location of the Ouachita frontal thrust (USGS and AGS fault compilation).

The Arkoma Basin is controlled by three distinct fault geometries: NE-, E-W-, and NW-striking faults (Figures 5 and 6). Northeast and east-west trending faults reflect the dominant horst and graben Precambrian rift architecture, in which they are genetically related. Northwest trending transfer faults overprint the NE and E-W faults with dextral offsetting. Faults in the eastern part of the Arkoma Basin strike northeast, whereas in western Arkansas they strike due east. This change in fault strike across the eastern and western parts of the basin may suggest differences in the tectonic histories relative to location within the basin (Van Arsdale, 1990).

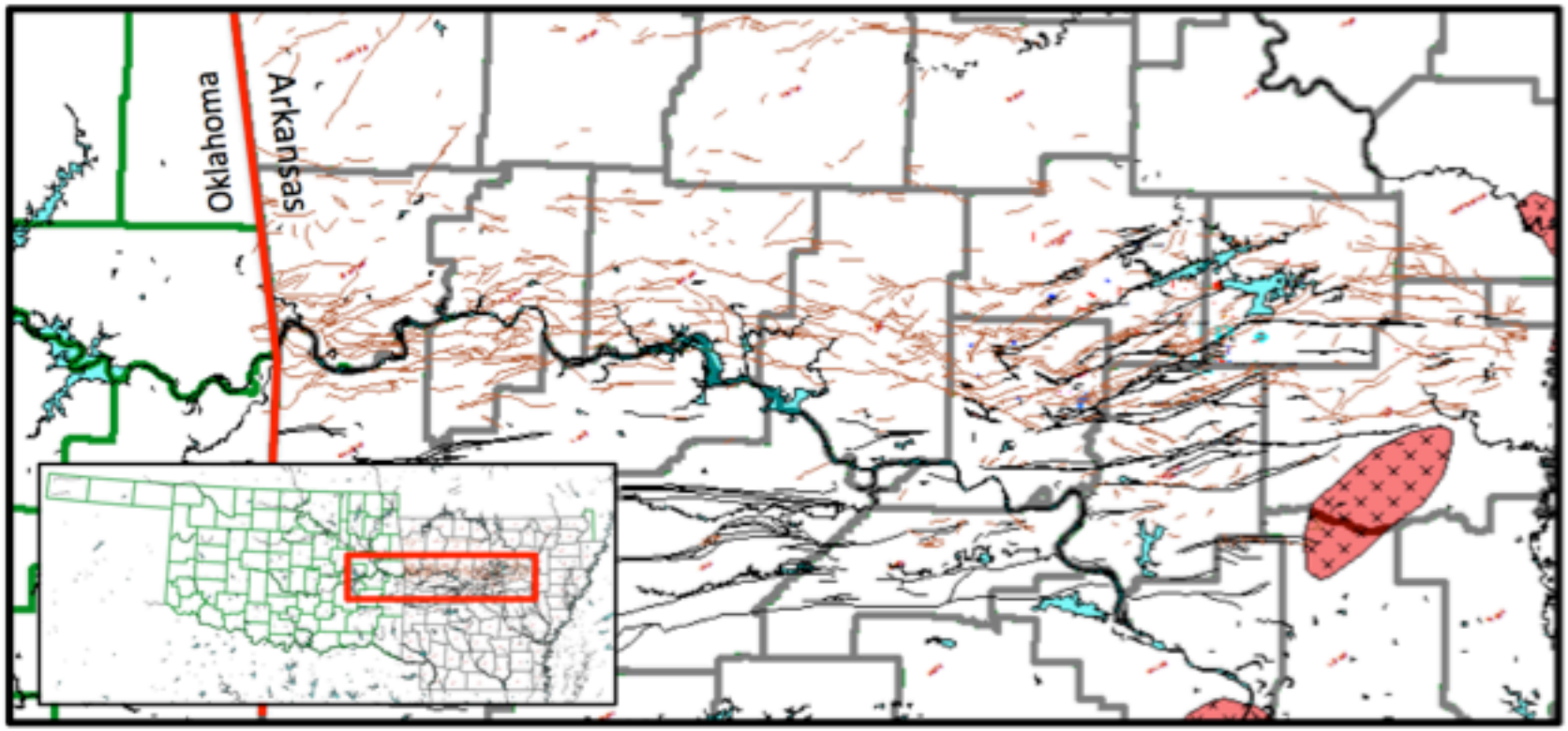

Figure 6: Study location as seen in Kingdom. Brown and black lines are surface faults from the Arkansas Geological Commission; red stippled areas represent Cretaceous igneous bodies.

There are two main structural regimes that characterize the faulting in the eastern area of the Arkoma Basin (Figure 7). Steep, deep, normal-dipping basement faults are continuous from the Proterozoic basement rock up to the base of the Pennsylvanian Morrowan series (Van Arsdale, 1990). The near-surface structural regime consists of high-angle listric normal growth faulting. These shallow Atokan-aged listric normal faults do not merge with the deep basement faults in the eastern Arkoma Basin, but may merge in the western side of the basin (Van Arsdale, 1990). The genetic relationship between the timing of these deep and shallow fault regimes were the main controls on the location of rapid foreland basin infilling during the Pennsylvanian (Van Arsdale, 1990).

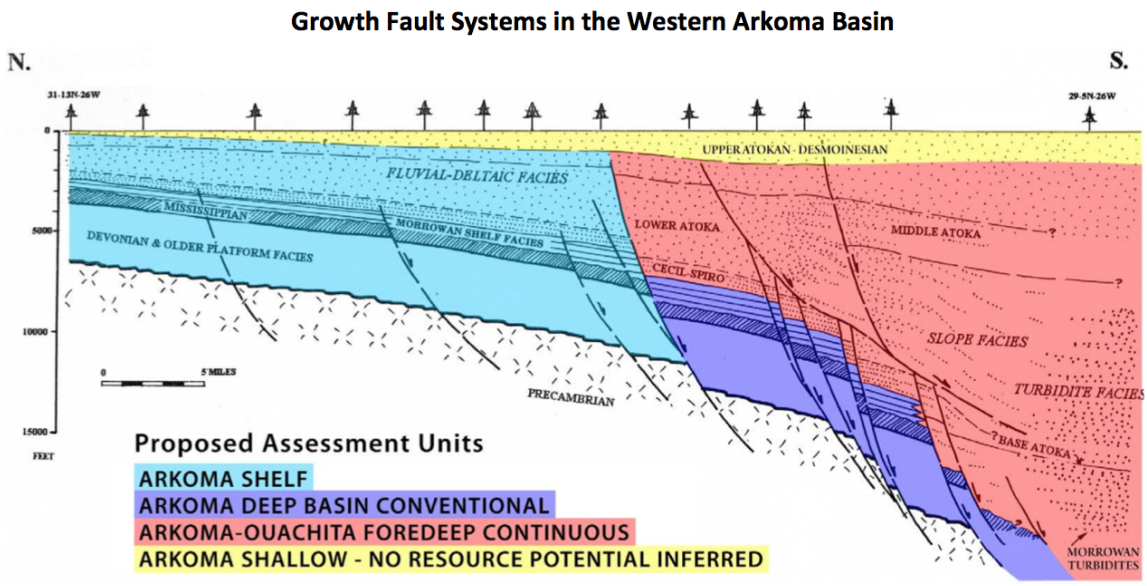

Figure 7: Schematic illustrating the two main fault systems in the Arkoma basin: deep-seated normal faults and shallow listric normal growth faults. From USGS: modified from Roberts, 1994 and Houseknecht et al., 1989.

CHAPTER 3: Methods

3.1 Methods

Basin modeling techniques aid the evaluation of the thermal and burial histories of sedimentary basins. Maturity indicators are used to evaluate the thermally induced changes to organic matter. These changes provide insight regarding the rate and extent of subsurface heating. In combination with data from multiple well logs and/or seismic data, basin models can be optimized to predict observed values and ultimately narrate the geologic history of an area.

A recently acquired and multifaceted well data set, generously provided by Southwestern Energy (SWN), will be used to perform a detailed analysis within the eastern portion of the Arkoma Basin. The dense well set from SWN covers nearly 1,400 square miles and is located in the central-western portion of Arkansas. In most cases, the available log curves for the eastern portion of the study include gamma ray, resistivity, density, neutron, spontaneous potential, and sonic logs. Southwestern Energy has provided new thermal calibration data, such as vitrinite reflectance, rock-eval, and apatite fission track analysis (AFTA) for 23 new localities within the central-eastern Arkoma Basin. The new calibration and extensive well log data from SWN are combined with previously published thermal maturation data and a detailed basin analysis is performed. IHS Kingdom is used for log analysis, formation top picking, and map generation. Basin modeling and evaluation of the petroleum system is executed using Schlumberger's 1D basin modeling software, PetroMod1D. Single point well locations are constructed from scratch in the PetroMod Well Editor with formation top picks and other data exported

from Kingdom. Fifty1D models are constructed along two sections that span across the three main fault configurations in the central-eastern Arkoma Basin. The PetroMod software does not allow the user to construct a gridded 2D cross section from the calibrated 1D models, therefore, this study will combine 1D output models and manually construct cross sections to examine lateral thermal variations in the basin.

3.2 Basis for the Geologic Framework

Input values for erosion estimation, lithology, age, porosity, thermal maturity, depth, thickness, and heat flow are required parameters for analysis within PetroMod1D. In order to extract the depths and thicknesses of the intervals of interest across the basin so they can be imported into the modeling software, Kingdom is used to pick the formation tops associated with each of the tectonically significant surfaces. The log characteristics used to identify the formation tops were based on published literature and previous research done by individuals at SWN. The gamma ray signatures for the formation tops interpreted in the Billiot-A well are shown in Figure 8a. Cross-section A to A' displays the general variability seen in the gamma ray logs across a northeast-southwest trending fault configuration (Figure 8b). The log signatures in Figures 8a and 8b can be compared to annotated lithologies as illustrated in a generalized stratigraphic section of the Arkoma Basin (Figure 9). A full list of formation tops used in the study can be found in Table 1.

Calibration data (vitrinite reflectance and AFTA) provide important constraints in the reconstruction of basin models. Furthermore, access to a plentiful repository of well log data to create a variety of geological maps allow for even further refinement of the

models. The opportunity to synthesize both unpublished regional maps and multiple current calibration data sets was utilized in this study to its fullest extent.

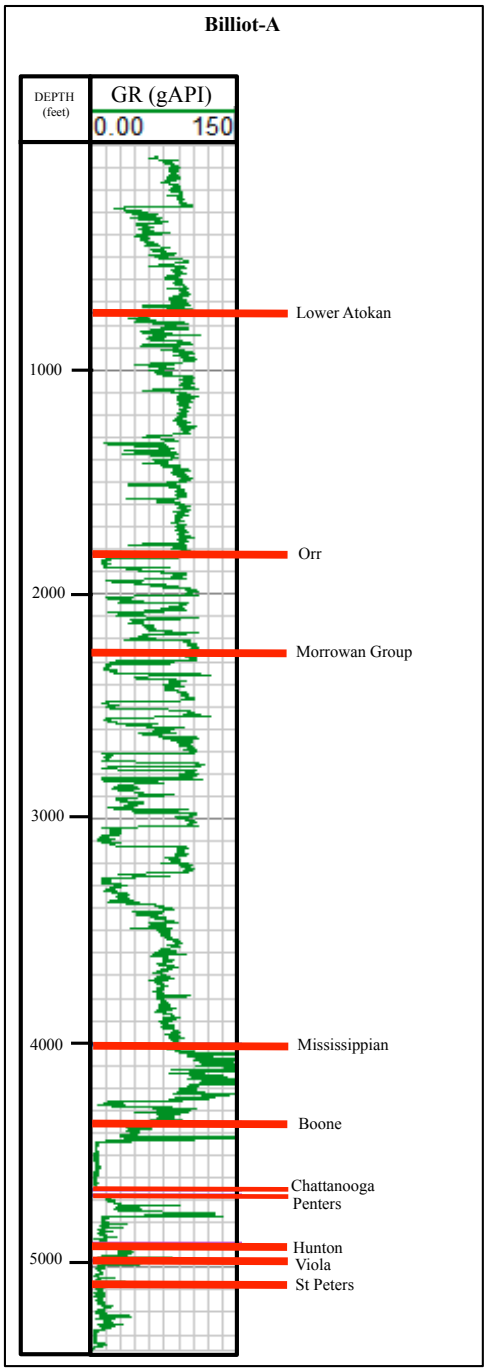

Figure 8a: Interpreted formation tops and associated Gamma Ray log signatures as seen in IHS Kingdom for the Billiot-A well. Picks displayed are for events modeled in PetroMod1D.

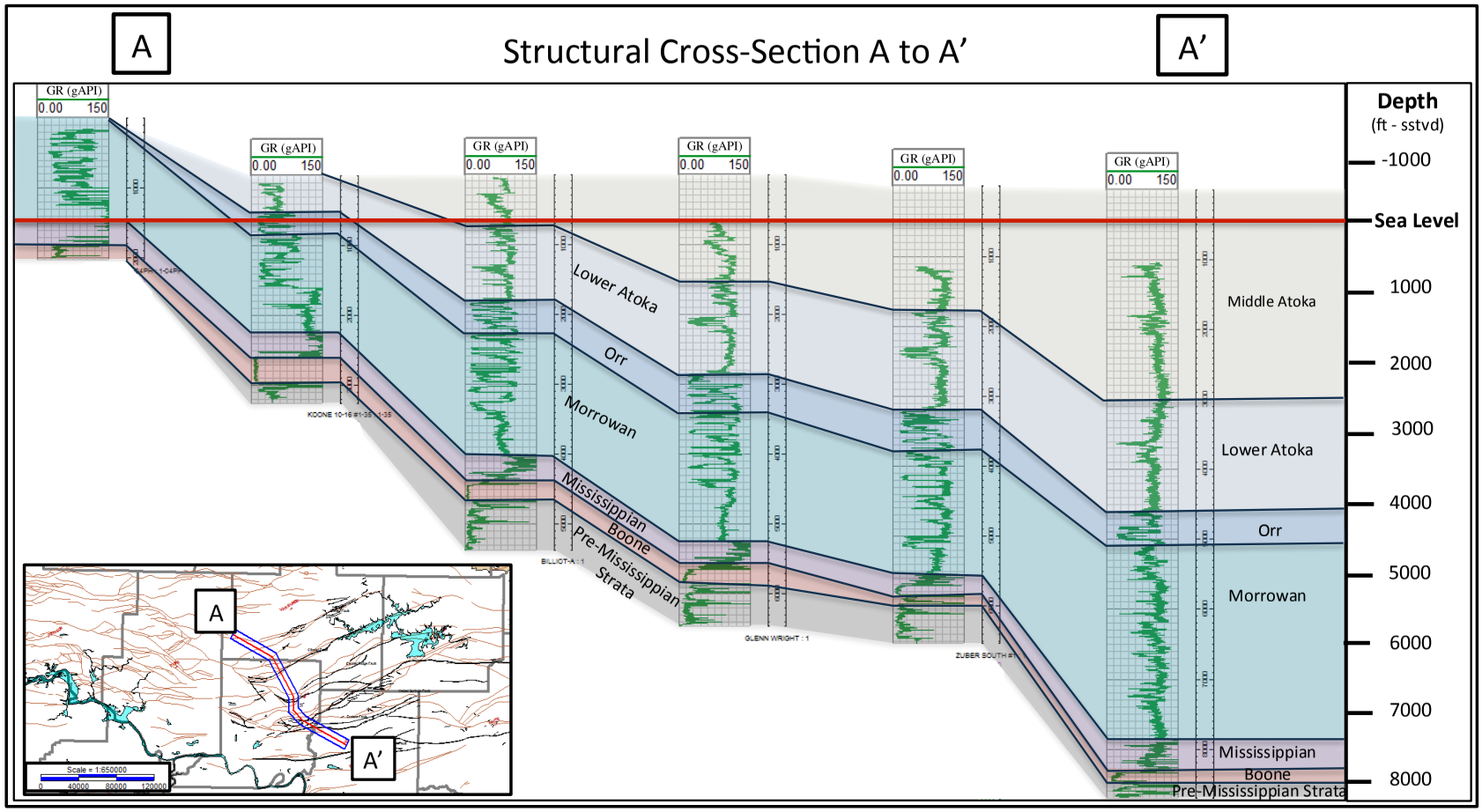

Figure 8b: Gamma ray log signatures across Line A to A' as seen in Kingdom. The structure deepens towards the southeast. Plan-view thumbnail to the left shows line crosses several key NE-SW trending faults. Actual locations of the faults are not displayed within the line. Wells from A to A': OHU 10-17 1-04, Koone 10-16 1-36, Billiot-A 1, Glenn Wright 1, Zuber South 1, and McLung 1-33.

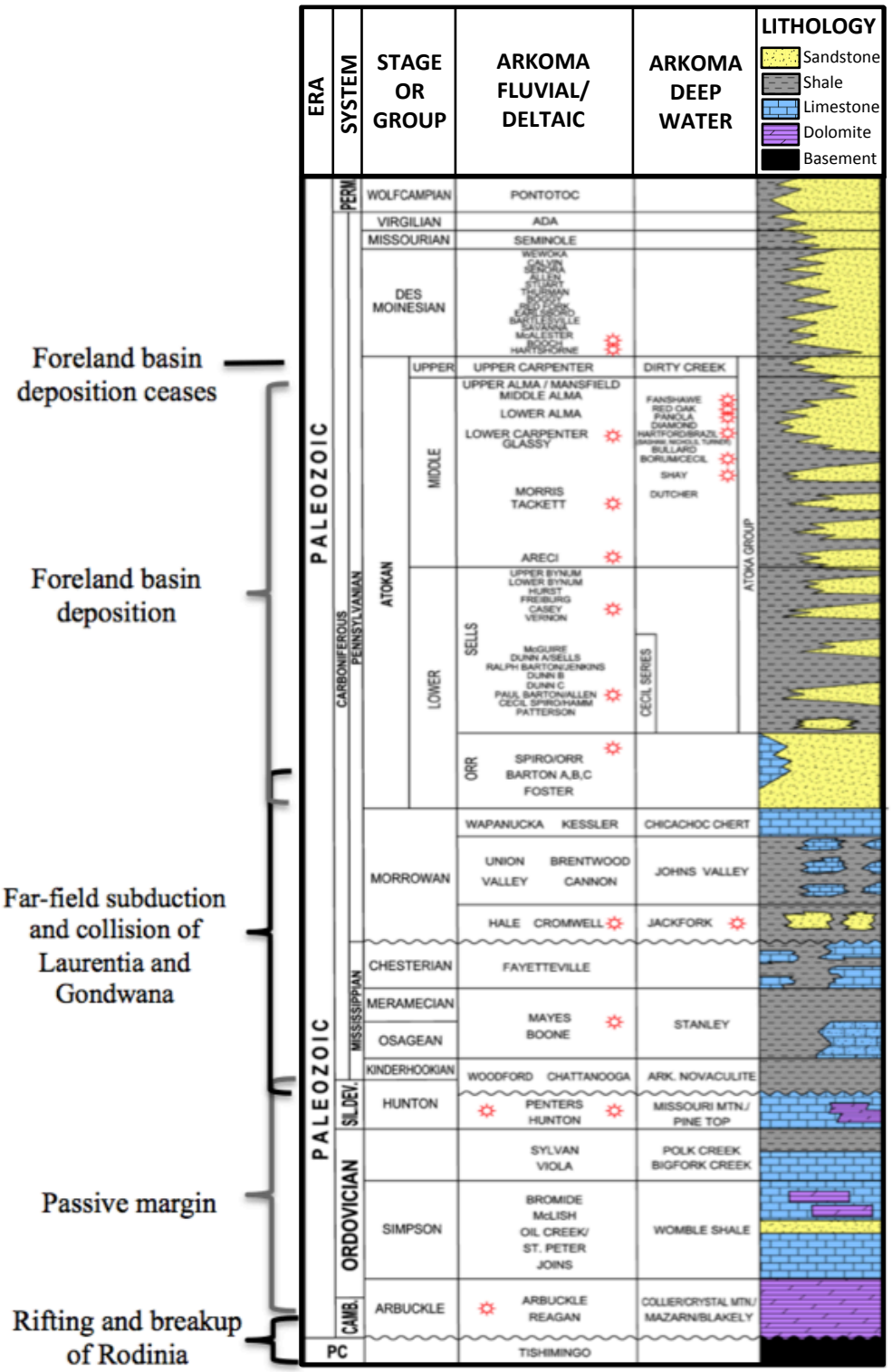

Figure 9: A generalized stratigraphic section of the Arkoma Basin. Tectonic settings are expressed on the left side of the column. Stratigraphic column modified from SWN.

Nine isochore and four structure maps were generating for the Arkansas portion of the Arkoma Basin. The number of wells used in the interpolations varied for each map. Logs were scrutinized for the presence of faults, and if applicable, those wells were eliminated from the map interpretation. Isochore and structure maps were gridded in Kingdom using the flex gridding algorithm, which combines minimum curvature and minimum tension algorithms into a single routine. The four structure maps produced are as follows: (from oldest) 1. St. Peters Formation (Simpson Group – Ordovician System); 2. Mississippian-Pennsylvanian Unconformity; 3. Morrowan Group (Early Pennsylvanian); and 4. Orr Formation (Early Lower Atoka – Middle Pennsylvanian). Nine isochore maps were produced: 1. Mississippian System; 2. Morrowan Group (Early Pennsylvanian); 3. Lower Atoka Group (Middle Pennsylvanian); 4. Sells Group (Lower Atoka Group – Middle Pennsylvanian); and 5-9. Upward succession of time-transgressive maps within the Middle Atoka Group (Middle Pennsylvanian). Map descriptions and interpretations are discussed in Chapter 4.

3.3 Inputs Required for 1D Models

The basin development of the study area has been modeled from 50 wells with the PetroMod1D forward modeling program. Forward modeling uses inferred starting conditions to arrive at values known at present day. The basin history is subdivided into an uninterrupted sequence of chronostratigraphic events. These events, along with their required ages and durations, must be specified as being either times of deposition, nondeposition, or erosion. From the geological input at the well location (thickness and ages of sediments, estimated magnitude and timing of erosion and estimated heat-flow

history), the program starts simulation of the geological development from the base of the sedimentary section and calculates various parameters such as vitrinite reflectance, temperature, and pressure as a function of time. The calculated values of these parameters for the present-day situation are then compared with data that constrain the thermal history such as the present-day bottom-hole temperature (BHT) and thermal maturity indicators (vitrinite reflectance and AFTA). Achieving an agreeable match between the measured and calculated values required several simulations. Input parameters were modified and the program was executed again until match was achieved. By assigning the actual latitudes-longitudes, surface elevation, and depth information for each well, a plan-view and 3D basemap showing the well localities and their associated data can be created in the Well Editor to directly compare calibration values as a function of distance.

1) Heat Flow, Geothermal Gradient, and Surface Temperatures

It is critical to control for the present-day temperature profile in the application of estimating paleotemperatures. Temperature-history reconstruction can be done reliably by use of at least two calibration tools, such as vitrinite reflectance (Ro%) and equilibrated or Horner-corrected bottom-hole temperatures (Welte et al., 1997).

PetroMod requires present-day and paleo-heat flow to reconstruct the temperature history of basins and the thermal maturation of source rock organic matter (Welte et al., 1997). Heat flow measures the conductive component of heat transferred through the Earth's crust to the surface (Welte et al., 1997). Heat flow is the product of geothermal gradient and thermal conductivity and it is expressed in milliwatts per square meter (mW/m^2). The geothermal gradient can be measured in a borehole as the rate of

temperature change with increasing depth in the Earth's interior. The thermal conductivity measures the property of a material to conduct heat.

Although now considered one of the most active basins for unconventional natural gas production, published heat-flow data in the central-eastern Arkoma Basin area are scarce. Some heat-flow values exist further east than the study area near the Mississippi Embayment, however, studies in other parts of the Arkoma Basin show that the difference in heat flow over a 50 km area can vary up to 15 mW/m^2. Heat-flow maps for the continental U.S. have been published (Blackwell and Richards, 2004), however, the granularity of these values for the Arkoma Basin is not sufficient for this study. This problem has been encountered before, as Lee et al. (1996) states that the geothermal gradient map of North America (Blackwell and Steele, 1991) contains a single heat-flow value for the Arkoma Basin. Because PetroMod places a heavy importance of heat flow as an input parameter for modeling, the approximation of heat flow was aided by producing a geothermal gradient map of the Arkoma Basin from 229 wells. Bottom-hole temperature data were collected manually from 169 well log headers on file at the log library provided by Southwestern Energy Company (SWN) as well as 60 BHTs from the National Geothermal Database. Because drilling activity distorts the temperature measurement from the true in-situ value, mathematical corrections are calculated to determine the in-situ temperature of the formation. Bottom-hole depth, temperature, fluid type, and time-since-circulation information were collected to create a repository of corrected bottom-hole temperatures and calculated geothermal gradient per well location. According to the amount of data available for the well and its proximity to other wells with time-since-circulation information, the Horner plot correction was the first choice

correction method used. If no time-since circulation information was available, bottom-hole temperatures were corrected by adding ±33 °F (±18 °C). The expected T_{eq} uncertainty is ±17 °F (±9 °C) (Corrigan, 2003).

Data from air-drilled wells were initially gathered. After the collection and calculation of geothermal gradients in these wells, additional data were taken from fluid-drilled wells to constrain trends at a finer granularity. A mean annual ground surface temperature was estimated to be 22.2 °C: the intercept of a least squares linear regression on 226 BHTs. The mean annual average surface air temperature in the vicinity of the wells is 19 °C (NCDC). Mean annual ground temperatures are generally a few degrees Celsius warmer than mean annual surface air temperature. These data suggest that the calculated mean of the annual ground surface temperature is within a reasonable margin of error. The geothermal gradient values were then reassigned to their respective well locations and imported into the Kingdom software for regional interpolation. In general, the values are in agreement with the map published by Byrnes and Lawyer (1999). 115 well locations were used by Byrnes and Lawyer (1999) to calculate the geothermal gradient of a region three times the size of the area of interest presented in this study. Furthermore, changes in the calculated geothermal gradient across a shorter distance may be more prominent in the interpreted map in this study. Different measurement methods or inaccurate readings of temperature and circulation information are possible causes for the local variations. Differences in geothermal gradients must be scrutinized on a case-by-case basis, as wells selected for the study cover varying depths and formations drilled. For basin modeling, geothermal gradient maps are of less utility than heat-flow maps (Lee et al., 1996). Changes in geothermal gradient may simply reflect changes in

lithology. Heat flow is conserved and therefore is a better indicator of the thermal state of the crust and upper mantle. The use of geothermal gradient in this study is used as a calibration tool for the areas lacking heat-flow data.

Heat flow was calculated in the western Arkoma Basin by Lee et al. (1996). From an Airy isostatic balance, the total change in heat flow from south to north due to the change in crustal heat production is approximately 5 to 15 mW/m^2. Overall, there is an observed 20 to 30 mW/m^2 increase in present-day heat flow from south to north. Heat-flow values of 35 to 40 mW/m^2 exist in the southernmost portion of the western Arkoma basin. In the central part of the basin, heat flow is ~58 ±12 mW/m^2. The heat flow increases to 66 ± 13 mW/m^2 on the northern end near the stable midcontinent platform. In this study, a present-day heat-flow value was calculated within PetroMod1D in conjunction with existing heat-flow trends from Lee et al. (1996). Corrected bottom-hole temperature measurements and present and assumed paleo-surface temperatures were used to calibrate the heat flow. Paleo-heat flow and the estimated amount of removed overburden were altered accordingly to attain a geologically acceptable match between the measured data and the projected vitrinite reflectance with respect to depth profile. The EASY%Ro algorithm of Sweeney and Burnham (1990) is employed to relate the influence of time and temperature on the increase of vitrinite reflectance.

The thermal-maturity data from a number of wells have been used to derive first order paleo-heat flow levels. In general, the vitrinite reflectance levels for the wells are too low if a constant (present-day) geothermal temperature since burial is assumed. The comparison of the effects of heat flow and its significant role in determining model output values is discussed in more detail in the results section.

2) Age Assignments, Lithologies, and Source Rock Properties

Table 1 lists the ages of the stratigraphic units and unconformities for which modeling calculations were executed. Radiometric ages were taken from Mankin et al. (1987) and research conducted by SWN. The ages at system and series boundaries were adjusted to the International Geologic Time Scale from the International Commission on Stratigraphy. Any slight errors in the estimated chronometric ages of each sample are not expected to affect the thermal history interpretation of either the AFTA or vitrinite reflectance data to any significant degree. Associated kerogen types and total organic carbon data are also presented in Table 1 (Johnson and Cardott, 1992; Byrnes and Lawyer, 1999).

The lithologies of the modeled stratigraphic units have important implications on thermal maturity and subsidence patterns. The following units are represented within the stratigraphic section of Figure 9. Shallow-water carbonates primarily controlled deposition during the Cambrian through Middle Mississippian. A stable shelf existed along the southern passive continental margin of North America at this time. The shallow-water carbonates consist of the Arbuckle, Viola, and Hunton Groups. The only significant break in carbonate deposition occurred in the Middle Ordovician with a terrigenous influx of sediment from the Simpson Group. The Late Devonian unconformity is marked by widespread erosion that resulted in the removal of portions of the Hunton Group. A transgressive surface, marked by the organic-rich black shale of the Chattanooga Formation, rests successively above the Late Devonian unconformity (Byrnes and Lawyer, 1999). The disconformable base of the Boone Formation was used as the modeled base of the Mississippian Period. The Boone Formation is generally

characterized as a fossiliferous limestone that is interbedded with chert (McFarland, 2004). The Mississippian-Chesterian consists of the Pitkin Limestone, Fayetteville Shale, Hindsville Limestone, and Moorefield shale. The Chesterian series is separated from the Early and Middle Mississippian Boone Formation by an unconformity. Sea withdrawal from the mid-continental shelf regions during the Late Mississippian marks a regional unconformity at the base of the Pennsylvanian. The increasing southward tilt of the Arkoma shelf north of the approaching Ouachita trough resulted in a truncation of the Chesterian sequence. The Early Pennsylvanian Morrowan Series is characterized by complex depositional patterns resulting from periods of gradual transgression and regression (Sutherland, 1988). The Hale Formation (Morrowan) is made up of two members, but can be generally described as being composed of silty shales, sandstones, and limy sandstones. The Bloyd Formation (Morrowan) is represented by a sequence of limestones that are separated by thick intervals of dark shale (McFarland, 2004). The Pennsylvanian Atokan Series is a thick sequence of marine silty sandstones and shales. In some areas, the series may reach up to 25,000 feet thick. The Atoka Formation is divided into three informal divisions that are based on depositional patterns in response to the Atokan structural history. The latest Atokan and Pennsylvaninan-Desmoinesian are composed of shallow-marine, deltaic, fluvial and coal-bearing sediments (Sutherland, 1988). Few published examples exist; however, evidence for westward transportation along the axis of the newly developed foreland basin is reflected by the east to west orientation of sediments in the central portion of the Arkoma Basin during the Upper Atoka (Sutherland, 1988).

Modeled stratigraphic unit	Chronostratigraphic age	Radiometric age of onset (Ma)	Principal Lithology	Principal kerogen type	Total organic carbon (%)
Upper Atoka Fm.	Early Pennsylvanian	306	ShSs	II/III	0.2-1.8
Middle Atoka Fm.	Early Pennsylvanian	308	ShSs	II/III	0.2-1.8
Lower Atoka Fm.	Early Pennsylvanian	311	ShSs	II/III	0.2-1.8
Morrowan Series	Early Pennsylvanian	318	ShSs	III	0.29-3.0
Unconformity		322			
Pitkin Ls., Fayetteville Sh., Hindsville Ls.	Middle/Late Mississippian	337	ShLs	II/III	
Unconformity		348			
Boone Fm.	Early/Middle Mississippian	353	Ls	II/III	
Unconformity		359			
Chattanooga	Late Devonian	375	Sh	II/III	2.0-12.5
Unconformity		395			
Penters	Devonian	402	LsSandy		
Unconformity		407			
Hunton Group	Silurian-Devonian	428	LsDolo		
Unconformity		445			
Viola	Late Ordovician	450	LsSh	I/II	
Unconformity		460			
Simpson Group	Middle Ordovician	485	Ls	I/II	
Arbuckle Group	Cambrian – Early Ordovician	486	Dolo		0.0 – 1.4

Table 1: Table of the stratigraphic units used for PetroMod1D models.

3.4 Measured Data and Calibration

Measured values of vitrinite reflectance and Apatite Fission Track Analysis (AFTA) data were obtained from 50 wells (Figure 2). New AFTA and vitrinite reflectance data were provided by Southwestern Energy for 23 wells in the study area. Data from these wells are integrated with previously published thermal-maturity data within the Arkoma Basin. The thermal maturation data in this study are geographically widespread; therefore, variation in sampling techniques and sources is taken into account. In each well, the synthesis of the two calibration methods will be used to provide a regionally coherent tectonic framework within which the structural development of the basin may be understood.

Data from the Arkansas Geological Commission (AGC) and selected wells that were analyzed in Houseknecht (1992) were used for calibration in this study. AGC well cutting samples from deep gas wells were collected at the Norman F. Williams Well Sample Library in Little Rock, Arkansas. Many of the samples that were analyzed are selected stratigraphically above, through, and below the Fayetteville and Chattanooga Formations in order to obtain a vertical maturation profile for a given well.

Maturation indicators are used as an index to determine the amount of thermal exposure a rock has been subjected to. The critical temperature at which an organic or inorganic chemical reaction takes place indicates the maturity level of the source rock and can be used to determine the potential for hydrocarbon generation and erosion estimation (Hagen, 1986). One of the key maturation indicators available for this study is vitrinite reflectance. Vitrinite reflectance is a time-temperature indicator used to measure the highest temperature that a source rock has experienced. Vitrinite reflectance is

measured in units of reflectance, Ro%, and is determined by measuring the reflectivity of vitrinite macerals under polarized light. As the temperature of host strata increases, the reflectance of vitrinite will increase, indicating higher levels of thermal maturity. The use of Ro data are considered the most appropriate measurement for characterizing the thermal maturity of sedimentary rocks and for understanding their thermal history (Houseknecht, 1993). However, Ro values may be influenced by variables that can cause suppression and an increase in reflectance (Houseknecht, 1993).

Apatite fission track analysis (AFTA) is a radiometric dating technique for the determination of the magnitude of the maximum temperature and the time at which cooling from that maximum temperature began. Fission tracks are trails of radiation damage that are produced within apatite grains at a near-constant rate through geological time. AFTA dating is suitable for determining low-temperature thermal events. In samples which have been subjected to temperatures less than ~50 °C since deposition, spontaneous fission tracks have a characteristic distribution of confined length tracts, but a "fission track age" can be calculated by calibration against other isotopic systems using age standards which also have this type of length distribution. In samples which have been subjected to temperatures greater than ~50 °C after deposition, fission tracks are shortened because of the gradual repair of radiation damage. The process for which tracks shrink from each end is known as fission track "annealing". The final length of each individual track is determined by the maximum temperature that track has experienced. As temperature increases, all existing tracks shorten to a length determined by the prevailing temperature, regardless of when they were formed. After the temperature has decreased, all tracks formed prior to the thermal maximum are frozen at the degree of

length reduction they attained at that time. Furthermore, the length of each track can be thought of as a maximum-reading thermometer, recording the maximum temperature to which it has been subjected. In thermal history scenarios in which a heating episode is followed by a cooling and reheating, the tracks formed during the second heating phase will undergo progressing shortening (SWN, 2004).

Vitrinite reflectance is a time-temperature indicator governed by a kinetic response in a similar manner to the annealing of fission tracks in apatite described above. The interpretation of vitrinite reflectance is based off of the distributed activation energy model by Sweeney and Burnham (1990), which describes the evolution of vitrinite reflectance with time and temperature. Because vitrinite reflectance continues to increase progressively with increasing temperature, vitrinite reflectance data allow direct estimation of maximum paleotemperatures in the range where AFTA only provide minimum estimates or where apatite fission tracks are totally annealed (generally above ~110 °C). AFTA data should allow tight constraints to be placed on the time of cooling and also the cooling history, because AFTA parameters are dominated by the effects of tracks formed after cooling from maximum paleotemperatures.

The AFTA data provide important controls on the post-Middle Jurassic cooling history. Constraints used to model the 50 wells in this study were constrained using the following parameters. Cooling from peak paleotemperatures began at some time between the end-Carboniferous (306 Ma) and the Middle Jurassic (165 Ma). Paleotemperatures greater than 100 °C for Carboniferous sediments now at the surface persisted until around the Lower Cretaceous (~145 to 125 Ma) (Arne, 1992; Geotrack). Depending on the location within the basin, local loading history will result in a variation in

paleotemperatures. Cooling from "peak" paleotemperatures of 75 to 85 °C occurred at the beginning of the Early Miocene (~25 to 20 Ma). To satisfy the criteria required by both AFTA and vitrinite reflectance data, five key depositional, non-depositional, and erosional events were implemented in the calibrated reconstructions. The significance of each event and its implications on the thermal evolution of the basin will be described in specific case studies.

Although minor, event timing per well varies according to location within the basin. The results of the time-transgressive isochore and structure maps produced in this study aided in determining event series timing. A major burial event was placed around the Atokan time, ~308 to 306 Ma, representing rapid deposition during main foreland wedge deposition. Modeled burial continued at a constant rate until a rate change at 280 Ma. From 280 Ma until the end of the Paleozoic (250 Ma), subsidence continued to occur. The rate change at 280 Ma exists because of restrictions required by Middle Atokan stratigraphic thicknesses and due to the suggested total duration of subsidence in foreland basins, as seen in subsidence histories presented by Xie and Heller (2009). Foreland basin subsidence is suggested to last a few to tens of millions of years (Xie and Heller, 2009). Ceased subsidence at the end of the Paleozoic (250 Ma) is followed by uplift until the Middle Jurassic (165 Ma), the maximum limit for the time at which cooling from peak paleotemperatures began. AFTA restrictions require paleotemperatures to remain above 100°C until 125 Ma (Lower Cretaceous), therefore, non-deposition persisted from 165 Ma until 130 Ma. Uplift and erosion was selected to initiate around 130 Ma to permit decreasing paleotemperatures to reach nearly 100 °C by 125 Ma. Present-day heat flow and paleo-heat flow were carefully adjusted to these

parameters and monitored through various simulations to determine a reasonable match that satisfies cooling restraints from AFTA data. Heat flow was held constant until the end of the Carboniferous. From there, the heat flow was lowered at a constant decreasing slope until the present day. Several simulations determined that the time at which the heat flow begins to decrease towards present day can be altered within a 10-15 million year bracket while still achieving the same vitrinite reflectance values. On a geologic time scale, the change in slope within this time range is negligible. Although the time restraints for the heat-flow deviation points are not strict parameters needed to determine the predicted vitrinite reflectance values, the heat-flow value itself plays a crucial role in predicted thermal maturity. In previous studies, there has been a great deal of emphasis on the calculation of "total removed overburden" to reconstruct the basin's history. However, it is equally important to segregate the burial events that constitute the maximum thickness because of the implications on timing of petroleum generation. The location of wells in relation to the migration of the foreland basin depocenter from east to west illustrate variations in thickness as a function of time and the effects of burial rate on thermal maturity. To acknowledge both vitrinite reflectance data and AFTA data, uplift and erosion had to occur in multiple intervals. Arrival at the same present-day vitrinite reflectance values can also be achieved by erosion occurring at a constant rate since time of initiation of uplift. However, a constant rate of uplift would not satisfy the paleotemperature boundaries provided by the AFTA data.

All 50 wells in the study area possessed a set of measured vitrinite reflectance data specific to that individual well. Wells were first calibrated to their distinct set of measured vitrinite reflectance values that fit the required geologic framework. Model-

predicted vitrinite reflectance was compared with measured data in the form of an output vitrinite reflectance with respect to depth plot (Figure 10). The profiles were extrapolated using the EASY%Ro (Sweeney and Burnham, 1990) and compared with the thermal maturity patterns of the Hartshorne coal bed. The vitrinite reflectance values of the Hartshorne coal bed are considered to be a good indicator for thermal maturity at the surface and in the shallow subsurface of the Arkoma Basin (Houseknecht, Hathon, and McGilvery, 1992). Surface vitrinite reflectance values are ~ 0.6% in the western end of the basin in Oklahoma. These surface values increase eastward to values greater than 2.0%, until the erosional edge of the coal bed is met in Pope County, Arkansas.

After a match was detected in a single well, measured data from proximal wells could be displayed within the output plot for comparison. Wells with a small number of measured values could be projected to shallower depths by using input parameters similar to nearby wells with more data. The constant comparison of calibration data to surrounding wells provided the basis for generating a set of burial and thermal history models adhering to a geologically coherent framework.

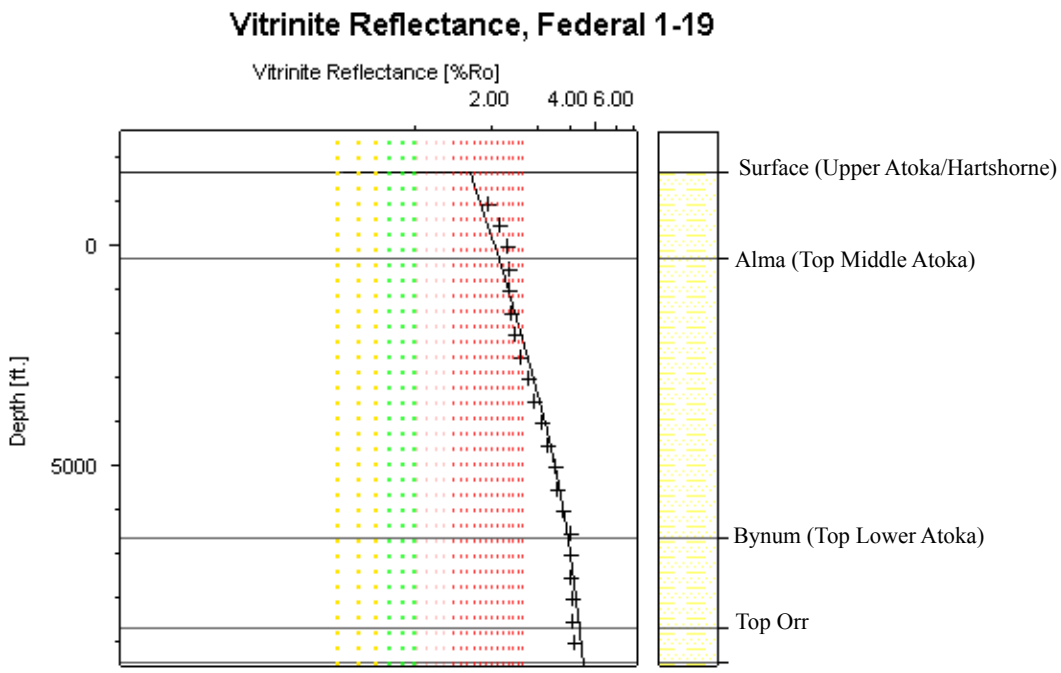

Figure 10: Model predicted vitrinite reflectance with respect to depth for Federal 1-19. Black crosses represent the measured data in which input parameters were calibrated against. Stippled colored areas denote the zones of hydrocarbon generation and destruction (hydrocarbon windows), expressed in terms of vitrinite reflectance (%Ro): 0.5-0.7, early mature (oil); 0.7-1.0, mid-mature (oil); 1.0-1.3, late mature (oil); 1.3-2.6, main gas generation. Modeled stratigraphic units (Table 1) are specified to the right of the reflectance plot.

CHAPTER 4: Results

4.1 Geothermal Gradient Map

Although not a direct input parameter in PetroMod1D, a geothermal gradient map may act as a reference for predicting heat-flow trends where heat-flow data do not exist. For each output model in PetroMod1D, a geothermal gradient was automatically calculated as a function of the lithology and the heat flow of that particular stratigraphic

column. Models were simulated several times by altering the present-day heat flow until a match was achieved between the modeled and measured geothermal gradients. The generated present-day geothermal gradient map of the Arkansas portion of the Arkoma Basin is seen in Figure 11. In general, geothermal gradients range from 20 °C/km to 35 °C/km. The south and southeast portions of the study area exhibit average geothermal gradients around 20 °C/km. The middle portion of the basin exceeds 30 °C/km and values in the north are seen steadily decreasing to around 27 °C/km. Higher heat-flow values are concentrated in the central eastern portion of the basin. The map is in agreement with the geothermal gradient map produced by Byrnes and Lawyer (1999) for the regional Arkoma Basin. Drastic lateral changes in geothermal gradient are evident in some areas in the map. In some places, a difference of 10 °C/km exists over a distance of less than three miles. As discussed in Chapter 3, these points may not reflect in-situ geological conditions due to the differing industry procedures used to measure bottom-hole temperature.

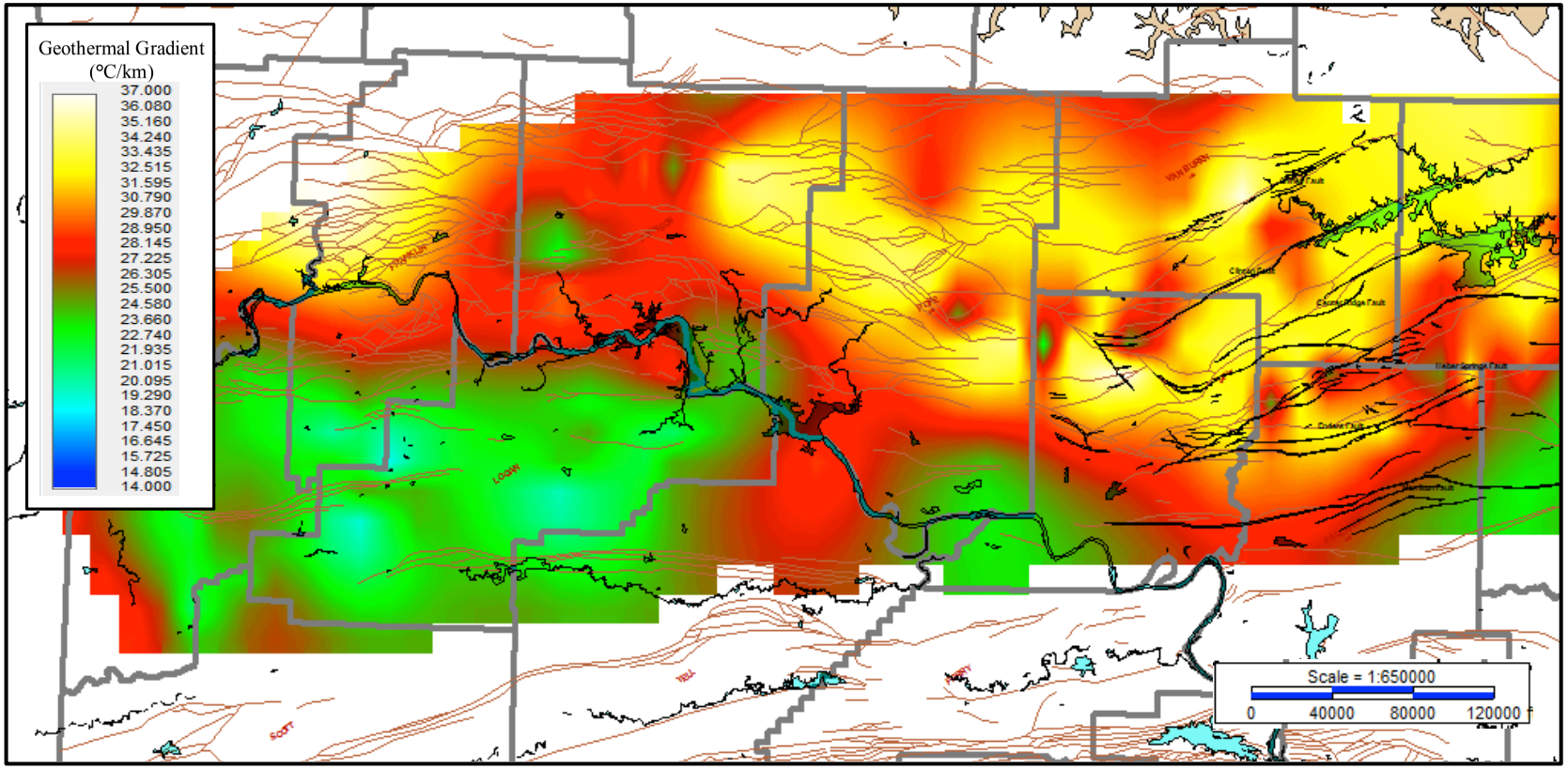

Figure 11: Map of the present day geothermal gradient in the Arkansas portion of the Arkoma Basin.

4.2 Structure and Isochore Maps

Figures 12-15 are present-day structure maps interpolated from well logs in Kingdom. Relative ages of the four different horizons are referenced in Figure 2. The St. Peters Formation (Ordovician) is the deepest structure map presented in this study (Figure 12). Present-day depths are strictly bounded by fault location. Downthrown terraces from E/W and NE/SW-striking normal faults result in an overall southward-deepening structure. The crosscutting relationship between present-day faulting and depth of the St. Peters Formation is evidence for tectonic movement and reactivation of deep basement faulting from foreland basin formation that continued to generate dip-slip displacement on the St. Peters Formation long after its deposition. Similarly, a structure map of the top of the Mississippian System shows a deepening to the south (Figure 13). E/W-striking normal faulting in the western portion of the basin shows nearly ~2,000 feet of relief occurring across faults. Structure follows the orientation of the faults in the eastern portion of the basin, however, displacement across the NE/SW-trending faults is more gradual. Within the NE/SW-trending faults, the structure dips toward the SW. Relief across the downthrown fault terraces is greatest along southernmost faults. In particular, depth is highly controlled by the boundaries of faults within Faulker and Conway counties.

The Early Pennsylvanian Morrowan Group shows an overall deepening structure to the southwest (Figure 14). In the eastern portion of the basin where a NE/SW fault configuration is dominant, the structure dips gently to the southeast. Relief across this fault configuration is significantly less prominent in the Morrowan Group than seen in the top Mississippian structure. Present-day depth of the Morrowan Group most mimics

the NW/SE to E/W-striking faults in the central and western portions of the basin. A structure map of the Lower Atokan Orr also shows deepening to the southwest (Figure 15). EW-striking faults in the west do not show much control over the south-dipping structure. Toward the east in the center of the basin, Morrowan structure more strictly follows the NW/SE-striking fault trend. NE/SW fault terraces furthest east do not show a significant change in depth.

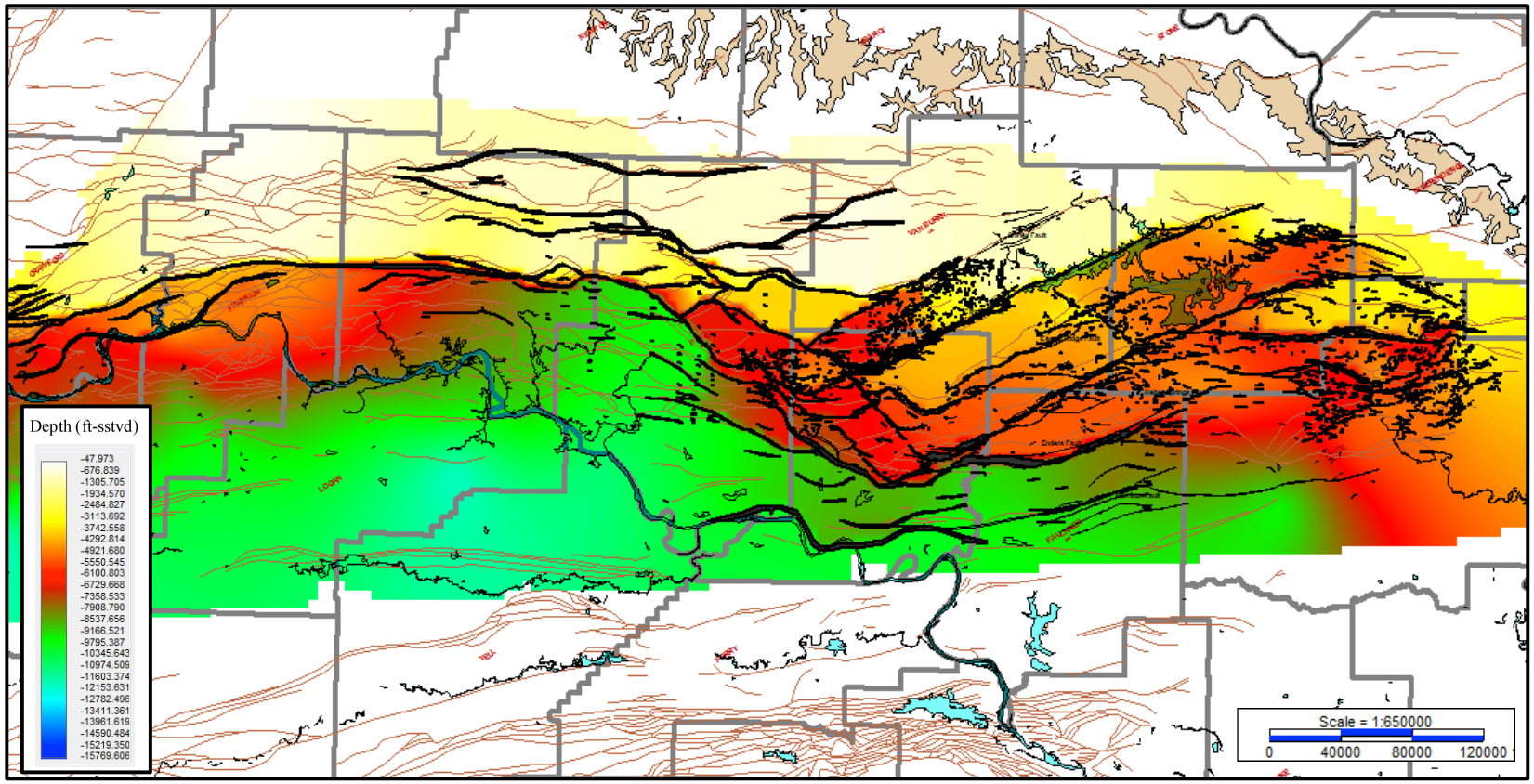

Figure 12: Structure map of the St. Peters Formation (Ordovician)

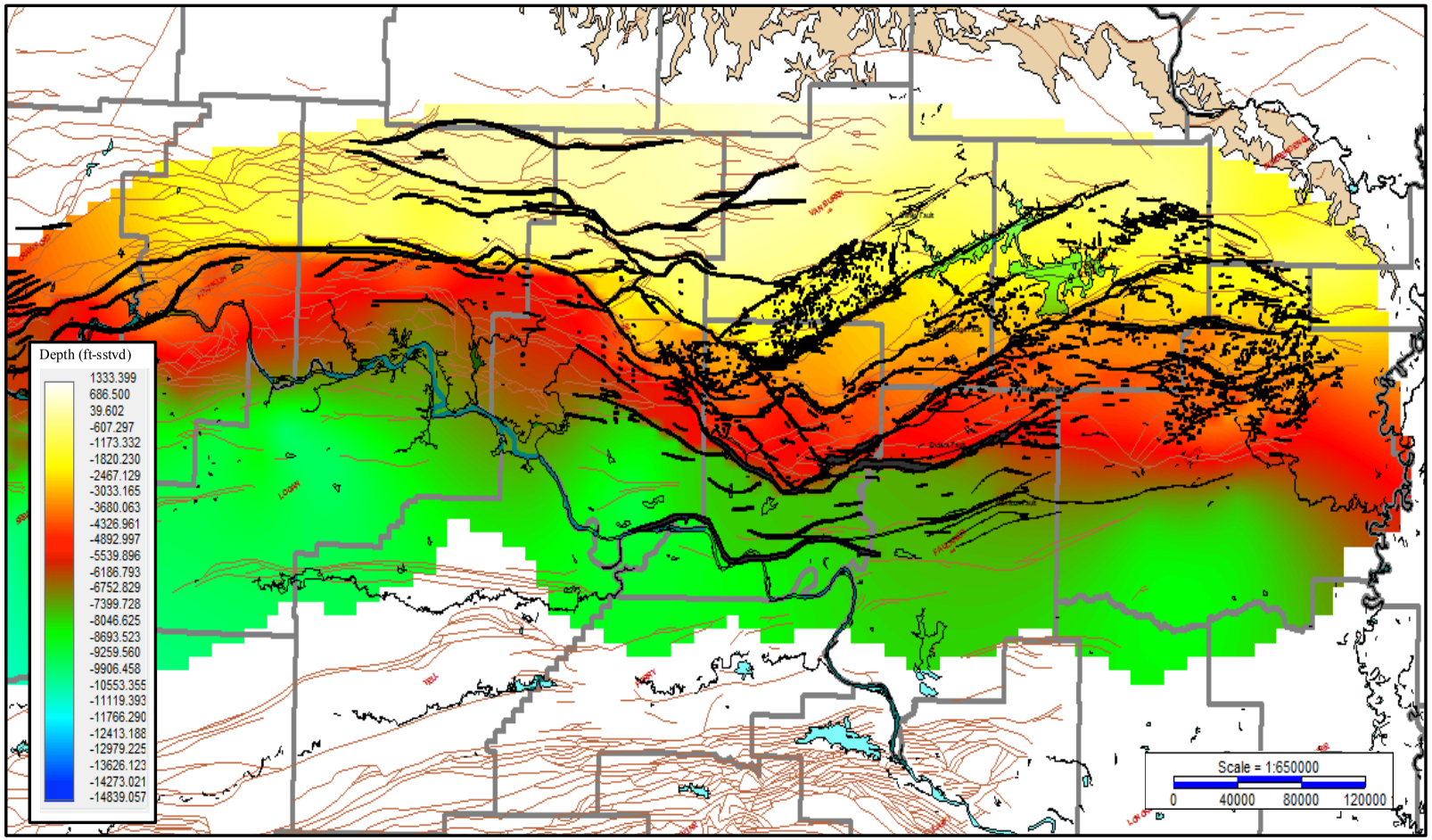

Figure 13: Structure map of the top Mississippian

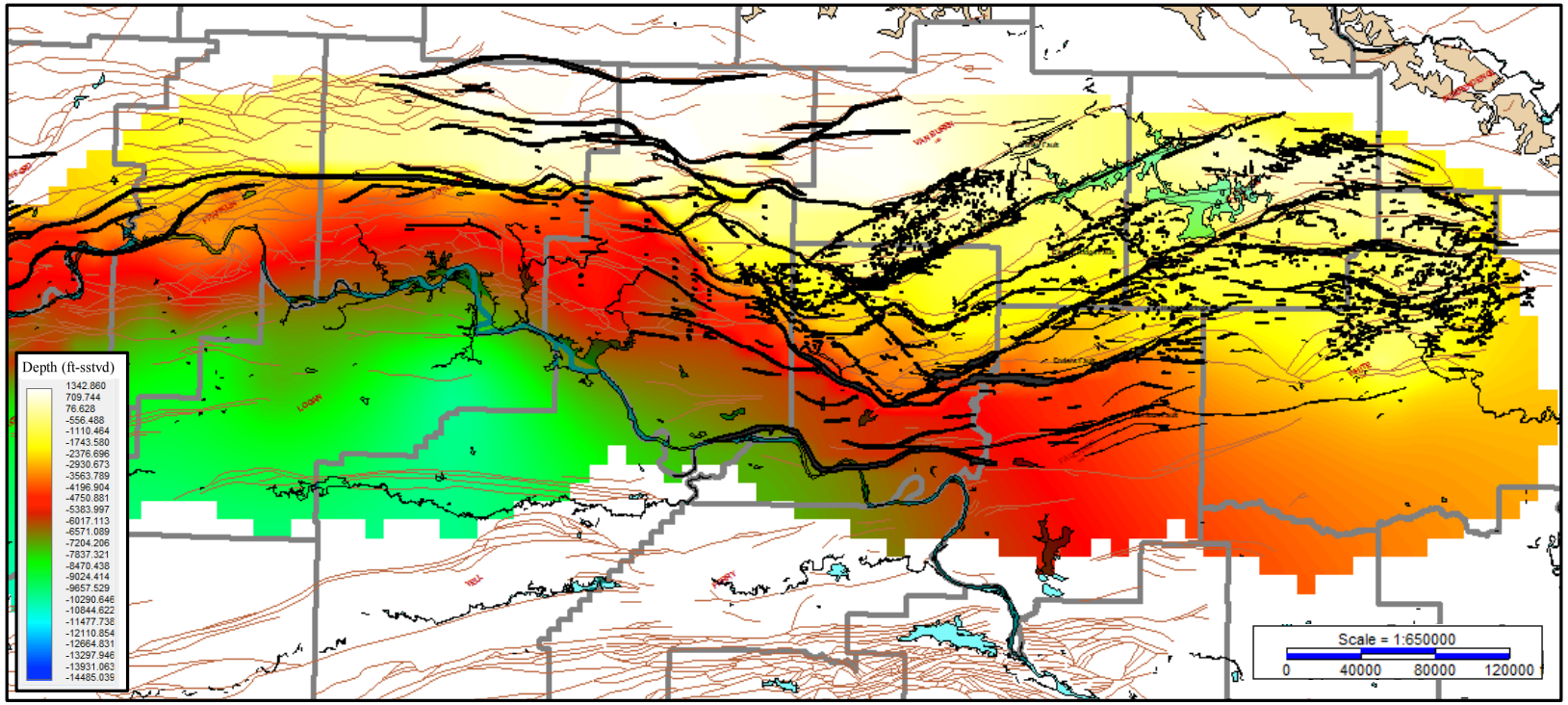

Figure 14: Structure map of the Morrowan Group (Early Pennsylvanian)

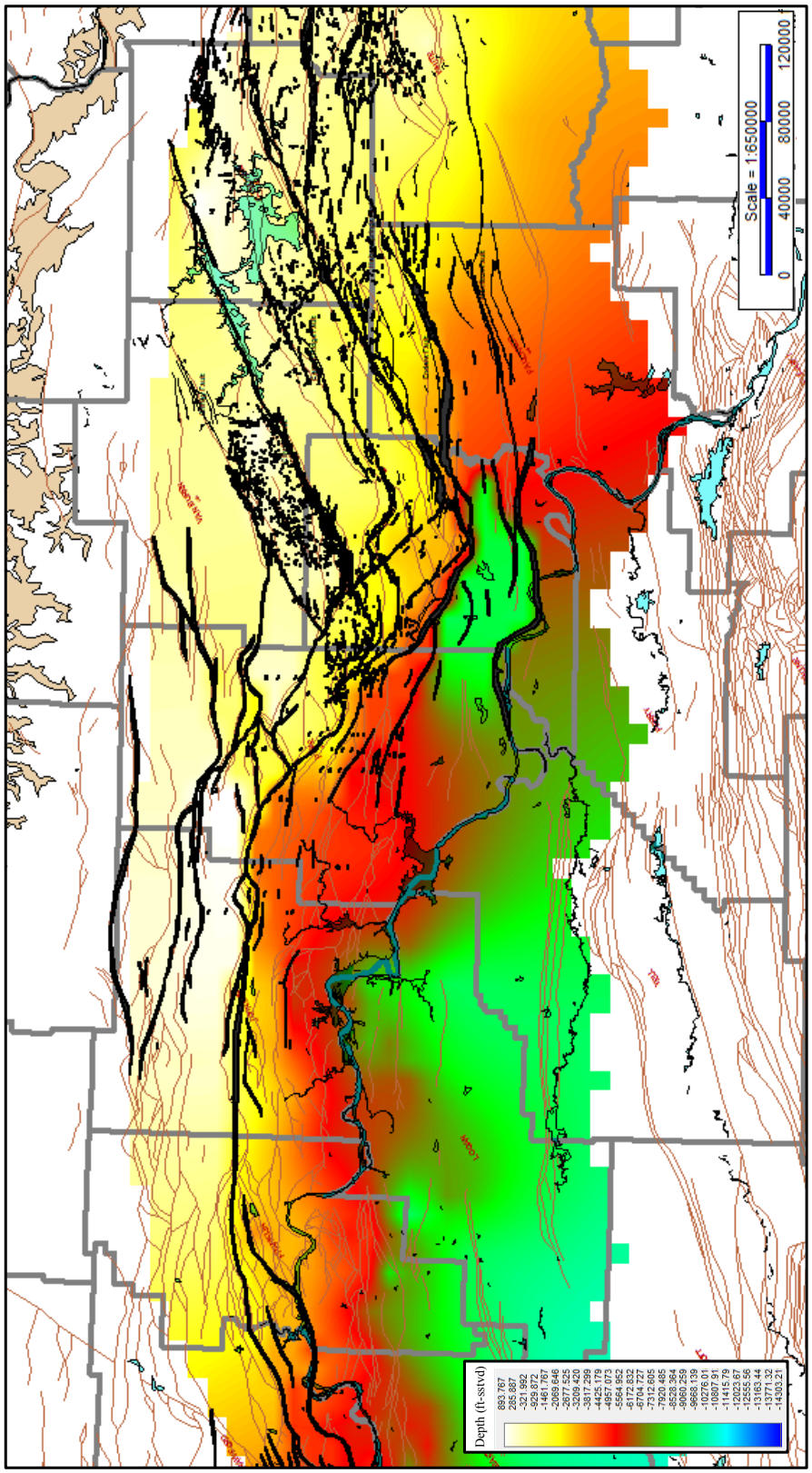

Figure 15: Structure map of the Orr Formation (Lower Atokan – Pennsylvanian)

A series of nine time-transgressive isochore maps were produced traversing the

Arkansas portion of the Arkoma Basin. Strata document the depositional history as the Arkoma area transformed from a passive stable shelf into a rapidly downwarping foreland basin. The isochore maps in Figures 16-24 are compared alongside a stratigraphic section of the Arkoma Basin that highlights the main tectonic controls on sedimentation throughout development of the foreland basin. The isochore map of the Mississippian-Osagean though the Mississippian-Chesterian stages clearly indicates greatest sediment thickness existing in the northeast portion of the basin (Figure 16). Deposition most representative of a passive margin setting is dominant in this section, although far-field subduction was occurring to the southeast of the Arkoma Basin area at this time. No significant changes in thickness due to plate flexure are seen in this section, however, an isochore map of the latest Mississippian may show the effects of the approaching orogenic wedge. A shift in the preferred location of deposition is most evident in an isochore map of the Early Pennsylvanian Morrowan Group (Figure 17). During this time, deposition is heavily concentrated in the southeast area of the developing Arkoma foreland basin and flexural downwarping of the subducting plate is a control on sedimentation. Figures 18-24 illustrate the changing thicknesses of strata within the Arkoma Basin as the formation of the foreland basin progresses. Depositional changes that take place during the Lower Atokan Group are shown in Figures 18 and 19. Figure 18, an isochore map from the top of the Morrowan Group to the top of the Lower Atokan Group, shows the thickness of the Lower Atokan Group in its entirety. Figure 19 shows the location of sediment that was deposited in the later half of the Lower Atokan Group. A comparison of the two thickness maps shows that deposition migrated from the east to the west with time. The concentration of rock is more or less equally distributed in

the east and west in Figure 18 compared to Figure 19, where deposition in the west has become more prominent. As a whole, the isochore maps show a distinct change in the preferred depositional location from commencement of the Pennsylvanian System. Figures 20-24 are time-transgressive stacked isochore maps that were deposited during a two million year time interval in the Middle Atokan Group. The extent of these maps is not as widespread as the intervals previously discussed due to extensive surface erosion; however, lateral changes in thickness can still be observed through time. As the Middle Atokan evolves through time, a continued westward shift in deposition is seen from the earliest sediment package (Figure 20) to the later stages of the Middle Atokan. Evident changes in thickness that originate in northern Yell and southern Polk counties in Figure 21 can be traced westward through Figure 24 to the western edge of Logan county.

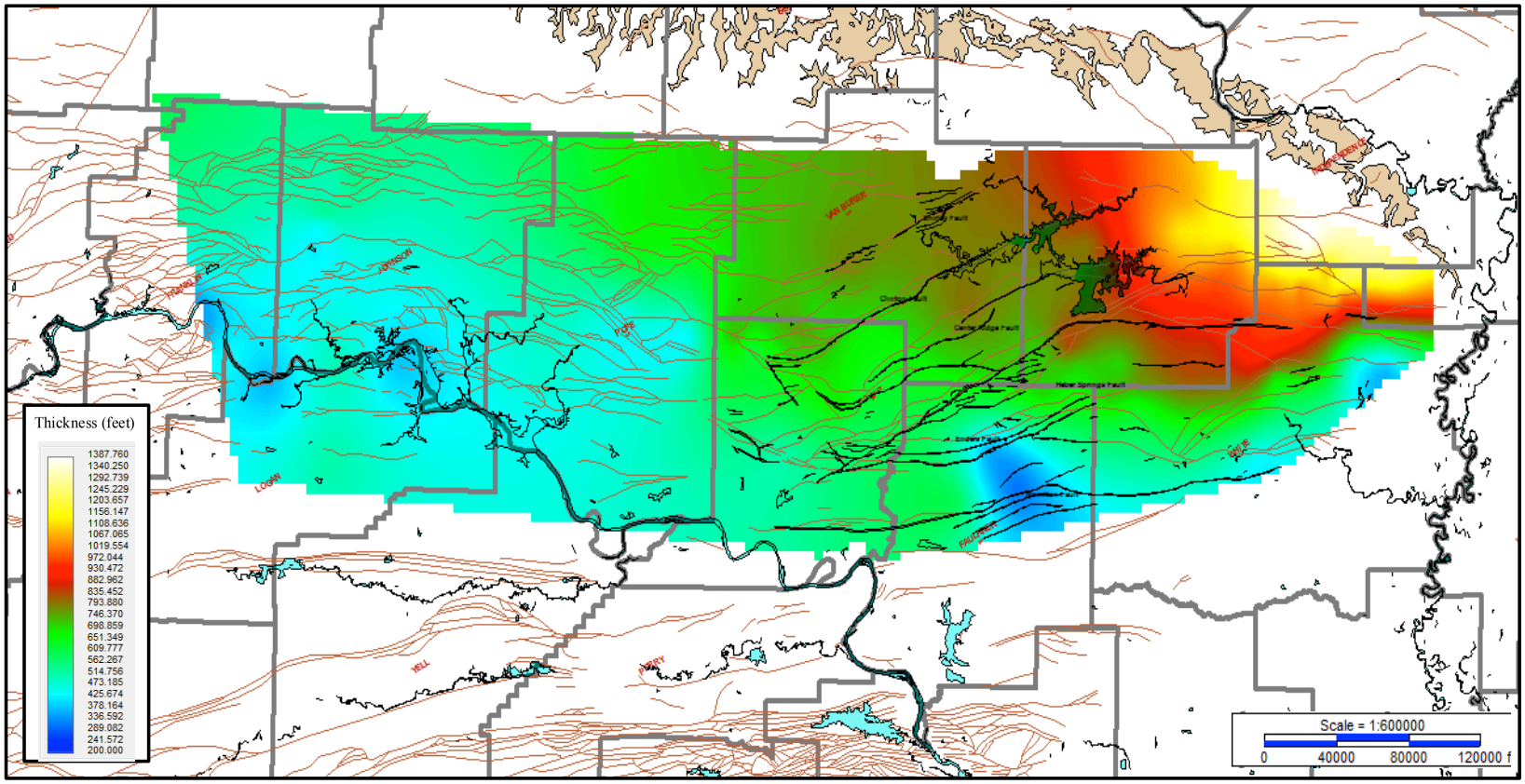

Figure 16: Isochore map of the Mississippian-Chesterian to Mississippian-Osagean

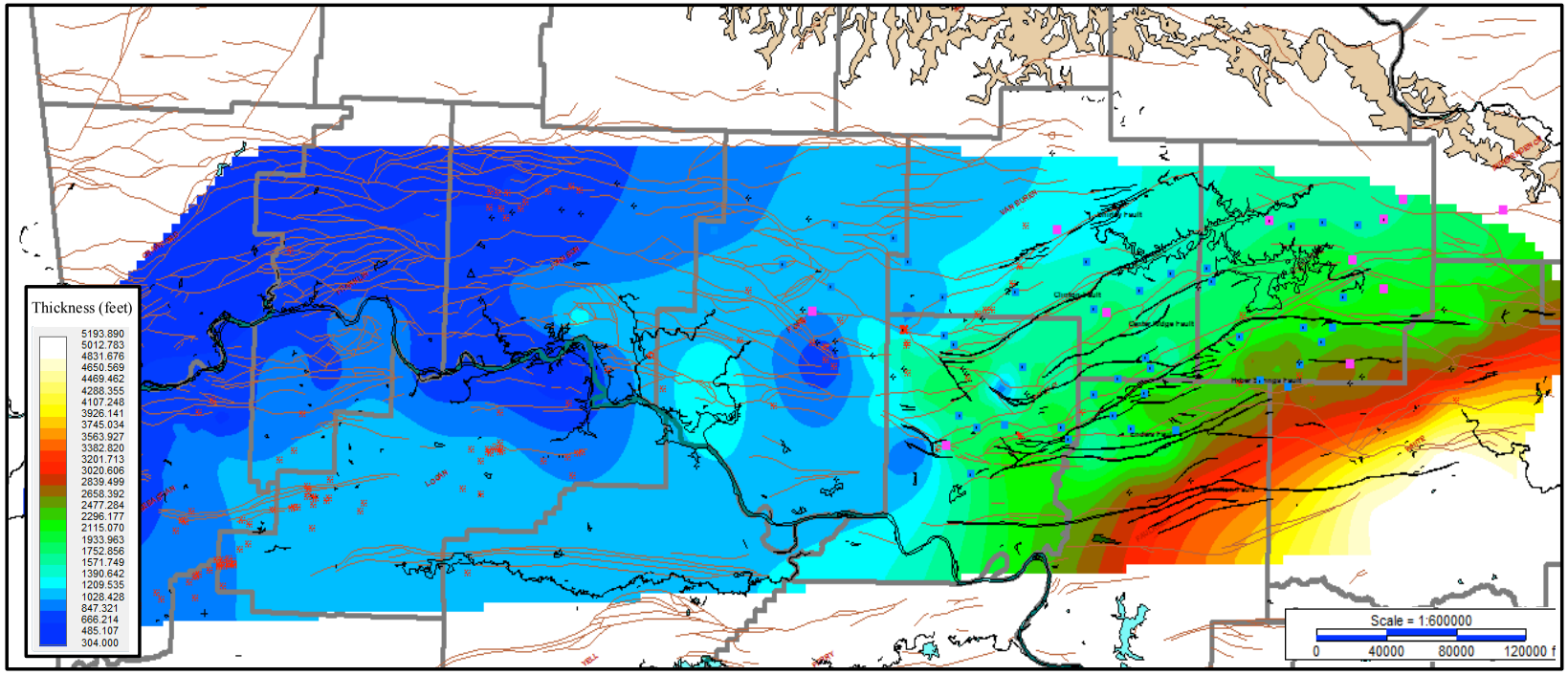

Figure 17: Isochore map of the Morrowan Group (Early Pennsylvanian)

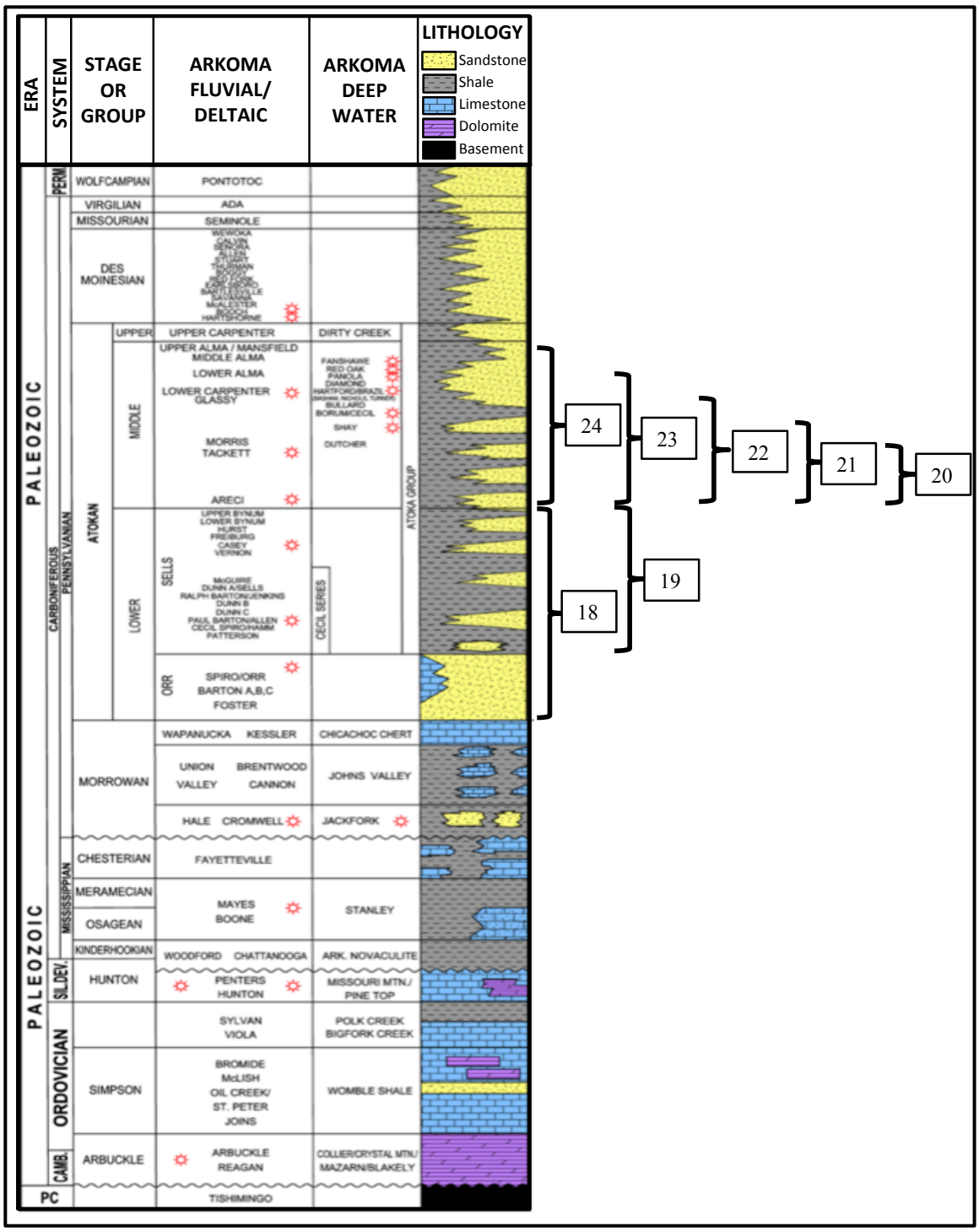

Figure 9 (modified): General stratigraphic section of the Arkoma Basin. Brackets correspond to their associated figures for each isochore map.

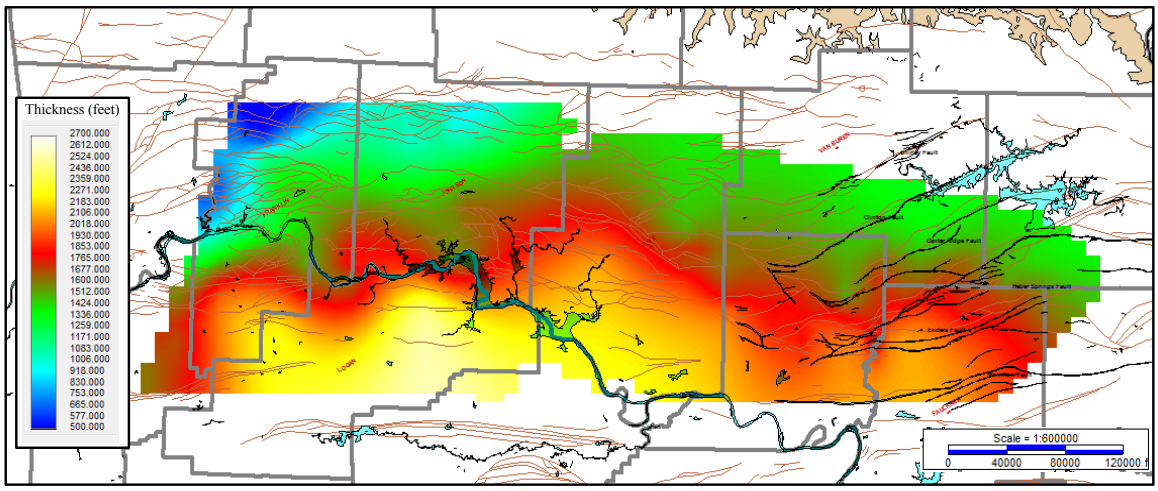

Figure 18: Isochore map of the Lower Atokan Group

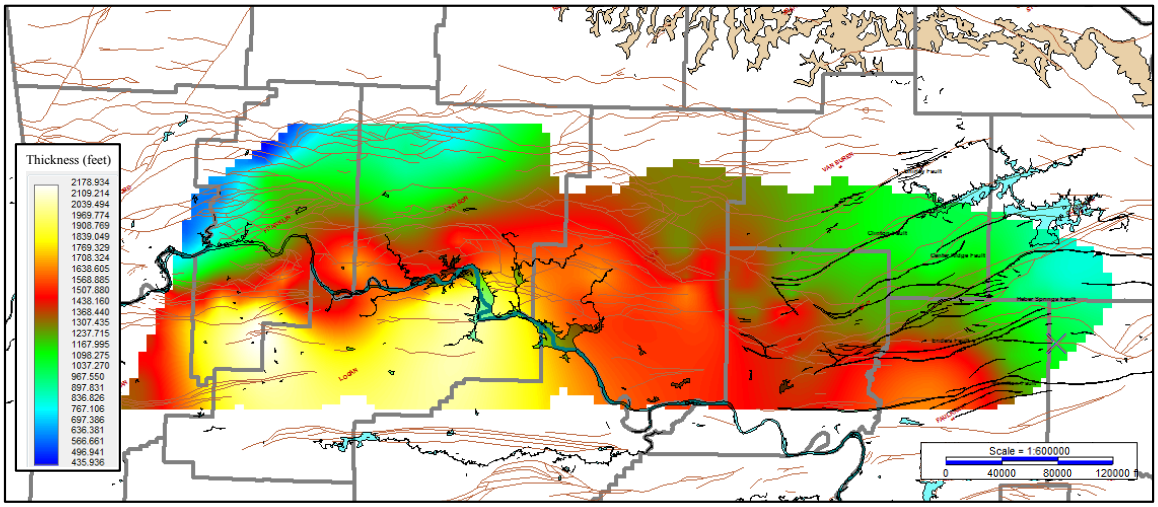

Figure 19: Isochore map of the later Lower Atokan Group

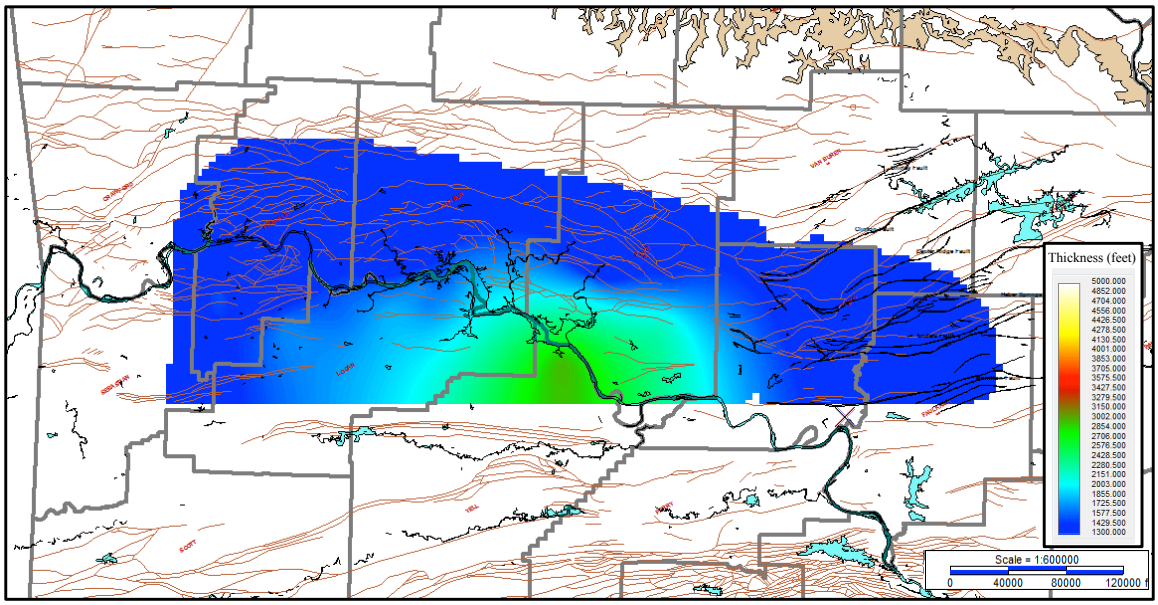

Figure 20: Isochore map of the Tackett to Bynum Formations

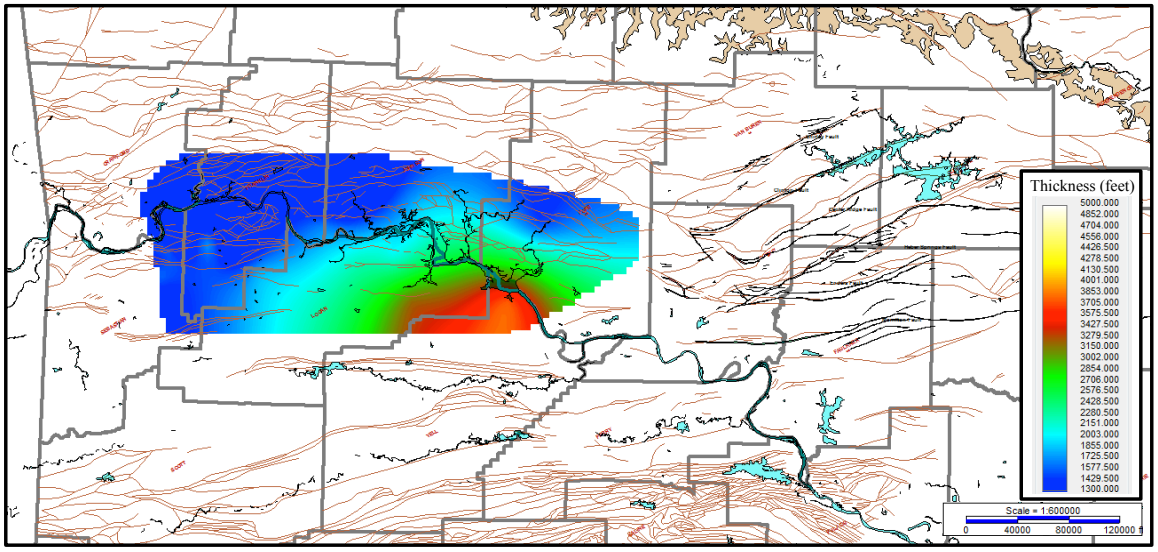

Figure 21: Isochore map of the Morris to Bynum Formations

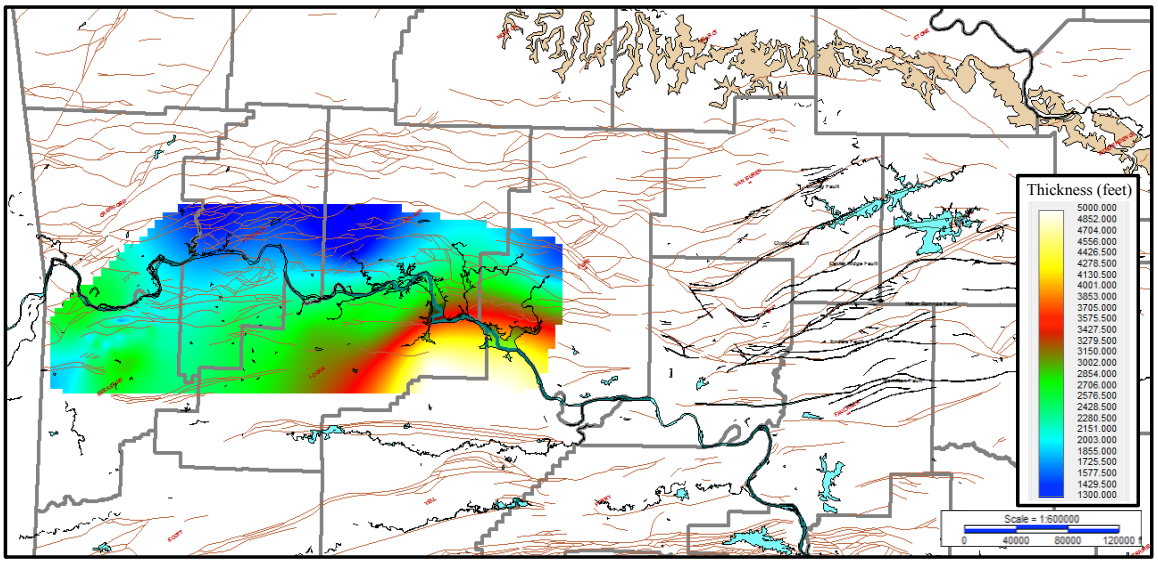

Figure 22: Isochore map of the Carpenter to Bynum Formations

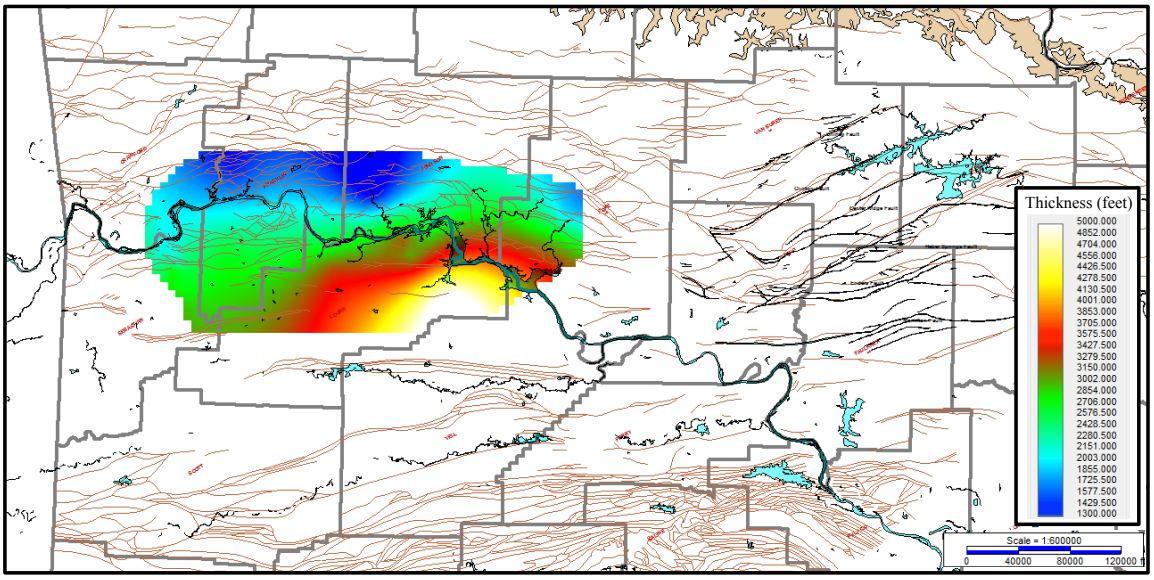

Figure 23: Isochore map of the Lower Alma to Bynum Formations

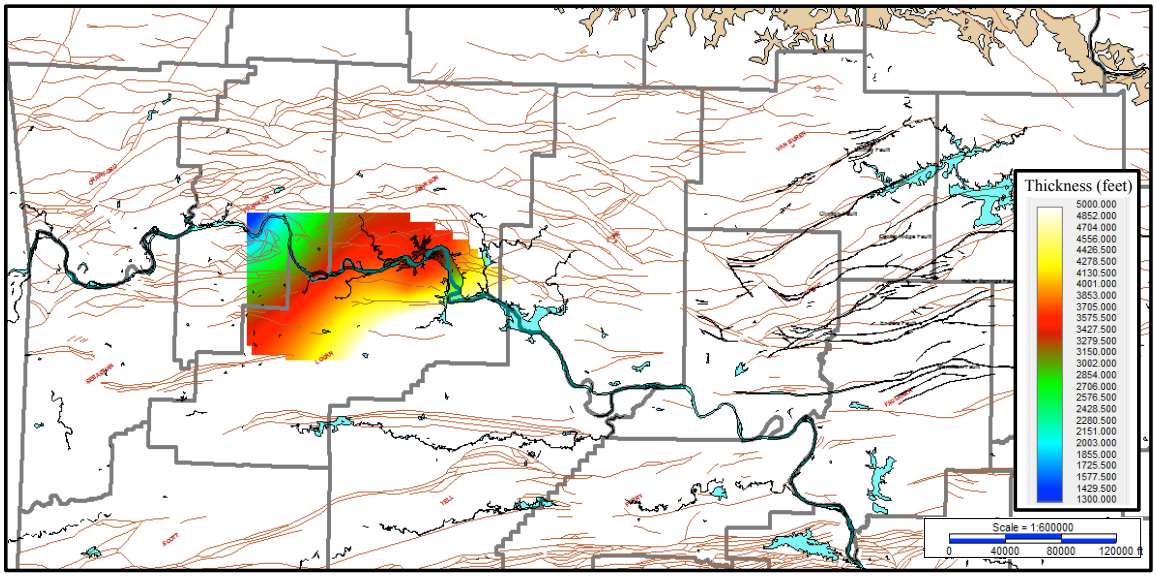

Figure 24: Isochore map of the Alma to Bynum Formations

4.3 PetroMod Basin Modeling

Vitrinite reflectance measurement data were available for all 50 wells in the study. Each well underwent an extensive analysis and numerous simulations were required before arriving at agreeable output models. Rather than presenting 50 separate well scenarios, results from the 50 models can more effectively be explained by form of a series of cross-sections from stitched 1D models. A case study for an individual well will first be discussed in detail. Results and logic from this case study may be applied to all other wells for which their data and output models reside in the appendix.

Making the connection: heat flow and erosion with measured maturity data

Results from the E.W. Moore Estate #1 well are first presented. The significance for discussion of this well is to compare the results from this study with the measured

vitrinite reflectance data presented by Houseknecht (1992) and the basin modeling results from Byrnes and Lawyer (1999). Models produced in that study used vitrinite reflectance data provided from the 5 wells in Houseknecht (1992) and 110 other undisclosed wells in the Arkoma Basin throughout Arkansas and Oklahoma. The location of the E.W. Moore Estate #1 well is presented in Figure 25. Figure 26a shows the comparison of the best-fit model-predicted vitrinite reflectance with respect to depth with the measured vitrinite reflectance data in Houseknecht (1992). Several simulations were required to fit the predicted projection to the measured values for each model. Input parameters, such as heat flow and erosion, were used to calibrate the model. Only one parameter acted as a variable in each simulation. Initial replication of the depth vs. reflectance profile was attempted by using results from regional maps produced by Byrnes and Lawyer (1999), the vitrinite reflectance measurements from Houseknecht (1992), and stratigraphic tops interpreted from well logs within the Kingdom Software. Selected stratigraphic tops can be seen along the y-axis in the model predicted vitrinite reflectance with respect to depth plots. The well penetrates what is considered deep strata in the basin (Cambrian Arbuckle Dolomite) while also preserving section from foreland basin development in the Middle Atokan. The Middle Atokan – Upper Atokan contact is located at the surface of the well. The measured data generally display a continuous increase in reflectance with depth until nearing strata in the mid-Morrowan. At this point, the sublinear relationship between vitrinite reflectance and depth is interrupted by a dogleg pattern. Below the dogleg, there is a decrease in the slope of the reflectance profile and values no longer adhere to the expected linear relationship between vitrinite reflectance and depth. Houseknecht (1992)

emphasizes that faults or unconformities are not the cause for the change in slope of the vitrinite-reflectance profiles.

By using an assumed near-constant geothermal gradient, their minimum and maximum models report that the estimated total removed overburden for the E. W. Moore #1 well range from 12,000 feet to thicknesses nearing 20,000 feet. Replication of the Byrnes and Lawyer (1999) models first began by using an estimated total removed overburden of 20,000 feet and a heat flow of 53 mW/m^2. The overburden value was taken from Figure 6 in Byrnes and Lawyer (1999) using the ±25% minimum and maximum overburden error range. Results for heat flow were not presented by Byrnes and Lawyer (1999), therefore, initial models in this study kept the value for overburden constant while varying the heat flow to: (1) determine the heat flow needed to achieve the present-day geothermal gradient and (2) observe the different combinations of removed overburden and heat flow that produce similar predicted vitrinite-reflectance profiles. A model that increases the heat flow and decreases the overburden will produce a similar vitrinite-reflectance profile to a model in which the heat flow is decreased and the overburden is increased. The dense well data set in this study provides tight constraints on the different combinations of overburden and heat flow. Each well contains a unique set of vitrinite reflectance and/or AFTA data. Cross-validation of the constraints required by the measured data in multiple wells allows for a greater limitation on possible parameter combinations. Because this study combines previously published thermal-maturity data in the area with firsthand data from SWN, the data set in this study is the most comprehensive data set known to date. Results from the first simulation in the E. W. Moore #1 well using the estimated total removed overburden of 20,000 feet and heat flow

of 53 mW/m^2 exhibit an EASY%Ro projection that is significantly lower than that required by the Houseknecht (1992) measured values (Figure 26b). In addition, the output predicted present-day geothermal gradient generated by using these input parameters is less than the measured geothermal gradient for the area around the well. The output results for the present-day geothermal gradient indicate that a higher input heat-flow value must be used in the models. For the next simulation, overburden was again held constant while the heat flow was adjusted to generate an output present-day geothermal gradient closest to that of the measured data.

Figure 26c displays calibration results where overburden is held constant at 20,000 feet and the heat flow is increased to 57 mW/m^2. The heat flow is constant through time. The output model shows that the EASY%Ro curve has shifted to the right towards the higher vitrinite reflectance measured values. However, the projection still remains slightly lower than the measured data points. Although the projection shows that the input model parameters produce a lower than needed vitrinite reflectance with respect to depth projection, a heat-flow value of 57 mW/m^2 generates an output present-day geothermal gradient that is in agreement with measured present-day geothermal gradient data. This means that a present-day heat flow of 57 mW/m^2 is a sufficient input value for the present-day heat flow in the E. W. Moore #1 well, but the paleo-heat flow must be higher than 57 mW/m^2 in order for the EASY%Ro projection to match measured thermal-maturity data. Similarly, if the overburden were a smaller value, such as 17,000 feet, the input value for the present-day heat flow would still need to be 57 mW/m^2, but the paleo-heat flow would need to be even higher than the paleo-heat flow used for an overburden value of 20,000 feet. A higher heat flow compensates for less overburden.

These same parameters were used on the proximal McLung well. Results were similar to that of the E.W. Moore #1 well, and predicted profiles were still significantly lower than that of the measured values. A heat flow of 57 mW/m^2 was used because when coupled with the thermal conductivity calculated by the lithological section within PetroMod1D, a present-day geothermal gradient is generated to that similar of the geothermal gradient in the area (28-29 °C/km).

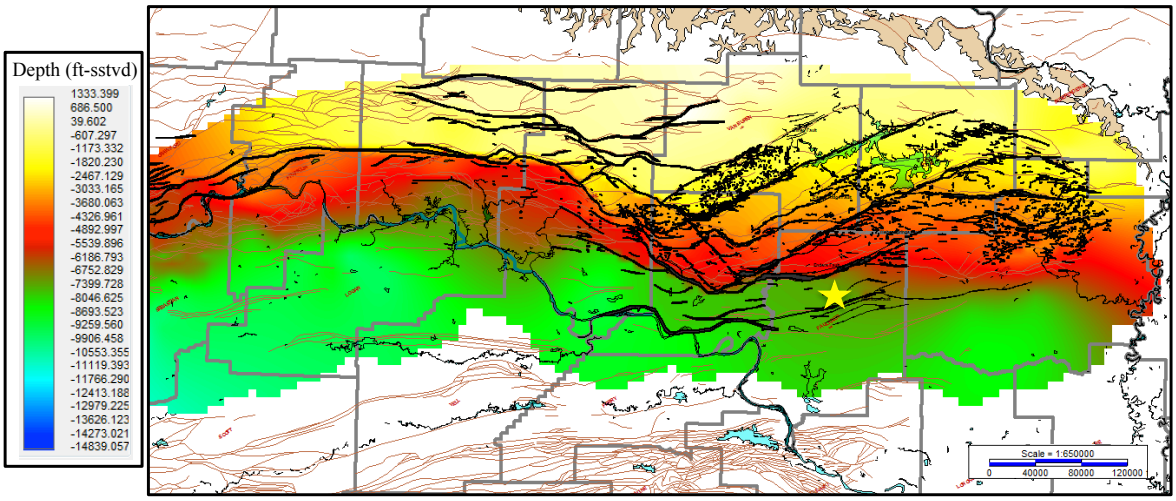

Figure 25: Structure map of the top Mississippian. Yellow star represents the location of the E. W. Moore #1 well.

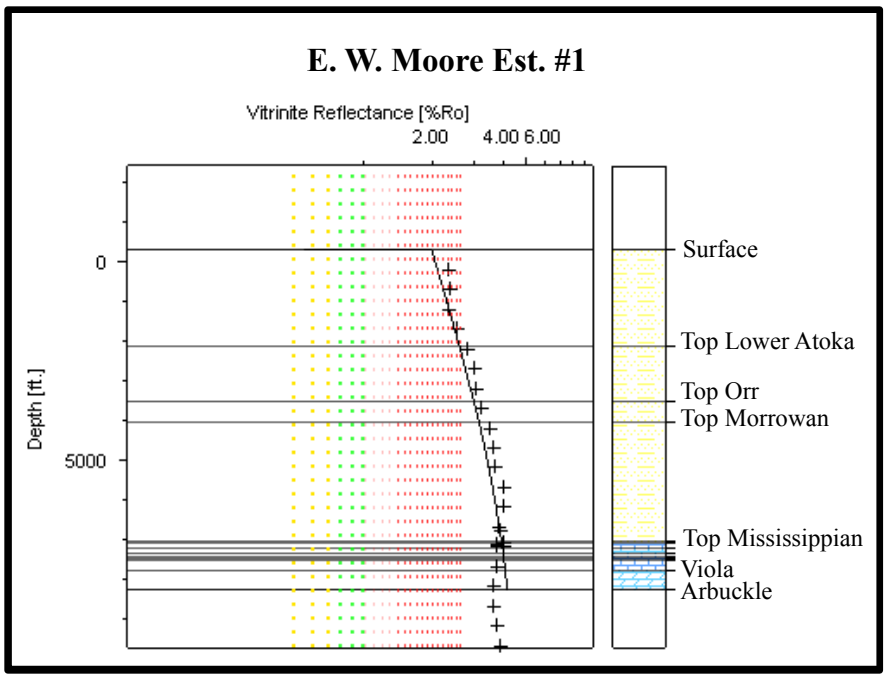

Figure 26a: Model best-fit predicted vitrinite reflectance with respect to depth for the E. W. Moore #1 well. Black crosses are measured reflectance values. Erosion is 19,800 feet. Heat flow is variable. Heat flow is 60 mW/m^2 from time of deposition until around 310 Ma. From 310 Ma to present day, the heat flow is decreasing linearly from 60 mW/m^2 to 57 mW/m^2. Stippled colored areas denote the zones of hydrocarbon generation and destruction (hydrocarbon windows), expressed in terms of vitrinite reflectance (%Ro): 0.5-0.7, early mature (oil); 0.7-1.0, mid-mature (oil); 1.0-1.3, late mature (oil); 1.3-2.6, main gas generation. Modeled stratigraphic units (Table 1) are specified to the right of the reflectance plot.

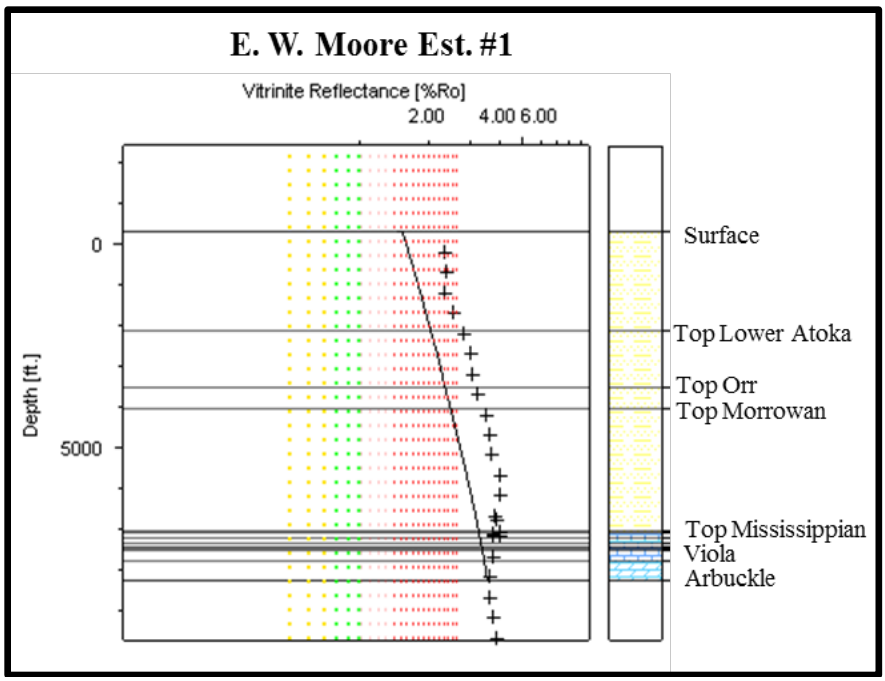

Figure 26b: First attempt model-predicted vitrinite reflectance with respect to depth for the E. W. Moore #1 well. Erosion is held constant at 20,000 feet. Heat flow is held constant through time with a value of 53 mW/m^2. Stippled colored areas denote the zones of hydrocarbon generation and destruction (hydrocarbon windows), expressed in terms of vitrinite reflectance (%Ro): 0.5-0.7, early mature (oil); 0.7-1.0, mid-mature (oil); 1.0-1.3, late mature (oil); 1.3-2.6, main gas generation. Modeled stratigraphic units (Table 1) are specified to the right of the reflectance plot.

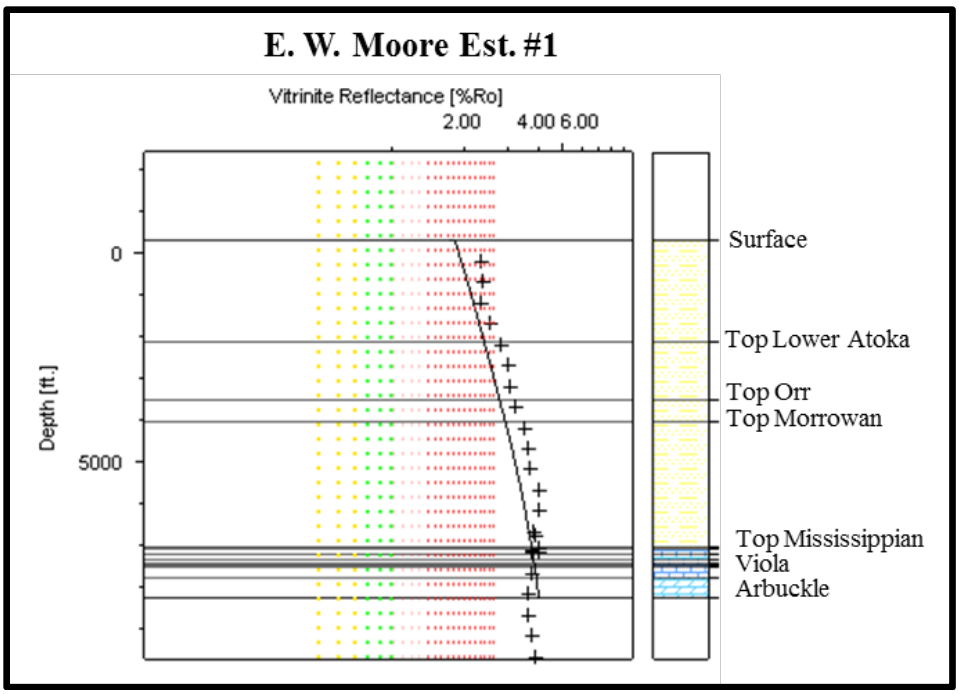

Figure 26c: Second attempt model-predicted vitrinite reflectance with respect to depth for the E. W. Moore #1 well. Erosion is held constant at 20,000 feet. Heat flow is held constant at 57 mW/m^2. Stippled colored areas denote the zones of hydrocarbon generation and destruction (hydrocarbon windows), expressed in terms of vitrinite reflectance (%Ro): 0.5-0.7, early mature (oil); 0.7-1.0, mid-mature (oil); 1.0-1.3, late mature (oil); 1.3-2.6, main gas generation. Modeled stratigraphic units (Table 1) are specified to the right of the reflectance plot.

Models that used a constant present-day heat flow with input erosion values within 1,000 feet of the estimations provided by the results of Byrnes and Lawyer (1999) consistently generated predicted reflectance values lower than that of the needed measured values. Byrnes and Lawyer hold their geothermal gradient constant through time, but there is no mention of the specific constraints placed on heat flow. The best fit predicted vitrinite reflectance with respect to depth profile for the E.W. Moore #1 well was achieved with a paleo-heat flow higher than that used for present day. A heat flow of 60 mW/m^2 was used as an input parameter from the time of the earliest modeled

stratigraphic top until 310 Ma during the Lower Atokan (Figure 26a). The heat flow was then lowered at a constant rate through time until reaching a present-day heat flow of 57 mW/m^2. The primary tectonic activity since the formation of the Arkoma foreland basin in the Pennsylvanian has been uplift and erosion. For this reason, the most significant change in heat flow was chosen to occur at the time of collision. Although igneous activity existed east of the Arkoma Basin in the Mississippi Embayment during the Cretaceous, AFTA data provide evidence that the thermal history of the Arkoma Basin was not affected.

A total of 19,800 feet of eroded overburden was needed to fit measured vitrinite reflectance and AFTA data: 13,500 feet of burial occurred from 306 Ma to 280 Ma followed by an additional 6,300 feet of burial from 280 Ma to 244 Ma. Burial curves for foreland basins are classically thought to accelerate with time, as reflected by their convex-up shape (Xie and Heller, 2009; Sinclair and Naylor, 2012). Accelerations in the curve are common indicators of the onset of orogenesis and the formation of the foreland basin (Sinclair and Naylor, 2012). The rapid, accelerating subsidence histories of pro-foreland basins are short-lived and are generally less than 40 million years in duration (Sinclair and Naylor, 2012). As time progresses, the redistribution of sediment due to the migration of the thrust load results in a flattening basin geometry (Xie and Heller, 2009). The duration of rapid initial subsidence seen in the models in this study are generally 20 to 25 million years. A slower rate of burial extends until the end of the Paleozoic. Burial curves in this study show similar geometries to the foreland basin subsidence curves within Figure 6 of Xie and Heller (2009). The combination of measured maximum paleotemperatures from the vitrinite reflectance data with the cooling parameters set by

the AFTA data generate a possible burial history model solution that involves sediment uplift exhibiting a stair-stepping geometry (Figures 27 and 28). The estimated amount of eroded overburden for this well is in agreement with surrounding wells that also have independent measured vitrinite reflectance and AFTA data.

Heat-flow values are also constrained by literature described in Chapter 3 as well as by calibration with the present-day geothermal gradient. Figure 29 compares the model predicted temperature and maximum temperatures with respect to time for the E.W. Moore #1 well. The heat flow, amount of eroded overburden, and timing of the erosion were all adjusted until requirements for AFTA and vitrinite reflectance data are met. Sweeney and Burnham (1990) overlays were displayed on burial history models after all models were calibrated. In the case of the E.W. Moore well (Figure 27), all rocks in the present-day stratigraphic section entered the early mature phase of oil generation around the early Permian (~285 Ma). Oil generation was short lived and strata existing in the present day hit the oil floor by the middle of the Permian (~265 Ma) as a result of continued burial. By the end of the Permian, maximum paleotemperatures had been reached and nearly all present-day strata were within the dry gas window. In PetroMod1D, the two separate yet continuous burial events must exist in order for a stair-stepping uplift movement to be modeled. Although the same vitrinite reflectance values can be achieved by simply eroding rocks at a constant rate through time, AFTA restraints would not be met. However, although the temperature constraints are now within the bounds required by the AFTA data during uplift, the presence of the two main burial events actually further complicate the timing of thermal maturity. In E.W. Moore #1, a steep initial burial curve outpaces the changing temperature of the deepening strata. This

temperature lag results in delayed thermal maturity. When burial rate begins to slow at 280 Ma, the temperature is again able to begin catching up with increasing depth. Although there are no unique solutions for the amount of erosion, the timing of the erosion, and the input heat flow, improving the accuracy of thermal reconstruction for individual wells can be considerably achieved with abundant well log and calibration data. Furthermore, slight adjustments in these required parameters to fit a geologically rational and sound framework will in turn produce an even more coherent regional model.

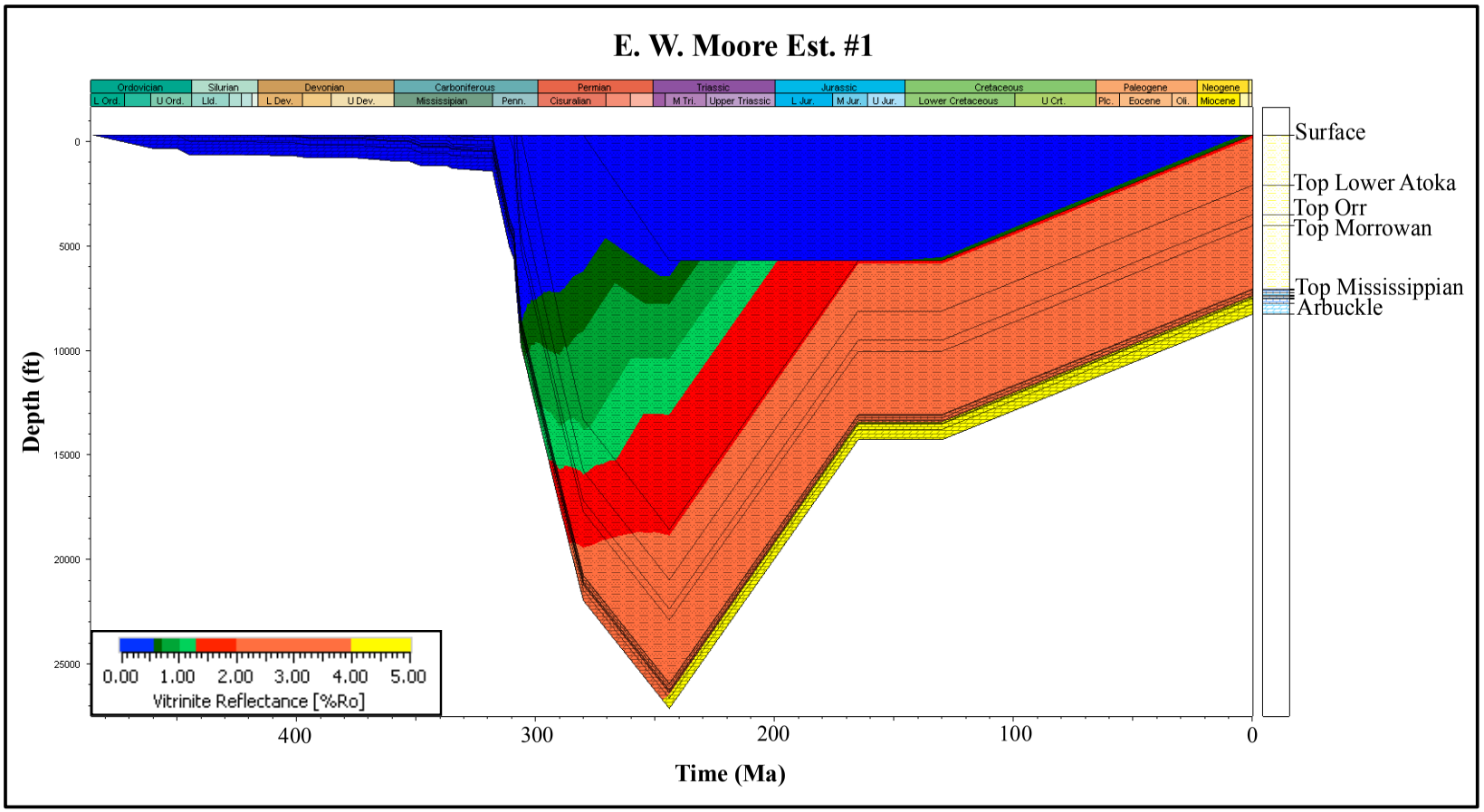

Figure 27: Sweeney and Burnham (1990) EASY%Ro projection on the calibrated 1D burial history model for E. W. Moore #1. Colored areas denote the zones of hydrocarbon generation and destruction (hydrocarbon windows), expressed in terms of vitrinite reflectance (%Ro): 0.5-0.7, early mature (oil); 0.7-1.0, mid-mature (oil); 1.0-1.3, late mature (oil); 1.3-2.0, overmature for oil, thermal cracking to gas; 2.0-4.0, dry gas; 4.0-5.0, upper limit of dry-gas preservation.

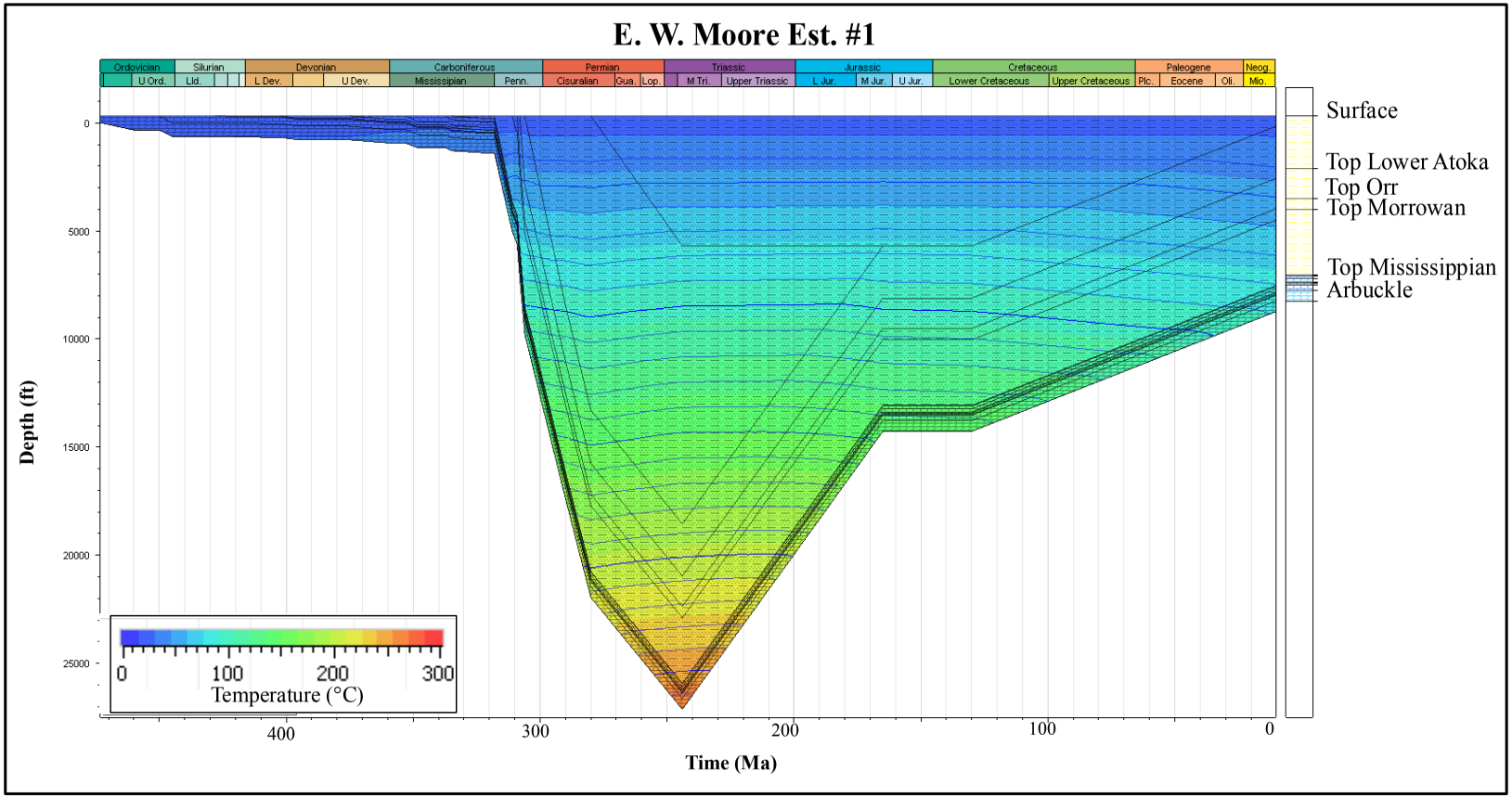

Figure 28: Temperature overlay on the calibrated 1D burial history model for the E. W. Moore #1 well.

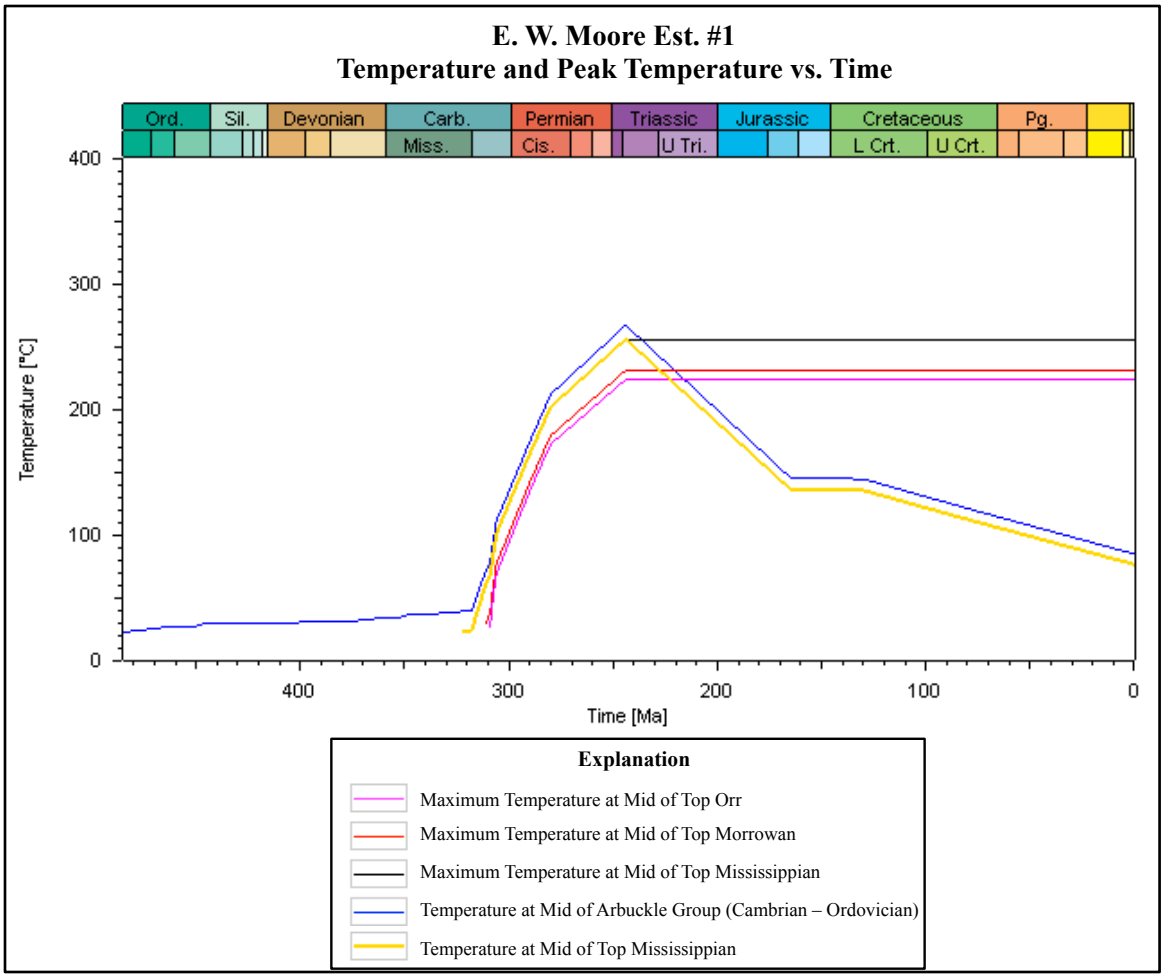

Figure 29: Model predicted temperature with respect to time for the E. W. Moore #1 well.

All output models discussed in the E.W. Moore #1 example were also generated for the other 49 wells. The data for these wells reside in the appendix. A regional comparison of model predicted thermal maturity can be seen in Figures 30a and 30b. Line B-B' consists of 10 different burial history output models that are overlain by well-specific calibrated Sweeney and Burnham (1990) thermal maturity projections. Vertical slices in line B-B' represent the burial history during the last 10 million years in a particular well. Although modeled as much more complex, stratigraphic divisions in this

display have been simplified into five main units. Lateral changes in unit thickness, thermal maturity, and depth can be observed from the cross-section. The northwest to southeast crossline, B-B', traverses the NE/SW-trending normal fault configuration. A comparison of model and measured vitrinite reflectance with respect to depth plots can be seen in Figure 31a. It can be observed that some of the measured values have slopes considerably steeper than what is allowed by the projection of Sweeney and Burnham (1990). As this might be a result of error in depth measurement from cutting groupings, calibrated vitrinite reflectance curves were adjusted to fit the upper half of the measured values.

Wells along line B-B' are shown hanging at their appropriate subsea true vertical depths. The datum for sea level has been moved above the vertical sections for visualization purposes. Well spacing is set at an equal distance between the wells. The stratigraphic units correlated in this cross-section are deepening to the southeast as they traverse the NE/SW-striking down-to-the-south normal fault configuration. In the direction of B to B', the thermal maturity patterns for the Lower Atoka and Morrowan Groups show an increase in thermal maturity with respect to depth. The greatest change in thermal maturity occurs between wells 3 and 4. The predicted and measured vitrinite reflectance values can be compared in Figure 31. Measured values in Brown are significantly lower (Ro% ~1.65) than those in the Thomas well (Ro% ~2.2%). The two wells are less than three miles apart, the thickness of their Morrowan section is relatively similar, and their present-day depths are comparable. It is highly unlikely that the Thomas well was brought to depths hundreds of feet deeper than the Brown well and uplifted again to match the present-day depth of the Brown well. An unrealistic amount

of overburden would need to have been removed from the Thomas well. Thermal maturities from neighboring wells are most comparable to that of the Thomas well. Therefore, it is not assumed that any anomalous thermal activity has produced the drastic contrast in vitrinite reflectance values between these two wells. Low thermal-maturity values in the Brown well may be a result of laboratory measurement error, but could also be attributed to an increase in the thermal conductivity of the overburden rock. Figure 31b displays how the geometry of an EASY%Ro projection is affected by an increase in thermal conductivity. In Figure 31b, the thermal conductivity for the entire Morrowan Group was significantly increased. The result is a shift to the right on the vitrinite reflectance with respect to depth profile. In other words, higher vitrinite reflectance values are assigned to shallower rocks without having to change the heat flow or overburden. This change can be compared to the best-fit projection in Figure 26a. However, the lithological and organic characteristics used to generate the models were selected to fit actual measured wellbore data. No other thermal anomalies are seen in the cross section. Expected relationships between depth and thermal maturity are evident.

Vitrinite reflectance values at the surface of Line B-B' increase from northwest to southeast. As the formation tops within Line B-B' deepen to the southeast, younger strata exist at the surface toward B'. Higher reflectance values of younger strata exist at equal present-day depths of older strata in the northwest. The increase in thermal maturity from B to B' is evidence that wells in the southeast were subjected to higher temperatures and hence greater overburden that was subsequently removed.

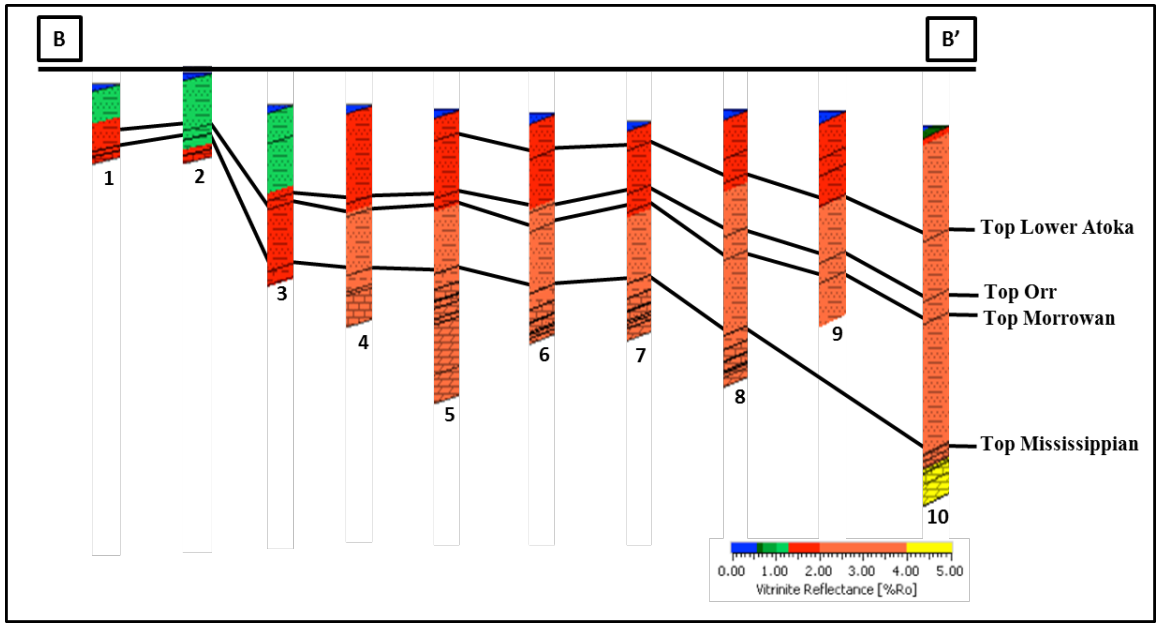

Figure 30a: Cross section from B – B' of 1D burial history output models with the Sweeney and Burnham (1990) overlay. Corresponding well locations are identified in Figure 30b.

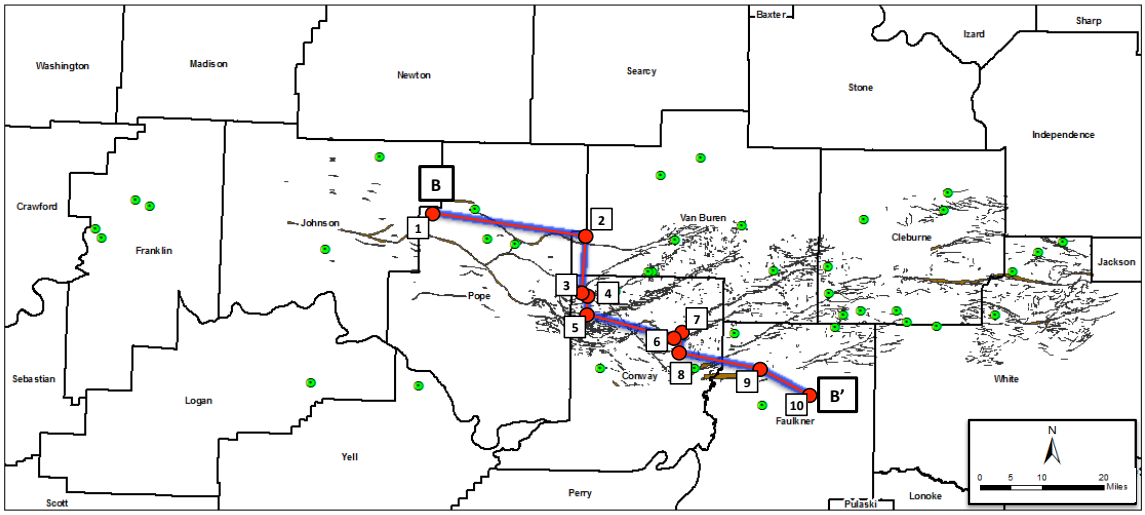

Figure 30b: Location of wells used in the cross section B – B'. Wells are denoted by red circles.

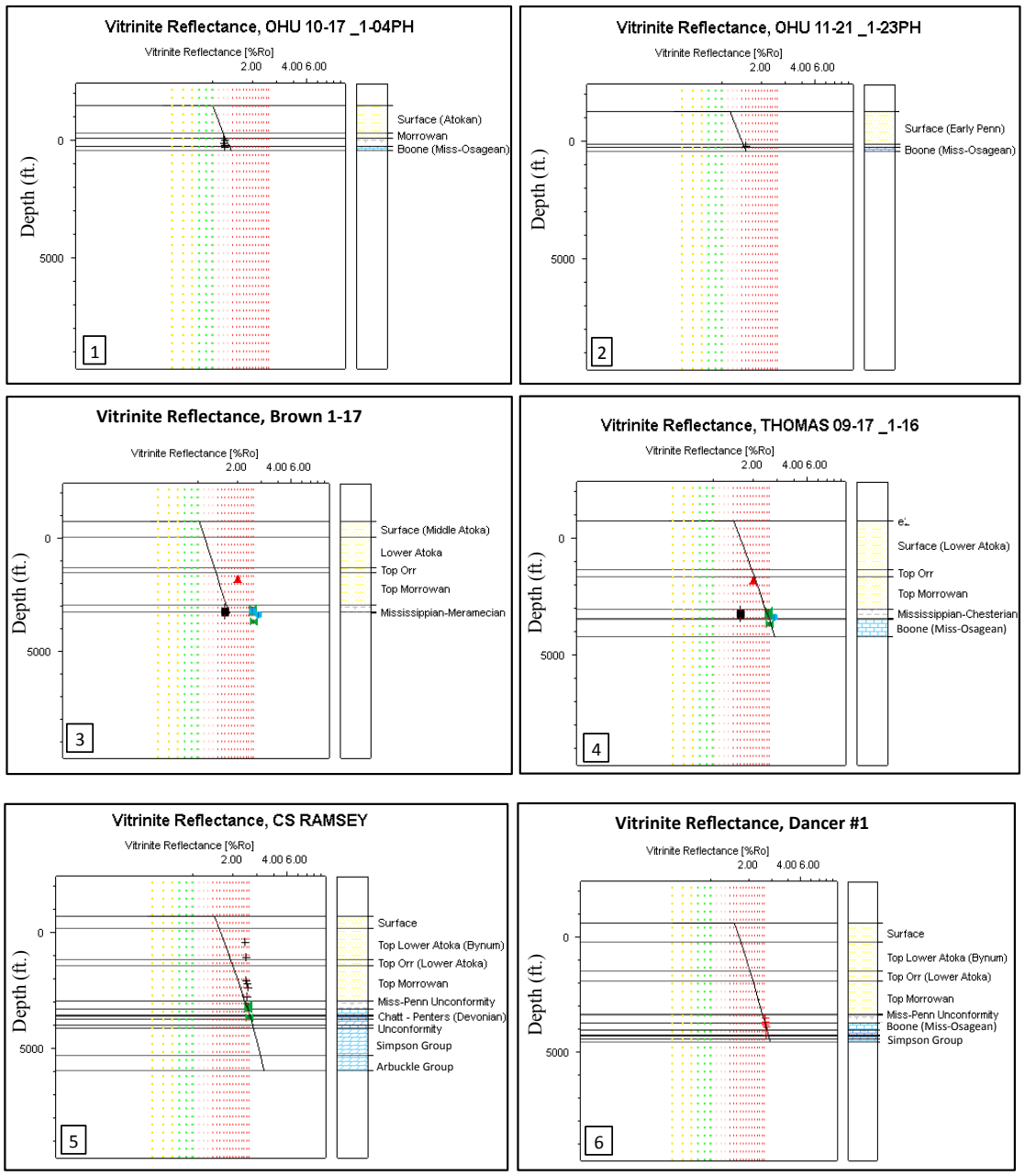

Figure 31a: See following page for explanation.

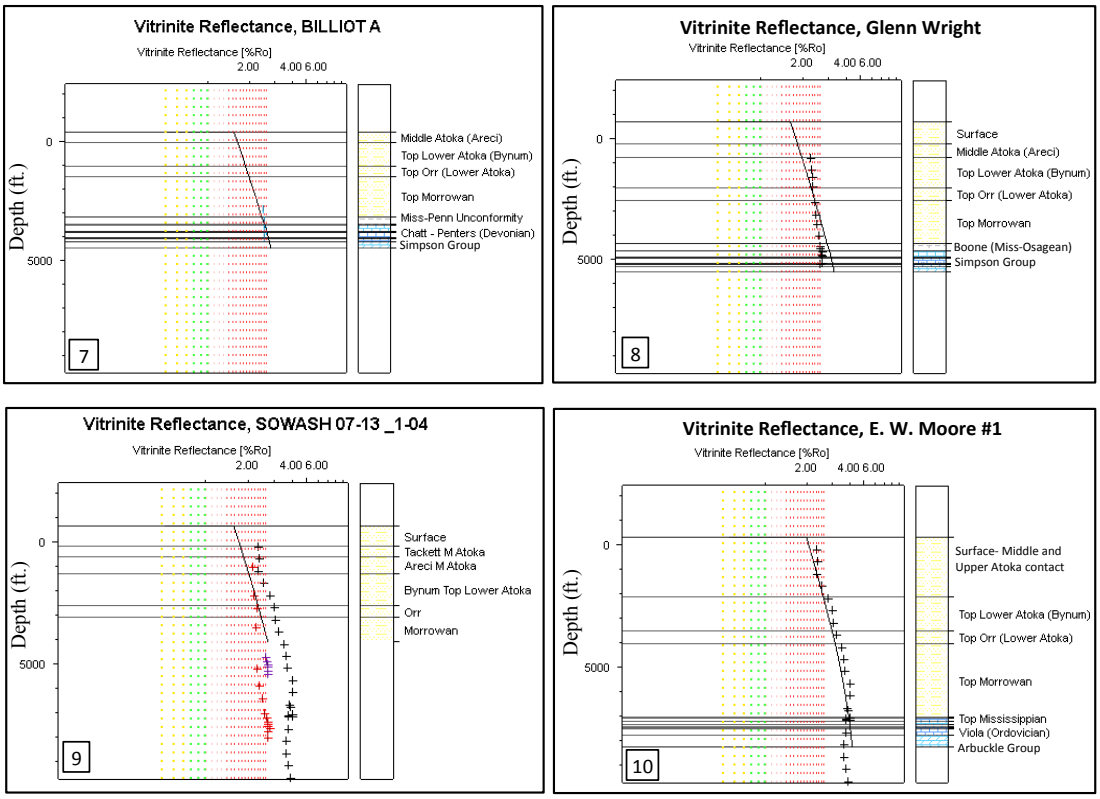

Figure 31a: Model predicted vitrinite reflectance with respect to depth profiles for wells along Line B – B'. Well locations for profiles 1-10 are indicated in Figure 30b. Plotted points represent measured values. Multiple symbols display measured data from proximal wells that were used as comparison for calibration. Stippled colored areas denote the zones of hydrocarbon generation and destruction (hydrocarbon windows), expressed in terms of vitrinite reflectance (%Ro): 0.5-0.7, early mature (oil); 0.7-1.0, mid-mature (oil); 1.0-1.3, late mature (oil); 1.3-2.6, main gas generation. Modeled stratigraphic units (Table 1) are specified to the right of the reflectance plot.

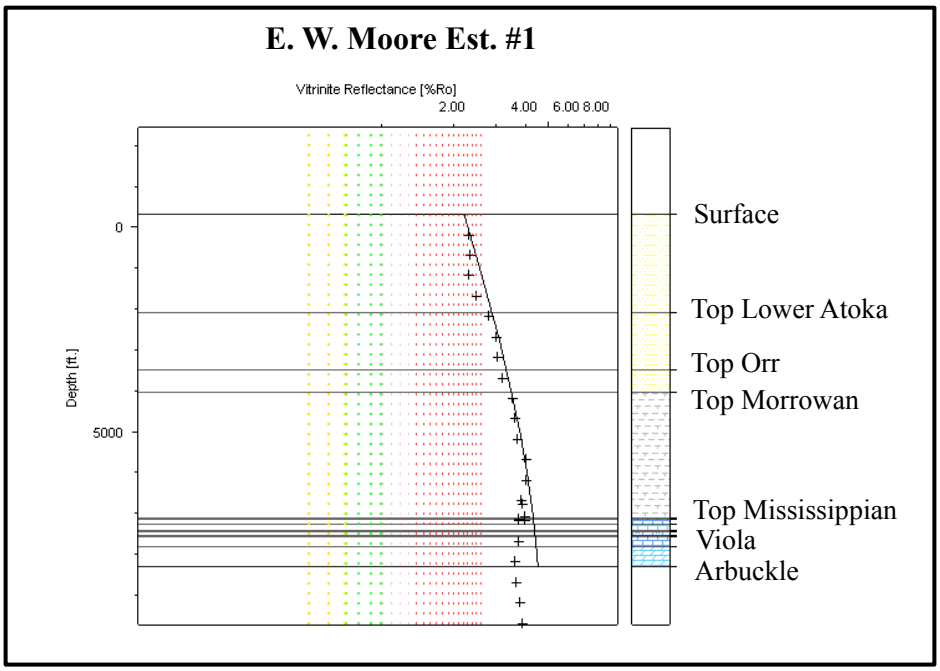

Figure 31b: Model-predicted vitrinite reflectance with respect to depth for the E. W. Moore Est. #1 well. Thermal conductivity is increased for the entire Morrowan Group. An increase in the EASY%Ro curve is observed. Stippled colored areas denote the zones of hydrocarbon generation and destruction (hydrocarbon windows), expressed in terms of vitrinite reflectance (%Ro): 0.5-0.7, early mature (oil); 0.7-1.0, mid-mature (oil); 1.0-1.3, late mature (oil); 1.3-2.6, main gas generation. Modeled stratigraphic units (Table 1) are specified to the right of the reflectance plot.

Line C-C' extends from the western portion of the Arkoma Basin near Oklahoma, into the central southern area, and further into the eastern portion of the basin (Figure 32b. The expected depth versus vitrinite reflectance patterns present throughout the cross section (Figure 32a). Variations in thermal maturity within separate stratigraphic units are consistent with depth, and no obvious thermal anomalies are evident. As evidence from the shallowing of formation tops, strata at the present-day surface increases in age from west to east. The greatest burial depths are seen in wells 3 and 4. The youngest formation top pictured in this cross section, Top Lower Atoka, remains at the greatest present-day burial depth in these wells and also exhibits the highest vitrinite reflectance values. The

surface reflectance values for wells 3 and 4 are also higher than all other wells in the section. Therefore, wells 3 and 4 were subjected to higher temperatures and greater burial depths, and subsequently more erosion and uplift than the other wells in the cross section. The relationship between erosion, heat flow, and thermal maturity from west to east along Line C-C' demonstrate that increasing maturation from west to east across the basin is primarily the result of increasing overburden and consequential erosion (Figures 33 and 34). The results are in agreement with Byrnes and Lawyer (1999).

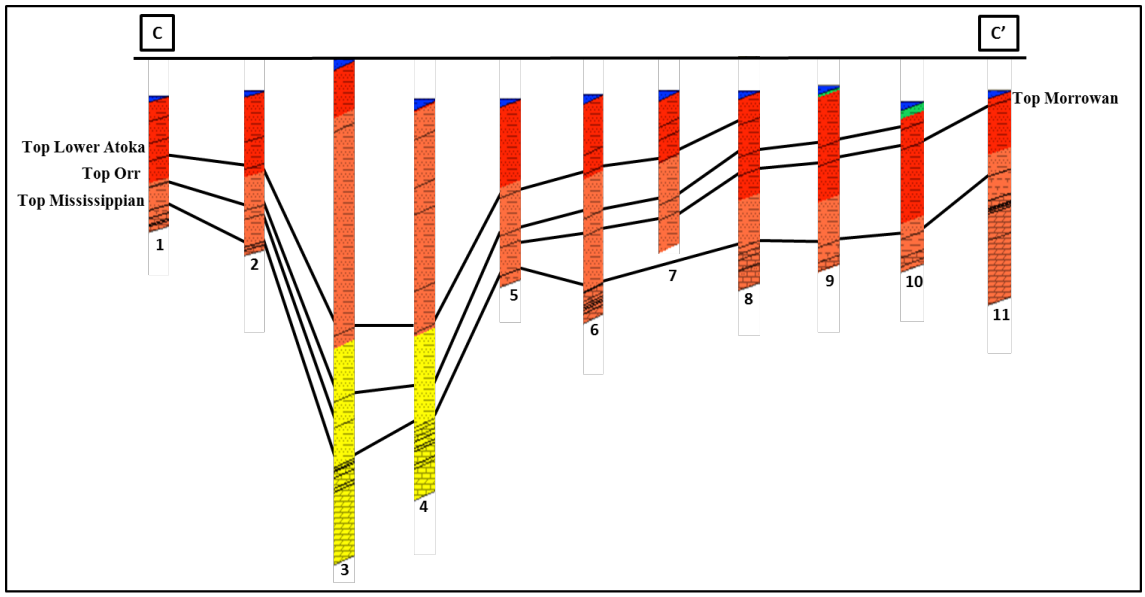

Figure 32a: Cross section from C – C' of 1D burial history output models with the Sweeney and Burnham (1990) overlay. Corresponding well locations are identified in Figure 32b.

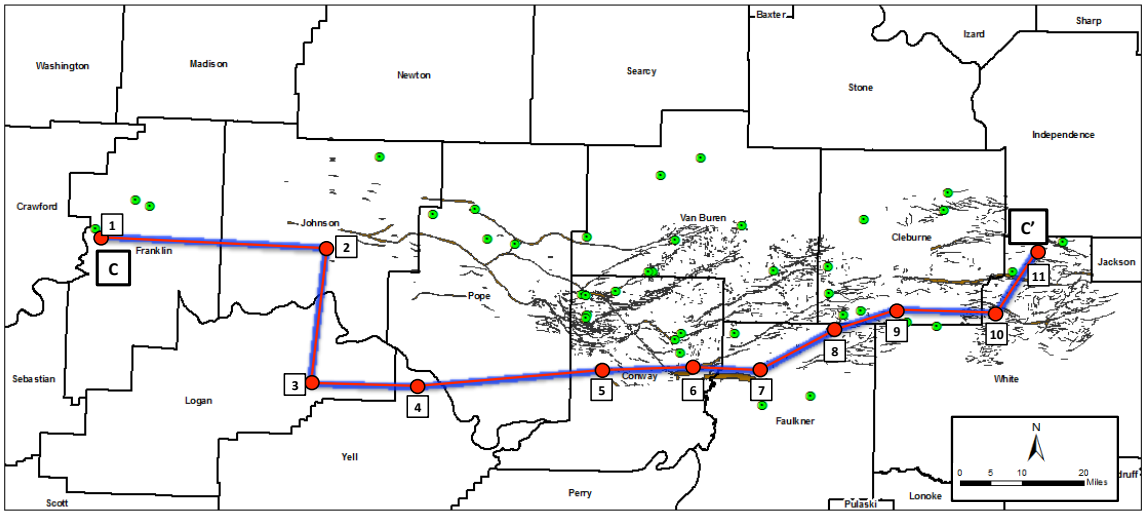

Figure 32b: Location of wells used in the cross section C – C'. Wells are denoted by red circles.

A regional map of the total removed overburden was constructed from the estimates provided by relative uplift analysis, vitrinite reflectance, and stratigraphic projection (Figure 33). The amount of eroded overburden reaches thicknesses of nearly 19,000 feet in the southernmost portion of the Arkoma Basin. Modeled erosion decreases to the north, with estimated thickness approaching 11,000 feet. Trends generally follow those made from previous publications. Thickness proportions of the two key burial events were carefully selected. Simulation shows that the prediction of modeled vitrinite reflectance values is highly dependent on initial timing and burial depths. Once initial thicknesses and heat-flow values were established and in agreement with measured vitrinite reflectance and AFTA data, the selection of input parameters for other wells in the region could be forecasted as a function of relative well location in the basin. The paleo-heat flow values needed to achieve a best-fit vitrinite reflectance with respect to

depth profile are shown in Figure 34. Values are as low as 56 mW/m^2 in the south towards the Ouachita Frontal Thrust and they increase to values between 76 and 78 mW/m^2 in the north. The map is in agreement with present-day heat-flow trends from Lee et al. (1996) in which values increased by 20 to 30 mW/m^2 from south to north. The south to north increase is evident in the paleo-heat flow map of Figure 34. However, vitrinite reflectance and AFTA data require that paleo-heat flow be higher than present-day heat flow, therefore, the values shown in Figure 34 are higher than in the present-day map by Lee et al. (1996). Although infrequent, thermal anomalies exist in the paleo-heat flow map. The heat-flow anomalies must exist in order to fit both the vitrinite reflectance and erosional patterns in the neighboring area. As with the E. W. Moore #1 well, heat-flow trends were adjusted to fit the measured thermal-maturity data and the estimated amount of overburden were in agreement with that reported by Byrnes and Lawyer (1999). The map demonstrates that the combination of erosion and heat flow dictate the prediction of measured vitrinite reflectance values. Similar heat-flow values in different areas of the basin do not infer parallel estimates of eroded overburden; the designation of heat flow and overburden are only permitted according to the measured vitrinite reflectance and AFTA data.

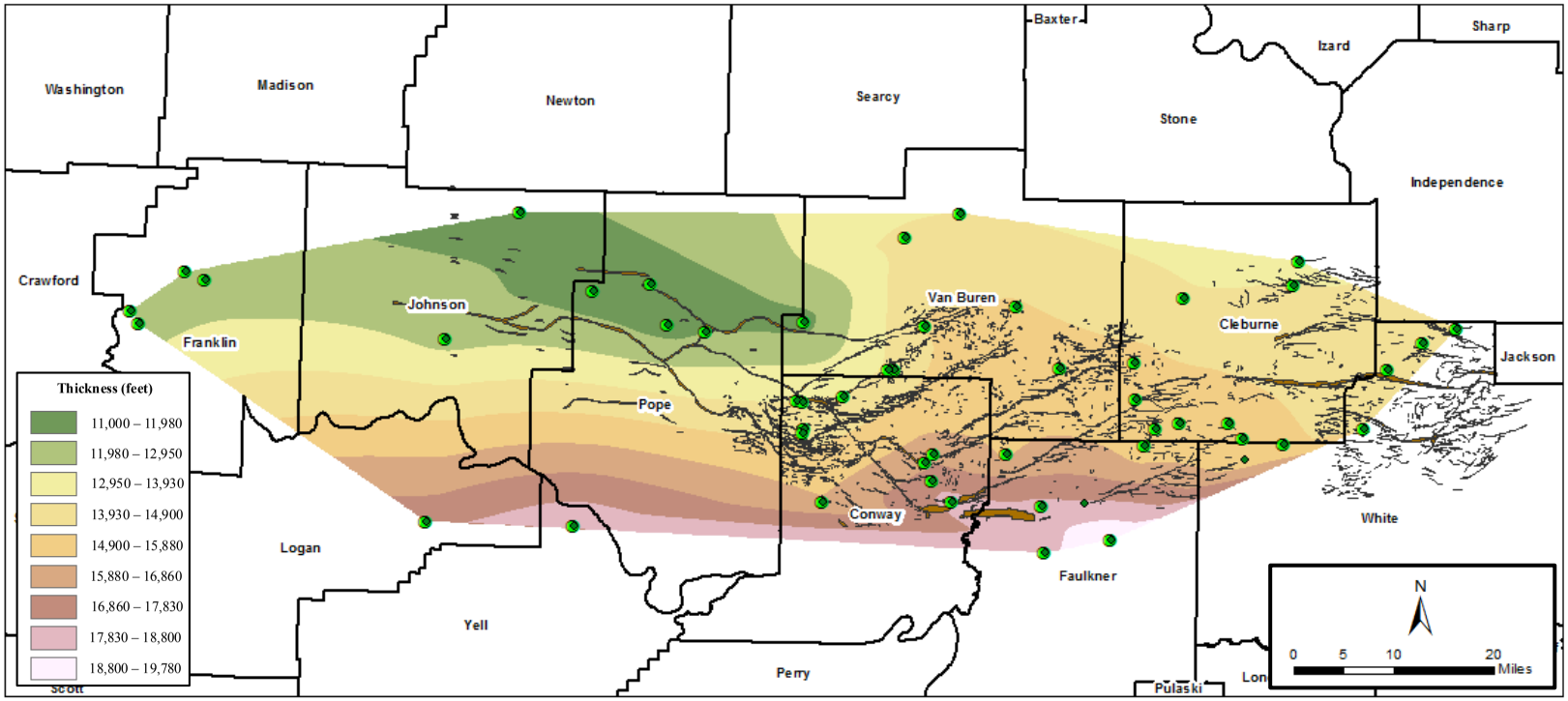

Figure 33: Estimated total removed overburden. Green circles represent the wells in which estimates were calculated.

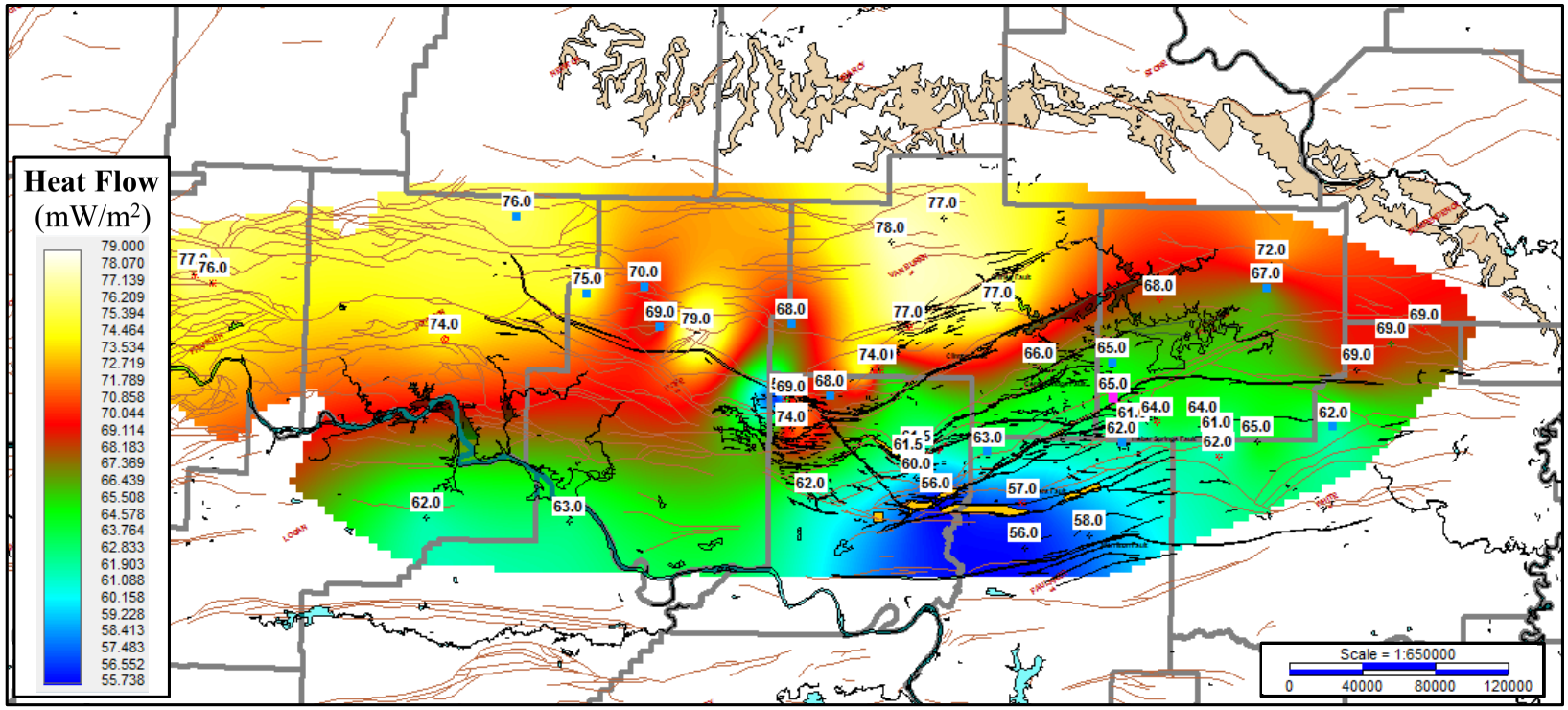

Figure 34: Paleo-heat flow map of the values used to fit thermal maturity data in the 50 basin models.

CHAPTER 5: Discussion

Constraints on heat flow obtained from the vitrinite reflectance and AFTA results indicate that maximum heating involved both elevated basal heat flow and significantly deeper burial on the top-Carboniferous unconformity (now exposed at the present-day ground surface). However, it is not clear from the results whether the time of maximum paleotemperatures (between ~306 Ma and 165 Ma) corresponds with the time of maximum burial. The constrained thermal histories obtained from calibration data show that the peak source rock maturation of the drilled Carboniferous-Ordovician sequence, corresponding to vitrinite reflectance values of ~1.9 to 3.0 (Ro%) (dry gas window to post-mature) at the present-day ground surface, was reached at some time between deposition of the youngest preserved Late Atokan sediment (~306 Ma) and the Middle Jurassic (165 Ma). Previous studies initially attributed the high thermal maturities in the eastern portion of the Arkoma Basin to raised heat flow from Cretaceous igneous activity in the Mississippi Embayment (Byrnes and Lawyer, 1999). However, zircon and AFTA data are consistent thermal maturity remaining unaltered and could not be associated spatially with the Cretaceous plutons, and that maximum thermal exposure occurred in the Late Paleozoic (Desborough et al., 1985; Arne, 1992).

Basinwide late and post-Paleozoic uplift and erosion make it difficult to establish the original thickness and extent of the middle and upper Atokan, Desmoinesian, and Upper Pennsylvanian-Permian sections. Calibration data in conjunction with well log interpretations enable reconstruction and validate the thermal history and subsequently the amount of sediments eroded atop the Paleozoic surface unconformity.

The estimated eroded overburden calculated in this study is within the accepted range established by previous workers and generates a match between predicted and measured maturity. The slope and variance of the %Ro versus depth trend exhibited by the data are consistent with what would be anticipated for increasing maturity with depth trends, assuming the range of present-day geothermal gradients in the region and assuming some variance associated with differences resulting from short- and long-term burial (Byrnes and Lawyer, 1999). Single well analysis is not sufficient enough to draw conclusions regarding overall erosion or heat-flow patterns in the Arkoma Basin. The comprehensive and concentrated data set in this study emphasizes that a rational configuration of present and paleo-heat flows can adequately explain lateral variations in thermal maturity. Variance in the thermal maturity for wells that do not fit the surrounding geologic framework may be attributed to laboratory error in the measurement of vitrinite reflectance.

Former studies estimate the amount of uplift and erosion ranging from 5,000 to 20,000 feet. Present and paleo-heat flow values and geothermal gradients are justified by Lee et al. (1996) and by the aid of present-day geothermal gradient mapping from 229 corrected bottom-hole temperatures. Many basin modeling studies in other basins have been able to calibrate their thermal and burial history models by using a constant heat flow through time. However, the notably high degree of thermal maturation within the Arkoma Basin has been identified by several previous researchers (Houseknecht, 1986; Byrnes and Lawyer, 1999). The models in this study were first run using a constant present-day heat flow to arrive at measured calibration values. This study found that using a constant heat flow through time results in a high, geologically unreasonable

amount of overburden needed to meet vitrinite reflectance and apatite fission track analysis values.

The results from this study utilize the most comprehensive set of thermal maturation data to date. On an average, estimated eroded overburden was in a difference of 1,000 to 3,000 feet from previous basin models created (Byrnes and Lawyer, 1999). The overall trend of erosion is in good agreement with previous models. This study established a consistent and coherent basinwide method for arrival at measured calibration values; the structure and isochore maps created in this study acted as aids to the timing of depocenter migration, and therefore could be used to place timing constraints on heat-flow values. For modeled %Ro values to successfully match measured %Ro values in models involving increasing estimates of removed overburden, it is necessary to either decrease the geothermal gradient/heat flow or assume earlier erosion through time. However, some amounts of estimated erosion yielded improbable heat-flow values that were too high or low for the areas where measured geochemical data were available. Because measured data were provided for every well, error in thermal maturity measurements could be more readily identified. On the other hand, abundant calibration data require numerous simulations and complex modeling to fit restrictions required by the measured data.

CHAPTER 6: Conclusions

Fifty 1D basin models were generated to estimate the burial and thermal histories of the Arkansas portion of the Arkoma Basin. Nine supplemental geological maps were

interpolated from an extensive well data set. The tectonically significant stratigraphic units chosen for structure and isochore mapping illustrate the depositional evolution within the Arkoma Basin as it exists at first as a stable shelf environment on a passive margin and then through its transition into a fully-formed foreland basin. The isochore maps exhibit relationships between tectonic history and relative location and orientation of focused deposition throughout time. As the effects of far-field subduction from the approaching tectonic load are felt around the transition from Late Mississippian into Early Pennsylvanian, stratigraphic thicknesses mimic the geometry of the downwarping subducting plate. Migration of the basin depocenter from east to west is clearly displayed in the Atokan Series by changes in the orientation and location of deposition in the basin. Conclusions made from the isochore maps relating the timing of rapid burial with the east to west migration of the downwarping south-dipping subducting plate were used to refine the input parameters for the basin models. AFTA and vitrinite reflectance data provided time-temperature calibration requirements. A geologically agreeable tectonic history was reconstructed for the basin by careful adjustment and balance of paleo-heat flow values, timing and stratigraphic thicknesses during main foreland basin formation, and the relative timing/magnitude of uplift throughout the present day. Input parameters for an individual well were chosen with high regard to the constraints required by nearby wells. Structure maps and calibrated Sweeney & Burnham (1990) EASY%Ro output burial history models indicate that patterns of increasing thermal maturity generally reflect those of increasing depth and erosion. Although some anomalous thermal-maturity values do exist, a rational configuration of present and paleo-heat flows can adequately explain lateral variations in thermal maturity.

REFERENCES

Amsden, T.W., 1980, Hunton Group (Late Ordovician, Silurian and Early Devonian) in the Arkoma basin of Oklahoma: OGS Bulletin **129**, 136.

Arbenz, J.K., 2008, Structural framework of the Ouachita Mountains: Oklahoma Geological Survey, Circular **112A**, 1-40.

Arne, D.C., 1992, Evidence from apatite fission-track analysis for regional Cretaceous cooling in the Ouachita Mountain fold belt and Arkoma basin of Arkansas: AAPG Bulletin, **76**, 392-402.

Beaumont, C., 1981, Foreland basins: Royal Astronomical Society Geophysical Journal, **65**, 291-329.

Blackwell, D. D., and M. Richards, 2004, Geothermal Map of North America. American Association of Petroleum Geologists, 1 sheet, scale 1:6,500,000.

Byrnes, A. P., and G. Lawyer, 1999, Burial, maturation, and petroleum generation history of the Arkoma Basin and Ouachita Foldbelt, Oklahoma and Arkansas: Natural Resources Research, **8**, 3-26.

Cardott B. J., L. A. Hemish, C. R. Johnson, K. V. Luza, 1986, The relationship between coal rank and present geothermal gradient in the Arkoma Basin, Oklahoma: Oklahoma Geological Survey Special Publication **86**-4, 6-15.

Comer, J. B., 1992, Organic geochemistry and paleogeography of Upper Devonian formations in Oklahoma and Northwestern Arkansas: Oklahoma Geological Survey, Circular 93

Corrigan, J., P. F. Cervany, R. Donelick, and S. C. Bergman, 1998, Postorogenic denudation along the late Paleozoic Ouachita trend, south central United States of America: Magnitude and timing constraints from apatite fission track data: Tectonics, **17** (4), 587–603, doi:10.1029/98TC01316.

Corrigan, J., 2003, Correcting Bottom Hole Temperature Data: ZetaWare, Inc. Utilities. Web. 20 Nov. 2013. www.zetaware.com/utilities/bht/default.html.

Frezon, S. E., and E. E. Glick, 1959, Pre-Atoka rocks of northern Arkansas: U. S. Geological Survey Professional Paper, 314-H, 171-189.

Frezon, S.E., 1962, Correlation of Paleozoic rocks from Coal County, Oklahoma, to Sebastian County, Arkansas: OGS Circular **58**, 53.

Hagen, E. S., 1986, Hydrocarbon maturation in Laramide-style basins—Constraints from the northern Bighorn Basin, Wyoming and Montana: Laramie, Ph.D. dissertation, University of Wyoming, 215.

Hendricks, J. D., 1988, Bouguer gravity of Arkansas: U. S. Geological Survey Professional Paper **1474**, 31.

Hildenbrand, T. G., and J. D. Hendricks, 1995, Geophysical setting of the Reelfoot rift and relations between rift structures and the New Madrid seismic zone: chap. E of Shedlock, K., and A. Johnston, eds., Investigations of the New Madrid seismic zone: U. S. Geological Survey Professional Paper, **1538.**

Houseknecht, D. W. and S. M. Matthews, 1985, Thermal maturity of Carboniferous strata, Ouachita Mountains: American Association of Petroleum Geologists Bulletin, **69**, 335-345.

Houseknecht, D. W., 1986, Evolution from passive margin to foreland basin: the Atoka Formation of the Arkoma Basin, south-central U.S.A.: in Allen, P.A., and P. Homewood, eds., Foreland basins: International Association of Sedimentologists, **8**, 327-345.

Houseknecht, D.W., and L.A. Hathon, 1989, Preservation of sandstone reservoir quality and methane reserves in overmature strata of Arkoma basin: AAPG Bulletin, v. 73, 1160.

Houseknecht D. W., L. A. Hathon, and T. A. McGilvery, 1992, Thermal maturity of Paleozoic strata in the Arkoma Basin: Oklahoma Geological Survey, Circular **93**, 122-132.

Houseknecht, D.W., D.F. Bensley, L.A. Hathon, and P.H. Kastens, 1993, Rotational reflectance properties of Arkoma basin dispersed vitrinite: insights for understanding reflectance populations in high thermal maturity regions: Organic Geochemistry, **20**, 187-196.

Lee, Y., D. Deming, and K. F. Chen, 1996, Heat Flow and Heat Production in the Arkoma Basin and Oklahoma Platform, Southeastern Oklahoma: Journal of Geophysical Research, **101**, 25,387-25,401.

Mankin, C. J., et al., 1987, Correlation of stratigraphic units in North America, Texas-Oklahoma tectonic region: American Association of Petroleum Geologists Correlation Chart Series, 1 sheet.

Meckel, L. D. Jr., D. G. Smith, and L. A. Wells, 1992, Ouachita Foredeep Basins: Regional Paleogeography and Habitat of Hydrocarbons: in Macqueen, R. W., and D. A. Leckie: AAPG Memoir 55, Foreland Basins and Fold Belts, **15**, 427-444.

Odum, J. K., E. A. Luzietti, W. J. Stephenson, K. M. Shedlock, and J. A. Michael, 1995, High-Resolution, Shallow, Seismic Reflection Surveys of the Northwest Reelfoot Rift Boundary Near Marston, Missouri: U. S. Geological Survey Professional Paper, **1538**.

Saleh, A., 2004, Correlation of Atoka and adjacent strata within a sequence stratigraphic framework, Arkoma Basin, Oklahoma (Doctoral dissertation). Retrieved from ProQuest Dissertations and Theses (Accession Order No. AAT 3122287).

Sinclair, H.D., and M. Naylor, 2012, Foreland basin subsidence driven by topographic growth versus plate subduction, Geological Society of America Bulletin, **124** no. 3-4, 368-379.

Spötl, C., D.W. Houseknecht, and S.J. Burns, 1996, Diagenesis of an 'overmature' gas reservoir: the Spiro sand of the Arkoma basin, USA: Marine and Petroleum Geology, **13**, 25-40.

Spoetl, C., D. W. Houseknecht, and R. C. Jacques, 1998, Kerogen maturation and incipient graphitization of hydrocarbon source rocks in the Arkoma Basin, Oklahoma and Arkansas; a combined petrogrpahic and Raman spectrometric study: Organic Geochemistry, **28**, no. 9-10, 535-542.

Sutherland, P. K. 1988, Late Mississippian and Pennsylvanian depositional history in the Arkoma basin area, Oklahoma and Arkansas: Geological Society of America Bulletin, **100**, no. 11, 1787-1802.

Sweeney, J. J., and A. K. Burnham, 1990, Evaluation of a simple model of vitrinite reflectance based on chemical kinetics: AAPG Bulletin, **74**, 1559-1570.

Thomas, W. A., 2006, Tectonic inheritance at a continental margin: GSA Today, **16**, no. 2, 4-11.

Van Arsdale, R. B., and E. S. Schweig, III, 1990, Subsurface structure of the eastern Arkoma Basin: AAPG Bulletin, **74**, 1030-1037.

Whitaker, A. E., and T. Engelder, 2006, Plate-scale stress fields driving the tectonic evolution of the central Ouachita salient, Oklahoma and Arkansas: Geological Society of America Bulletin, **118**, no. 5-6, 710-723.

Xie, X., and P. L. Heller, 2009, Plate tectonics and basin subsidence history: Geological Society of America Bulletin, **121**, no. 1-2, 55-64.

APPENDIX

A-1. Well locations

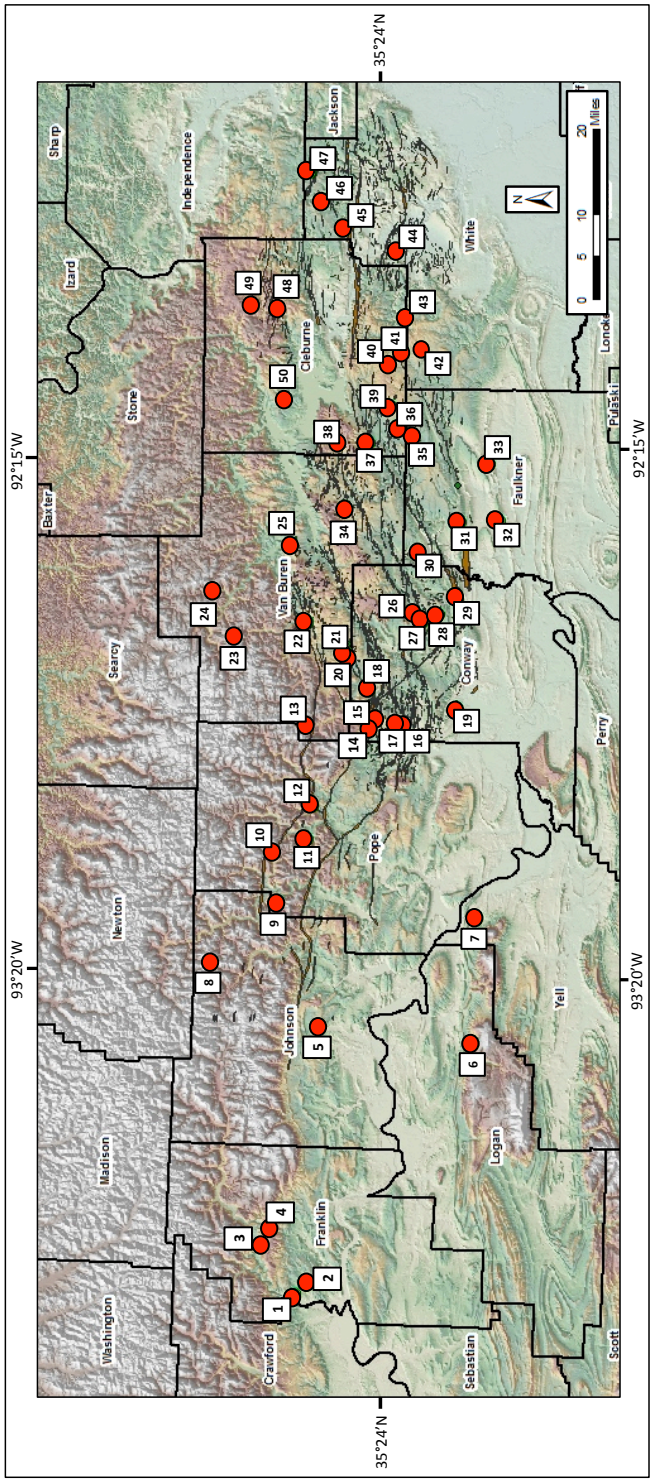

Figure 2: Location of the 50 wells used for modeling. Well numbering is specific to this map. Associated well names numbered on map: (1) Nixon B 10-28, (2), Wilson 1-17, (3) Cline 4-19, (4) Page 1-28, (5) Teague 1-21, (6) Federal 1-19, (7) McCray 1-22, (8) OHU 12-22 1-15, (9) OHU 11-21 1-23, (10) OHU 11-20 1-23 (11) OHU 10-19 1-07, (12) Parton 10-19 1-11, (13) OHU 10-17 1-04, (14) Brown 1-17, (15) Thomas 09-17 1-16, (16) Morrilton Lumber No. 1, (17) CS Ramsey No. 1, (18) Halbrook 09-16 4-18, (19) Kaufman No. 1, (20) Koone 10-16 1-35, (21) Hildreth 10-16 1-36, (22) Hankins 10-15 1-04, (23) Copeland 3, (24) Copeland 2, (25) Charles Hurley No. 1, (26) Billiot-A, (27) Dancer No. 1, (28) Glenn Wright No. 1, (29) Zuber South No. 1, (30) Harrison R 08-14 1-11, (31) Sowash 07-13, (32) McLung 1-33, (33) E. W. Moore #1, (34) Collums 10-13 1-27, (35) Sneed 08-11 1-06, (36) Landrum T, (37) Landrum Quitman No. 1, (38) Allen Cecil 10-12 7-25, (39) McNew 1-26, (40) Liles No. 1, (41) Snyder 09-10 1-35, (42) Patterson No. 1, (43) Rocka No. 1, (44) Neal 09-08 2-26, (45) Albert Est. No. 1, (46) Bobby and Lorette, (47) Sample 1, (48) Rackley 1-15, (49) A. C. Smith No. 1-2, (50) Hearst 1-23.

A-2. Burial history output models with Sweeney and Burnham (1990) overlay. Colored areas denote the zones of hydrocarbon generation and destruction (hydrocarbon windows), expressed in terms of vitrinite reflectance (%Ro): 0.5-0.7, early mature (oil); 0.7-1.0, mid-mature (oil); 1.0-1.3, late mature (oil); 1.3-2.0, overmature for oil, thermal cracking to gas; 2.0-4.0, dry gas; 4.0-5.0, upper limit of dry-gas preservation.

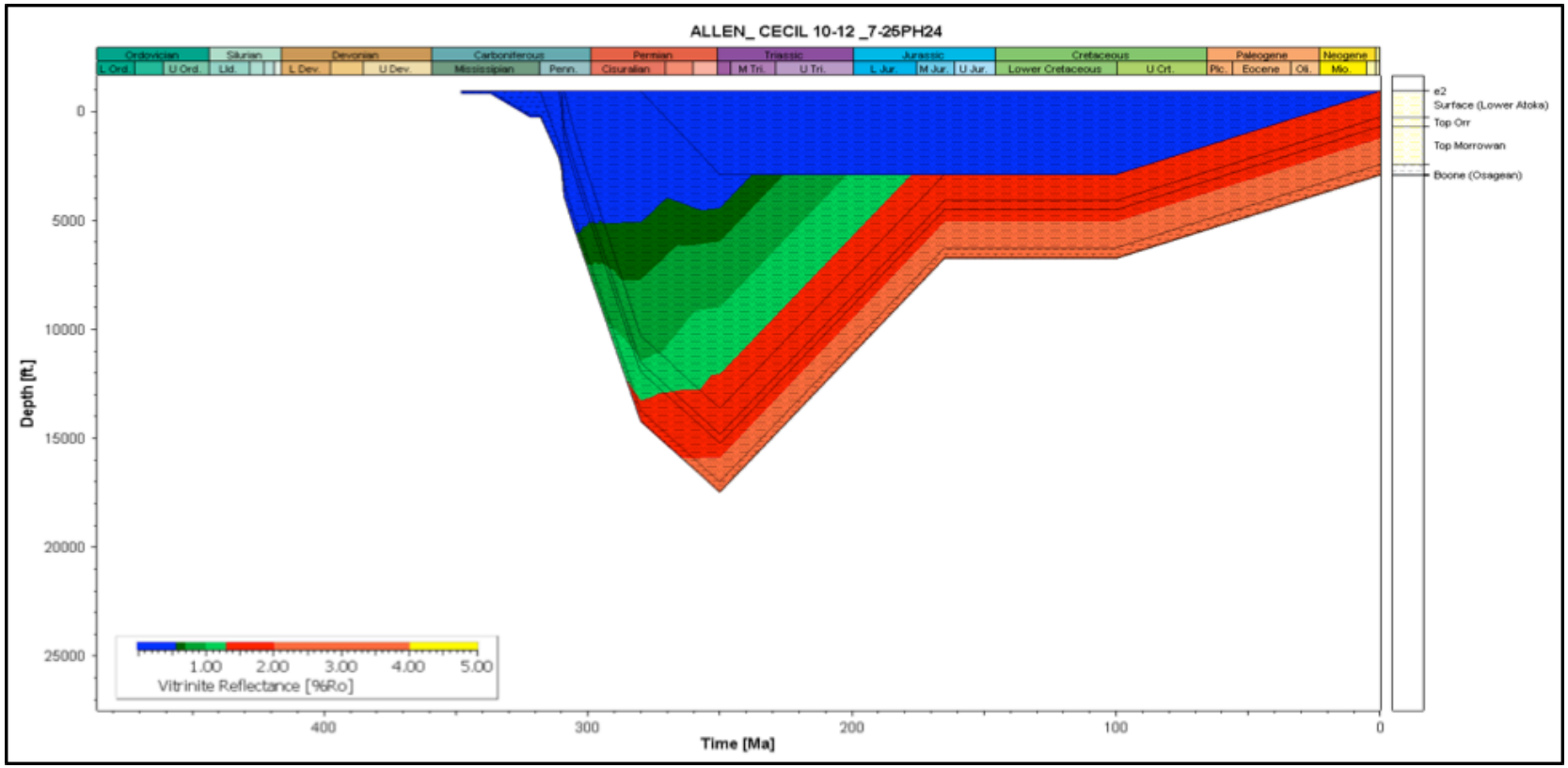

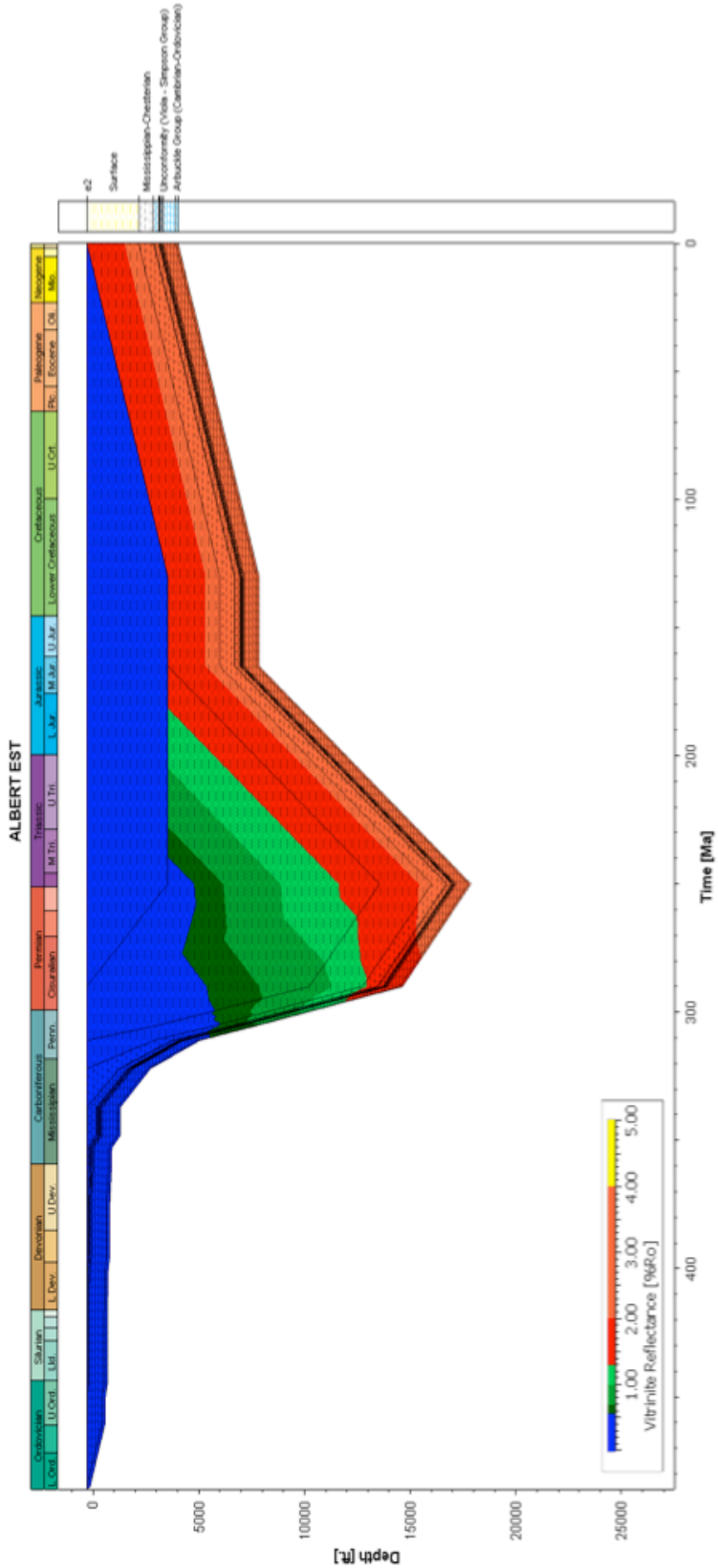
ALBERT EST
Surface
Mississippian-Chesterian
Unconformity (Viola - Simpson Group)
Arbuckle Group (Cambrian-Ordovician)
Ordovician
Silurian
Devonian
Carboniferous
Permian
Triassic
Jurassic
Cretaceous
Paleogene
Neogene
Time [Ma]
Depth [ft]
Vitrinite Reflectance [%Ro]
1.00
2.00
3.00
4.00
5.00

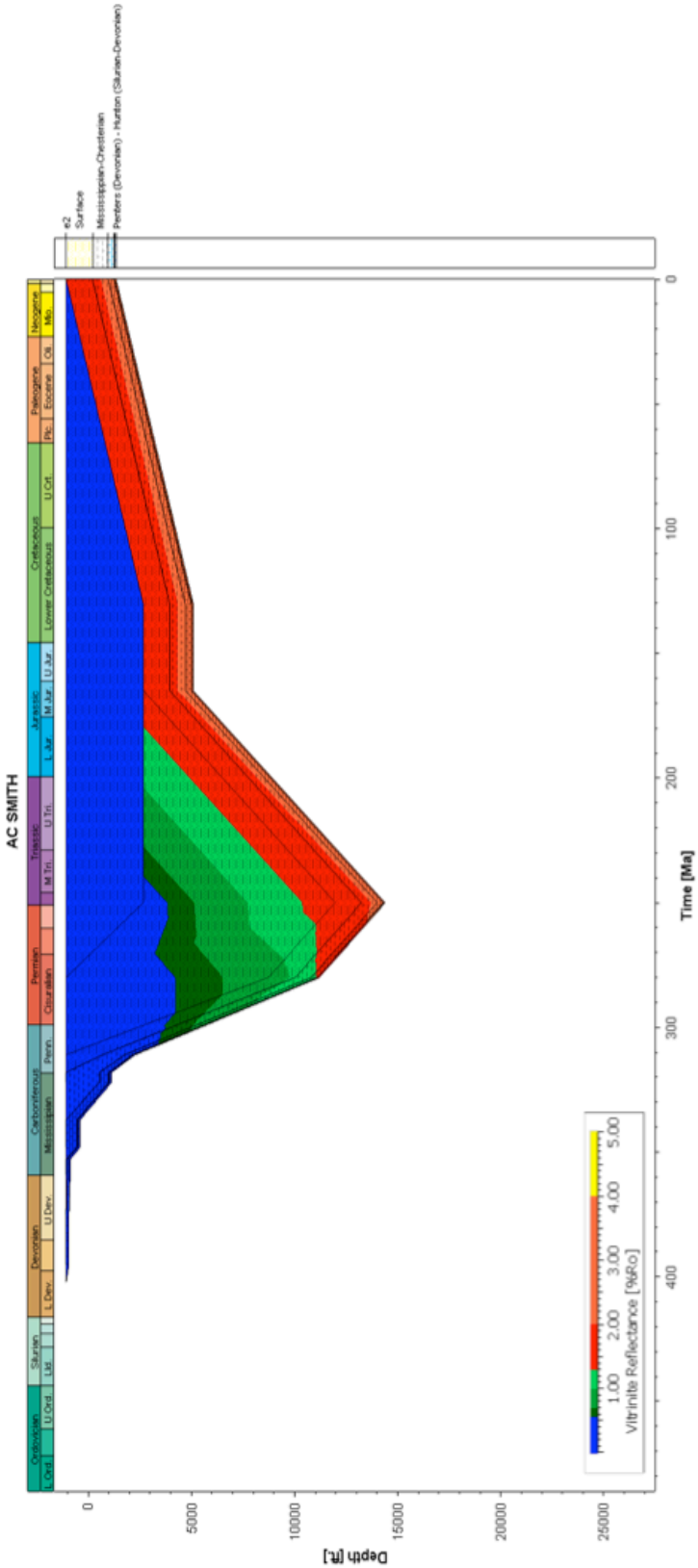
AC SMITH
Ordovician
Silurian
Devonian
Carboniferous
Permian
Triassic
Jurassic
Cretaceous
Paleogene
Neogene
L. Ord.
U. Ord.
Ltd.
L. Dev.
U. Dev.
Mississippian
Penn.
Cisuralian
M. Tri.
U. Tri.
L. Jur.
M. Jur.
U. Jur.
Lower Cretaceous
U. Cret.
Plc.
Eocene
Oli.
Mio.
Surface
Mississippian-Chesterian
Penters (Devonian) - Hunton (Silurian-Devonian)
Depth [ft]
0
5000
10000
15000
20000
25000
Time [Ma]
0
100
200
300
400
Vitrinite Reflectance [%Ro]
1.00
2.00
3.00
4.00
5.00

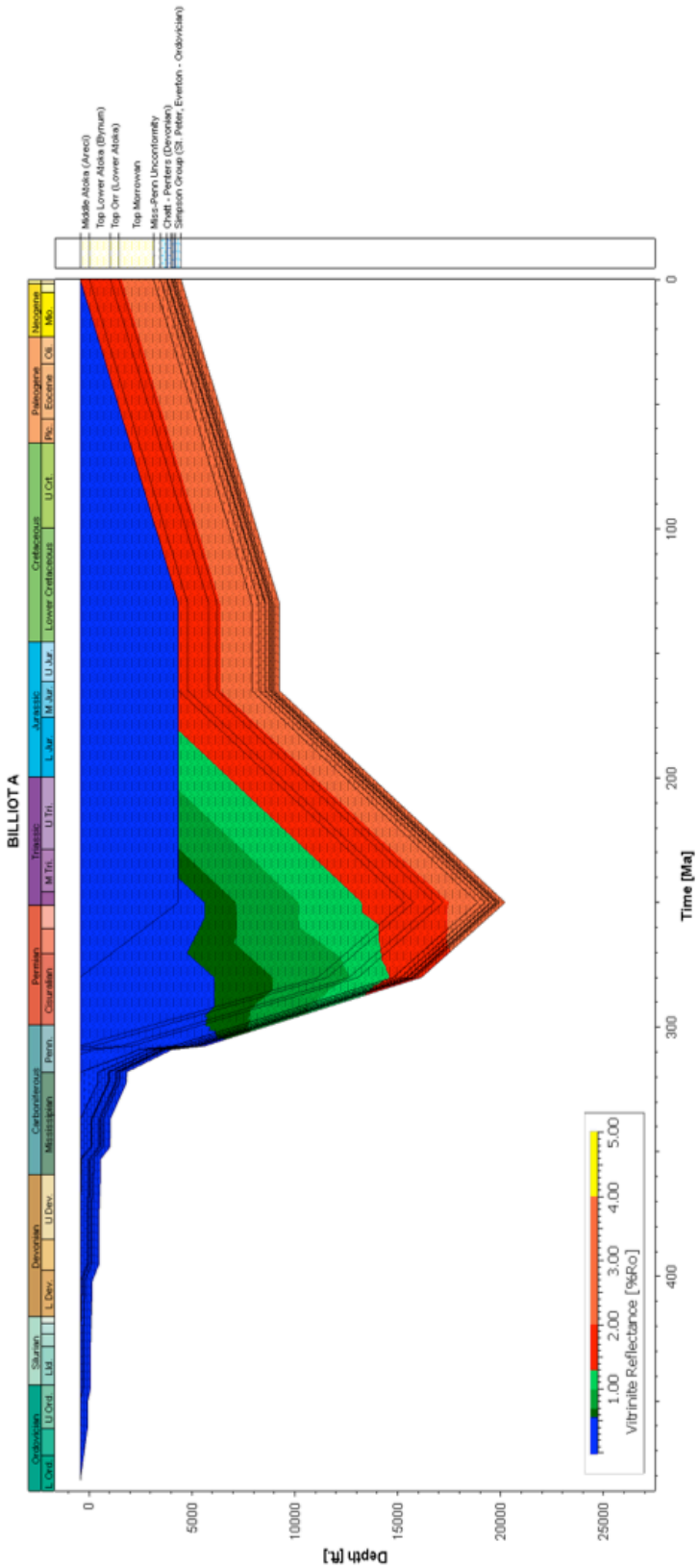
BILLIOT A
Middle Atoka (Arco)
Top Lower Atoka (Bynum)
Top Orr (Lower Atoka)
Top Morrowan
Miss-Penn Uncontormity
Chatt - Penters (Devonian)
Simpson Group (St. Peter, Everton - Ordovician)
Ordovician
Silurian
Devonian
Carboniferous
Permian
Triassic
Jurassic
Cretaceous
Paleogene
Neogene
L Ord
U Ord
Ltd
L Dev.
U Dev
Mississippian
Penn.
Cisuralian
M Tri.
U Tri.
L Jur
M Jur
U Jur
Lower Cretaceous
U Cret.
Plc.
Eocene
Olig.
Mio.
Depth [ft]
0
5000
10000
15000
20000
25000
Time [Ma]
0
100
200
300
400
Vitrinite Reflectance [%Ro]
1.00
2.00
3.00
4.00
5.00

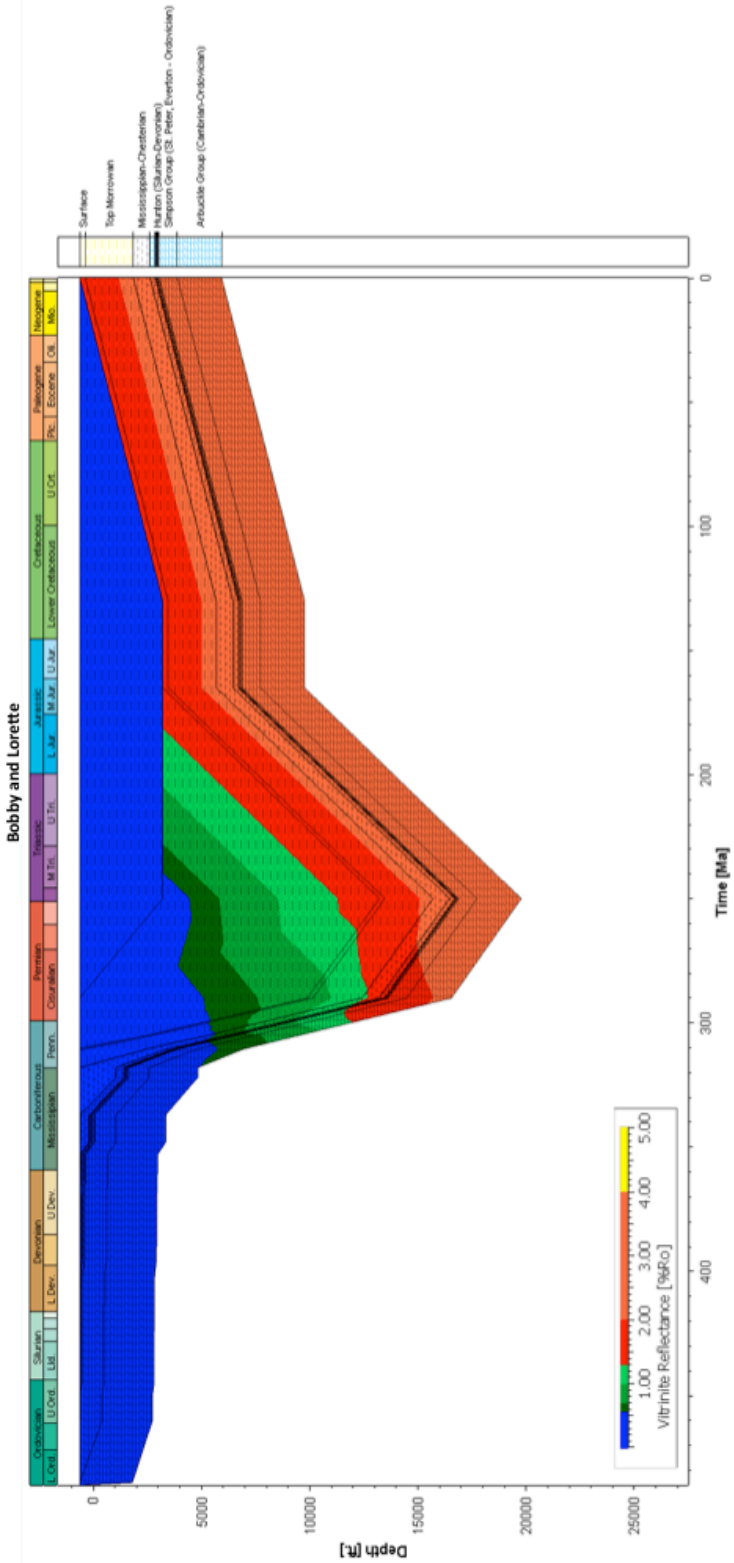
Bobby and Lorette
Surface
Top Morrowan
Mississippian-Chesterian
Hunton (Silurian-Devonian)
Simpson Group (St. Peter, Everton - Ordovician)
Arbuckle Group (Cambrian-Ordovician)
Ordovician
Silurian
Devonian
Carboniferous
Permian
Triassic
Jurassic
Cretaceous
Paleogene
Neogene
L Ord
U Ord
Lsil
L Dev
U Dev
Miss
Penn
Courtian
M Tri
U Tri
L Jur
M Jur
U Jur
Lower Cretaceous
U Cret
Plc
Eocene
Olig
Mio
Depth [ft]
0
5000
10000
15000
20000
25000
Time [Ma]
0
100
200
300
400
Vitrinite Reflectance [%Ro]
1.00
2.00
3.00
4.00
5.00

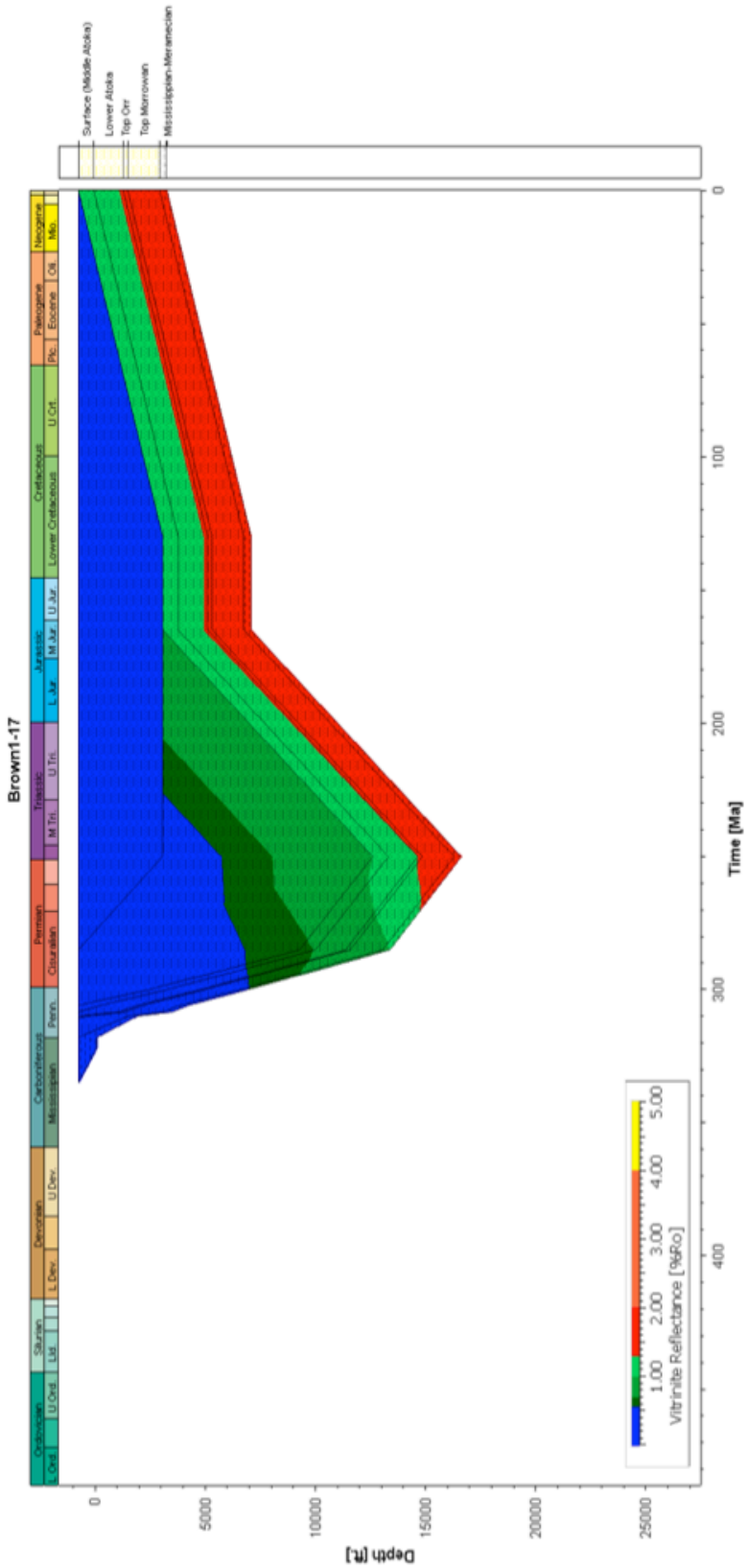
Brown1-17
Surface (Middle Atoka)
Lower Atoka
Top Orr
Top Morrowan
Mississippian-Meramecian
Cambrian
Ordovician
Silurian
Devonian
Carboniferous
Permian
Triassic
Jurassic
Cretaceous
Paleogene
Neogene
Cmb
U Ord
Lsd
L Dev
U Dev
Mississippian
Penn.
Guadalupian
M Tri
U Tri
L Jur
M Jur
U Jur
Lower Cretaceous
U Cret.
Pc.
Eocene
Olig.
Mio.
Vitrinite Reflectance [%Ro]
1.00
2.00
3.00
4.00
5.00
Depth [ft]
0
5000
10000
15000
20000
25000
Time [Ma]
400
300
200
100
0

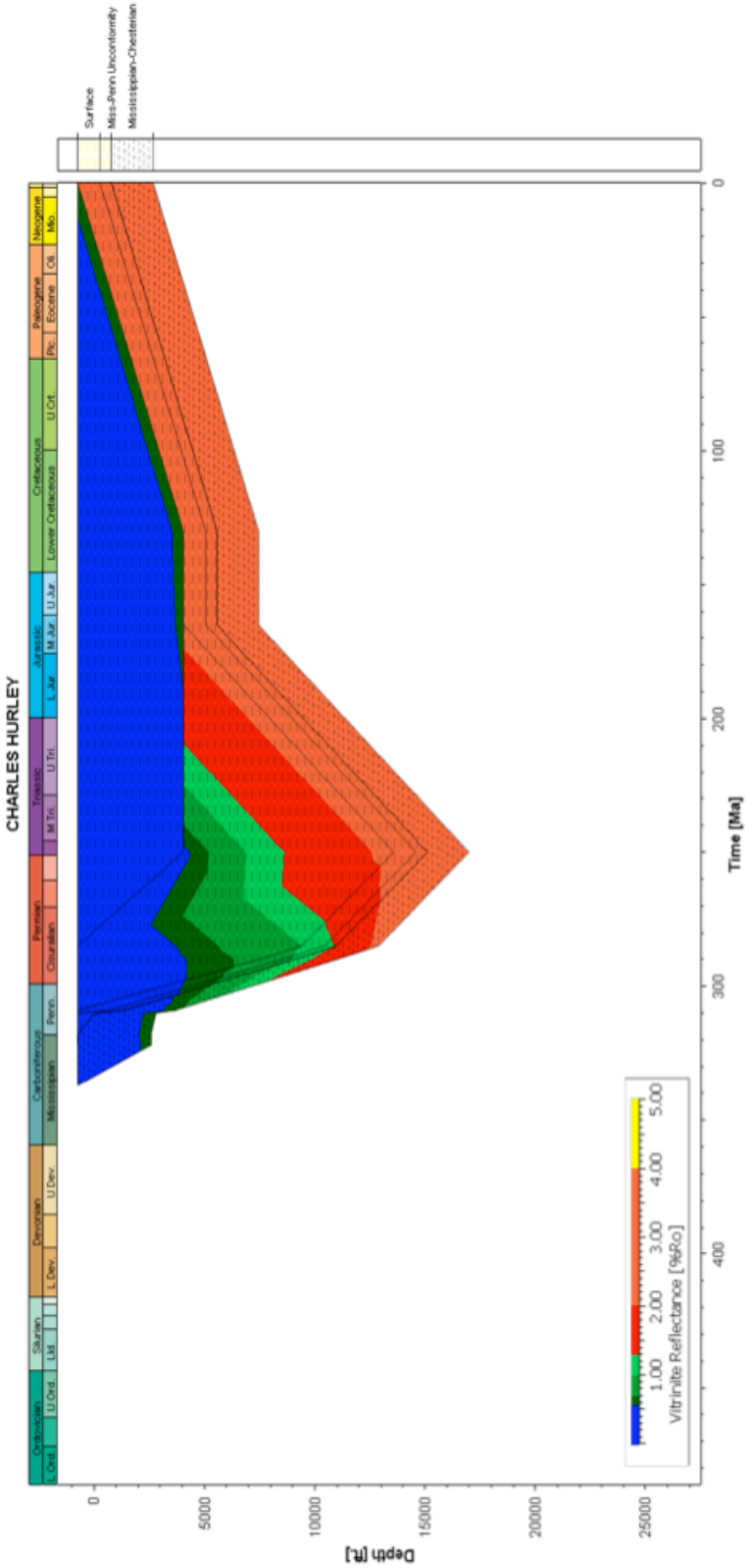
CHARLES HURLEY
Surface
Miss-Penn Uncontormity
Mississippian-Chesterian
Ordovician
L Ord.
U Ord.
Silurian
Ltl.
Devonian
L Dev.
U Dev.
Carboniferous
Mississippian
Penn.
Permian
Cisuralian
Triassic
M Tri.
U Tri.
Jurassic
L Jur.
M Jur.
U Jur.
Cretaceous
Lower Cretaceous
U Cret.
Paleogene
Plc.
Eocene
Oli.
Neogene
Mio.
Time [Ma]
0
100
200
300
400
Depth [ft]
0
5000
10000
15000
20000
25000
Vitrinite Reflectance [%Ro]
1.00
2.00
3.00
4.00
5.00

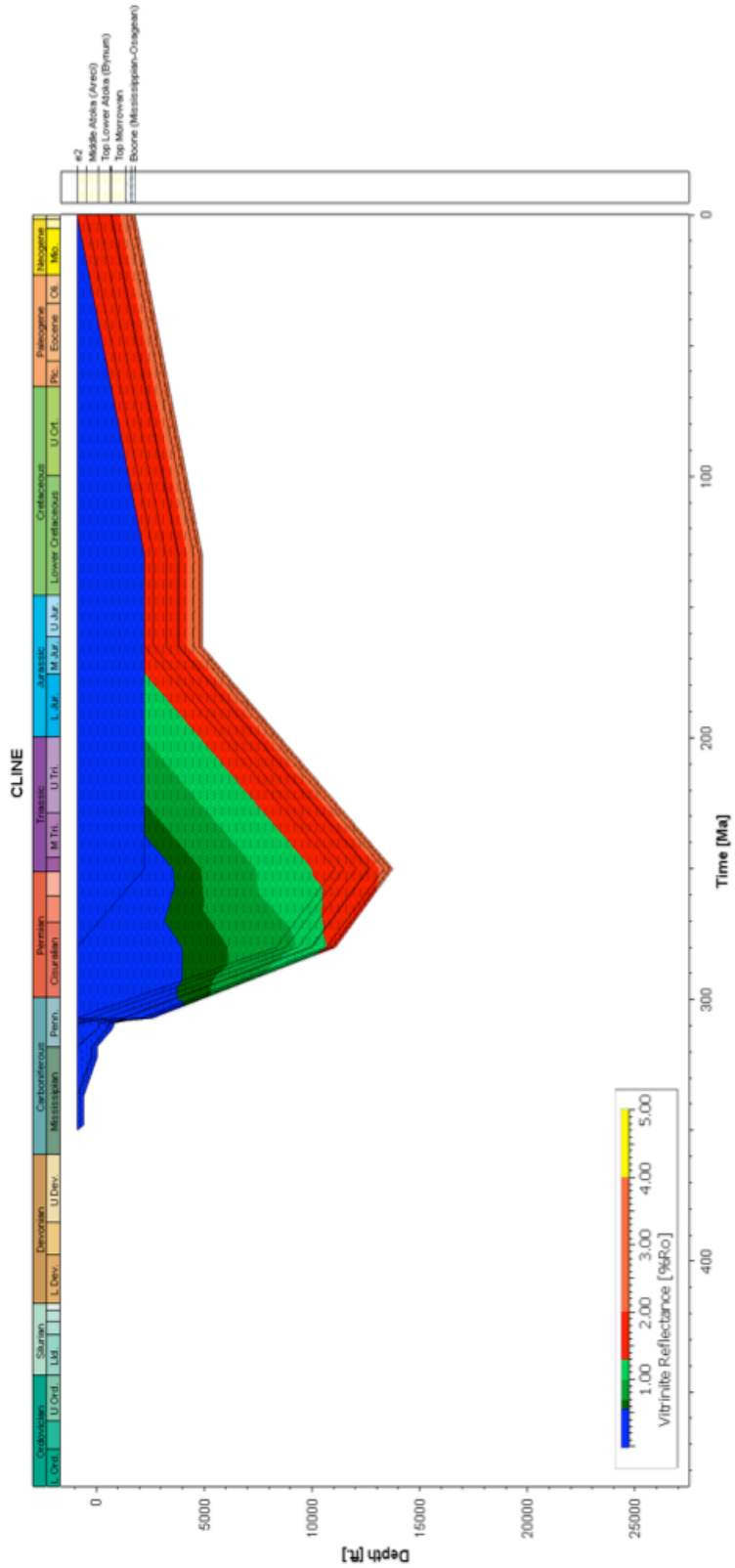
CLINE
Ordovician
Silurian
Devonian
Carboniferous
Permian
Triassic
Jurassic
Cretaceous
Paleogene
Neogene
Cmb
U Ord
Ltl
L Dev
U Dev
Miss
Penn
Cisuralian
M Tri
U Tri
L Jur
M Jur
U Jur
Lower Cretaceous
U Cret
Pc
Eocene
Ol
Mio
#2
Middle Atoka (Atoka)
Top Lower Atoka (Bynum)
Top Morrowan
Boone (Mississippian-Osagean)
Depth [ft]
0
5000
10000
15000
20000
25000
Time [Ma]
0
100
200
300
400
Vitrinite Reflectance [%Ro]
1.00
2.00
3.00
4.00
5.00

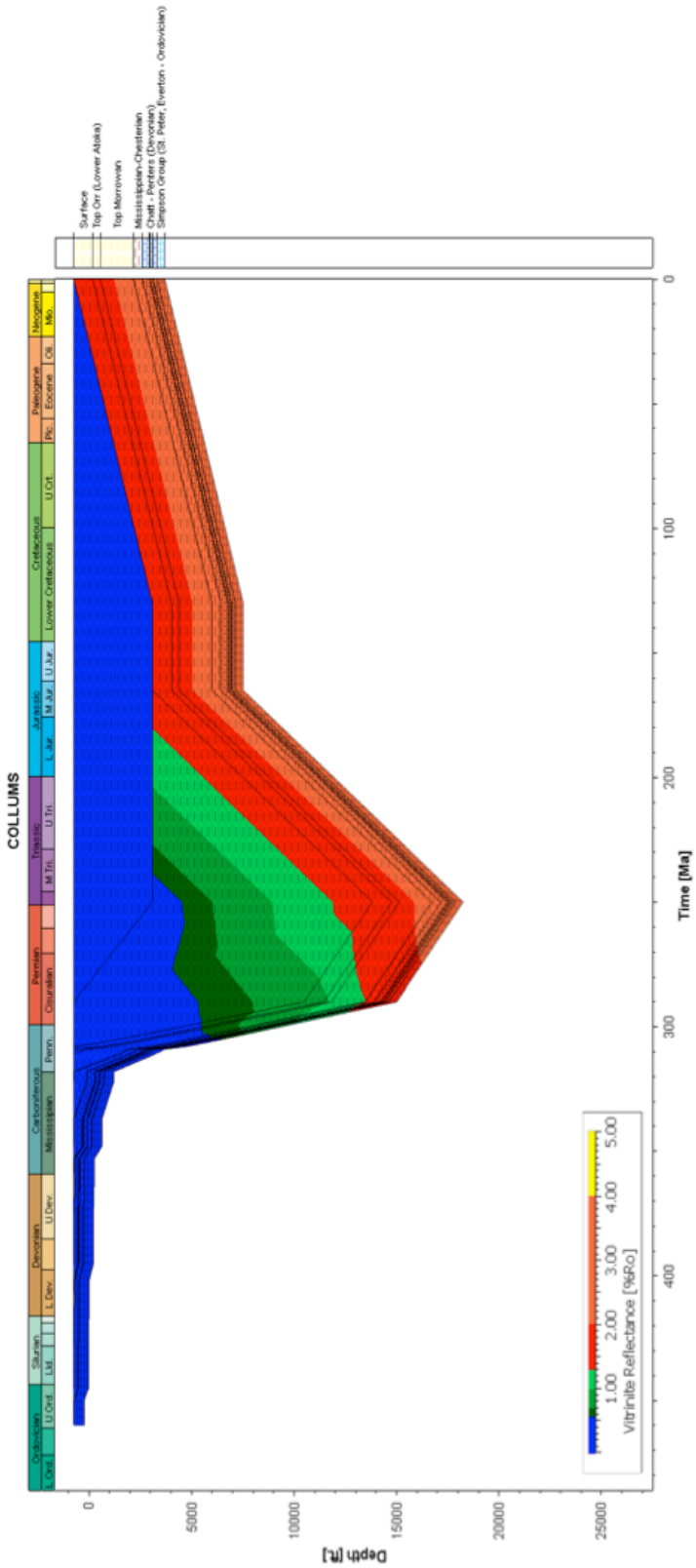
COLLUMS
Surface
Top Orr (Lower Atoka)
Top Morrowan
Mississippian-Chesterian
Chatt - Penters (Devonian)
Simpson Group (St. Peter, Everton - Ordovician)
Ordovician
Silurian
Devonian
Carboniferous
Permian
Triassic
Jurassic
Cretaceous
Paleogene
Neogene
Ord.
U.Ord.
Ltl.
L.Dev.
U.Dev.
Mississippian
Penn.
Cisuralian
M.Tri.
U.Tri.
L.Jur.
M.Jur.
U.Jur.
Lower Cretaceous
U.Cret.
Pic.
Eocene
Olig.
Mio.
Vitrinite Reflectance [%Ro]
1.00
2.00
3.00
4.00
5.00
Depth [ft]
0
5000
10000
15000
20000
25000
Time [Ma]
0
100
200
300
400

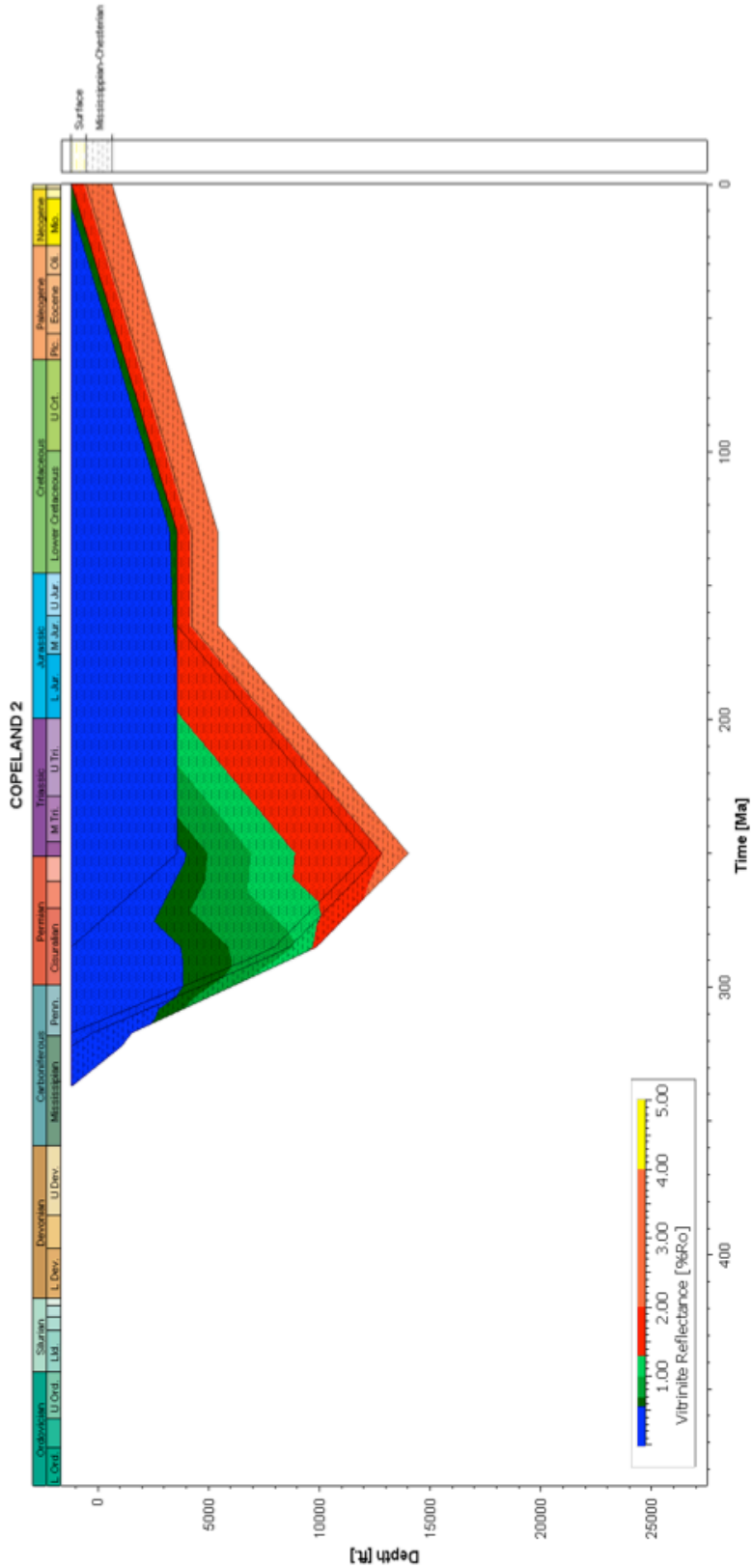
COPELAND 2
Cambrian
Ordovician
Silurian
Devonian
Carboniferous
Permian
Triassic
Jurassic
Cretaceous
Paleogene
Neogene
L. Ord.
U.Ord.
Ltd.
L. Dev.
U.Dev.
Mississippian
Penn.
Guadalupian
M.Tri.
U.Tri.
L.Jur.
M.Jur.
U.Jur.
Lower Cretaceous
U.Cret.
Pc.
Eocene
Ol.
Mio.
Surface
Mississippian-Chesterian
Time [Ma]
Depth [ft]
Vitrinite Reflectance [%Ro]
1.00
2.00
3.00
4.00
5.00

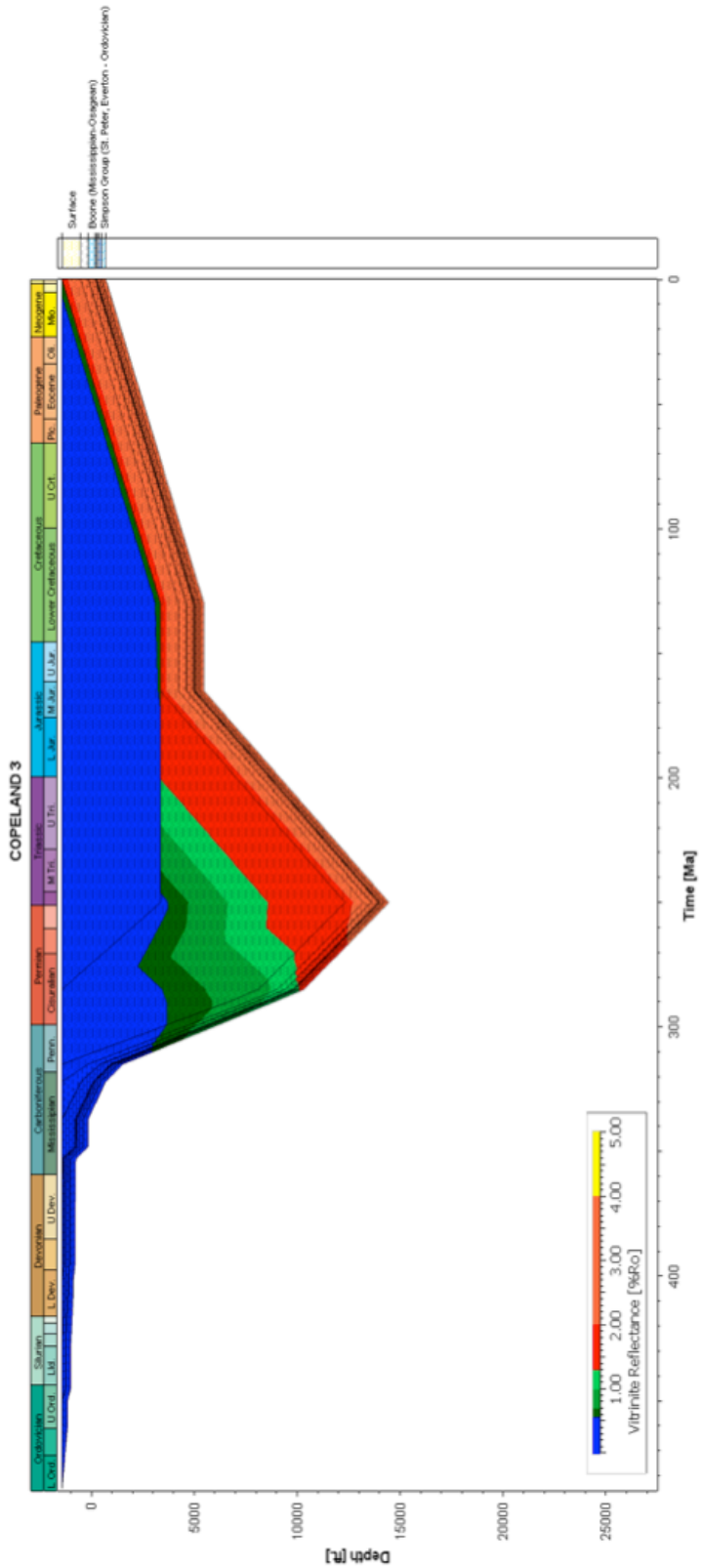
COPELAND 3
Surface
Eocene (Mississippian-Osagean)
Simpson Group (St. Peter, Everton - Ordovician)
Ordovician
L Ord.
U Ord.
Silurian
LM
Devonian
L Dev.
U Dev.
Carboniferous
Mississippian
Penn.
Permian
Cisuralian
Triassic
M Tri.
U Tri.
Jurassic
L Jur.
M Jur.
U Jur.
Cretaceous
Lower Cretaceous
U Cret.
Paleogene
Pc.
Eocene
Oli.
Neogene
Mio.
Time [Ma]
Depth [ft]
Vitrinite Reflectance [%Ro]
1.00
2.00
3.00
4.00
5.00

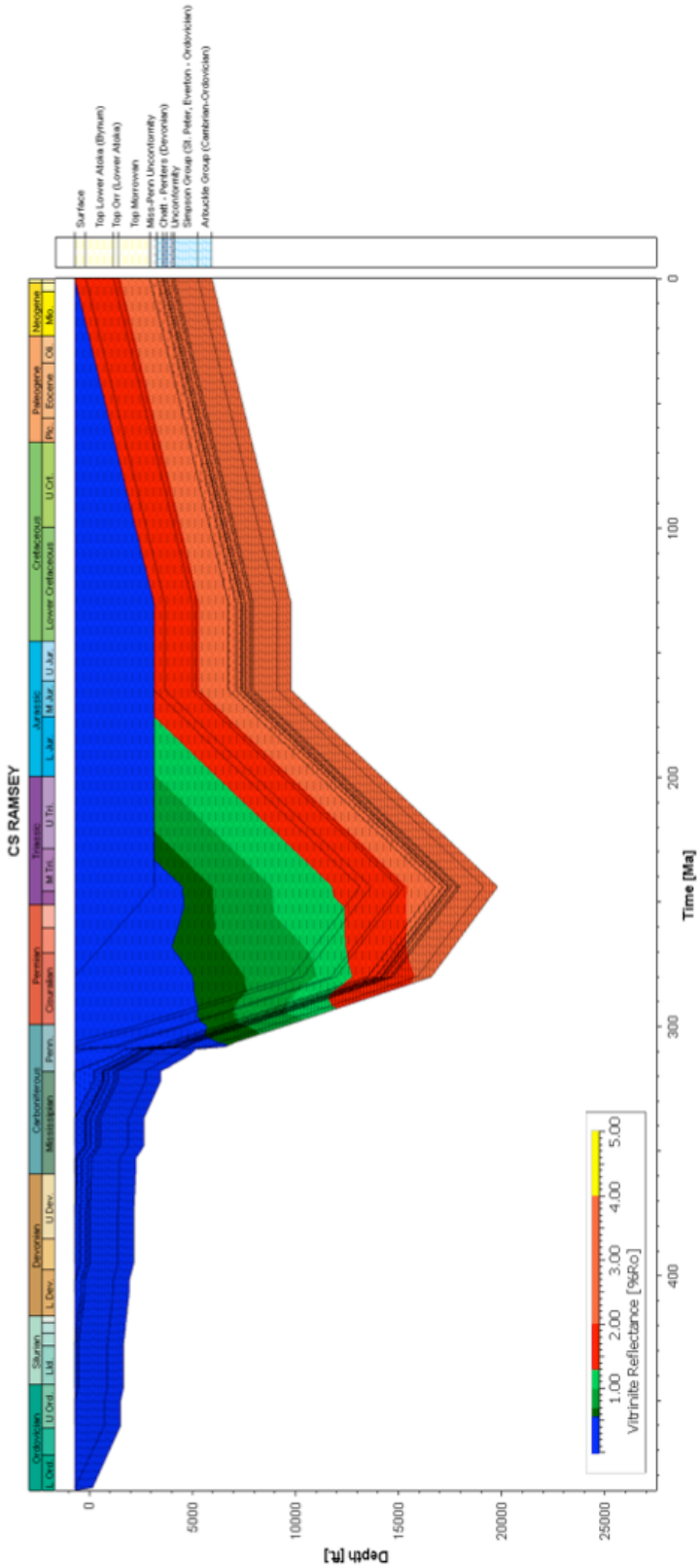
CS RAMSEY
Surface
Top Lower Atoka (Bynum)
Top Orr (Lower Atoka)
Top Morrowan
Miss.-Penn Unconformity
Chatt. - Porters (Devonian)
Unconformity
Simpson Group (St. Peter, Everton - Ordovician)
Arbuckle Group (Cambrian-Ordovician)
Ordovician
Silurian
Devonian
Carboniferous
Permian
Triassic
Jurassic
Cretaceous
Paleogene
Neogene
L Ord.
U Ord.
LM
L Dev.
U Dev.
Mississippian
Penn.
Cisuralian
M Tri.
U Tri.
L Jur.
M Jur.
U Jur.
Lower Cretaceous
U Crt.
Plc.
Eocene
Oli.
Mio.
Time [Ma]
Depth [ft]
Vitrinite Reflectance [%Ro]
1.00
2.00
3.00
4.00
5.00

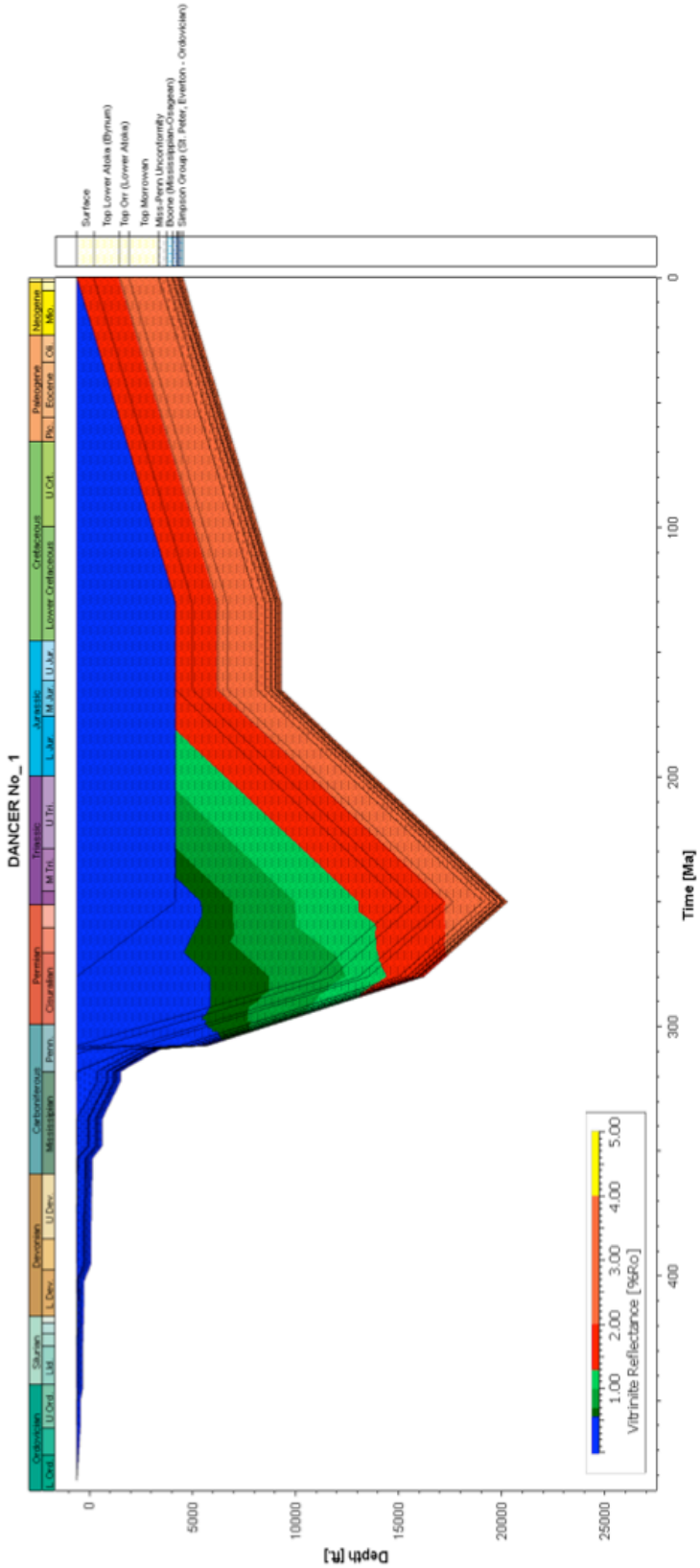
DANCER No_1
Surface
Top Lower Atoka (Bynum)
Top Orr (Lower Atoka)
Top Morrowan
Miss-Penn Unconformity
Boone (Mississippian-Osagean)
Simpson Group (Bil. Peter, Everton - Ordovician)
Ordovician
Silurian
Devonian
Carboniferous
Permian
Triassic
Jurassic
Cretaceous
Paleogene
Neogene
L.Ord.
U.Ord.
Ltl.
L.Dev.
U.Dev.
Mississippian
Penn.
Guadalupian
M.Tri.
U.Tri.
L.Jur.
M.Jur.
U.Jur.
Lower Cretaceous
U.Cret.
Pc.
Eocene
Oli.
Mio.
Time [Ma]
0
100
200
300
400
Depth [ft]
0
5000
10000
15000
20000
25000
Vitrinite Reflectance [%Ro]
1.00
2.00
3.00
4.00
5.00

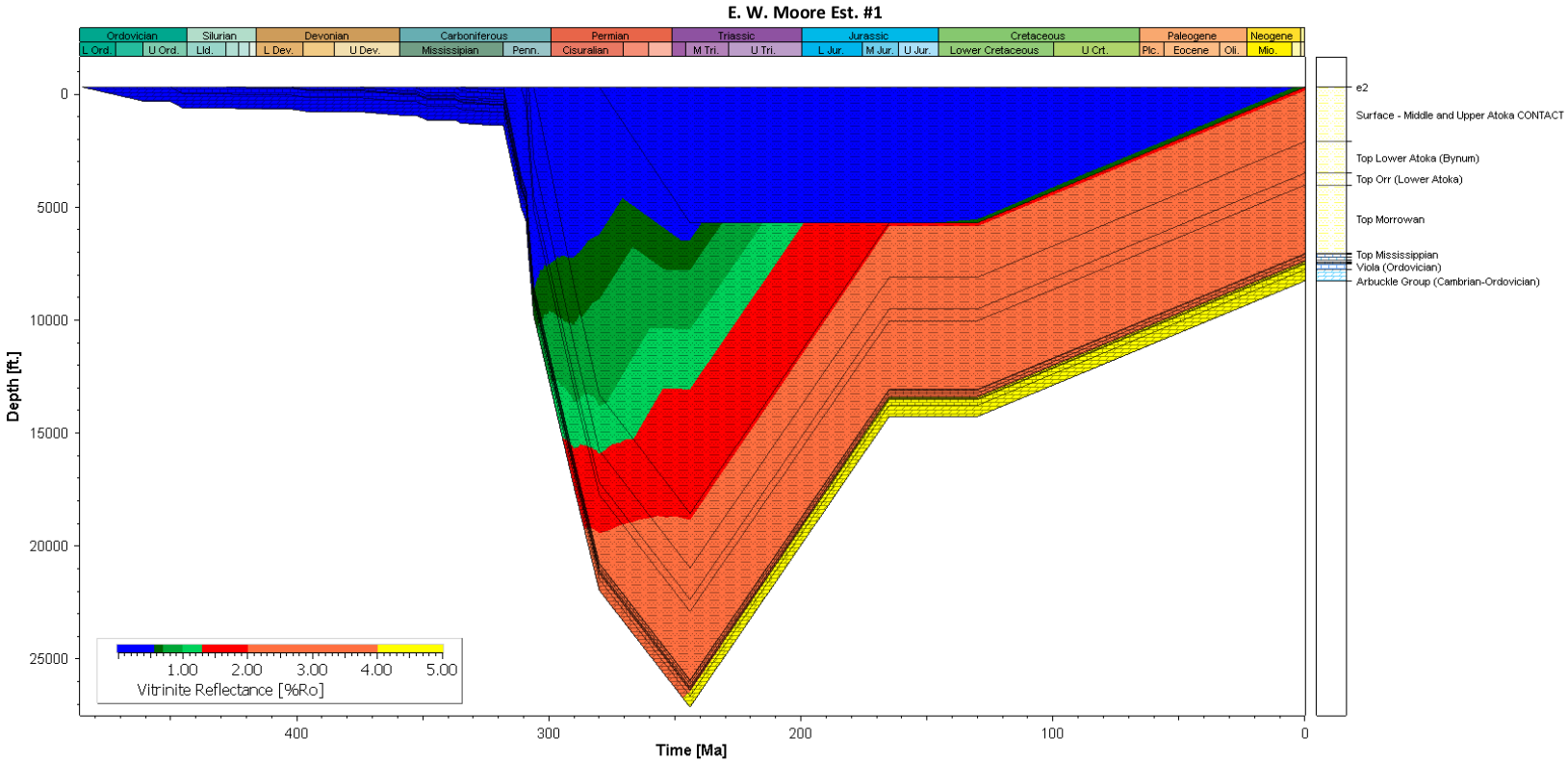
E. W. Moore Est. #1
Ordovician
Silurian
Devonian
Carboniferous
Permian
Triassic
Jurassic
Cretaceous
Paleogene
Neogene
L Ord.
U Ord.
Lld.
L Dev.
U Dev.
Mississipian
Penn.
Cisuralian
M Tri.
U Tri.
L Jur.
M Jur.
U Jur.
Lower Cretaceous
U Crt.
Plc.
Eocene
Oli.
Mio.
Depth [ft.]
0
5000
10000
15000
20000
25000
Time [Ma]
400
300
200
100
0
1.00
2.00
3.00
4.00
5.00
Vitrinite Reflectance [%Ro]
e2
Surface - Middle and Upper Atoka CONTACT
Top Lower Atoka (Bynum)
Top Orr (Lower Atoka)
Top Morrowan
Top Mississippian
Viola (Ordovician)
Arbuckle Group (Cambrian-Ordovician)

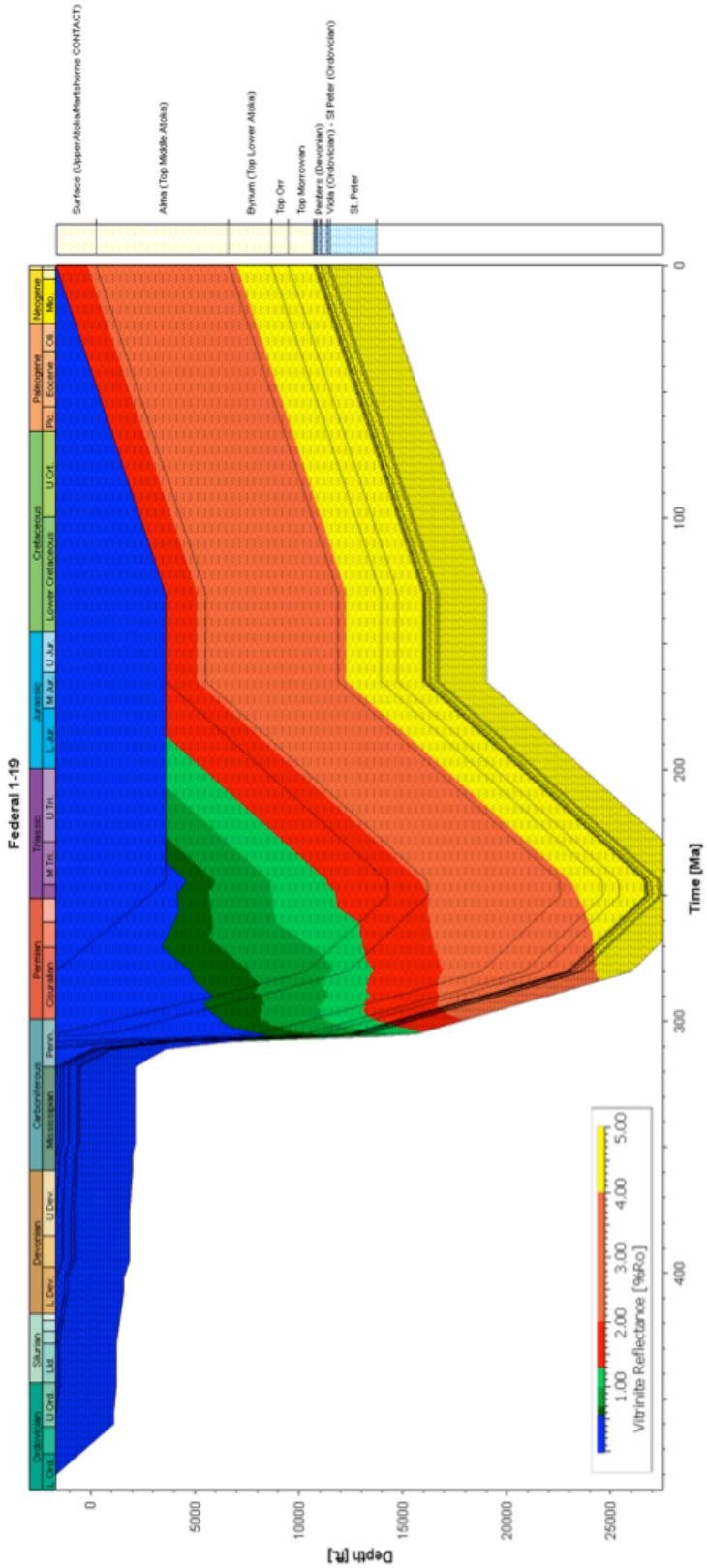
Federal 1-19
Surface (Upper Atoka/Hartshorne CONTACT)
Atoka (Top Middle Atoka)
Bynum (Top Lower Atoka)
Top Orr
Top Morrowan
Penters (Devonian)
Viola (Ordovician) - St Peter (Ordovician)
St. Peter
Ordovician
Silurian
Devonian
Carboniferous
Permian
Triassic
Jurassic
Cretaceous
Paleogene
Neogene
L Ord.
U Ord.
Ltl.
L Dev.
U Dev.
Mississippian
Penn.
Cisuralian
M Tri.
U Tri.
L Jur.
M Jur.
U Jur.
Lower Cretaceous
U Cret.
Plc.
Eocene
Oli.
Mio.
Time [Ma]
0
100
200
300
400
Depth [ft]
0
5000
10000
15000
20000
25000
Vitrinite Reflectance [%Ro]
1.00
2.00
3.00
4.00
5.00

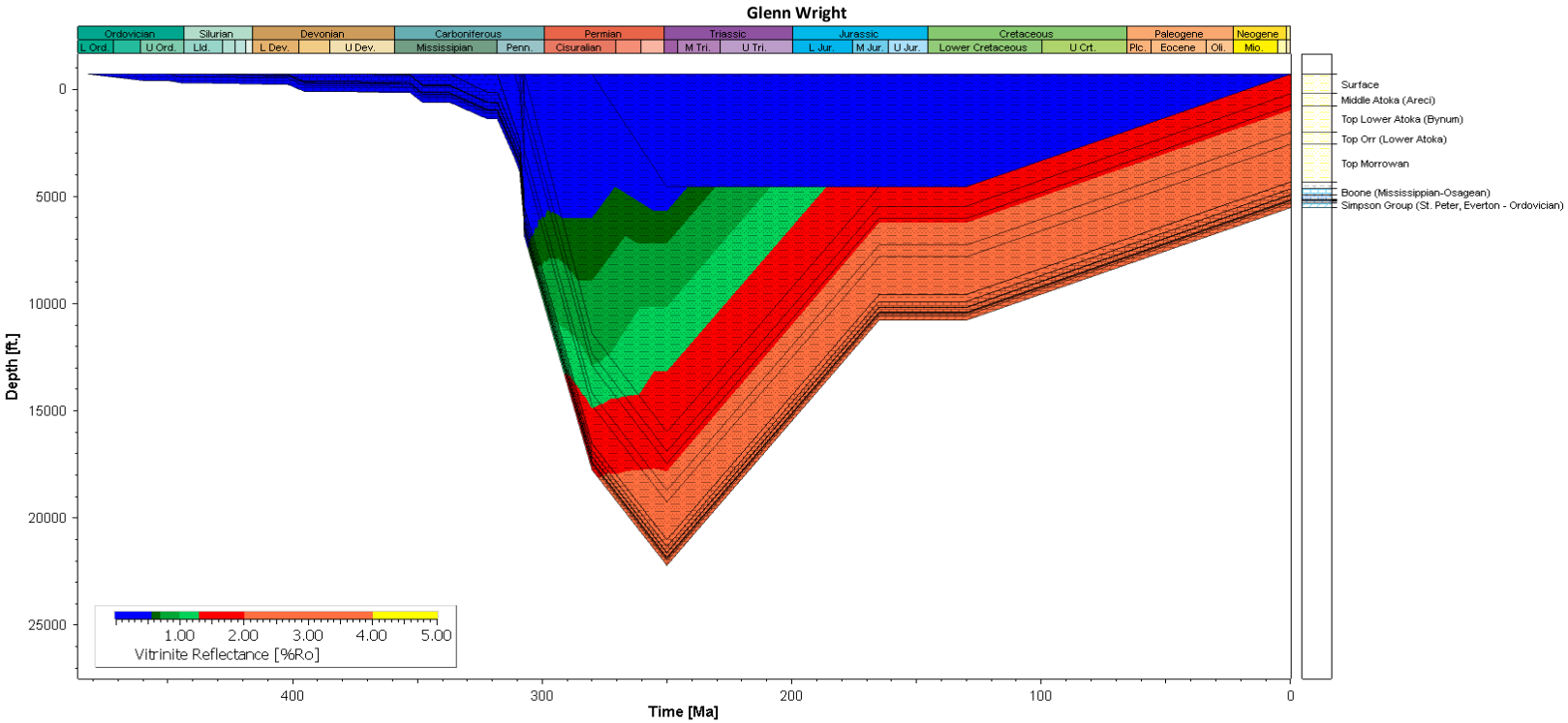
Glenn Wright
Ordovician
Silurian
Devonian
Carboniferous
Permian
Triassic
Jurassic
Cretaceous
Paleogene
Neogene
L Ord.
U Ord.
Lld.
L Dev.
U Dev.
Mississipian
Penn.
Cisuralian
M Tri.
U Tri.
L Jur.
M Jur.
U Jur.
Lower Cretaceous
U Crt.
Plc.
Eocene
Oli.
Mio.
Depth [ft.]
0
5000
10000
15000
20000
25000
Time [Ma]
400
300
200
100
0
1.00
2.00
3.00
4.00
5.00
Vitrinite Reflectance [%Ro]
Surface
Middle Atoka (Areci)
Top Lower Atoka (Bynum)
Top Orr (Lower Atoka)
Top Morrowan
Boone (Mississippian-Osagean)
Simpson Group (St. Peter, Everton - Ordovician)

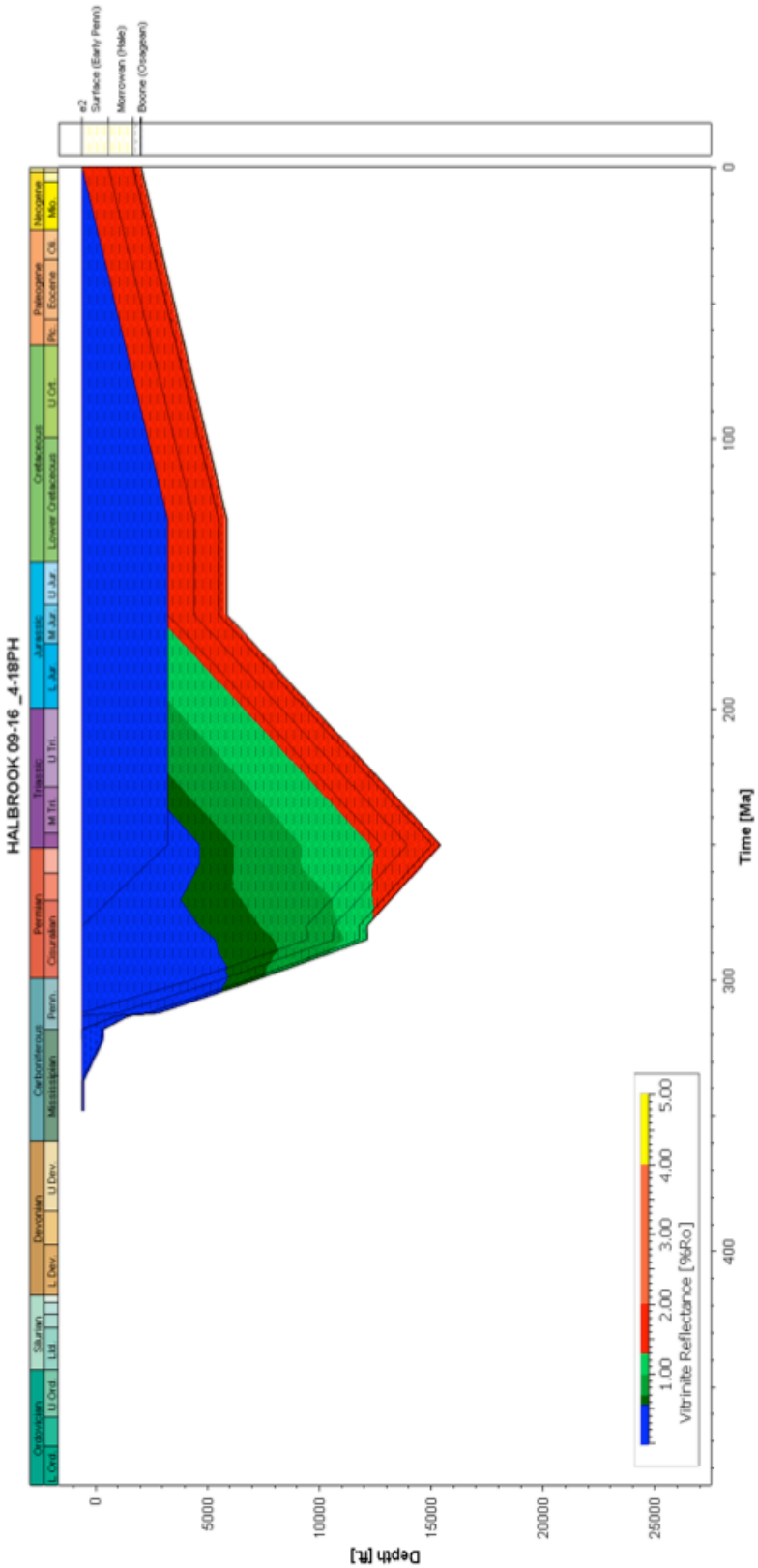
HALBROOK 09-16 _4-18PH
Ordovician
Silurian
Devonian
Carboniferous
Permian
Triassic
Jurassic
Cretaceous
Paleogene
Neogene
L Ord
U Ord
LM
L Dev
U Dev
Mississippian
Penn
Guadalupian
M Tri
U Tri
L Jur
M Jur
U Jur
Lower Cretaceous
U Cret
Pc
Eocene
Ol
Mio
Surface (Early Penn)
Morrowan (Hale)
Boone (Osagean)
Depth [ft]
0
5000
10000
15000
20000
25000
Time [Ma]
0
100
200
300
400
Vitrinite Reflectance [%Ro]
1.00
2.00
3.00
4.00
5.00

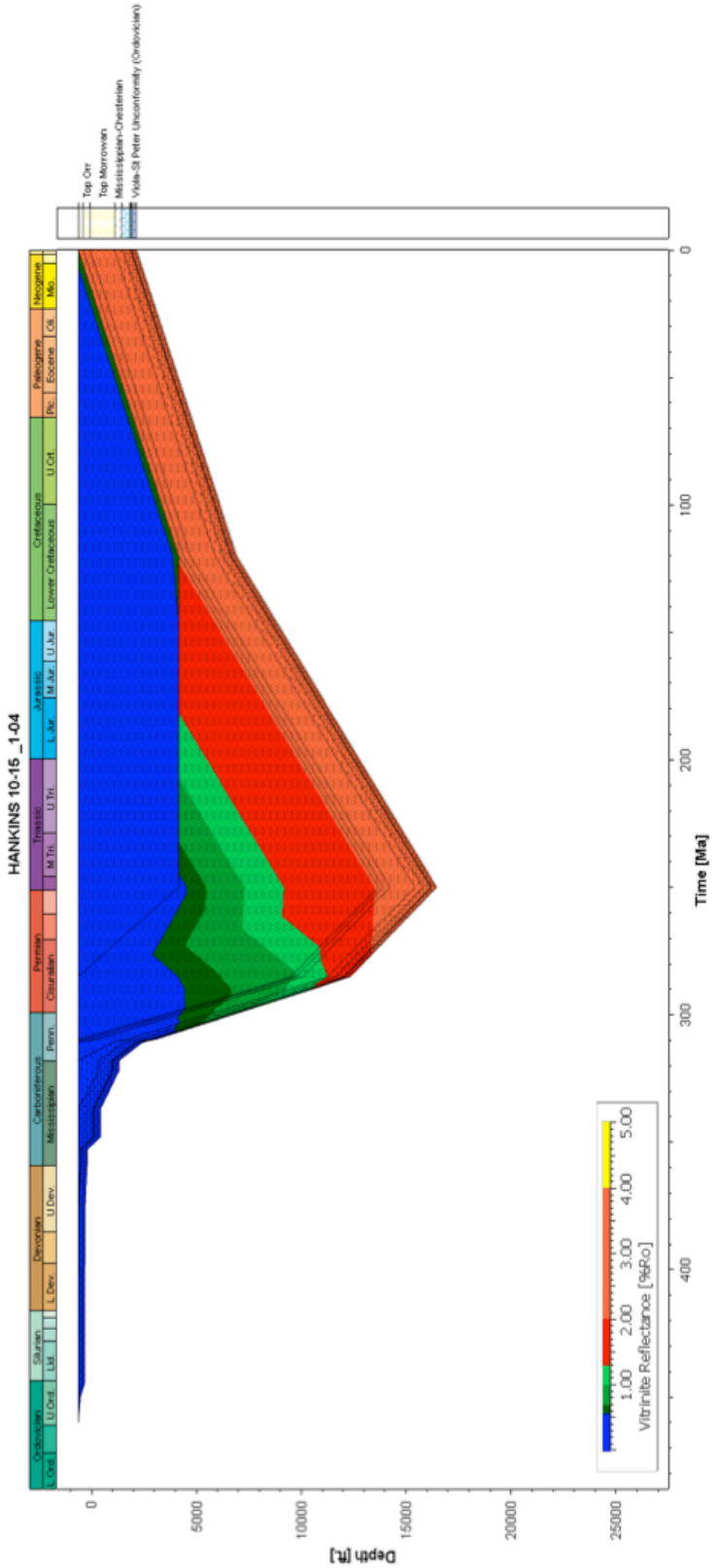
HANKINS 10-15 _1-04
Top Orr
Top Morrowan
Mississippian-Chesterian
Viola-St Peter Unconformity (Ordovician)
Ordovician
Silurian
Devonian
Carboniferous
Permian
Triassic
Jurassic
Cretaceous
Paleogene
Neogene
L Ord.
U Ord.
Ltd.
L Dev.
U Dev.
Mississippian
Penn.
Cisuralian
M Tri.
U Tri.
L Jur.
M Jur.
U Jur.
Lower Cretaceous
U Cret.
Pic.
Eocene
Oli.
Mio.
Time [Ma]
0
100
200
300
400
Depth [ft.]
0
5000
10000
15000
20000
25000
1.00
2.00
3.00
4.00
5.00
Vitrinite Reflectance [%Ro]

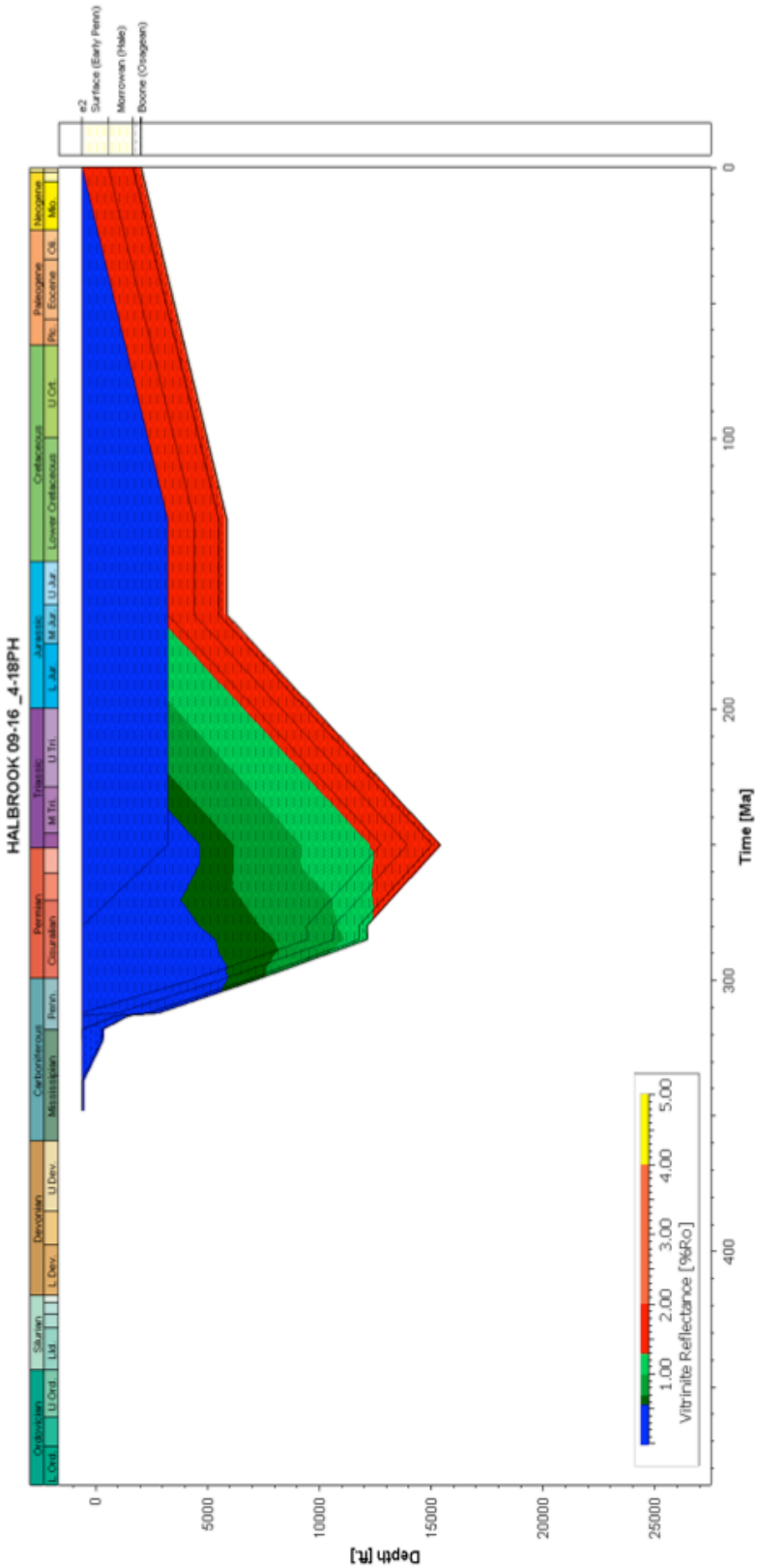
HALBROOK 09-16 _4-18PH
Ordovician
Silurian
Devonian
Carboniferous
Permian
Triassic
Jurassic
Cretaceous
Paleogene
Neogene
L Ord
U Ord
LM
L Dev
U Dev
Mississippian
Penn
Guadalupian
M Tri
U Tri
L Jur
M Jur
U Jur
Lower Cretaceous
U Cret
Pc
Eocene
Ol
Mio
Surface (Early Penn)
Morrowan (Hale)
Boone (Osagean)
Time [Ma]
Depth [ft]
Vitrinite Reflectance [%Ro]
1.00
2.00
3.00
4.00
5.00
0
5000
10000
15000
20000
25000
100
200
300
400

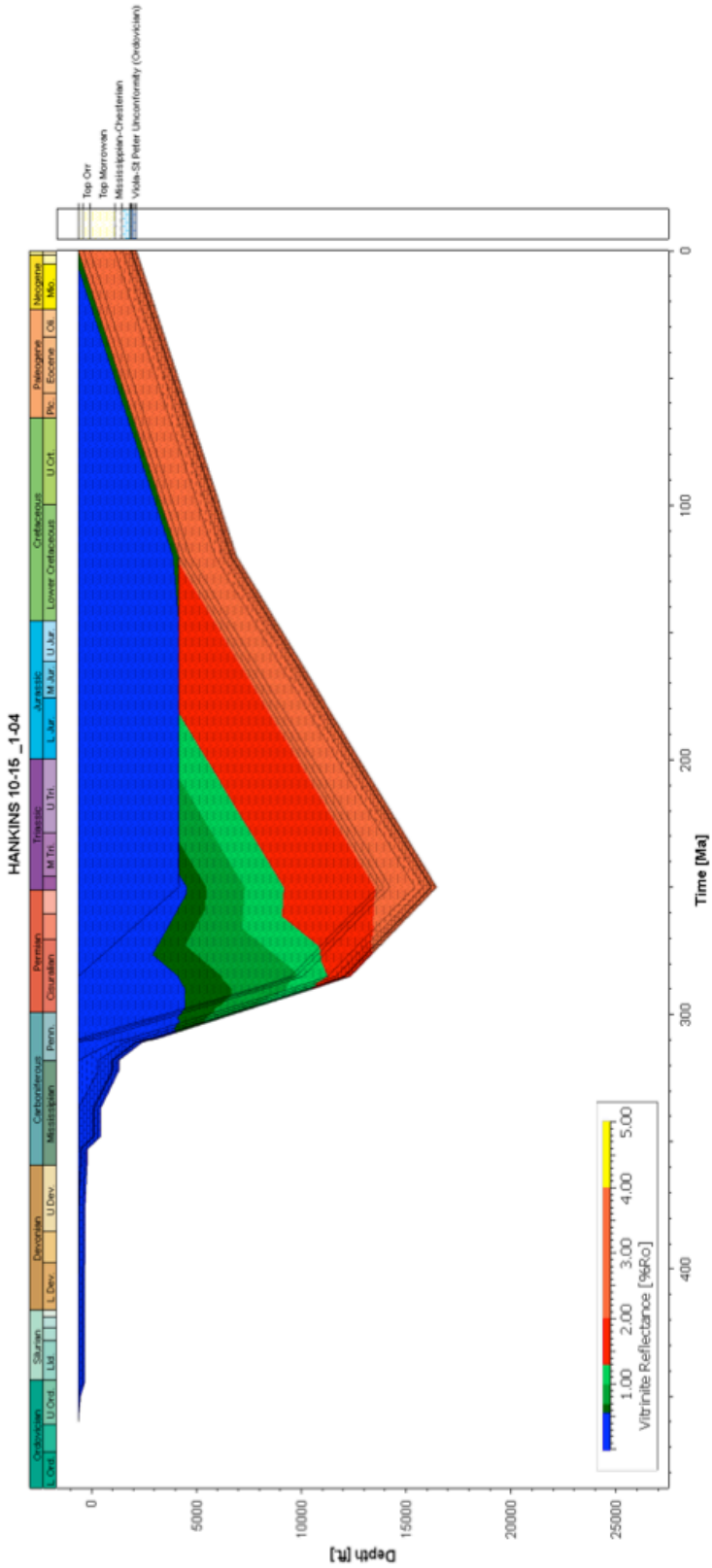
HANKINS 10-15 _1-04
Top Orr
Top Morrowan
Mississippian-Chesterian
Viola-St Peter Unconformity (Ordovician)
Ordovician
Silurian
Devonian
Carboniferous
Permian
Triassic
Jurassic
Cretaceous
Paleogene
Neogene
L Ord.
U Ord.
Ltd.
L Dev.
U Dev.
Mississippian
Penn.
Cisuralian
M Tri.
U Tri.
L Jur.
M Jur.
U Jur.
Lower Cretaceous
U Crt.
Plic.
Eocene
Oli.
Mio.
Depth [ft.]
0
5000
10000
15000
20000
25000
Time [Ma]
0
100
200
300
400
1.00
2.00
3.00
4.00
5.00
Vitrinite Reflectance [%Ro]

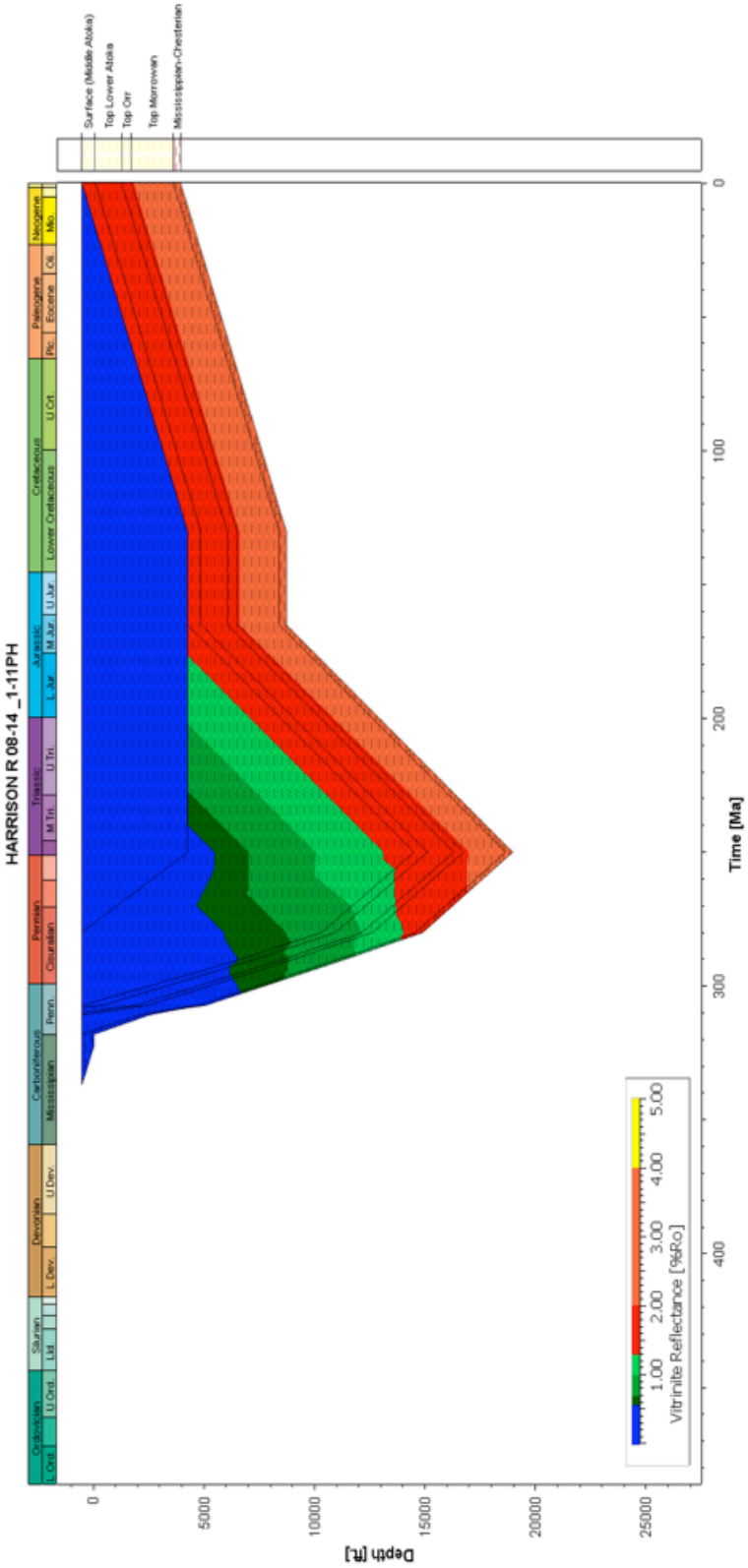
HARRISON R 08-14 _1-11PH
Surface (Middle Atoka)
Top Lower Atoka
Top Orr
Top Morrowan
Mississippian-Chesterian
Ordovician
Silurian
Devonian
Carboniferous
Permian
Triassic
Jurassic
Cretaceous
Paleogene
Neogene
L Ord
U Ord
Ltd
L Dev
U Dev
Mississippian
Penn
Cisuralian
M Tri
U Tri
L Jur
M Jur
U Jur
Lower Cretaceous
U Cret
Plc
Eocene
Ol
Mio
Time [Ma]
0
100
200
300
400
Depth [ft]
0
5000
10000
15000
20000
25000
Vitrinite Reflectance [%Ro]
1.00
2.00
3.00
4.00
5.00

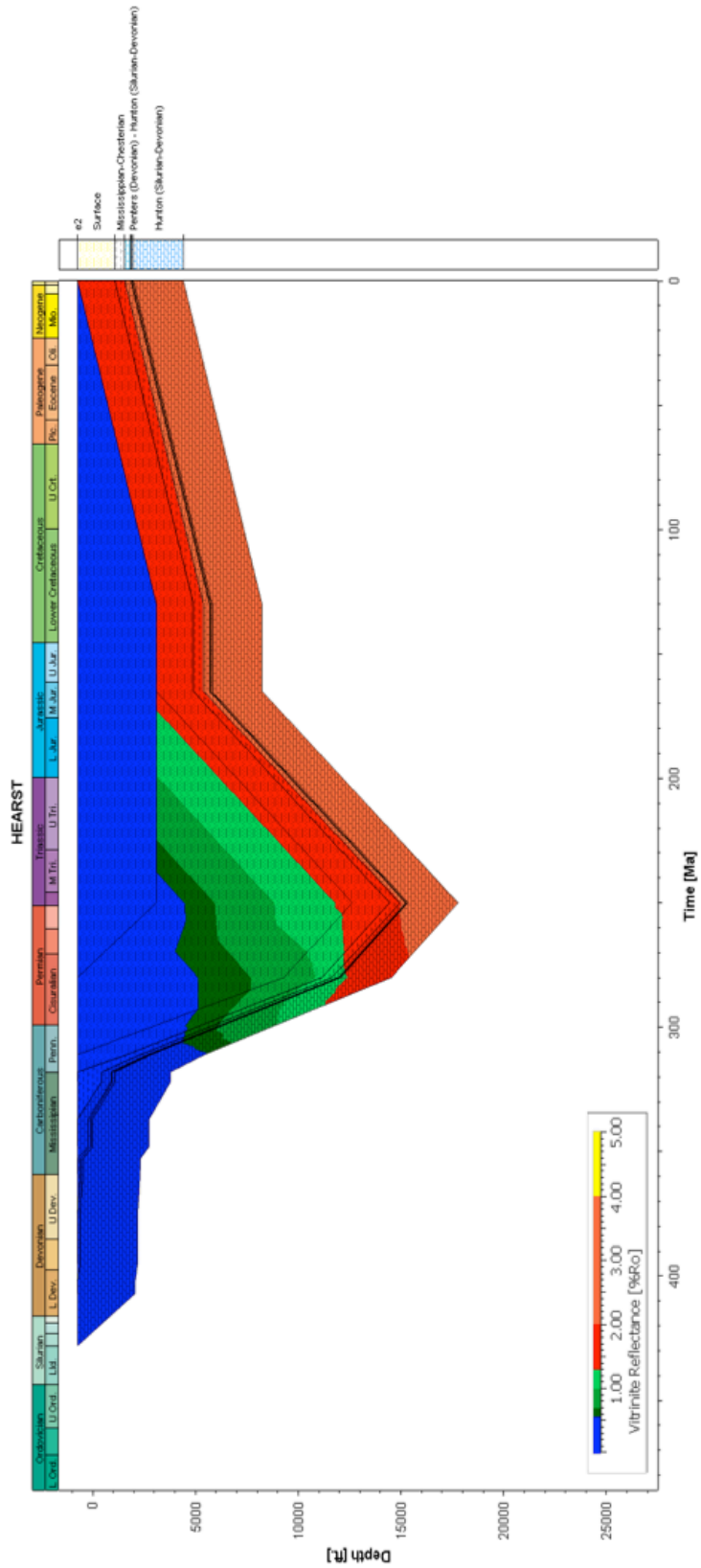
HEARST
Ordovician
Silurian
Devonian
Carboniferous
Permian
Triassic
Jurassic
Cretaceous
Paleogene
Neogene
L Ord.
U Ord.
Ltd.
L Dev.
U Dev.
Mississippian
Penn.
Cisuralian
M Tri.
U Tri.
L Jur.
M Jur.
U Jur.
Lower Cretaceous
U Cret.
Pc.
Eocene
Olig.
Mio.
e2
Surface
Mississippian-Chesterian
Penters (Devonian) - Hunton (Silurian-Devonian)
Hunton (Silurian-Devonian)
Vitrinite Reflectance [%Ro]
1.00
2.00
3.00
4.00
5.00
Depth [ft]
0
5000
10000
15000
20000
25000
Time [Ma]
0
100
200
300
400

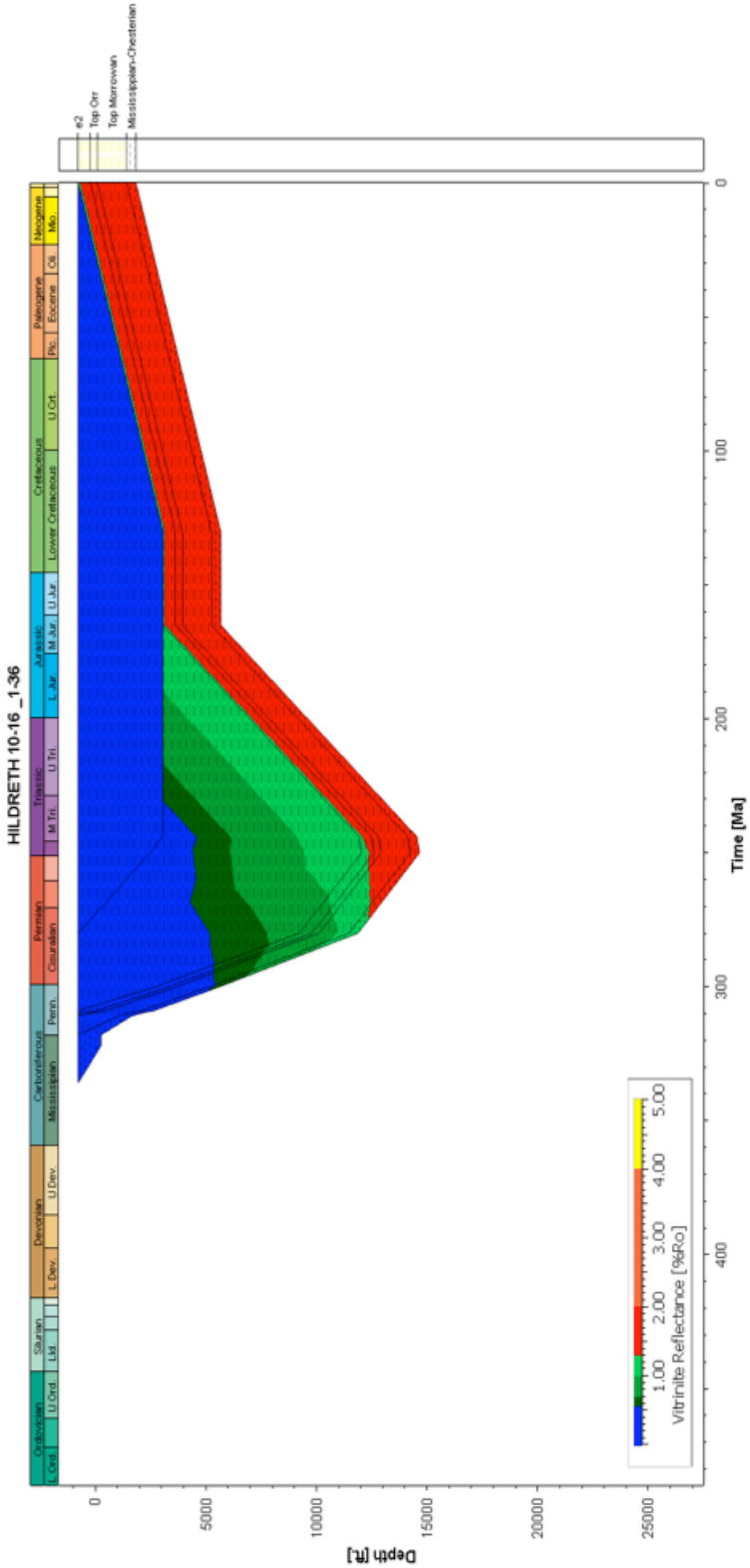
HILDRETH 10-16 _1-36
Ordovician
L Ord.
U Ord.
Silurian
Ltd.
Devonian
L Dev.
U Dev.
Carboniferous
Mississippian
Penn.
Permian
Cisuralian
Triassic
M Tri.
U Tri.
Jurassic
L Jur.
M Jur.
U Jur.
Cretaceous
Lower Cretaceous
U Crt.
Paleogene
Plc.
Eocene
Oli.
Neogene
Mio.
e2
Top Orr
Top Morrowan
Mississippian-Chesterian
Vitrinite Reflectance [%Ro]
1.00
2.00
3.00
4.00
5.00
Time [Ma]
0
100
200
300
400
Depth [ft]
0
5000
10000
15000
20000
25000

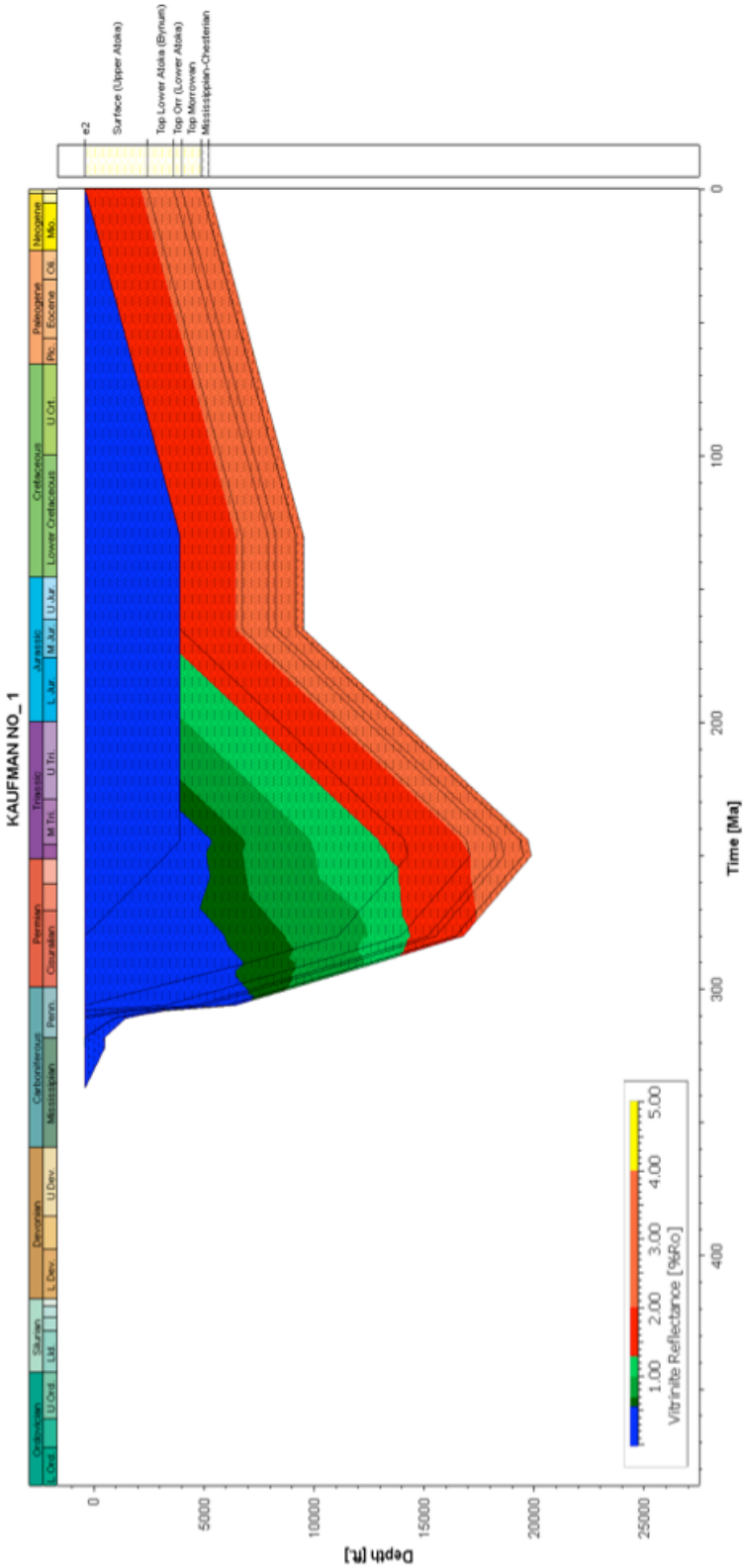
KAUFMAN NO_1
e2
Surface (Upper Atoka)
Top Lower Atoka (Bynum)
Top Orr (Lower Atoka)
Top Morrowan
Mississippian-Chesterian
Ordovician
L Ord.
U Ord.
Silurian
Ltd.
L Dev.
Devonian
U Dev.
Carboniferous
Mississippian
Penn.
Permian
Cisuralian
Triassic
M Tri.
U Tri.
Jurassic
L Jur.
M Jur.
U Jur.
Cretaceous
Lower Cretaceous
U Cret.
Paleogene
Pic.
Eocene
Oli.
Neogene
Mio.
Time [Ma]
0
100
200
300
400
Depth [ft]
0
5000
10000
15000
20000
25000
Vitrinite Reflectance [%Ro]
1.00
2.00
3.00
4.00
5.00

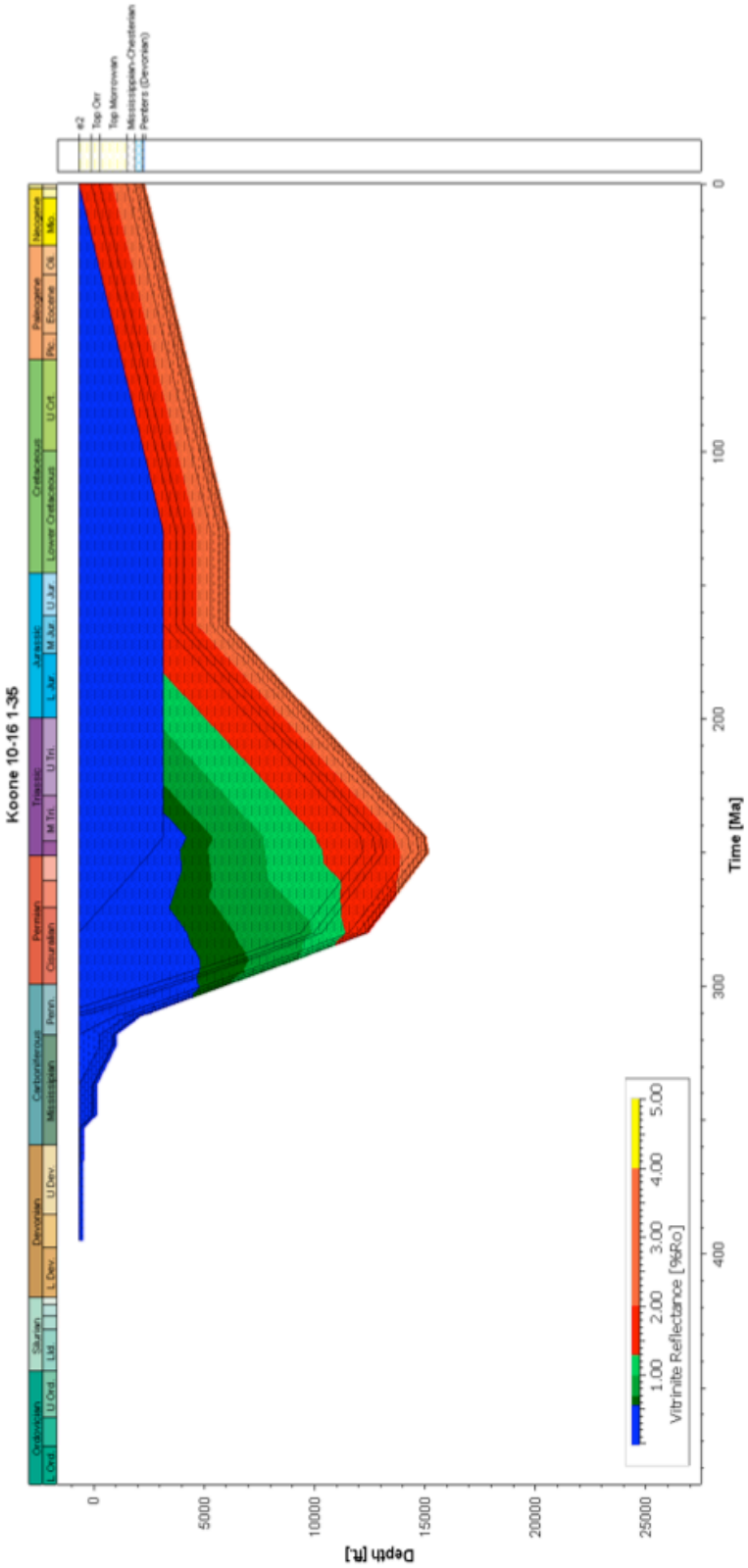
Koone 10-16 1-35
Ordovician
L Ord.
U Ord.
Silurian
Ltl.
L Dev.
Devonian
U Dev.
Carboniferous
Mississippian
Penn.
Permian
Cisuralian
Triassic
M Tri.
U Tri.
Jurassic
L Jur.
M Jur.
U Jur.
Cretaceous
Lower Cretaceous
U Cr.
Paleogene
Pic.
Eocene
Ol.
Neogene
Mio.
e2
Top Orr
Top Morrowan
Mississippian-Chesterian
Perters (Devonian)
Time [Ma]
0
100
200
300
400
Depth [ft]
0
5000
10000
15000
20000
25000
Vitrinite Reflectance [%Ro]
1.00
2.00
3.00
4.00
5.00

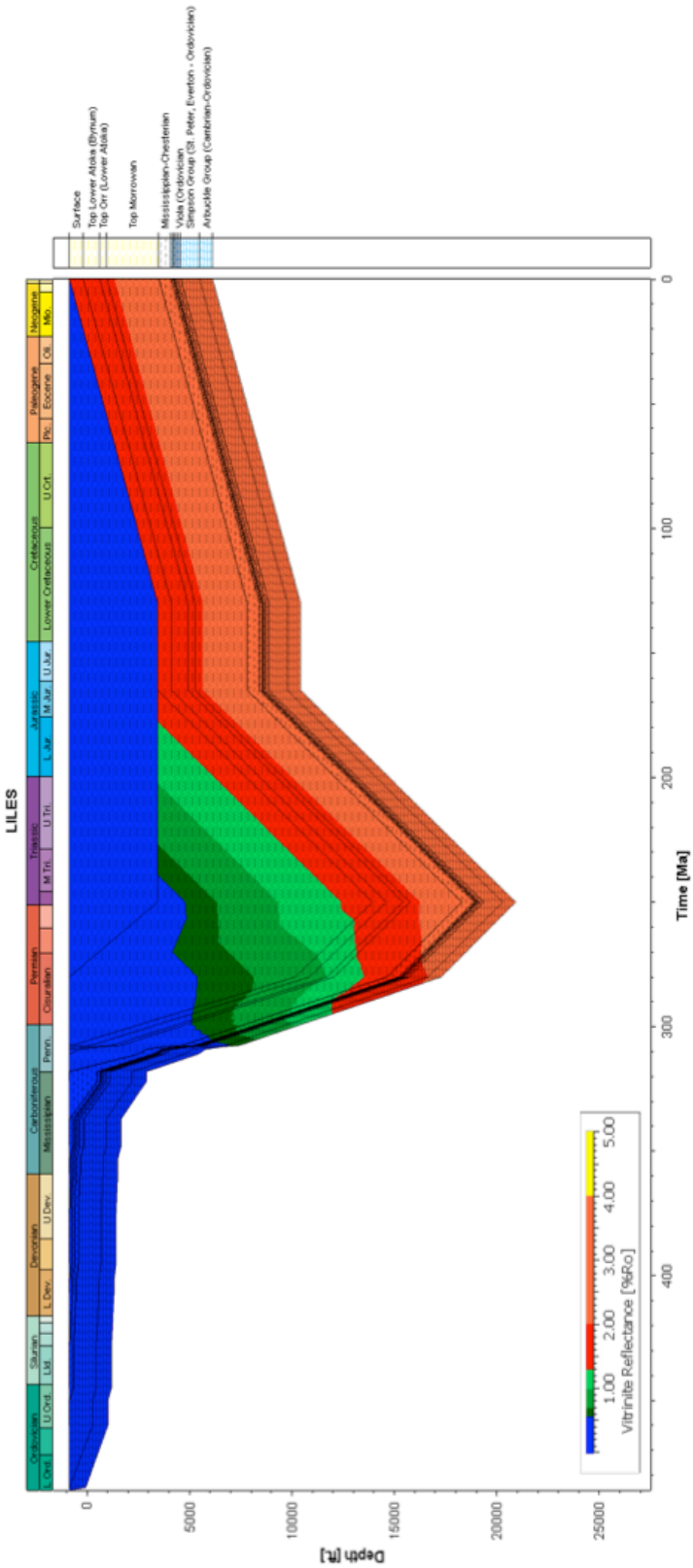
LILES
Surface
Top Lower Atoka (Bynum)
Top Orr (Lower Atoka)
Top Morrowan
Mississippian-Chesterian
Viola (Ordovician
Simpson Group (St. Peter, Everton - Ordovician)
Arbuckle Group (Cambrian-Ordovician)
Ordovician
Silurian
Devonian
Carboniferous
Permian
Triassic
Jurassic
Cretaceous
Paleogene
Neogene
L Ord.
U Ord.
Ltd.
L Dev.
U Dev.
Mississippian
Penn.
Cisuralian
M Tri.
U Tri.
L Jur.
M Jur.
U Jur.
Lower Cretaceous
U Cret.
Pc.
Eocene
Olig.
Mio.
Time [Ma]
Depth [ft]
0
5000
10000
15000
20000
25000
0
100
200
300
400
Vitrinite Reflectance [%Ro]
1.00
2.00
3.00
4.00
5.00

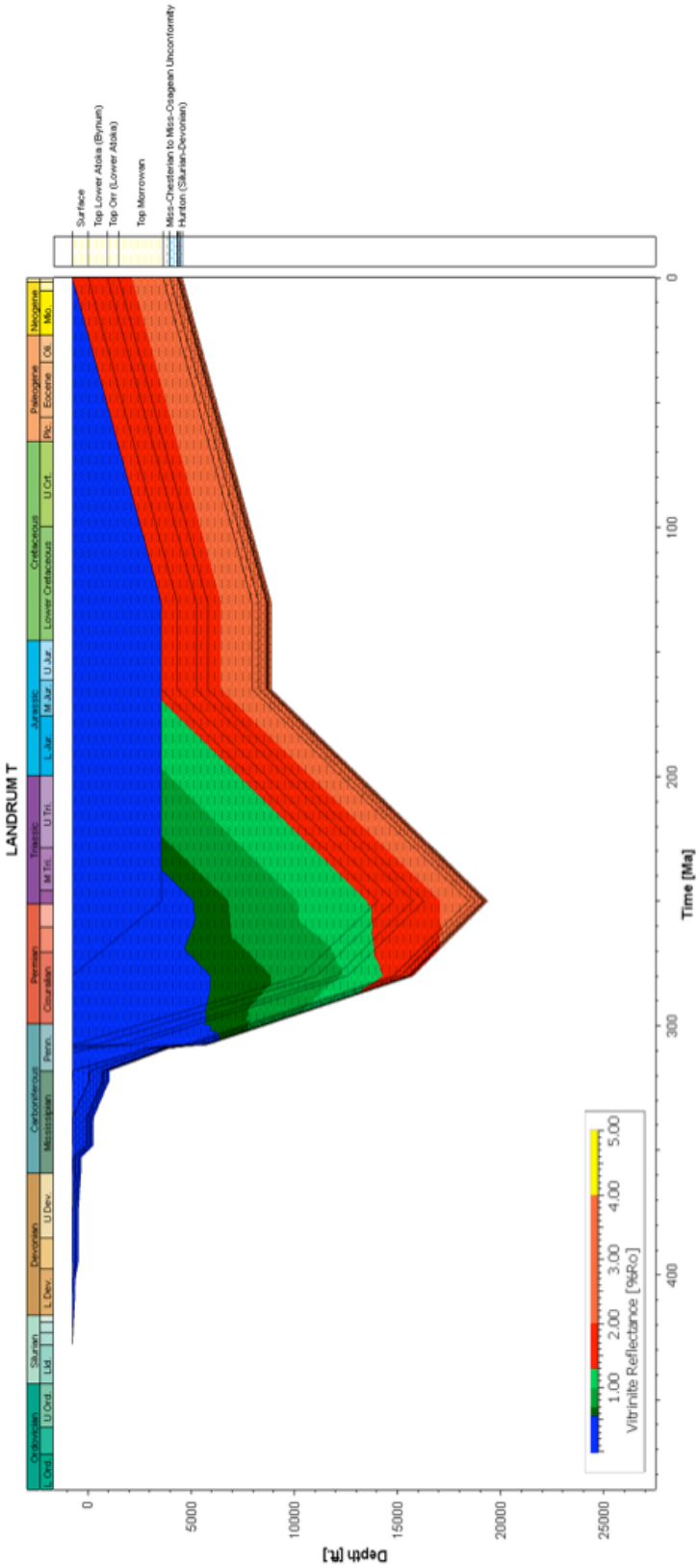
LANDRUM T
Surface
Top Lower Atoka (Bynum)
Top Orr (Lower Atoka)
Top Morrowan
Miss-Chesterian to Miss-Osagean Unconformity
Hunton (Silurian-Devonian)
Ordovician
Silurian
Devonian
Carboniferous
Permian
Triassic
Jurassic
Cretaceous
Paleogene
Neogene
L Ord
U Ord
Lsl
L Dev
U Dev
Mississippian
Penn.
Cisuralian
M Tri
U Tri
L Jur
M Jur
U Jur
Lower Cretaceous
U Crt
Plc
Eocene
Olig
Mio
Vitrinite Reflectance [%Ro]
1.00
2.00
3.00
4.00
5.00
Depth [ft]
0
5000
10000
15000
20000
25000
Time [Ma]
0
100
200
300
400

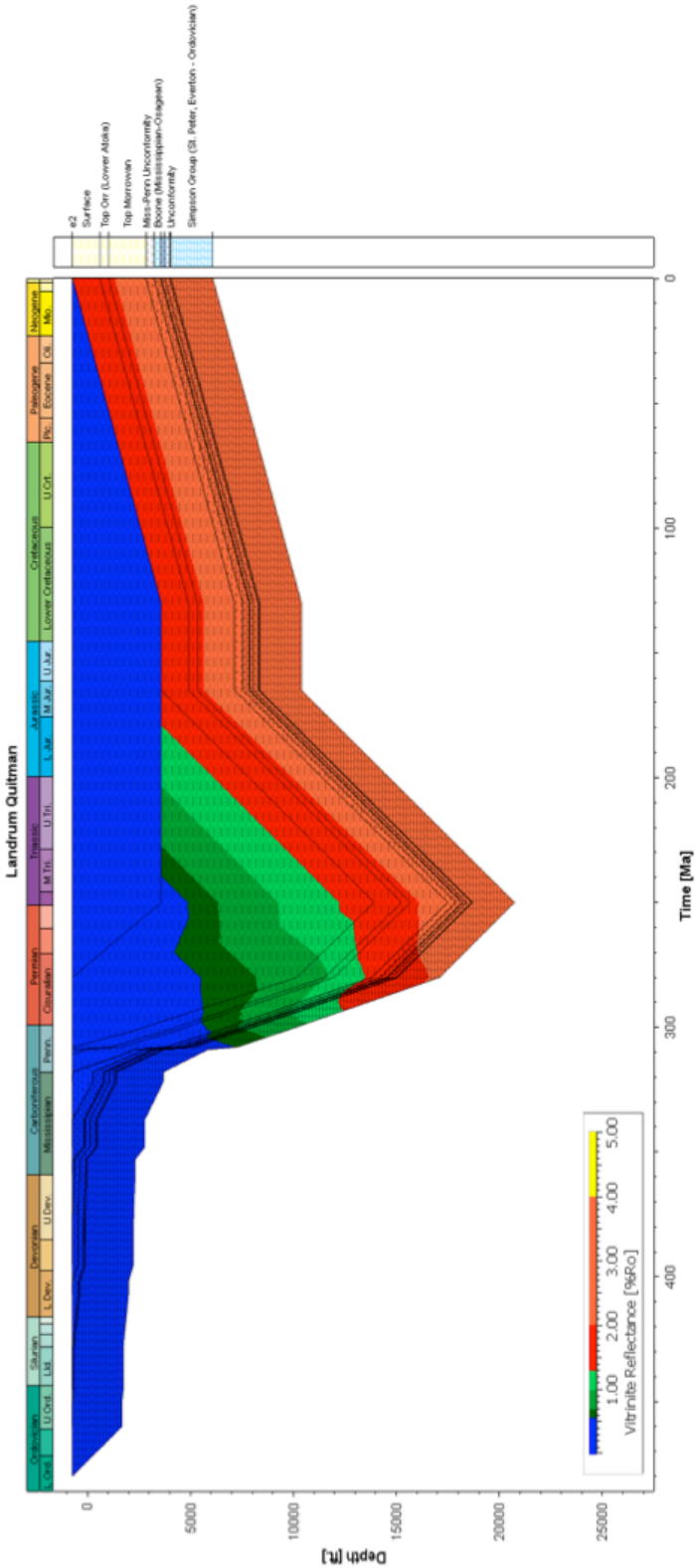
Landrum Quitman
Ordovician
Ord.
U.Ord.
Silurian
Ltd.
L.Dev.
Devonian
U.Dev.
Carboniferous
Mississippian
Penn.
Permian
Cisuralian
Triassic
M.Tri.
U.Tri.
Jurassic
L.Jur.
M.Jur.
U.Jur.
Cretaceous
Lower Cretaceous
U.Cret.
Paleogene
Pc.
Eocene
Ol.
Neogene
Mio.
e2
Surface
Top Orr (Lower Atoka)
Top Morrowan
Miss-Penn Unconformity
Boone (Mississippian-Osagean)
Unconformity
Simpson Group (St. Peter, Everton - Ordovician)
Depth [ft]
0
5000
10000
15000
20000
25000
Time [Ma]
0
100
200
300
400
Vitrinite Reflectance [%Ro]
1.00
2.00
3.00
4.00
5.00

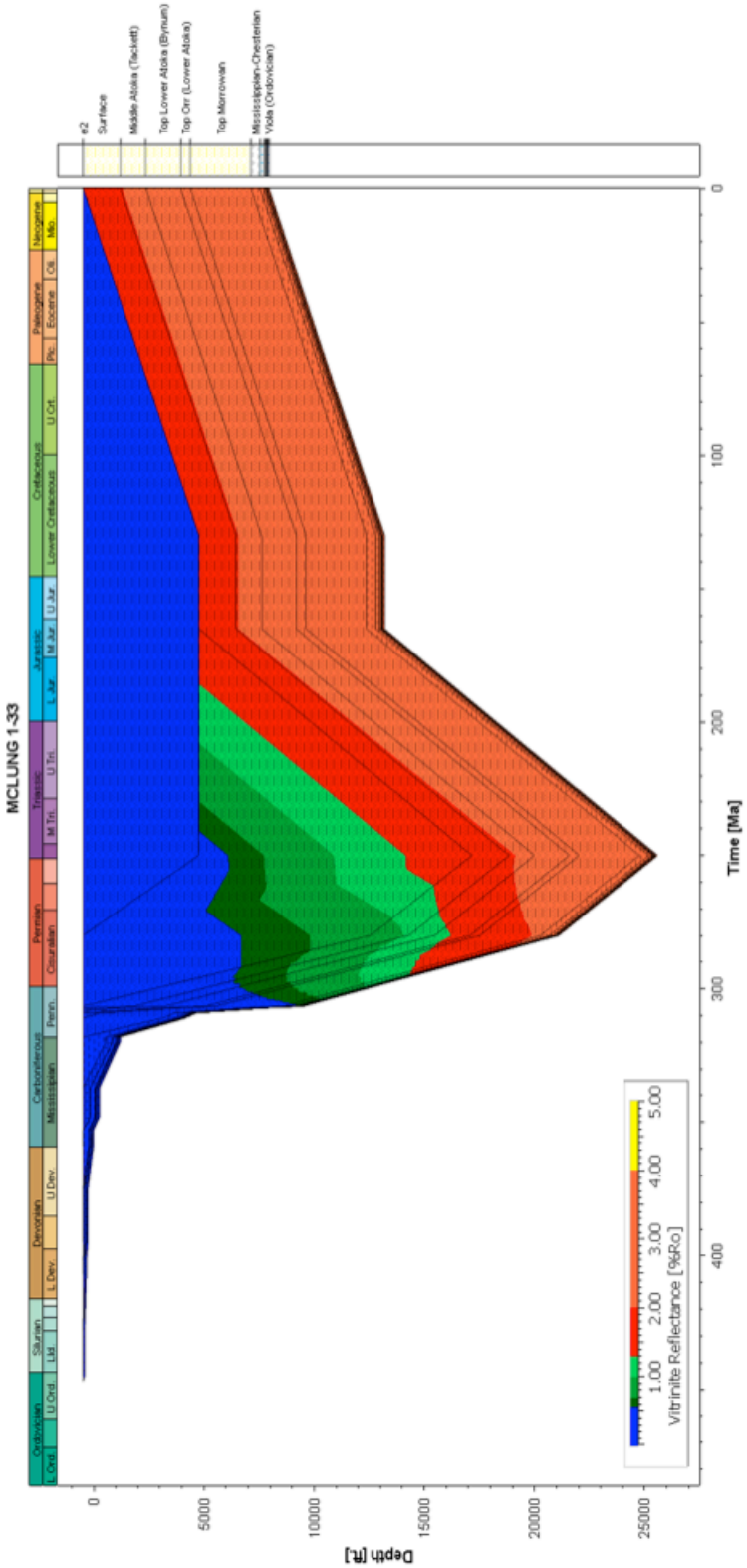
MCLUNG 1-33
e2
Surface
Middle Atoka (Tackett)
Top Lower Atoka (Bynum)
Top Orr (Lower Atoka)
Top Morrowan
Mississippian-Chesterian
Viola (Ordovician)
Ordovician
L Ord.
U Ord.
Silurian
Ltd.
Devonian
L Dev.
U Dev.
Carboniferous
Mississippian
Penn.
Permian
Cisuralian
Triassic
M Tri.
U Tri.
Jurassic
L Jur.
M Jur.
U Jur.
Cretaceous
Lower Cretaceous
U Cret.
Paleogene
Pic.
Eocene
Oli.
Neogene
Mio.
Time [Ma]
Depth [ft]
0
5000
10000
15000
20000
25000
100
200
300
400
Vitrinite Reflectance [%Ro]
1.00
2.00
3.00
4.00
5.00

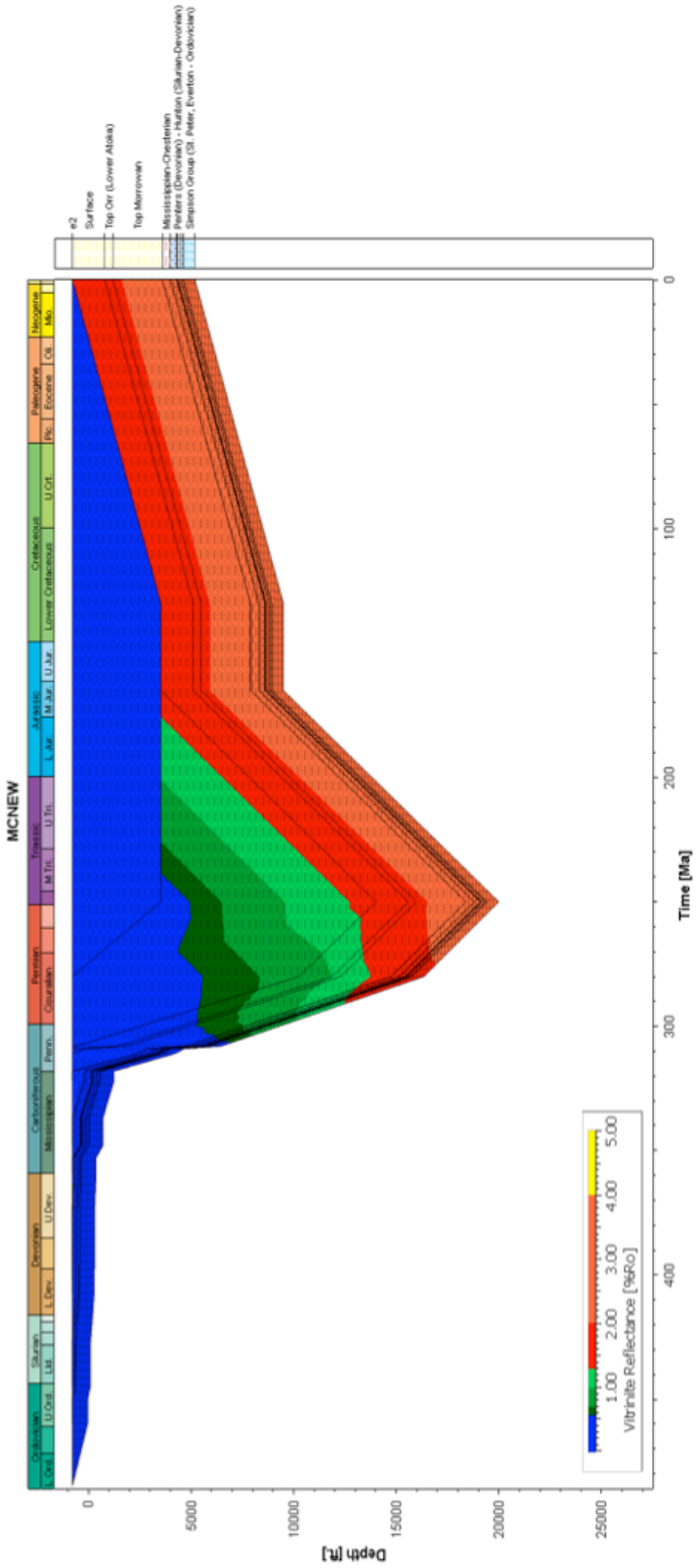
MCNEW
Ordovician
Silurian
Devonian
Carboniferous
Permian
Triassic
Jurassic
Cretaceous
Paleogene
Neogene
L Ord.
U Ord.
Ltl
L Dev.
U Dev.
Mississippian
Penn.
Cisuralian
M Tri.
U Tri.
L Jur.
M Jur.
U Jur.
Lower Cretaceous
U Cret.
Plc.
Eocene
Oli.
Mio.
e2
Surface
Top Orr (Lower Atoka)
Top Morrowan
Mississippian-Chesterian
Red River (Trenton-Ellenburger) Platten (Silurian-Devonian)
Simpson Group (St. Peter, Everton - Ordovician)
Time [Ma]
Depth [ft]
Vitrinite Reflectance [%Ro]
1.00
2.00
3.00
4.00
5.00

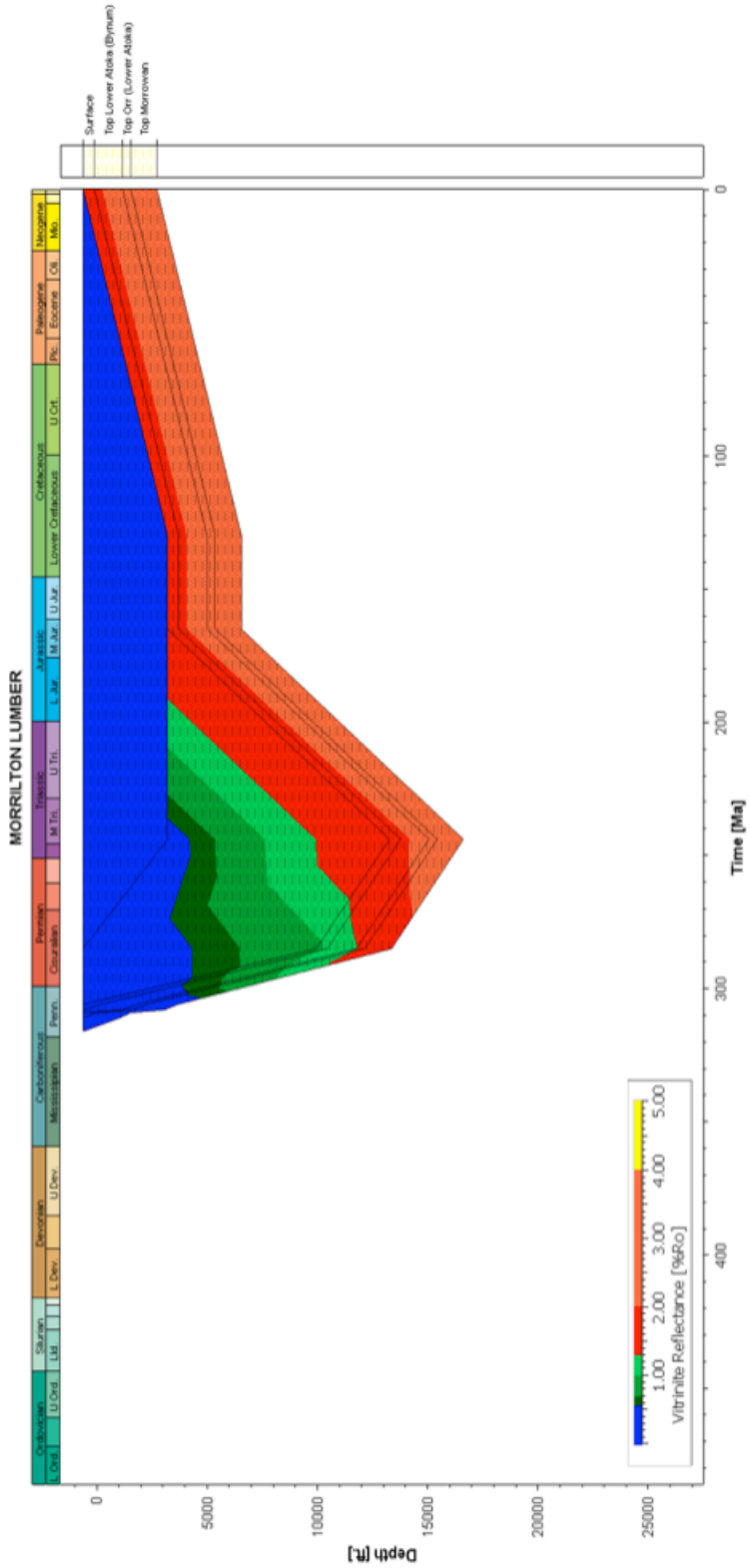
MORRILTON LUMBER
Surface
Top Lower Atoka (Bynum)
Top Orr (Lower Atoka)
Top Morrowan
Ordovician
Silurian
Devonian
Carboniferous
Permian
Triassic
Jurassic
Cretaceous
Paleogene
Neogene
L. Ord.
U. Ord.
Ltd.
L. Dev.
U. Dev.
Mississippian
Penn.
Cisuralian
M. Tri.
U. Tri.
L. Jur.
M. Jur.
U. Jur.
Lower Cretaceous
U. Cret.
Pic.
Eocene
Oli.
Mio.
Time [Ma]
0
100
200
300
400
Depth [ft]
0
5000
10000
15000
20000
25000
1.00
2.00
3.00
4.00
5.00
Vitrinite Reflectance [%Ro]

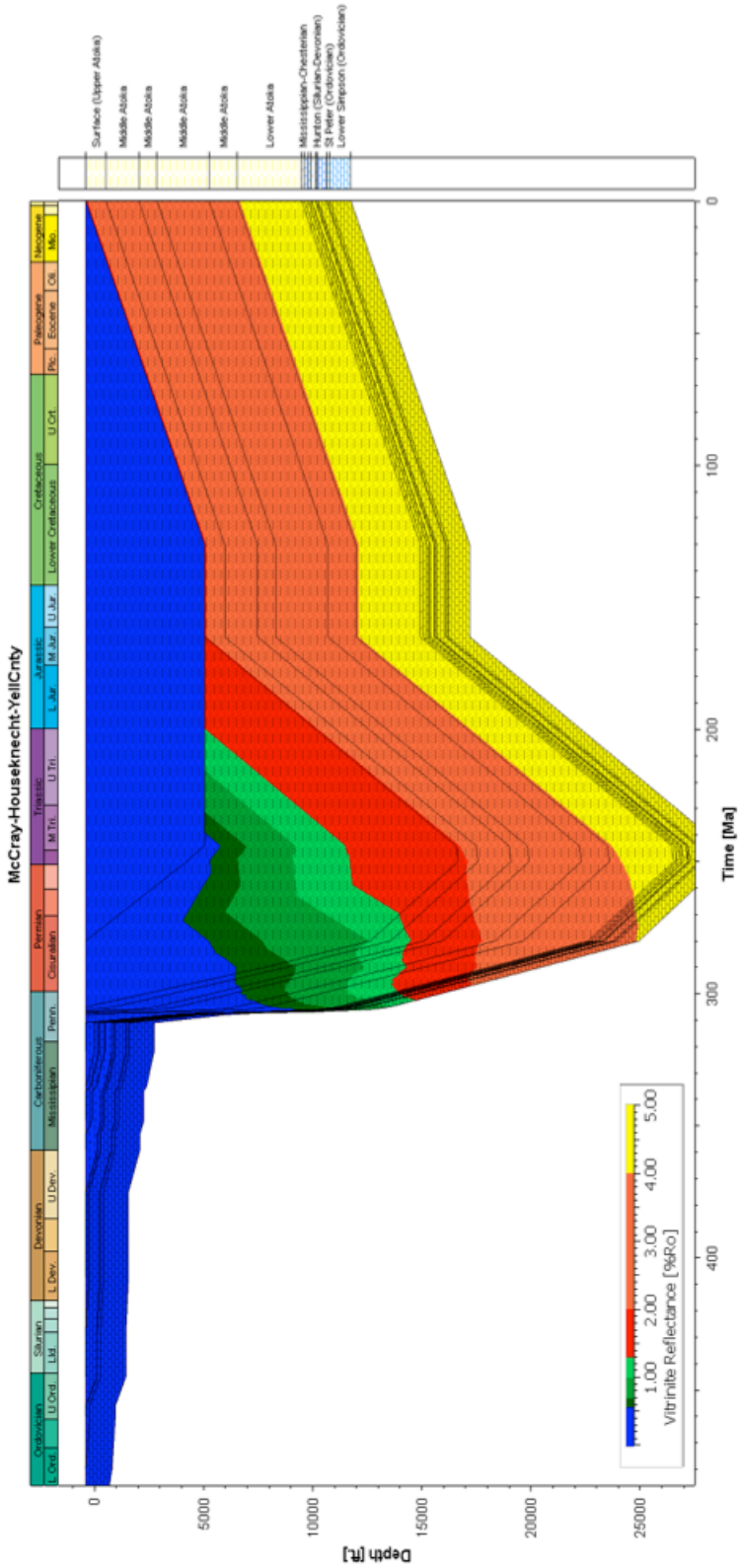
McCray-Houseknecht-YellCnty
Surface (Upper Atoka)
Middle Atoka
Middle Atoka
Middle Atoka
Middle Atoka
Lower Atoka
Mississippian-Chesterian
Hunton (Silurian-Devonian)
Sylvan (Ordovician)
Lower Simpson (Ordovician)
Ordovician
Silurian
Devonian
Carboniferous
Permian
Triassic
Jurassic
Cretaceous
Paleogene
Neogene
L Ord
U Ord
Ltd
L Dev
U Dev
Mississippian
Penn
Cisuralian
M Tri
U Tri
L Jur
M Jur
U Jur
Lower Cretaceous
U Crt
Pc.
Eocene
Ole
Mio
Time [Ma]
0
100
200
300
400
Depth [ft]
0
5000
10000
15000
20000
25000
Vitrinite Reflectance [%Ro]
1.00
2.00
3.00
4.00
5.00

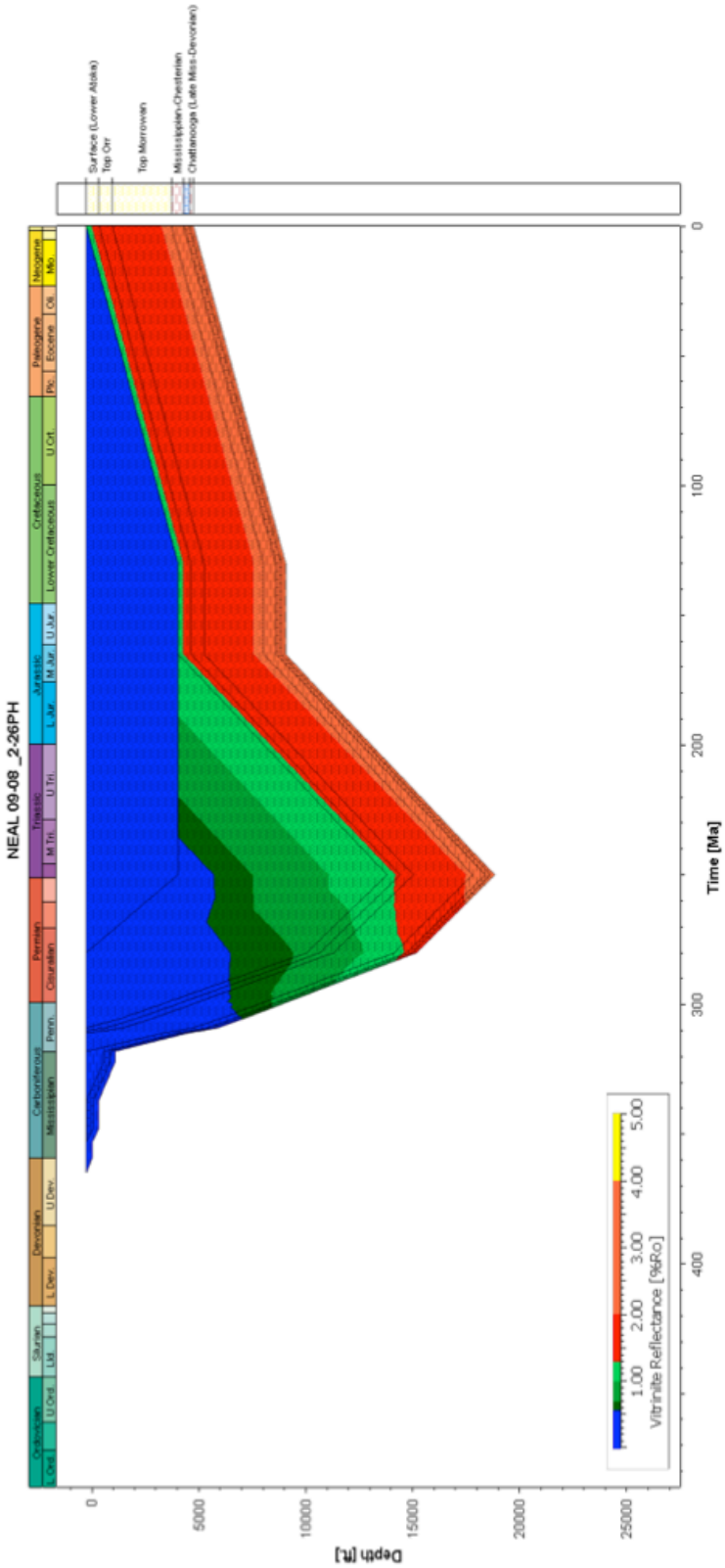
NEAL 09-08 _2-26PH
Surface (Lower Atoka)
Top Orr
Top Morrowan
Mississippian-Chesterian
Chattanooga (Late Miss-Devonian)
Ordovician
Silurian
Devonian
Carboniferous
Permian
Triassic
Jurassic
Cretaceous
Paleogene
Neogene
L Ord
U Ord
Ltl
L Dev
U Dev
Mississippian
Penn.
Cisuralian
M Tri.
U Tri.
L Jur.
M Jur.
U Jur.
Lower Cretaceous
U Cret.
Pc.
Eocene
Ol.
Mio.
Depth [ft]
0
5000
10000
15000
20000
25000
Time [Ma]
0
100
200
300
400
Vitrinite Reflectance [%Ro]
1.00
2.00
3.00
4.00
5.00

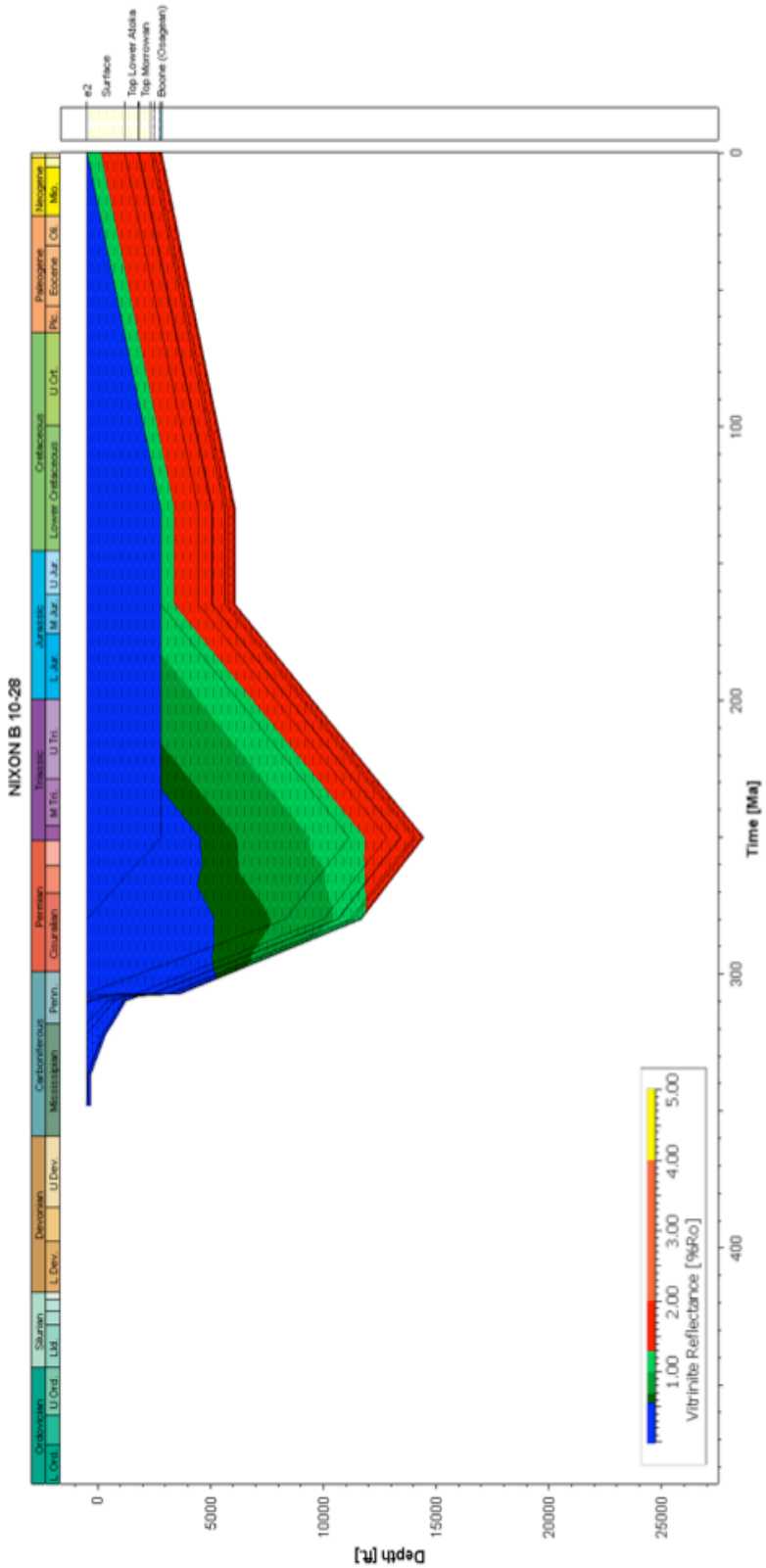
NIXON B 10-28
Ordovician
L Ord
U Ord
Silurian
Ltl
L Dev
Devonian
U Dev
Carboniferous
Mississippian
Penn.
Permian
Cisuralian
Triassic
M Tri
U Tri
Jurassic
L Jur
M Jur
U Jur
Cretaceous
Lower Cretaceous
U Crt
Paleogene
Pc.
Eocene
Ol.
Neogene
Mio
ss2
Surface
Top Lower Atoka
Top Morrowan
Boone (Osagean)
Vitrinite Reflectance [%Ro]
1.00
2.00
3.00
4.00
5.00
Time [Ma]
0
100
200
300
400
Depth [ft.]
0
5000
10000
15000
20000
25000

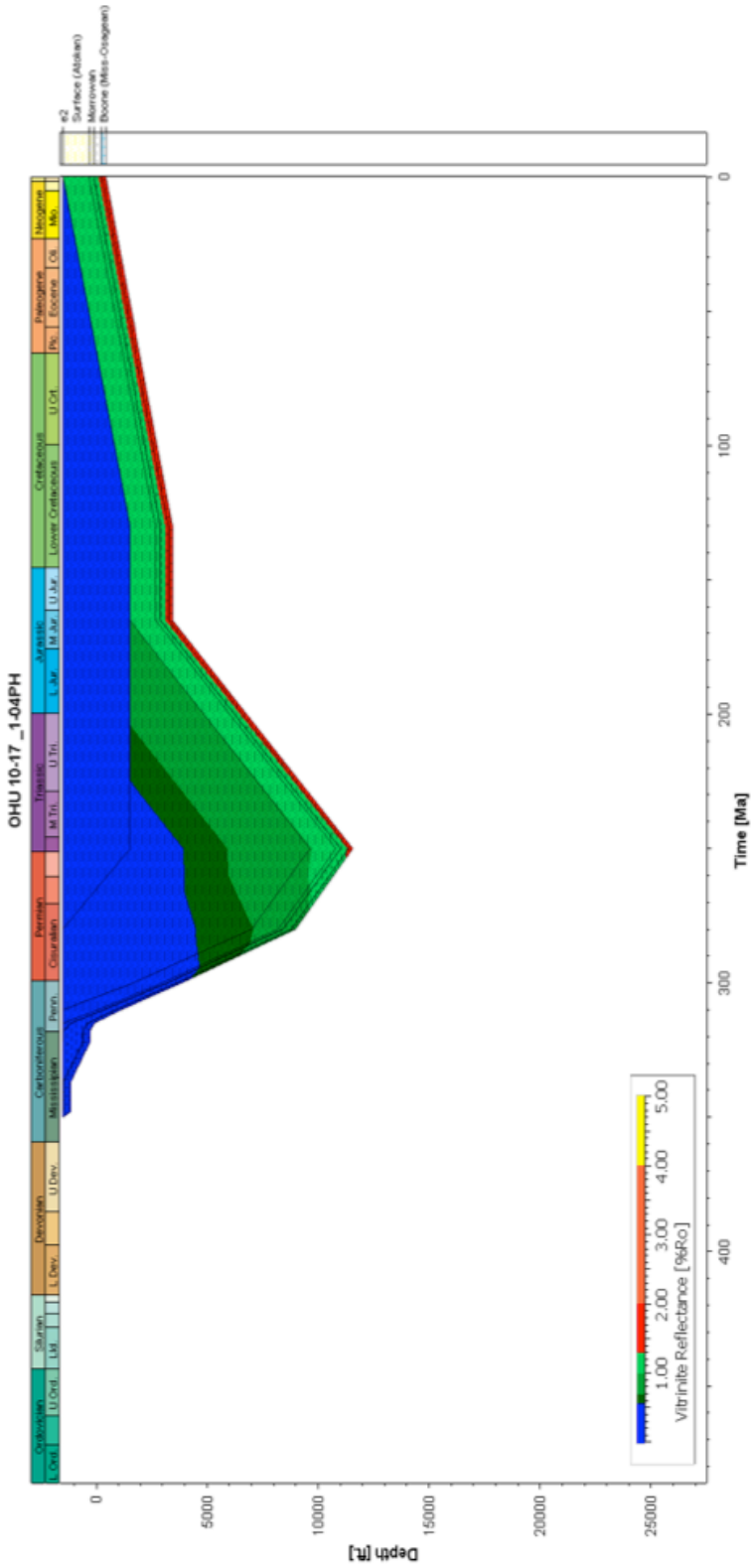
OHU 10-17 _1-04PH
Ordovician
L Ord
U Ord
Silurian
L Sil
L Dev
Devonian
U Dev
Carboniferous
Mississippian
Penn
Permian
Cisuralian
M Tri
Triassic
U Tri
L Jur
Jurassic
M Jur
U Jur
Cretaceous
Lower Cretaceous
U Cret
Paleogene
Pa
Eocene
Ol
Neogene
Mio
e2
Surface (Alluvium)
Morrowan
Boone (Miss-Osagean)
Time [Ma]
0
100
200
300
400
Depth [ft]
0
5000
10000
15000
20000
25000
Vitrinite Reflectance [%Ro]
1.00
2.00
3.00
4.00
5.00

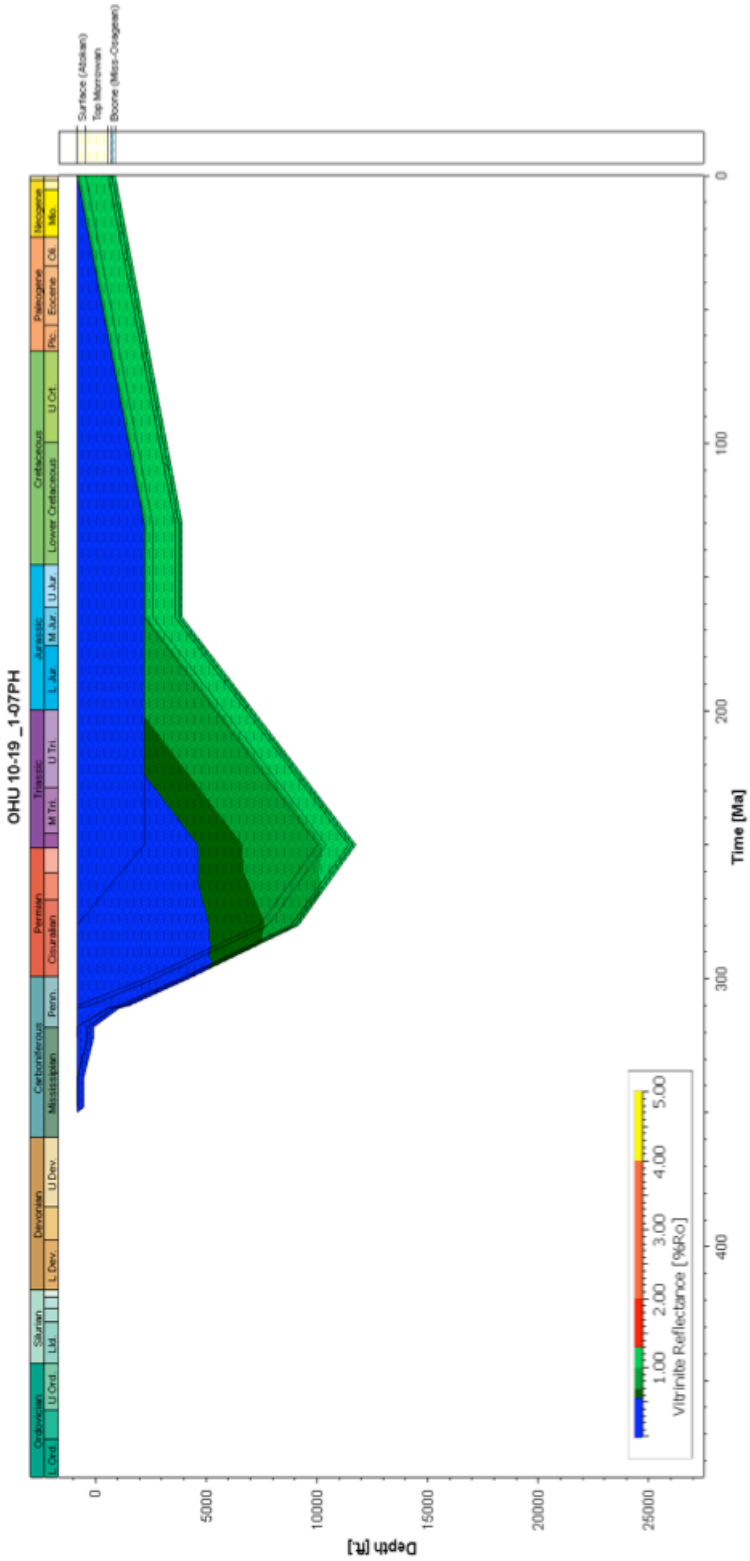
OHU 10-19 _1-07PH
Surface (Alcian)
Top Morrowan
Boone (Miss-Osagean)
Ordovician
Silurian
Devonian
Carboniferous
Permian
Triassic
Jurassic
Cretaceous
Paleogene
Neogene
L Ord.
U Ord.
Ltd.
L Dev.
U Dev.
Mississippian
Penn.
Cisuralian
M Tri.
U Tri.
L Jur.
M Jur.
U Jur.
Lower Cretaceous
U Crt.
Plc.
Eocene
Olig.
Mio.
Time [Ma]
0
100
200
300
400
Depth [ft]
0
5000
10000
15000
20000
25000
Vitrinite Reflectance [%Ro]
1.00
2.00
3.00
4.00
5.00

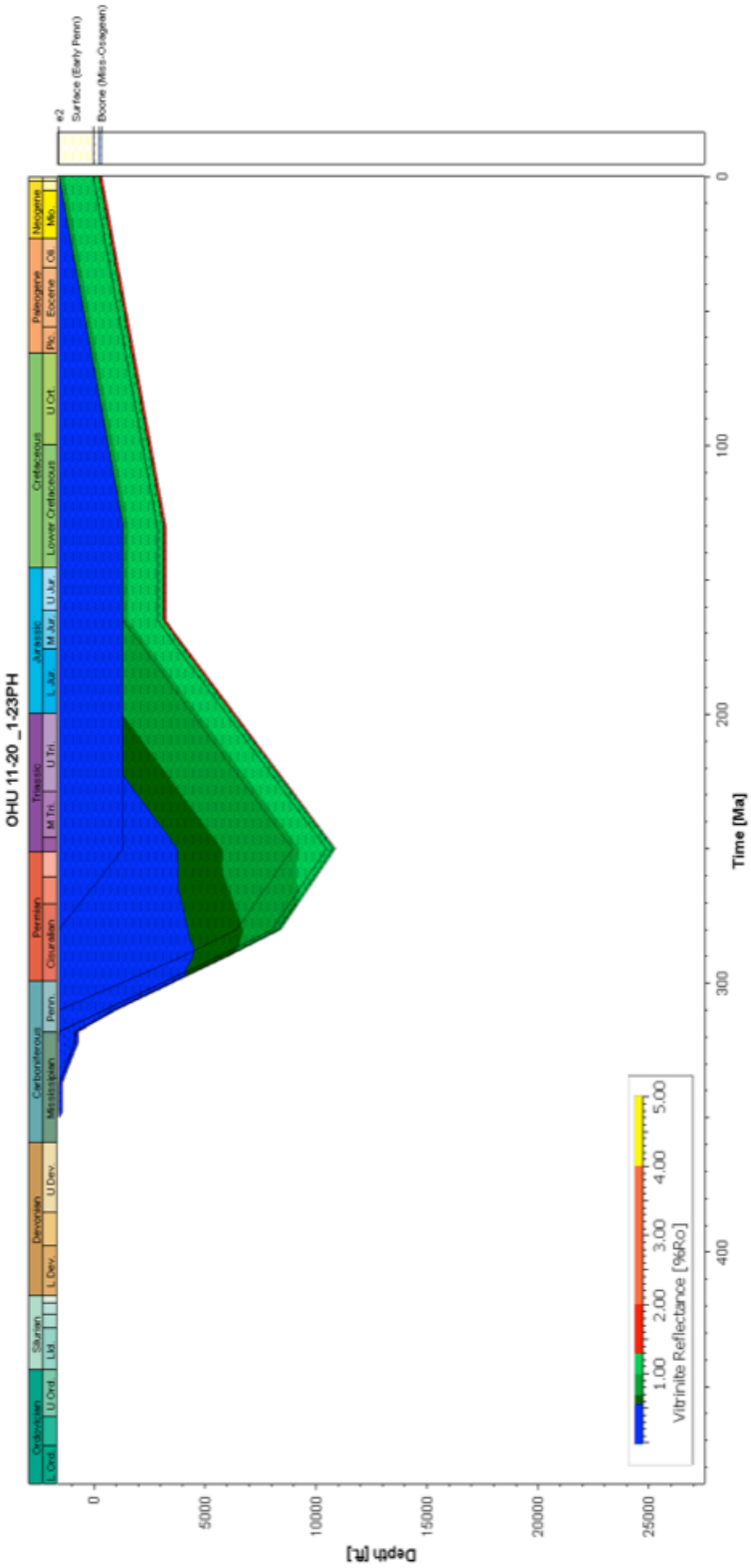
OHU 11-20 _1-23PH
Ordovician
L Ord.
U Ord.
Silurian
Ltd.
L Dev.
Devonian
U Dev.
Carboniferous
Mississippian
Penn.
Permian
Cisuralian
Triassic
M Tri.
U Tri.
Jurassic
L Jur.
M Jur.
U Jur.
Cretaceous
Lower Cretaceous
U Cret.
Paleogene
Pc.
Eocene
Oli.
Neogene
Mio.
e2
Surface (Early Penn)
Boone (Miss.-Osagean)
Vitrinite Reflectance [%Ro]
1.00
2.00
3.00
4.00
5.00
Depth [ft]
0
5000
10000
15000
20000
25000
Time [Ma]
400
300
200
100
0

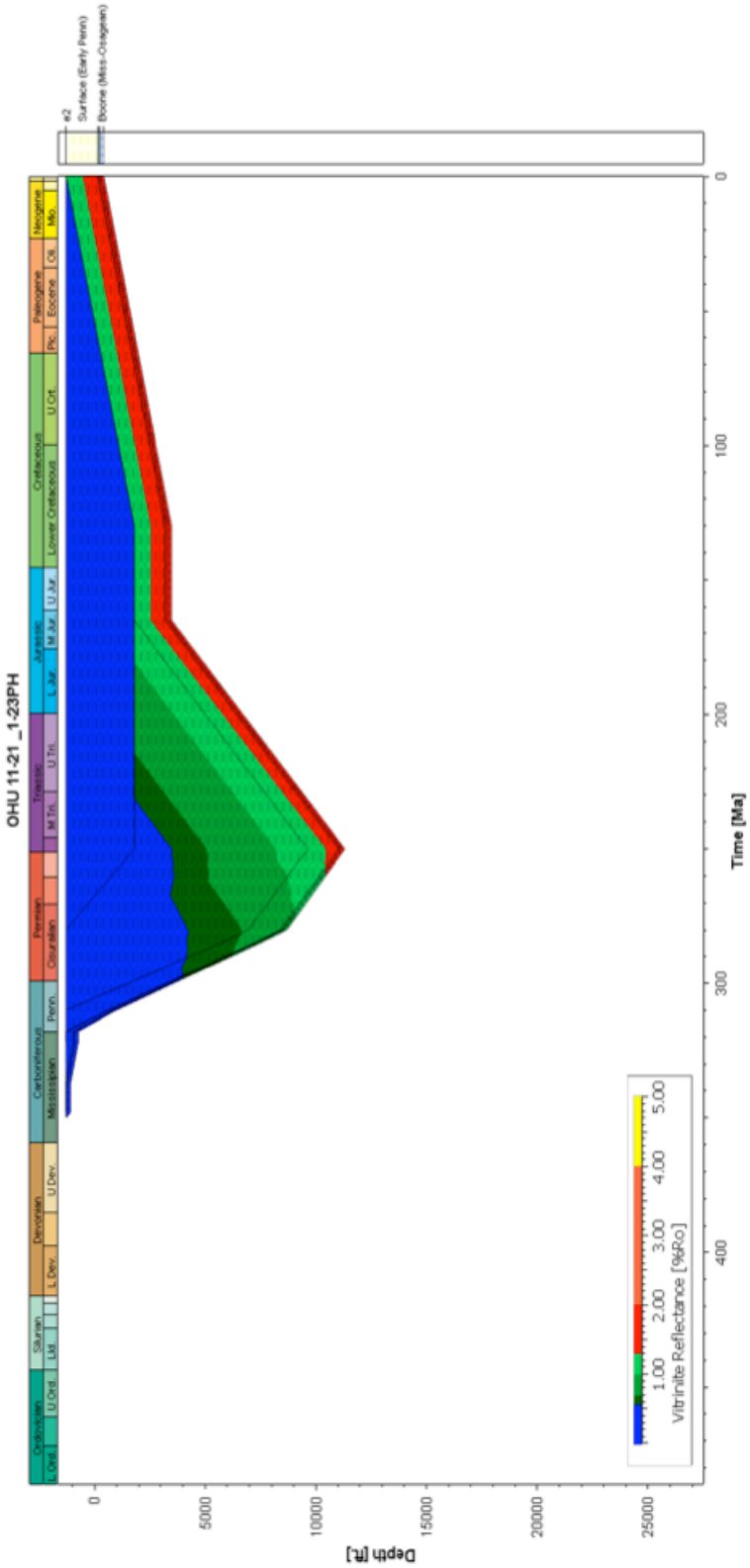
OHU 11-21 _1-23PH
Ordovician
L Ord.
U Ord.
Silurian
LMI.
Devonian
L Dev.
U Dev.
Carboniferous
Mississipian
Penn.
Permian
Cisuralian
Triassic
M Tri.
U Tri.
Jurassic
L Jur.
M Jur.
U Jur.
Cretaceous
Lower Cretaceous
U Crt.
Paleogene
Pic.
Eocene
Oli.
Neogene
Mio.
e2
Surface (Early Penn)
Boone (Miss.-Osagean)
Vitrinite Reflectance [%Ro]
1.00
2.00
3.00
4.00
5.00
Depth [ft]
0
5000
10000
15000
20000
25000
Time [Ma]
0
100
200
300
400

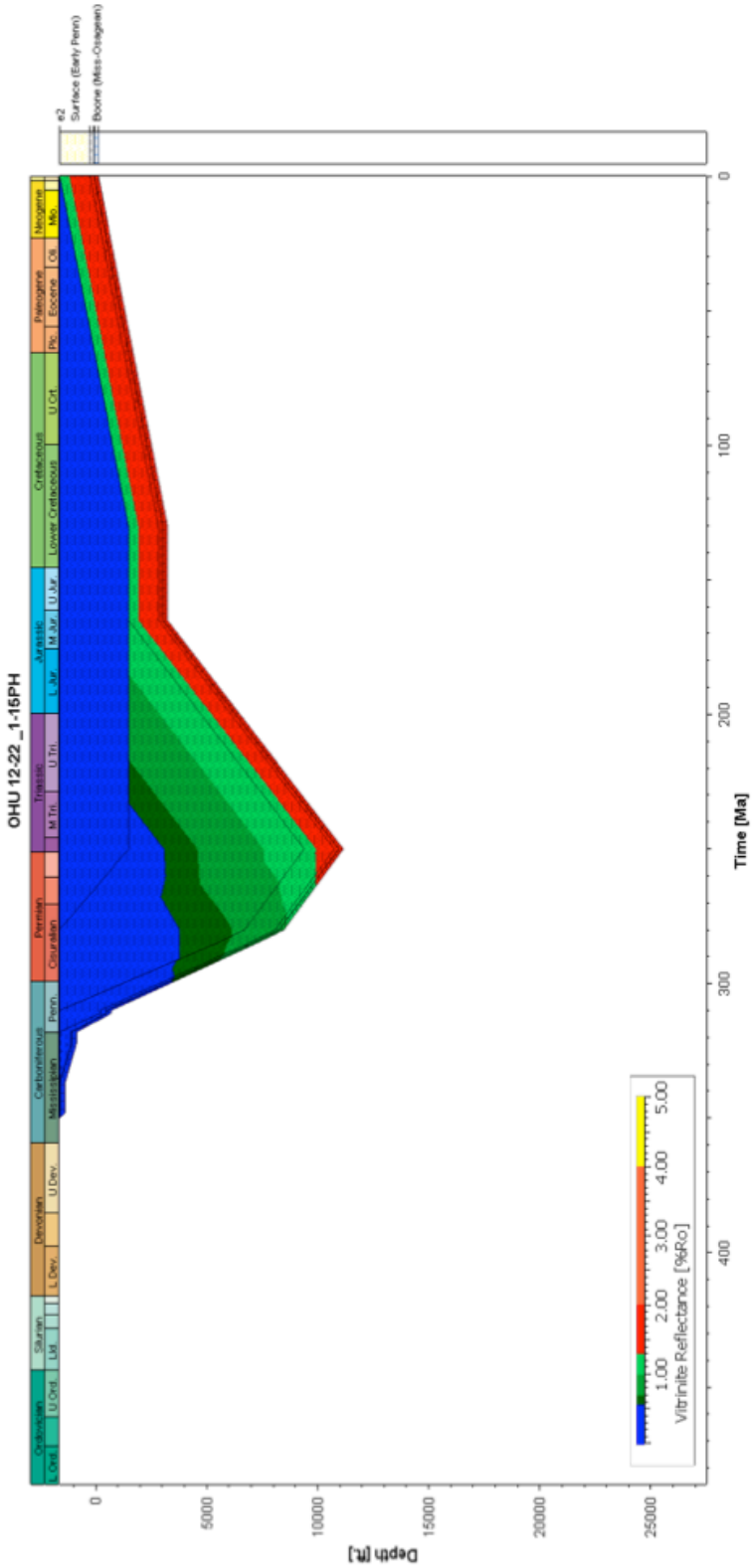
OHU 12-22 _1-15PH
Ordovician
L Ord.
U Ord.
Silurian
Ltd
L Dev.
Devonian
U Dev.
Carboniferous
Mississippian
Penn.
Permian
Cisuralian
M Tri.
Triassic
U Tri.
L Jur.
Jurassic
M Jur.
U Jur.
Cretaceous
Lower Cretaceous
U Cret
Paleogene
Pgc.
Eocene
Ol.
Neogene
Mio.
e2
Surface (Early Penn)
Boone (Miss-Ostegian)
Vitrinite Reflectance [%Ro]
1.00
2.00
3.00
4.00
5.00
Depth [ft]
0
5000
10000
15000
20000
25000
Time [Ma]
400
300
200
100
0

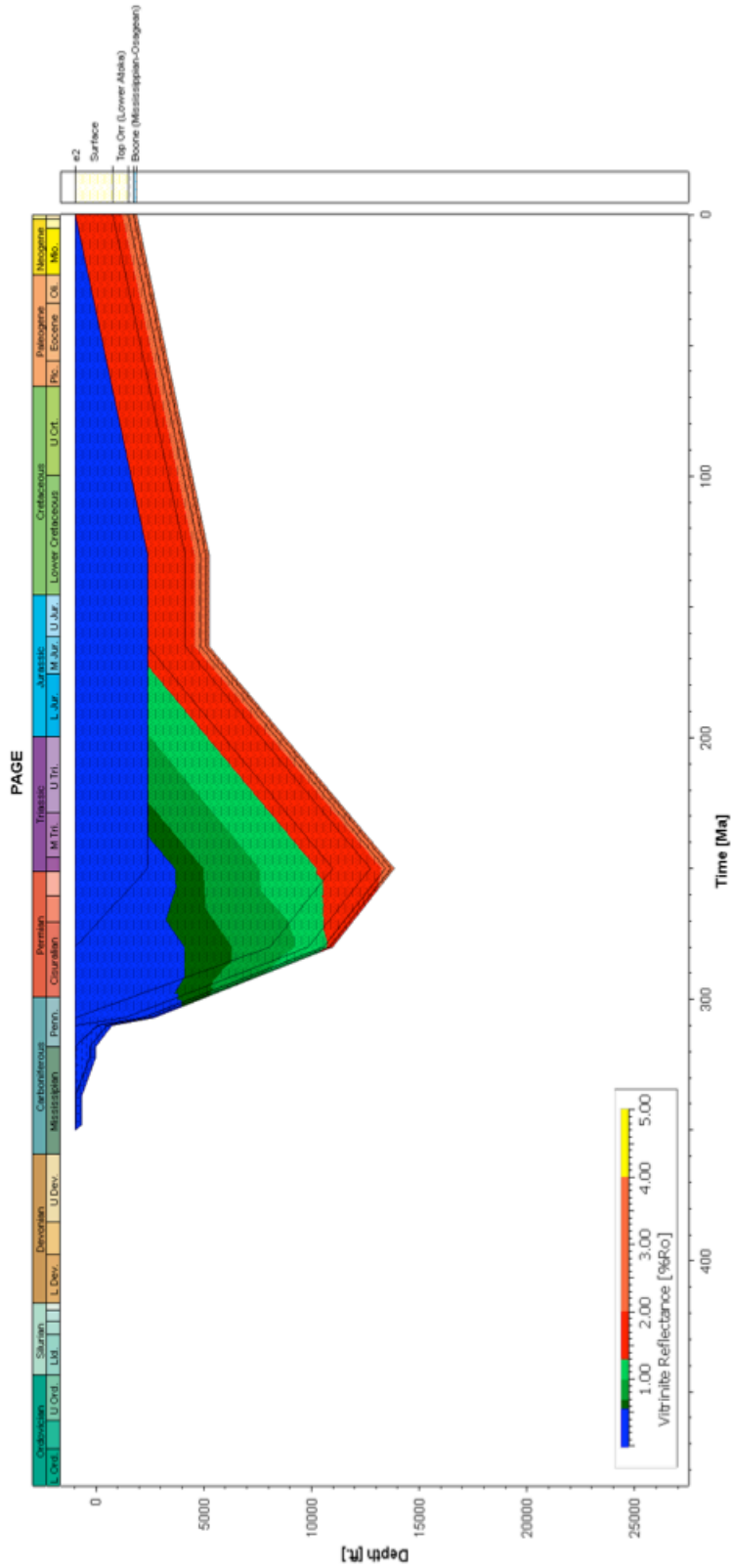
PAGE
Ordovician
Silurian
Devonian
Carboniferous
Permian
Triassic
Jurassic
Cretaceous
Paleogene
Neogene
Cmb
U Ord
Ltd
L Dev
U Dev
Mississippian
Penn.
Cisuralian
M Tri.
U Tri.
L Jur.
M Jur.
U Jur.
Lower Cretaceous
U Cret.
Plc.
Eocene
Ol.
Mio.
e2
Surface
Top Orr (Lower Atoka)
Boone (Mississippian-Osagean)
Depth [ft.]
0
5000
10000
15000
20000
25000
Time [Ma]
0
100
200
300
400
Vitrinite Reflectance [%Ro]
1.00
2.00
3.00
4.00
5.00

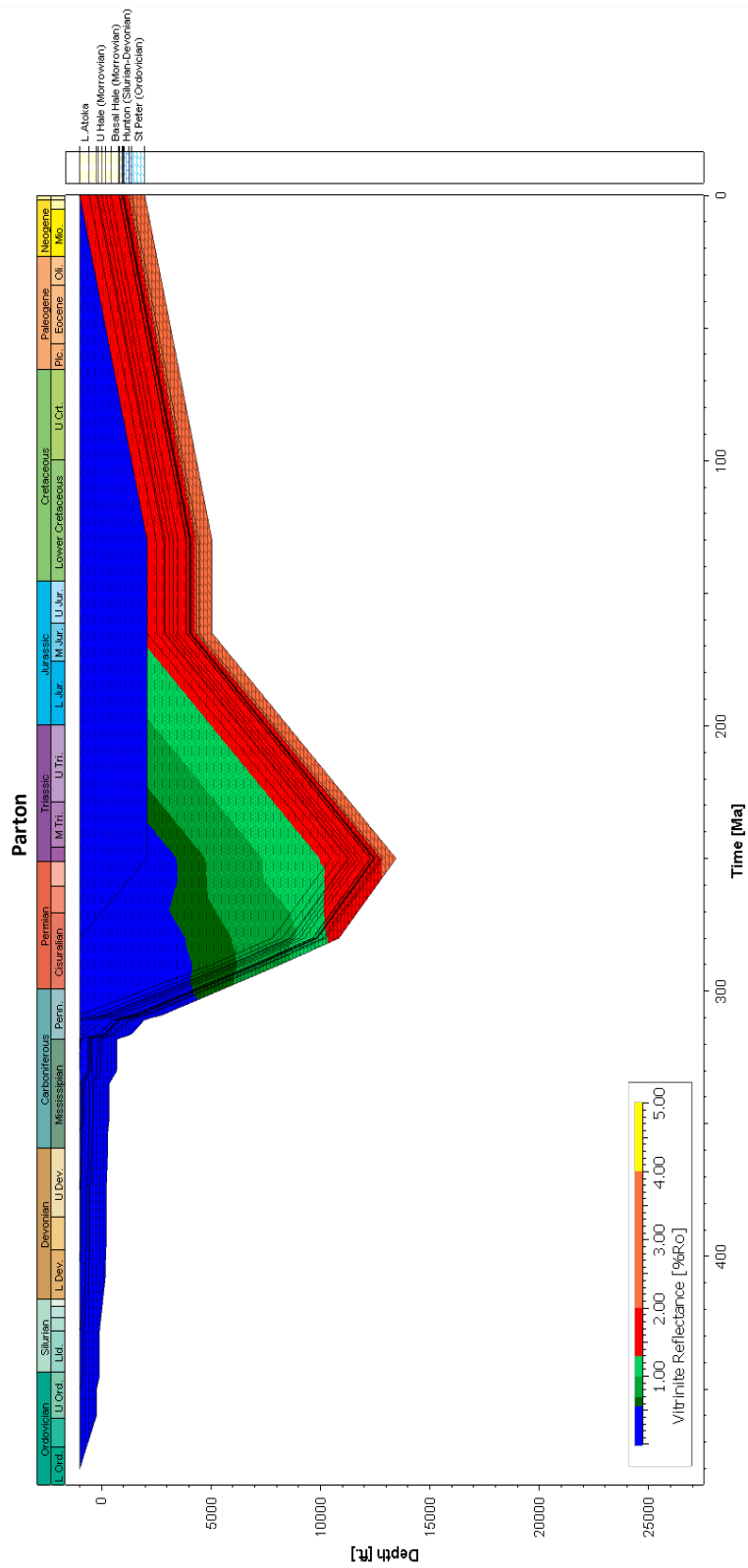
Parton
L. Atoka
U Hale (Morrowian)
Basal Hale (Morrowian)
Hunton (Silurian-Devonian)
St Peter (Ordovician)
Ordovician
L. Ord.
U Ord.
Silurian
Ltd.
Devonian
L. Dev.
U Dev.
Carboniferous
Mississipian
Penn.
Permian
Cisuralian
Triassic
M Tri.
U Tri.
Jurassic
L. Jur.
M. Jur.
U. Jur.
Cretaceous
Lower Cretaceous
U Crt.
Paleogene
Plc.
Eocene
Oli.
Neogene
Mio.
Time [Ma]
Depth [ft.]
Vitrinite Reflectance [%Ro]
1.00
2.00
3.00
4.00
5.00

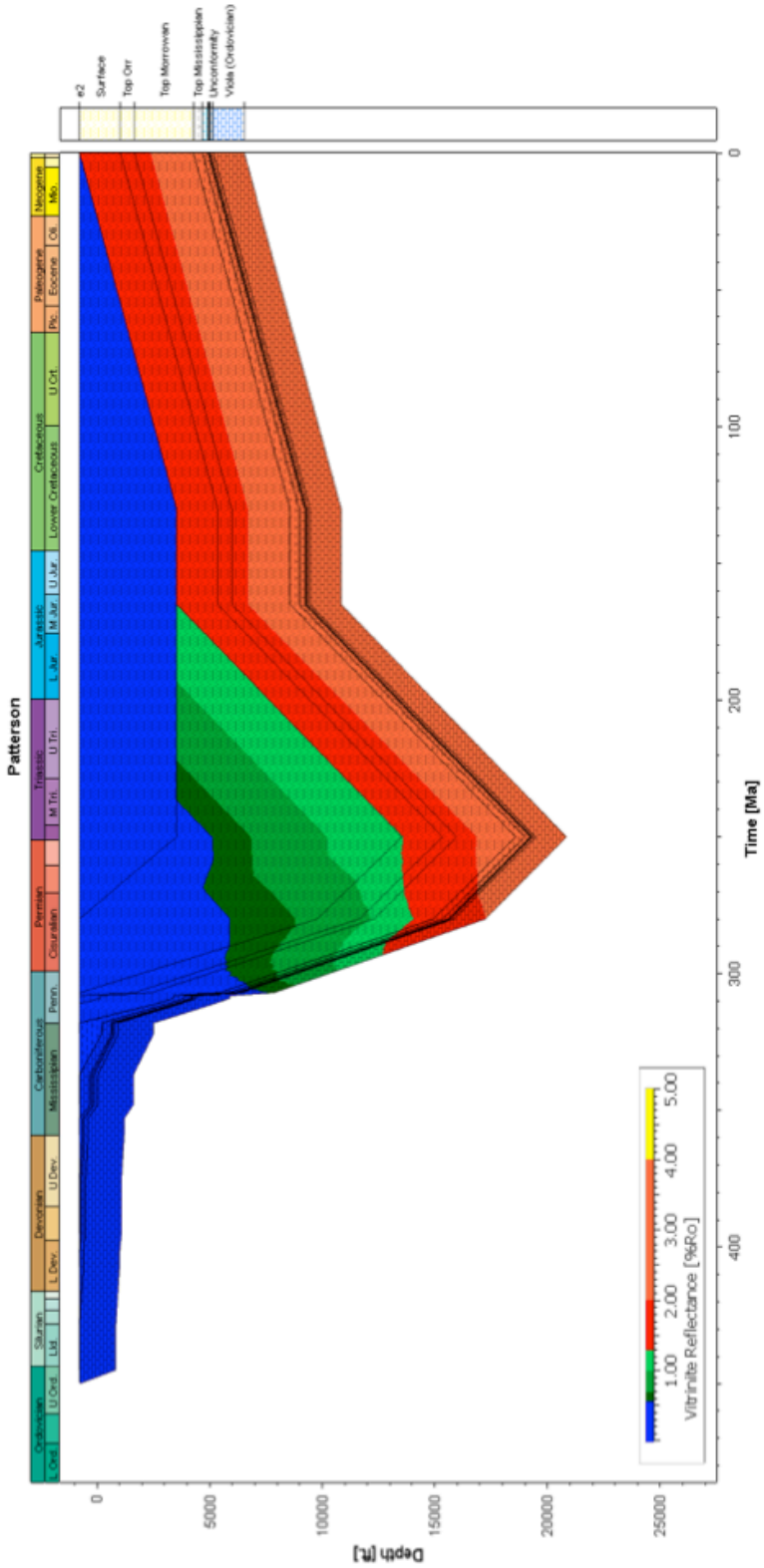
Patterson
Ordovician
L Ord.
U Ord.
Silurian
Ltd
Devonian
L Dev.
U Dev.
Carboniferous
Mississippian
Penn.
Permian
Cisuralian
Triassic
M Tri.
U Tri.
Jurassic
L Jur.
M Jur.
U Jur.
Cretaceous
Lower Cretaceous
U Cret.
Paleogene
Pgc.
Eocene
Ol.
Neogene
Mio.
e2
Surface
Top Orr
Top Morrowan
Top Mississippian
Unconformity
Viola (Ordovician)
Vitrinite Reflectance [%Ro]
1.00
2.00
3.00
4.00
5.00
Time [Ma]
0
100
200
300
400
Depth [ft]
0
5000
10000
15000
20000
25000

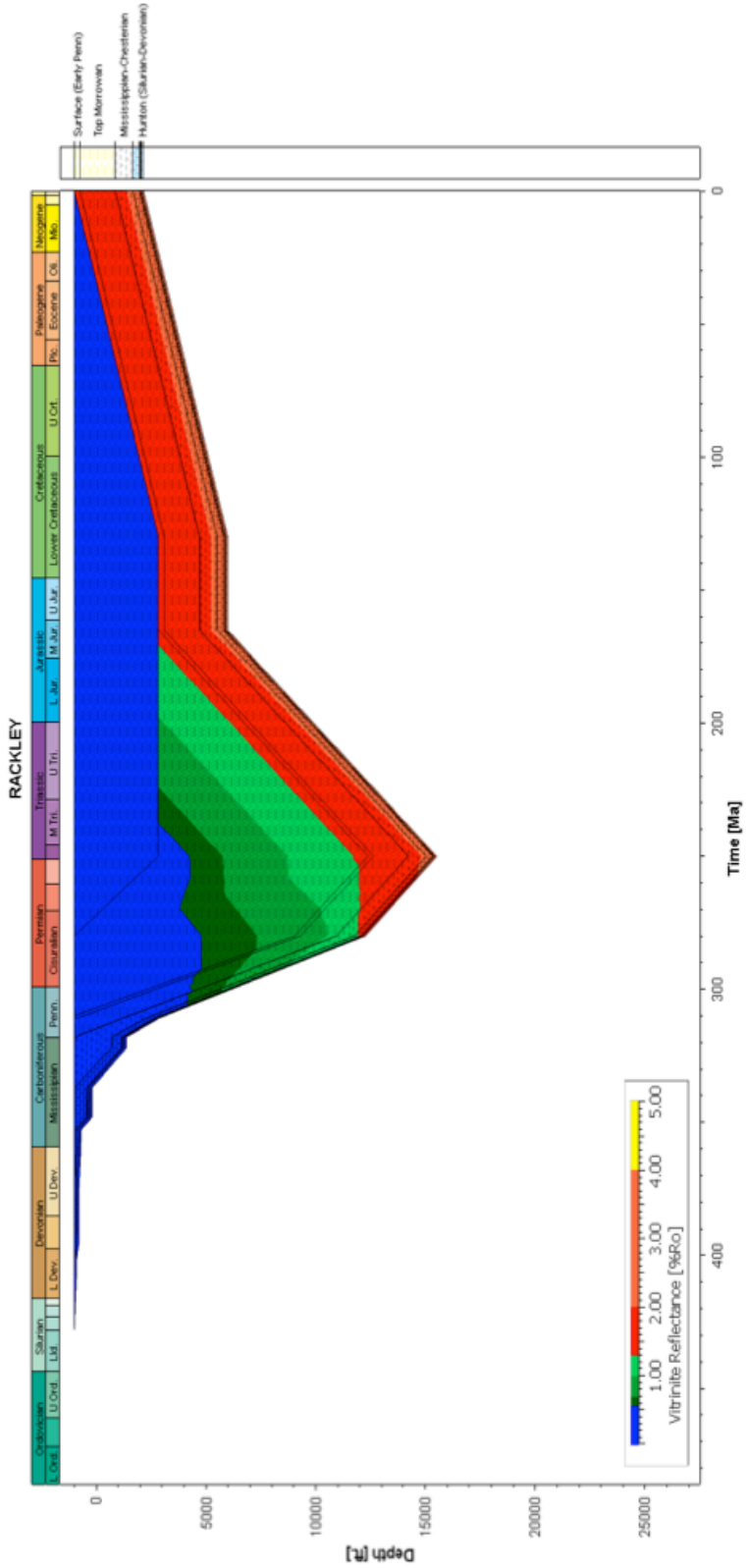
RACKLEY
Surface (Early Penn)
Top Morrowan
Mississippian-Chesterian
Hunton (Silurian-Devonian)
Ordovician
L. Ord.
U Ord.
Silurian
Ltd.
Devonian
L. Dev.
U Dev.
Carboniferous
Mississippian
Penn.
Permian
Cisuralian
Triassic
M Tri.
U Tri.
Jurassic
L. Jur.
M Jur.
U Jur.
Cretaceous
Lower Cretaceous
U Cret.
Paleogene
Pc.
Eocene
Oli.
Neogene
Mio.
Time [Ma]
0
100
200
300
400
Depth [ft]
0
5000
10000
15000
20000
25000
Vitrinite Reflectance [%Ro]
1.00
2.00
3.00
4.00
5.00

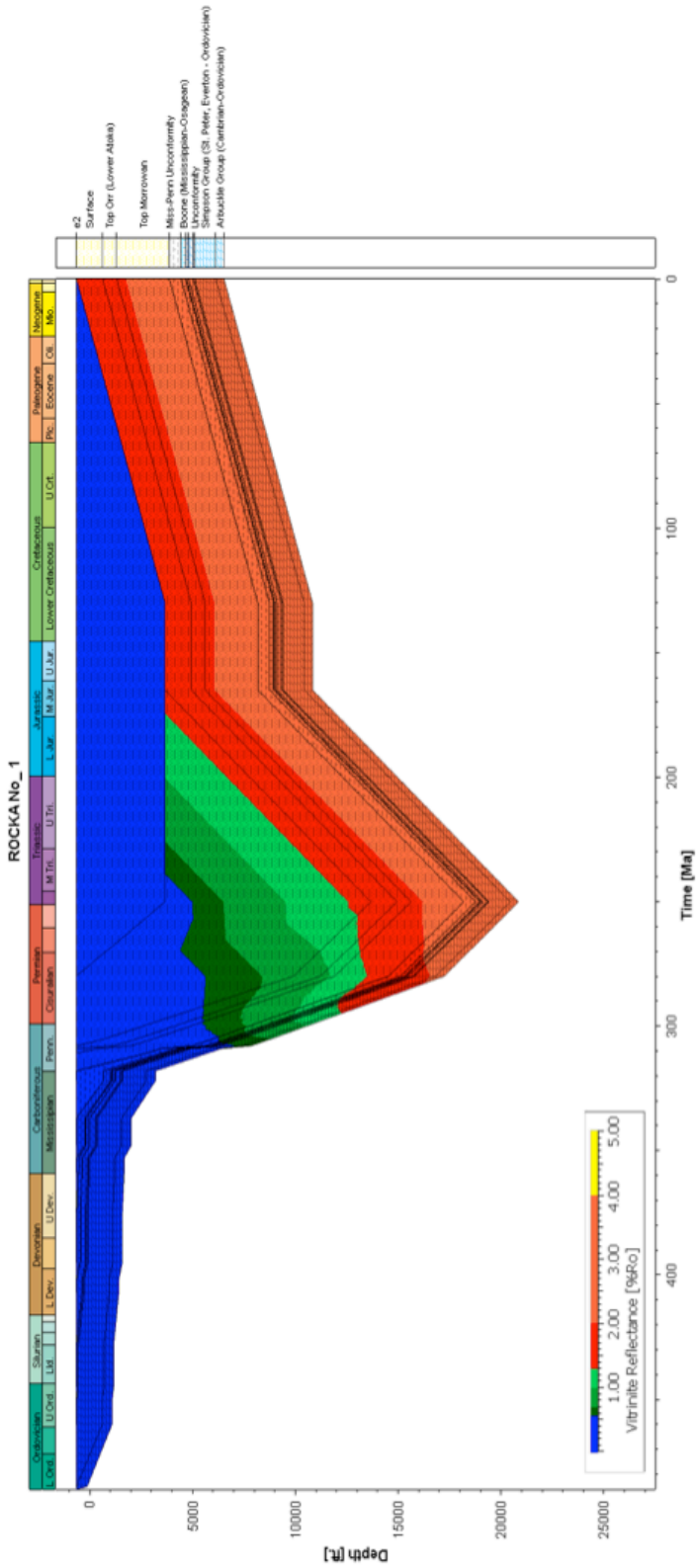
ROCKA No_1
Ordovician
L Ord.
U Ord.
Silurian
Ltd.
L Dev.
Devonian
U Dev.
Carboniferous
Mississippian
Penn.
Permian
Cisuralian
M Tri.
Triassic
U Tri.
L Jur.
Jurassic
M Jur.
U Jur.
Lower Cretaceous
Cretaceous
U Cret.
Pc.
Paleogene
Eocene
Ol.
Neogene
Mio.
e2
Surface
Top Orr (Lower Atoka)
Top Morrowan
Miss-Penn Unconformity
Boone (Mississippian-Osagean)
Unconformity
Simpson Group (St. Peter, Everton - Ordovician)
Arbuckle Group (Cambrian-Ordovician)
Depth [ft]
0
5000
10000
15000
20000
25000
Time [Ma]
0
100
200
300
400
Vitrinite Reflectance [%Ro]
1.00
2.00
3.00
4.00
5.00

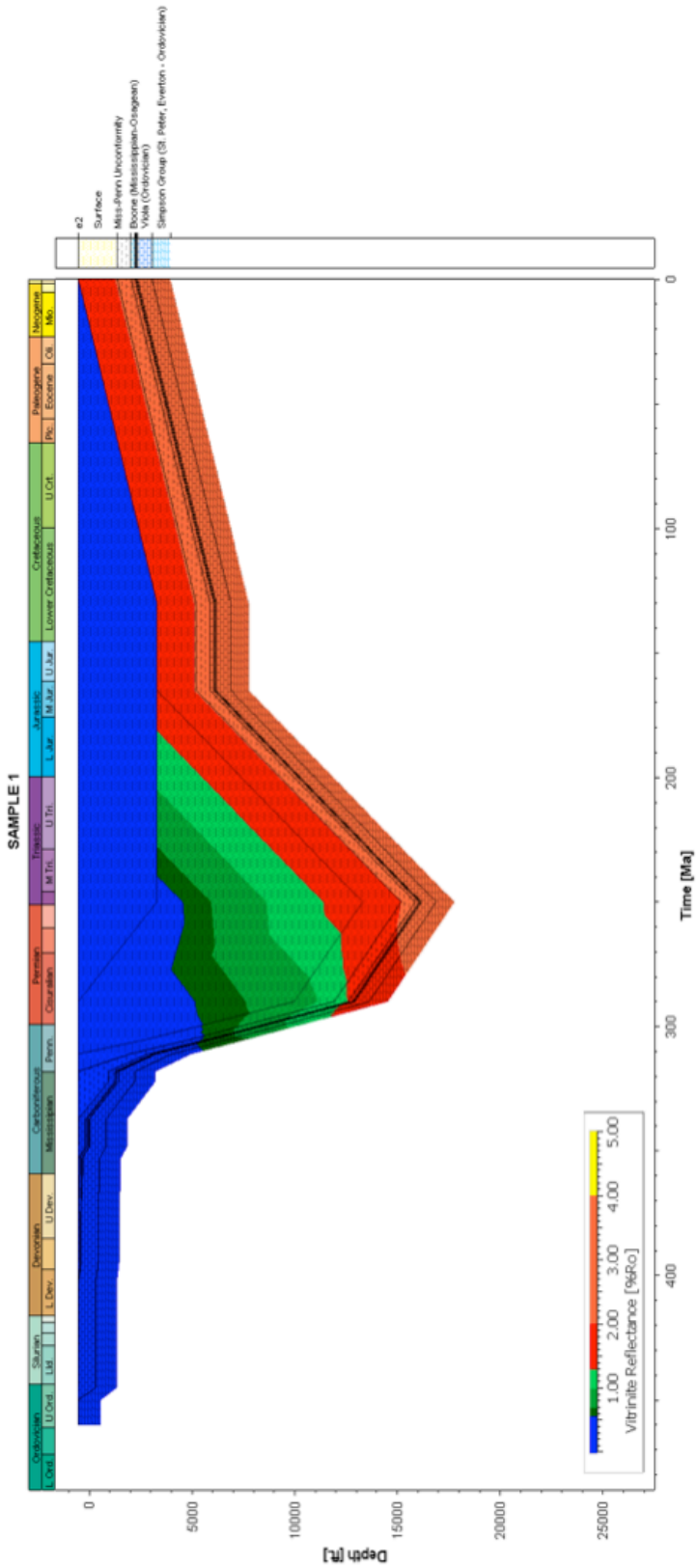
SAMPLE 1
Ordovician
Silurian
Devonian
Carboniferous
Permian
Triassic
Jurassic
Cretaceous
Paleogene
Neogene
L Ord.
U Ord.
Ltl.
L Dev.
U Dev.
Mississippian
Penn.
Cisuralian
M Tri.
U Tri.
L Jur.
M Jur.
U Jur.
Lower Cretaceous
U Cret.
Pic.
Eocene
Oli.
Mio.
e2
Surface
Miss-Penn Unconformity
Boone (Mississippian-Osagean)
Viola (Ordovician)
Simpson Group (Sil. Peter, Everton - Ordovician)
Depth [ft]
0
5000
10000
15000
20000
25000
Time [Ma]
0
100
200
300
400
Vitrinite Reflectance [%Ro]
1.00
2.00
3.00
4.00
5.00

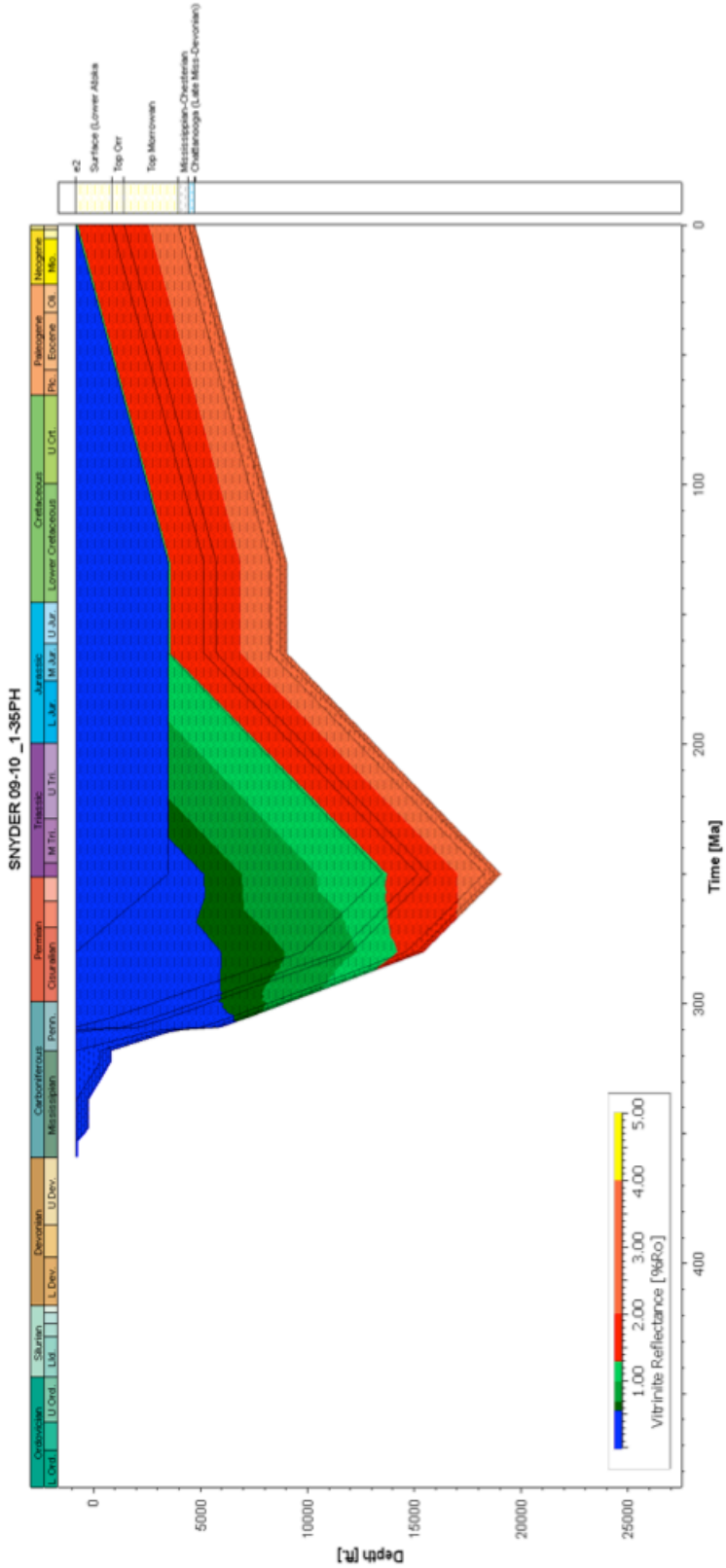
SNYDER 09-10_1-35PH
Ordovician
Silurian
Devonian
Carboniferous
Permian
Triassic
Jurassic
Cretaceous
Paleogene
Neogene
L Ord.
U Ord.
Ltd.
L Dev.
U Dev.
Mississippian
Penn.
Cisuralian
M Tri.
U Tri.
L Jur.
M Jur.
U Jur.
Lower Cretaceous
U Cret.
Plc.
Eocene
Olig.
Mio.
e2
Surface (Lower Atoka
Top Orr
Top Morrowan
Mississippian-Chesteran
Chattanooga (Late Miss-Devonian)
Depth [ft]
0
5000
10000
15000
20000
25000
Time [Ma]
0
100
200
300
400
Vitrinite Reflectance [%Ro]
1.00
2.00
3.00
4.00
5.00

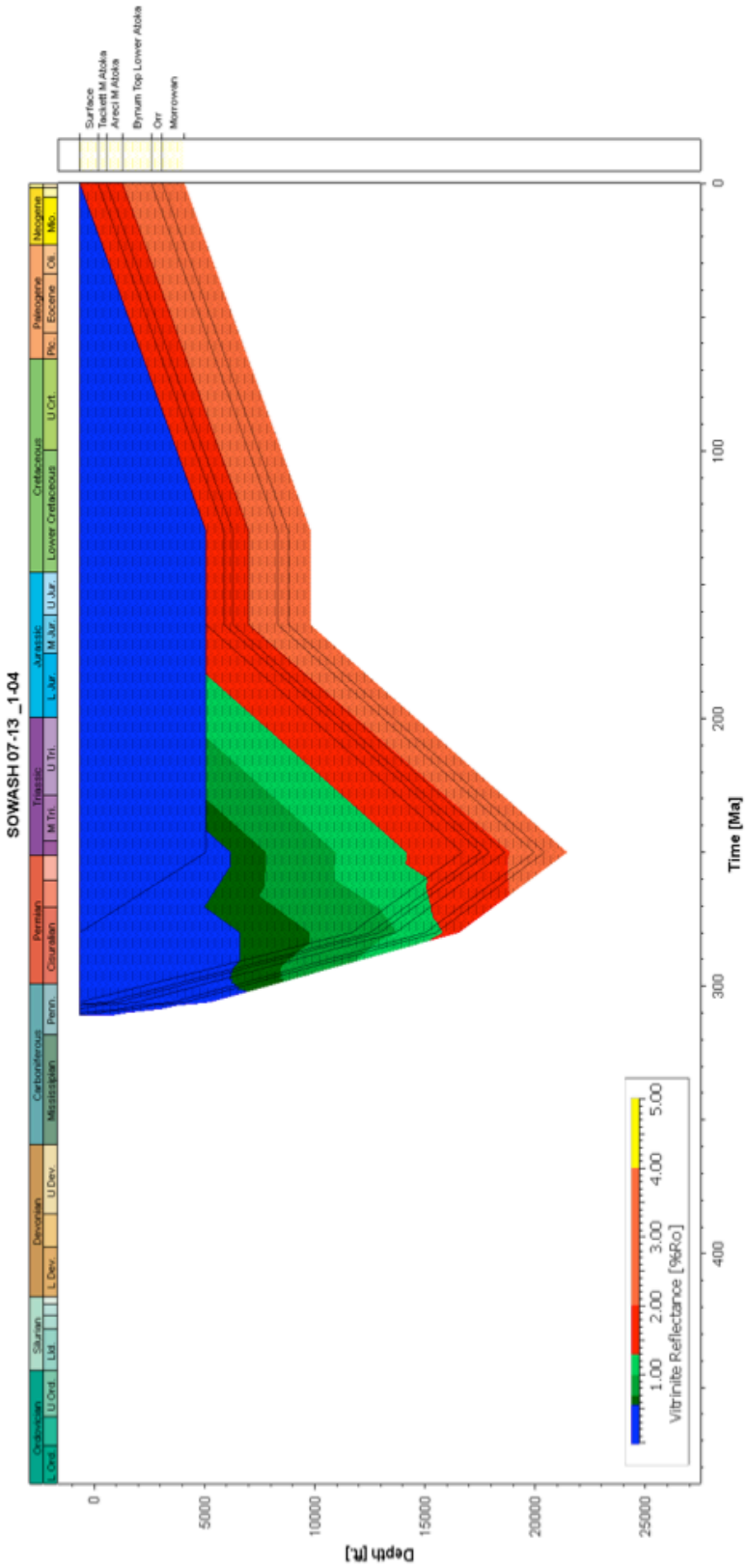
SOWASH 07-13 _1-04
Surface
Tackett M Atoka
Arecl M Atoka
Bynum Top Lower Atoka
Orr
Morrowan
Ordovician
Silurian
Devonian
Carboniferous
Permian
Triassic
Jurassic
Cretaceous
Paleogene
Neogene
L Ord.
U Ord.
Ltd
L Dev.
U Dev.
Mississippian
Penn.
Cisuralian
M Tri.
U Tri.
L Jur.
M Jur.
U Jur.
Lower Cretaceous
U Crt.
Plc.
Eocene
Oli.
Mio.
Vitrinite Reflectance [%Ro]
1.00
2.00
3.00
4.00
5.00
Time [Ma]
0
100
200
300
400
Depth [ft]
0
5000
10000
15000
20000
25000

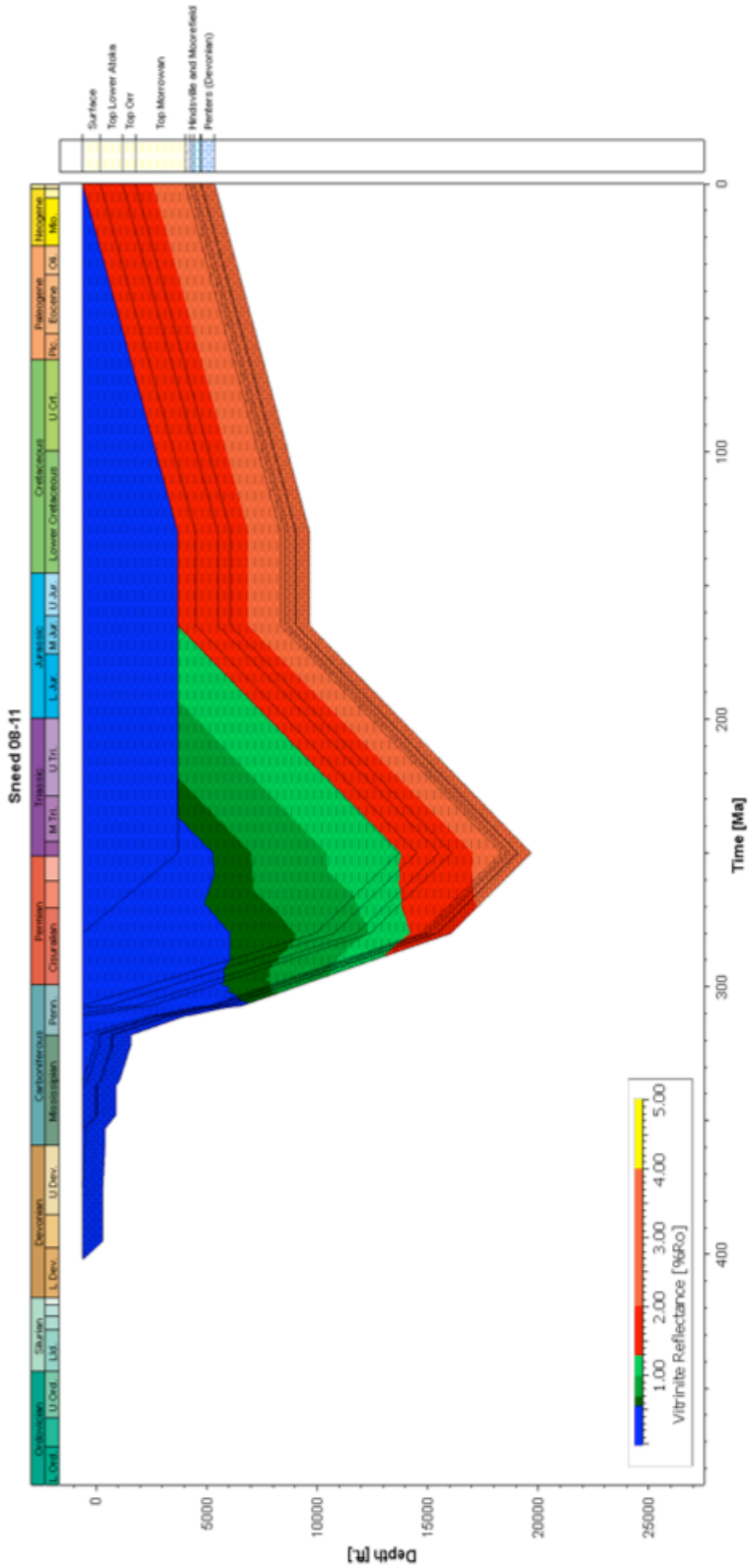
Sneed 08-11
Surface
Top Lower Atoka
Top Orr
Top Morrowan
Hindsville and Moorefield
Penters (Devonian)
Ordovician
Silurian
Devonian
Carboniferous
Permian
Triassic
Jurassic
Cretaceous
Paleogene
Neogene
L Ord.
U Ord.
L Dev.
U Dev.
Mississippian
Penn.
Cisuralian
M Tri.
U Tri.
L Jur.
M Jur.
U Jur.
Lower Cretaceous
U Cret.
Plc.
Eocene
Olig.
Mio.
Depth [ft]
0
5000
10000
15000
20000
25000
Time [Ma]
0
100
200
300
400
Vitrinite Reflectance [%Ro]
1.00
2.00
3.00
4.00
5.00

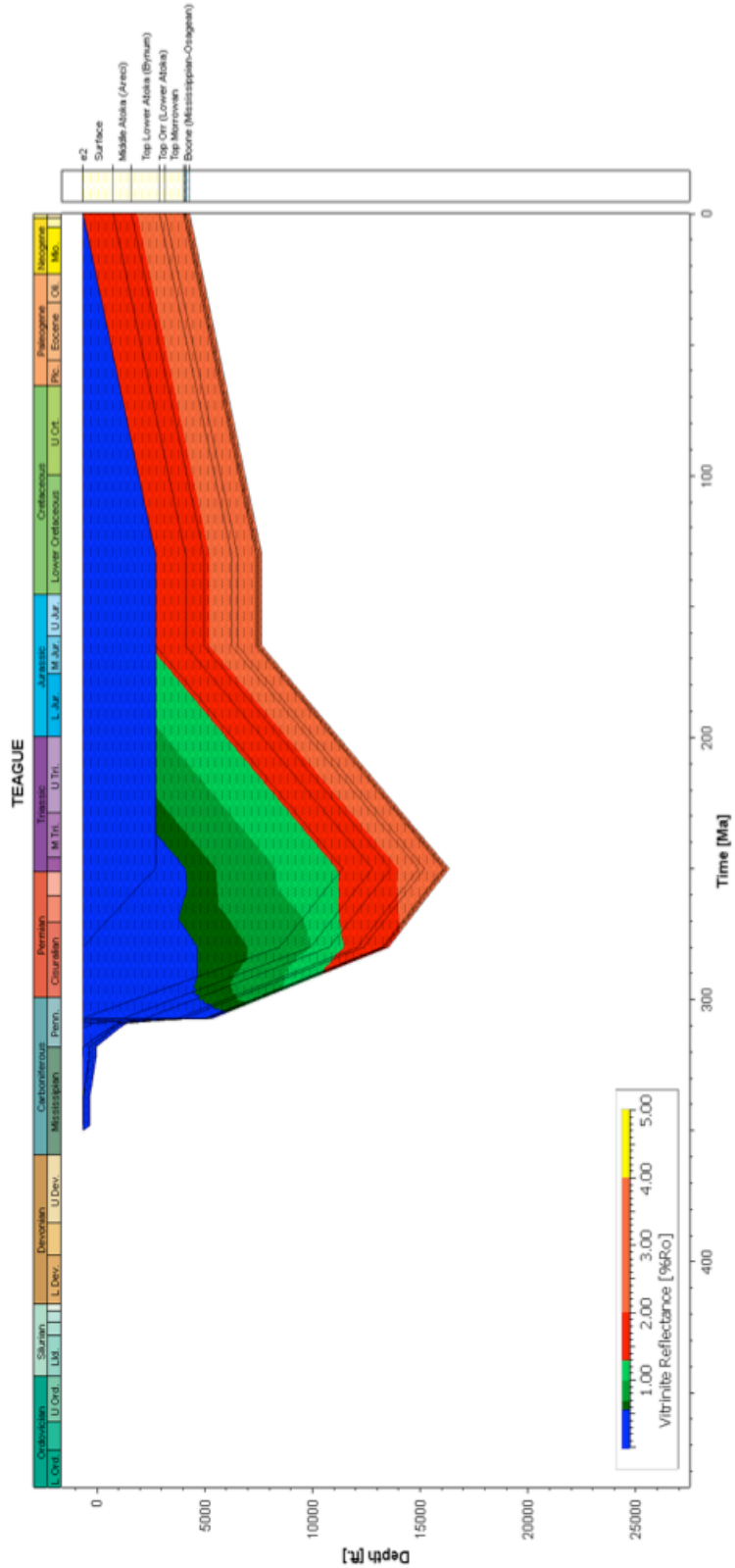
TEAGUE
Ordovician
Silurian
Devonian
Carboniferous
Permian
Triassic
Jurassic
Cretaceous
Paleogene
Neogene
L Ord.
U Ord.
Ltl
L Dev.
U Dev.
Mississippian
Penn.
Cisuralian
M Tri.
U Tri.
L Jur.
M Jur.
U Jur.
Lower Cretaceous
U Cret.
Pc.
Eocene
Ol.
Mio.
e2
Surface
Middle Atoka (Arenci)
Top Lower Atoka (Bynum)
Top Orr (Lower Atoka)
Top Morrowan
Boone (Mississippian-Osagean)
Depth [ft.]
0
5000
10000
15000
20000
25000
Time [Ma]
0
100
200
300
400
Vitrinite Reflectance [%Ro]
1.00
2.00
3.00
4.00
5.00

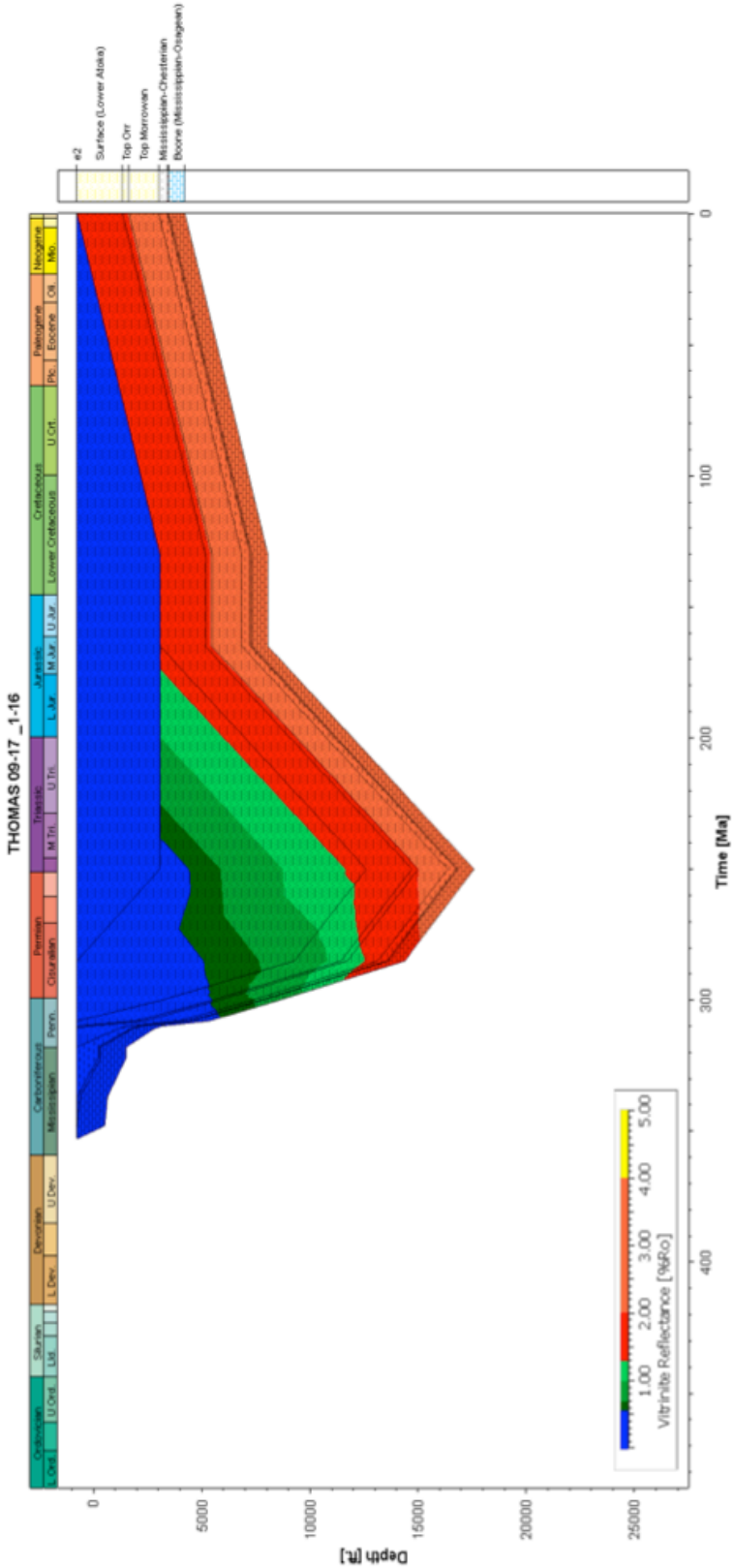
THOMAS 09-17 _1-16
Ordovician
Silurian
Devonian
Carboniferous
Permian
Triassic
Jurassic
Cretaceous
Paleogene
Neogene
L Ord
U Ord
Ltl
L Dev
U Dev
Miss
Penn
Cisuralian
M Tri
U Tri
L Jur
M Jur
U Jur
Lower Cretaceous
U Crt
Plc.
Eocene
Oli
Mio
e2
Surface (Lower Atoka)
Top Orr
Top Morrowan
Mississippian-Chesterian
Boone (Mississippian-Osagean)
Vitrinite Reflectance [%Ro]
1.00
2.00
3.00
4.00
5.00
Depth [ft]
0
5000
10000
15000
20000
25000
Time [Ma]
0
100
200
300
400

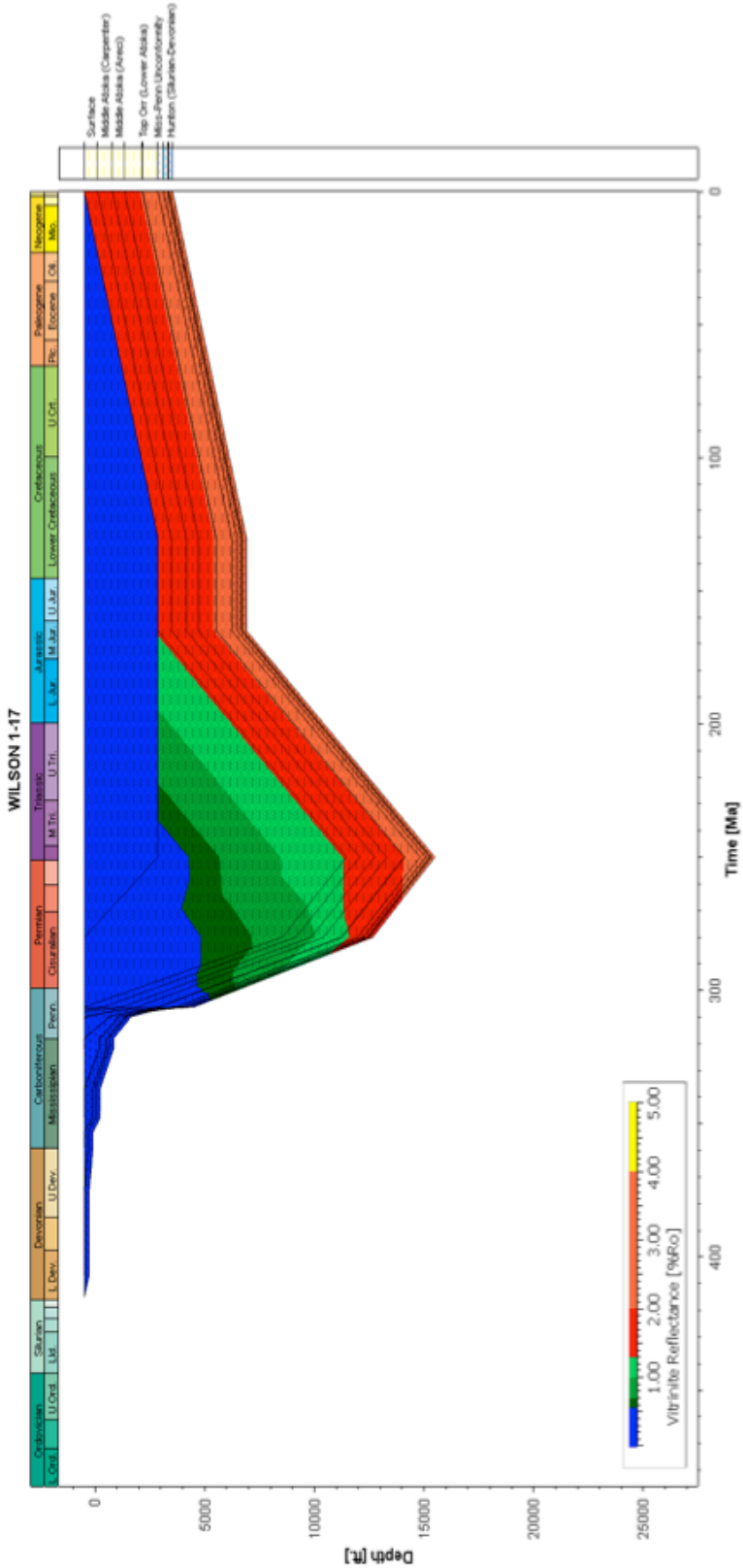
WILSON 1-17
Surface
Middle Abiska (Carpenter)
Middle Abiska (Arctic)
Top Orr (Lower Abiska)
Miss-Penn Unconformity
Hurton (Silurian-Devonian)
Ordovician
L Ord.
U Ord.
Silurian
Ltd.
Devonian
L Dev.
U Dev.
Carboniferous
Mississippian
Penn.
Permian
Cisuralian
Triassic
M Tri.
U Tri.
Jurassic
L Jur.
M Jur.
U Jur.
Cretaceous
Lower Cretaceous
U Crt.
Paleogene
Plc.
Eocene
Ol.
Neogene
Mio.
Time [Ma]
0
100
200
300
400
Depth [ft]
0
5000
10000
15000
20000
25000
Vitrinite Reflectance [%Ro]
1.00
2.00
3.00
4.00
5.00

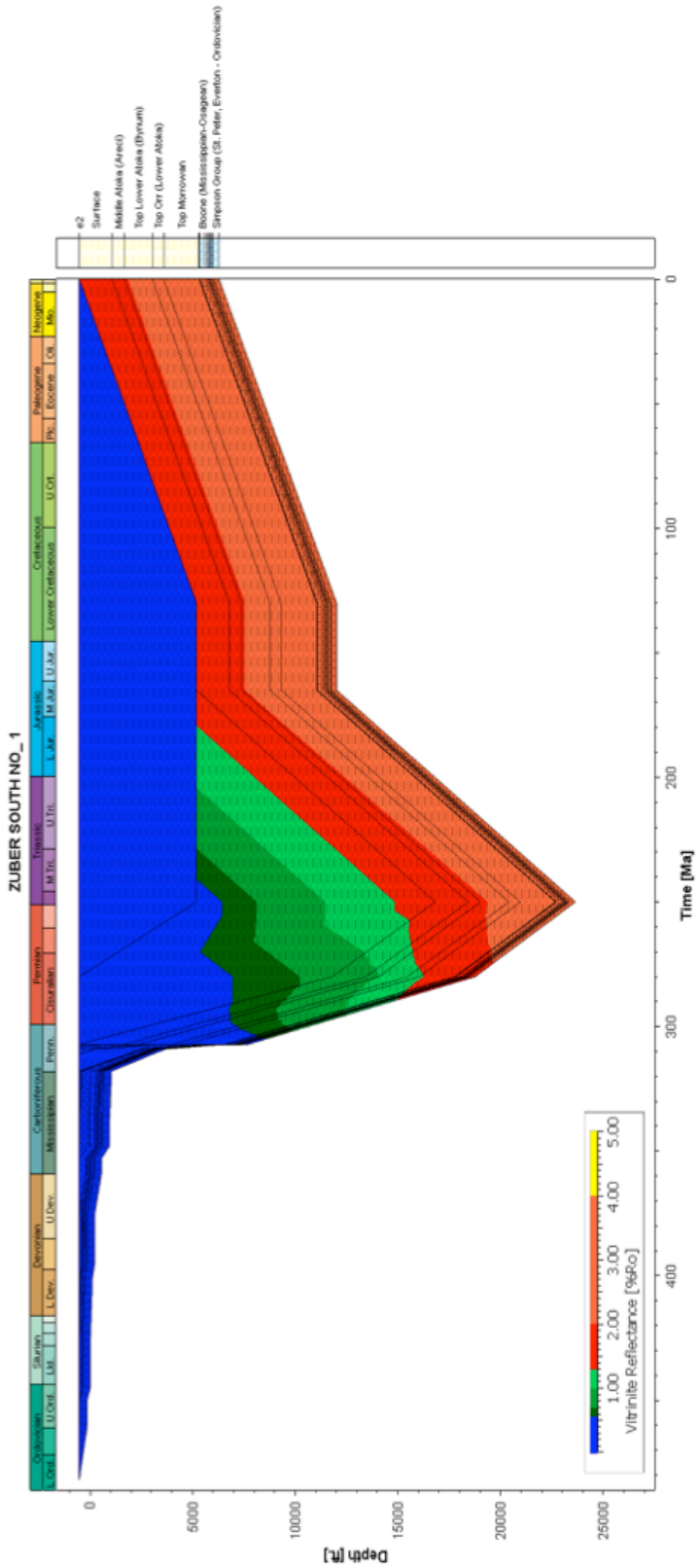
ZUBER SOUTH NO_1
e2
Surface
Middle Atoka (Area1)
Top Lower Atoka (Byrum)
Top Orr (Lower Atoka)
Top Morrowan
Boone (Mississippian-Osagean)
Simpson Group (St. Peter, Everton - Ordovician)
Ordovician
Silurian
Devonian
Carboniferous
Permian
Triassic
Jurassic
Cretaceous
Paleogene
Neogene
L.Ord.
U.Ord.
L.M.
L.Dev.
U.Dev.
Miss.
Penn.
Cisuralian
M.Tri.
U.Tri.
L.Jur.
M.Jur.
U.Jur.
Lower Cretaceous
U.Cret.
Plc.
Eocene
Oli.
Mio.
Depth [ft]
0
5000
10000
15000
20000
25000
Time [Ma]
0
100
200
300
400
Vitrinite Reflectance [%Ro]
1.00
2.00
3.00
4.00
5.00

A-3. Model-predicted vitrinite reflectance with respect to depth profiles. The sublinear black line represents the best-fit vitrinite reflectance EASY%Ro projection after calibration to the measured data points seen in the plot. Ro projections were first modeled to match the vitrinite reflectance data points collected from each given well. For wells with a small number of measured values, data from proximal wells were used to further calibrate the projections to shallower depths. If applicable, the figures below specify if sample points from multiple wells are displayed in the output models. Variations in marker styles represent individual wells. Otherwise, assume black projection curve is fit to the given well. Colored areas denote the zones of thermal maturity by use of vitrinite reflectance: 0.5-0.7, early mature (oil); 0.7-1.0, mid-mature (oil); 1.0-1.3, late mature (oil); 1.3-2.6, main gas generation. Modeled stratigraphic units (Table 1) are specified on the right of the reflectance profile.

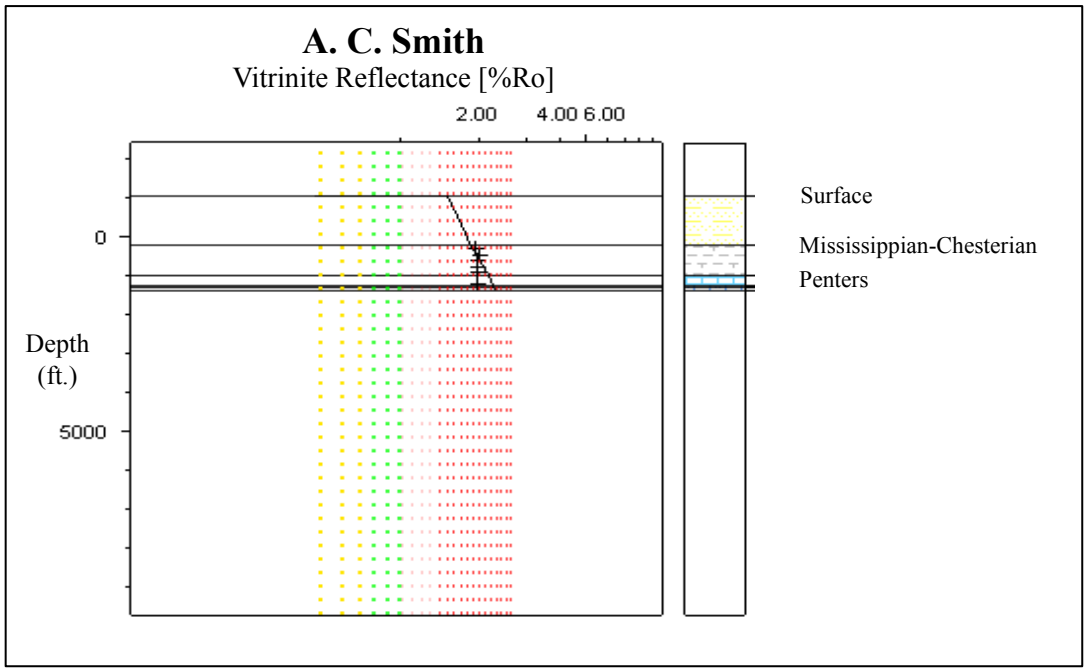

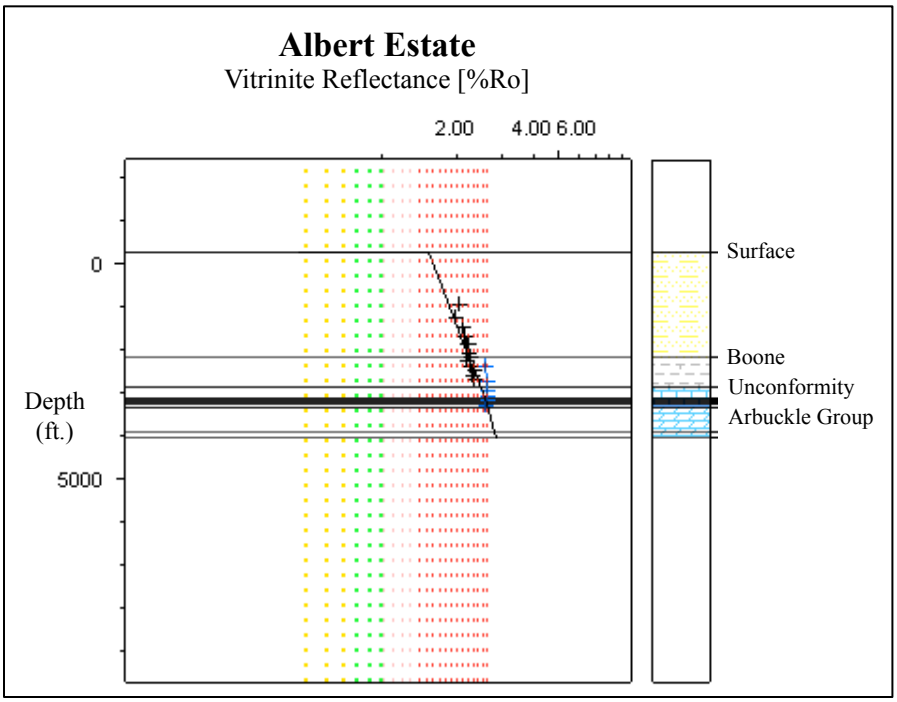

Wells in the surrounding area are displayed in the output model. Albert Estate: blue crosses, Sample 1: black crosses, Bobby and Lorette Reaper 10-7: black crosses

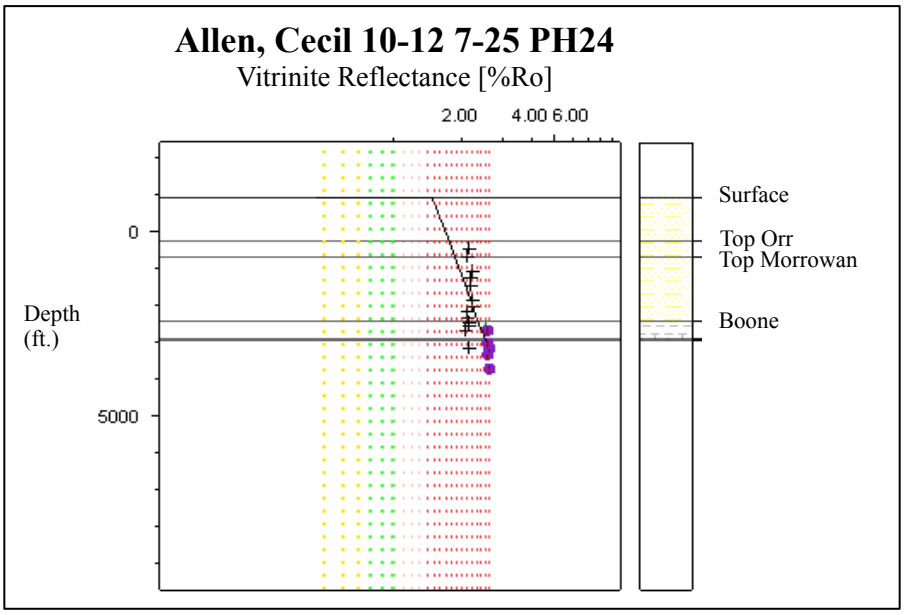

Wells in the surrounding area are displayed in the output model. Allen, Cecil: single green cross at 2,589' sstvd, Collums 10-13 #1-27: black crosses, Landrum Quitman No. 1: purple circles

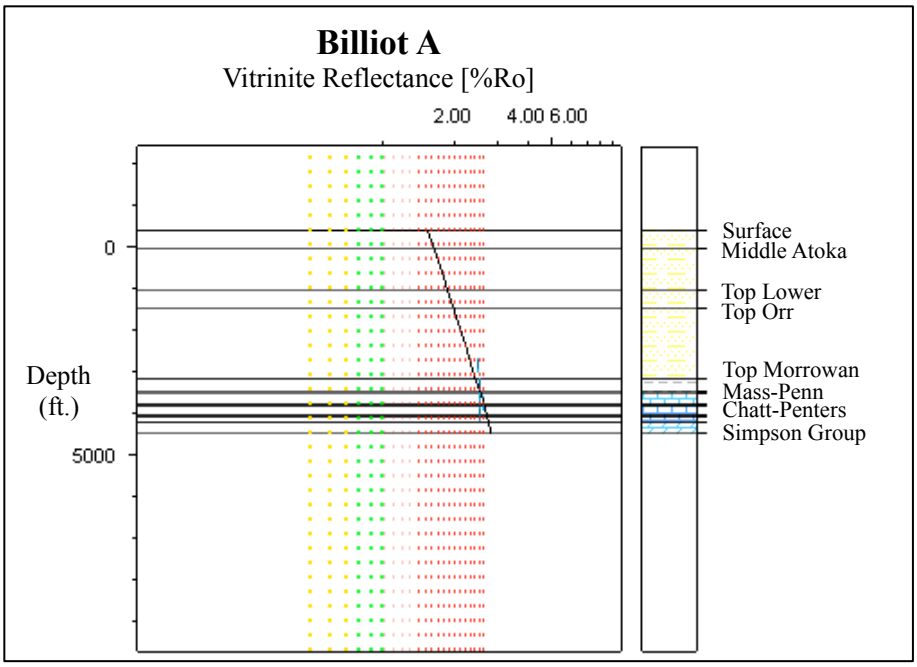
Billiot A
Vitrinite Reflectance [%Ro]
2.00
4.00 6.00
0
5000
Depth
(ft.)
Surface
Middle Atoka
Top Lower
Top Orr
Top Morrowan
Mass-Penn
Chatt-Penters
Simpson Group

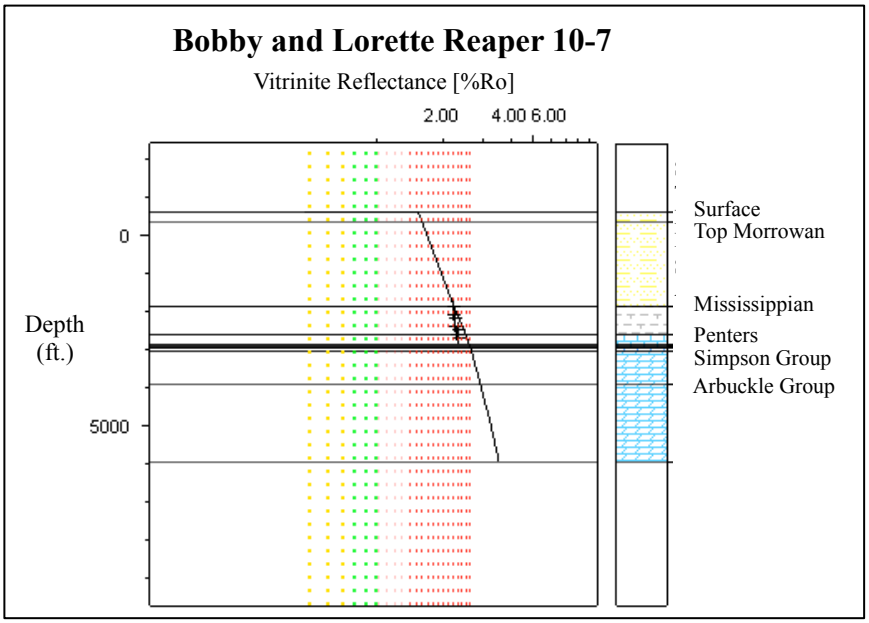
Bobby and Lorette Reaper 10-7
Vitrinite Reflectance [%Ro]
2.00
4.00 6.00
0
5000
Depth
(ft.)
Surface
Top Morrowan
Mississippian
Penters
Simpson Group
Arbuckle Group

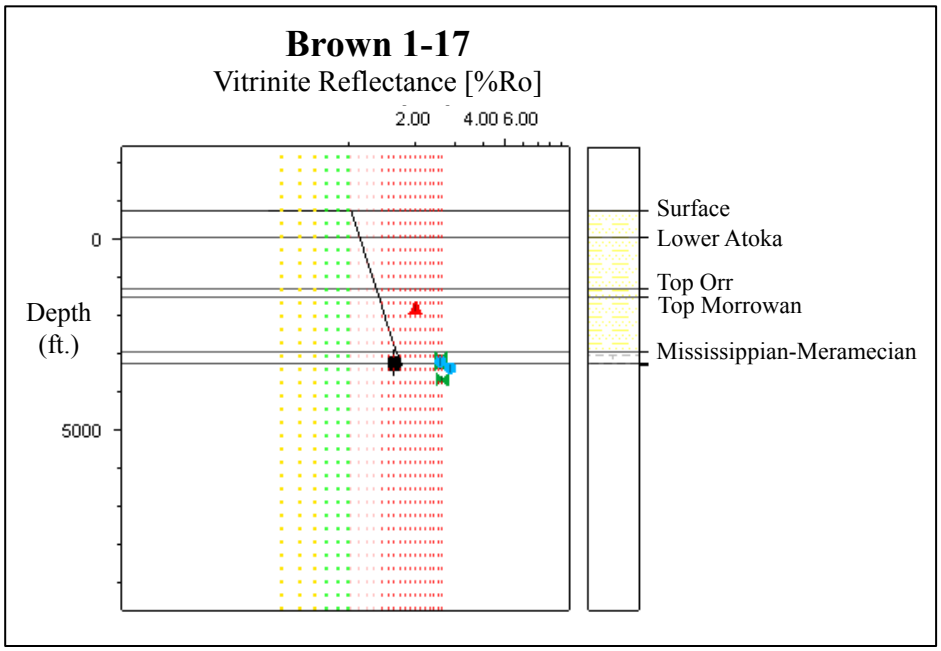

Wells in the surrounding area are displayed in the output model. Brown 1-17: black crosses, CS Ramsey: green bow ties, Halbrook 09-16: red triangle, Thomas 09-17: blue circles

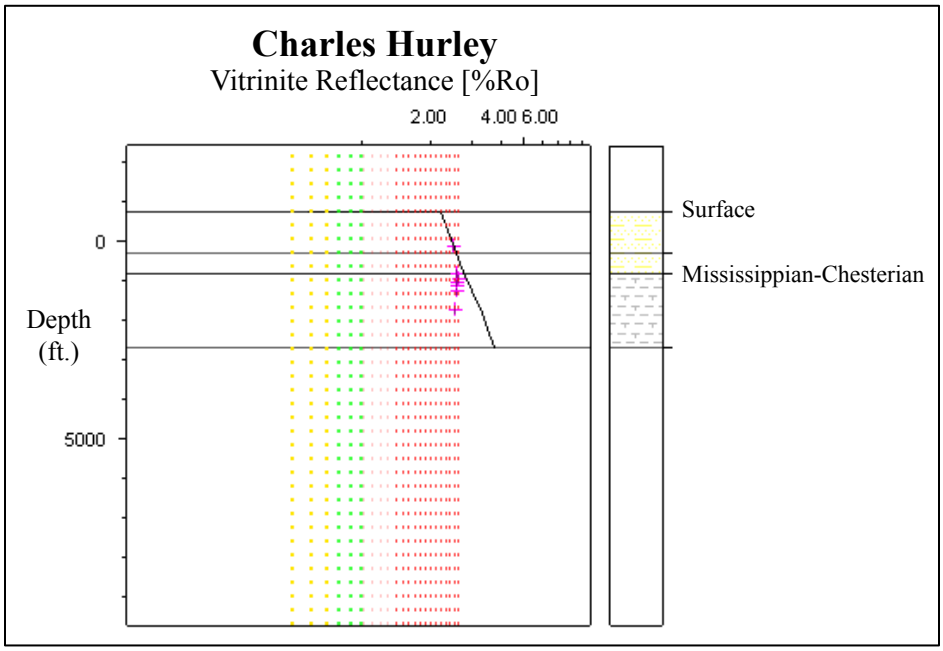

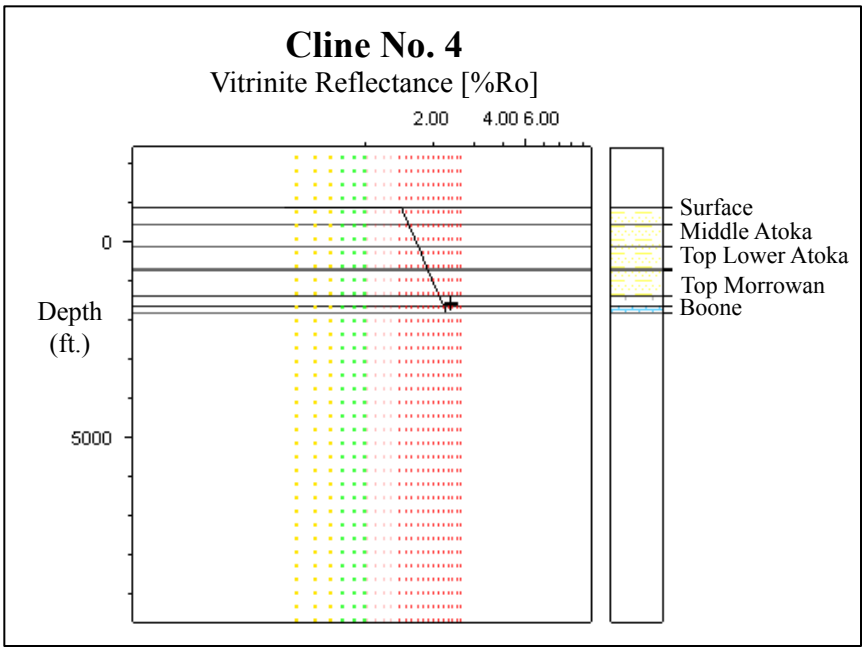

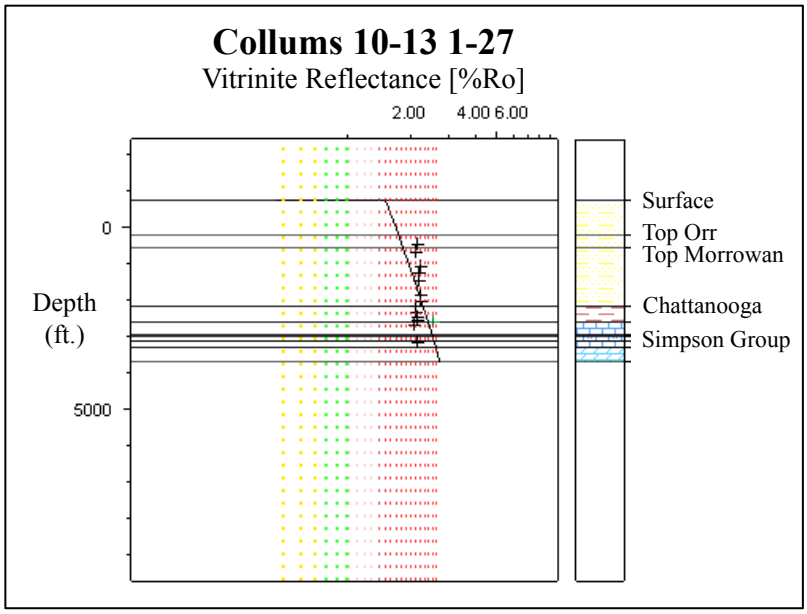

Wells in the surrounding area are displayed in the output model. Collums 10-13 1-27: black crosses, Allen Cecil 10-12 7-25: single green cross

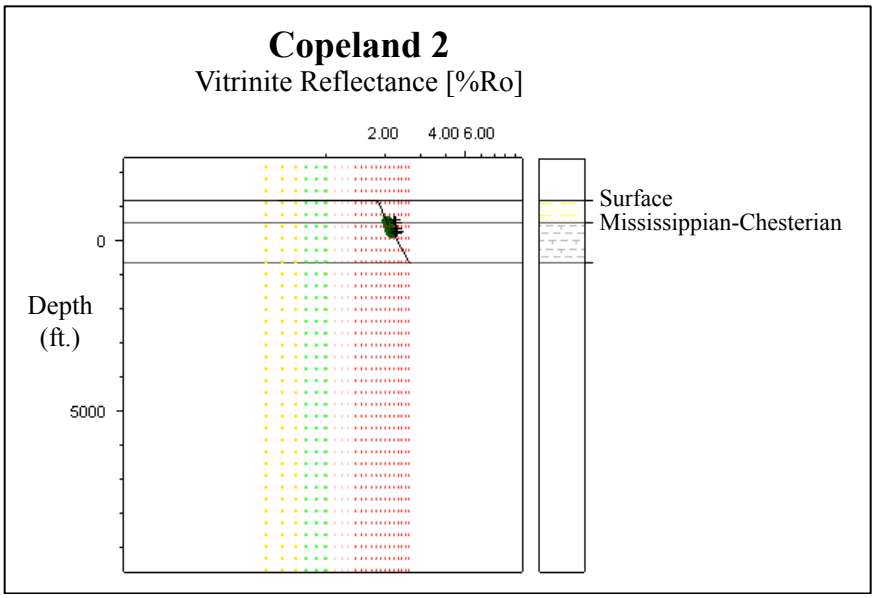

Wells in the surrounding area are displayed in the output model. Copeland 2: green circles, Copeland 3: black crosses

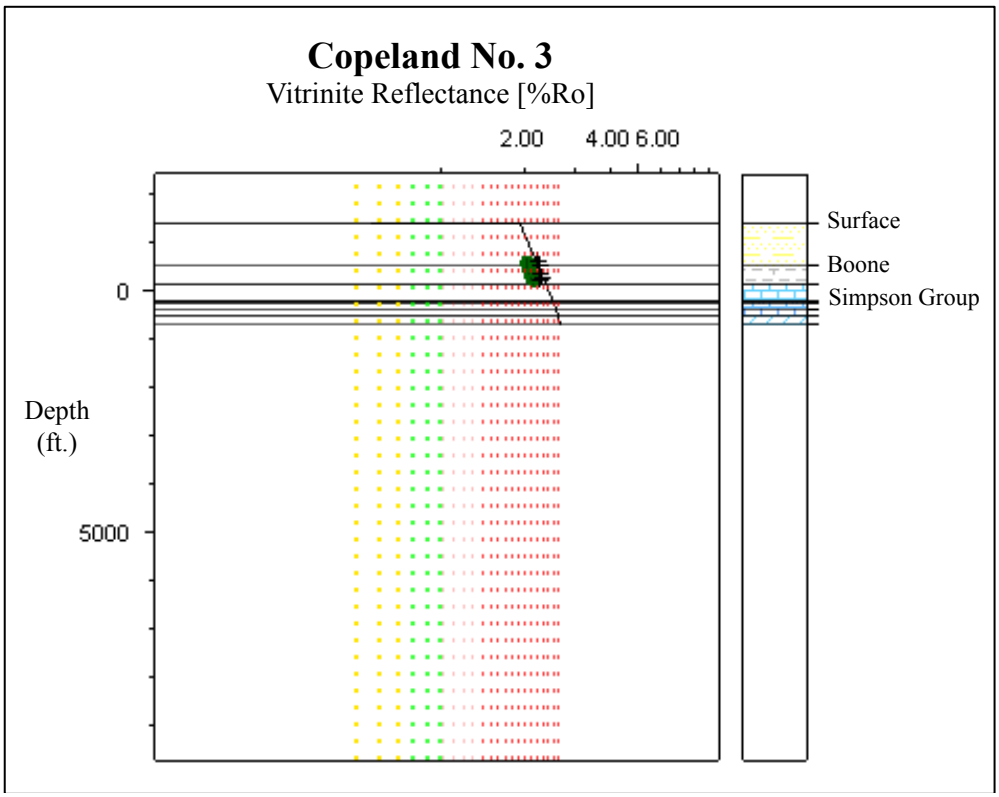

Wells in the surrounding area are displayed in the output model. Copeland 3: black crosses, Copeland 2: green circles

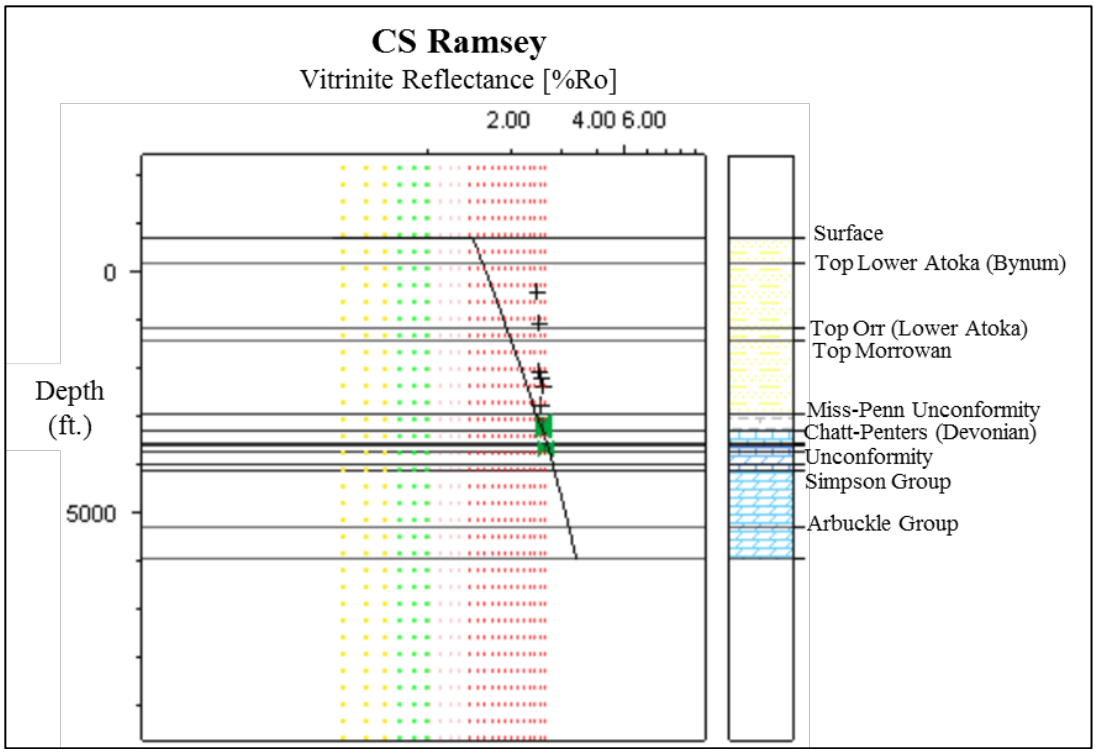
CS Ramsey
Vitrinite Reflectance [%Ro]
2.00
4.00 6.00
0
5000
Depth
(ft.)
Surface
Top Lower Atoka (Bynum)
Top Orr (Lower Atoka)
Top Morrowan
Miss-Penn Unconformity
Chatt-Penters (Devonian)
Unconformity
Simpson Group
Arbuckle Group

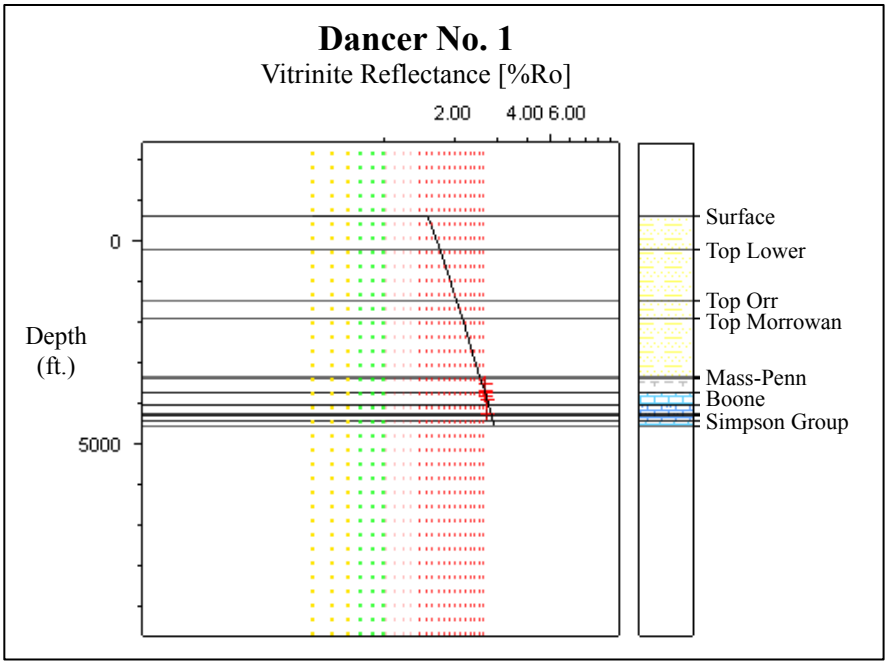
Dancer No. 1
Vitrinite Reflectance [%Ro]
2.00
4.00 6.00
0
5000
Depth
(ft.)
Surface
Top Lower
Top Orr
Top Morrowan
Mass-Penn
Boone
Simpson Group

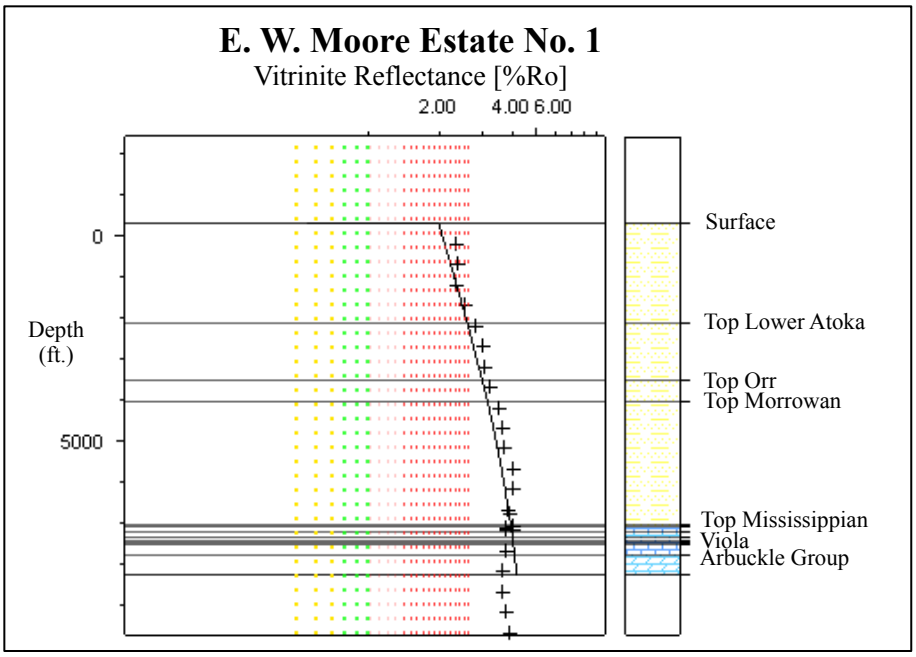
E. W. Moore Estate No. 1
Vitrinite Reflectance [%Ro]
2.00
4.00 6.00
0
5000
Depth
(ft.)
Surface
Top Lower Atoka
Top Orr
Top Morrowan
Top Mississippian
Viola
Arbuckle Group

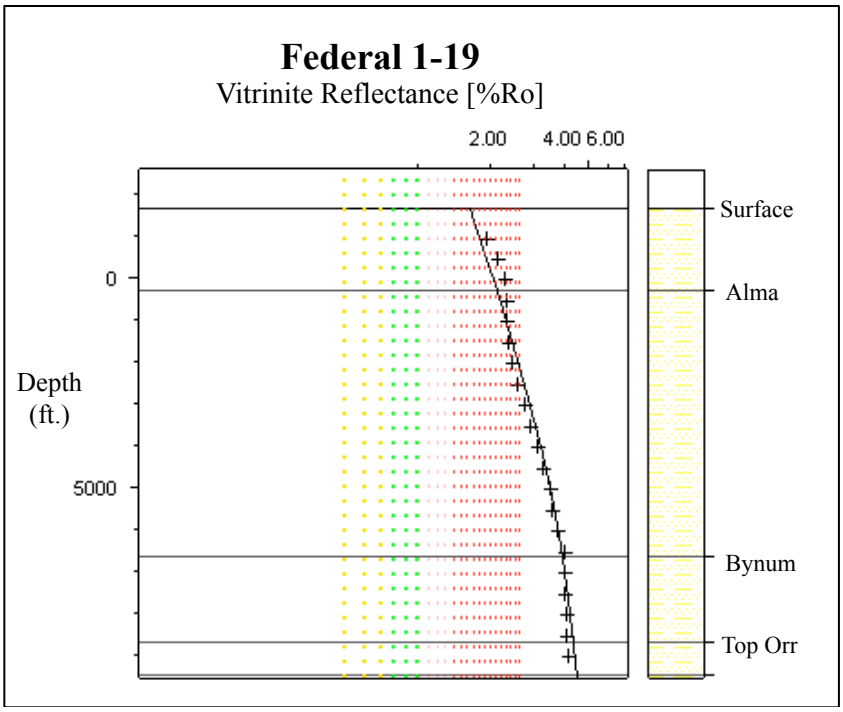
Federal 1-19
Vitrinite Reflectance [%Ro]
2.00
4.00 6.00
0
5000
Depth
(ft.)
Surface
Alma
Bynum
Top Orr

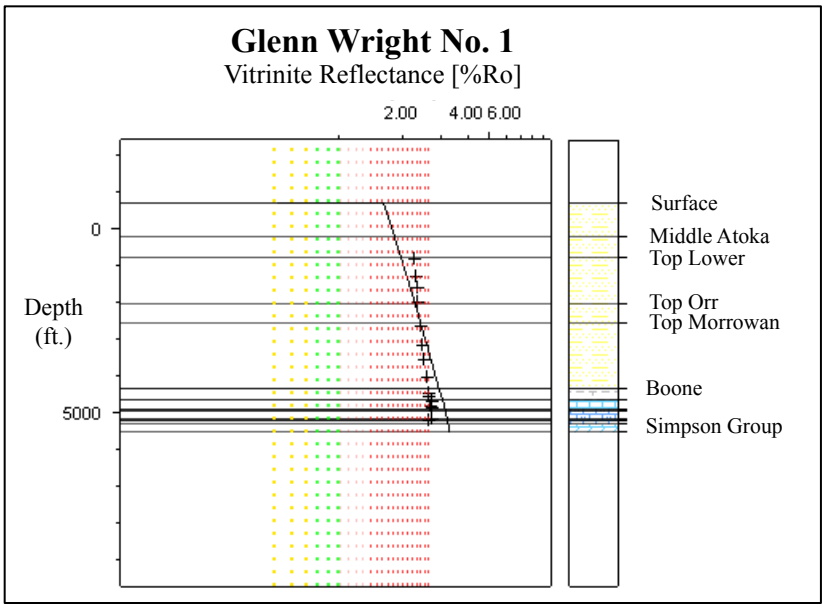

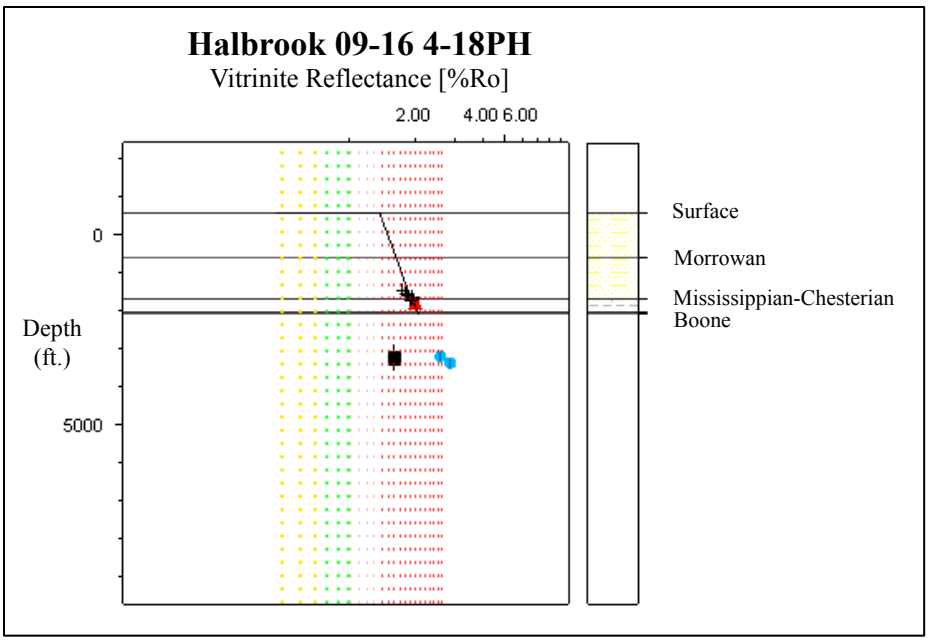

Wells in the surrounding area are displayed in the output model. Halbrook 09-16 4-18: red triangle, Brown 1-17: black crosses at 3,100' sstvd, Hildreth 10-16 1-36: black crosses at 1,400' sstvd, Thomas 09-17 1-16: blue circles

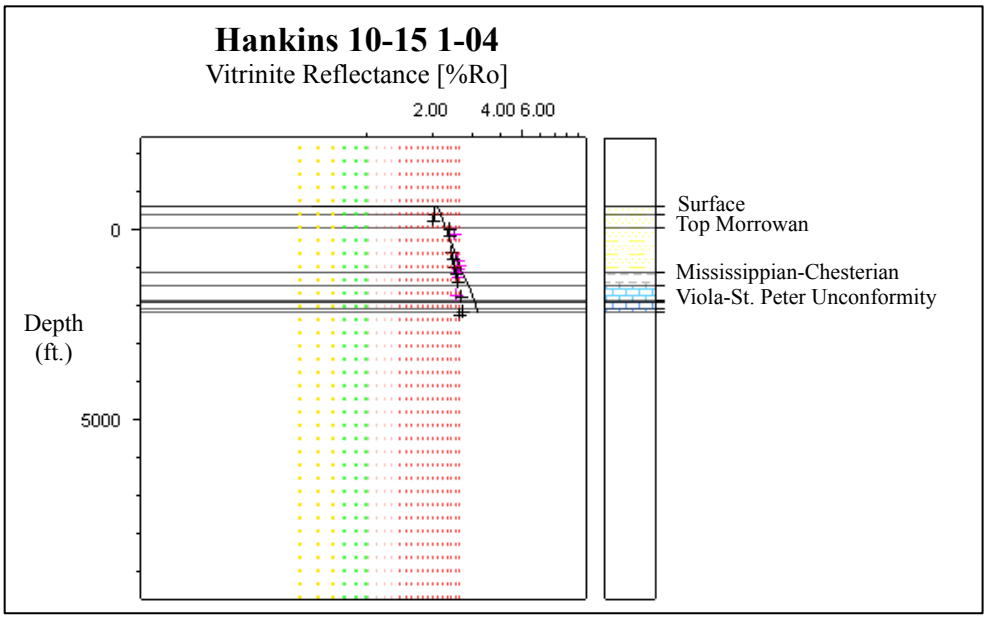

Wells in the surrounding area are displayed in the output model. Hankins 10-15 1-04: black crosses, Charles Hurley No. 1: pink crosses

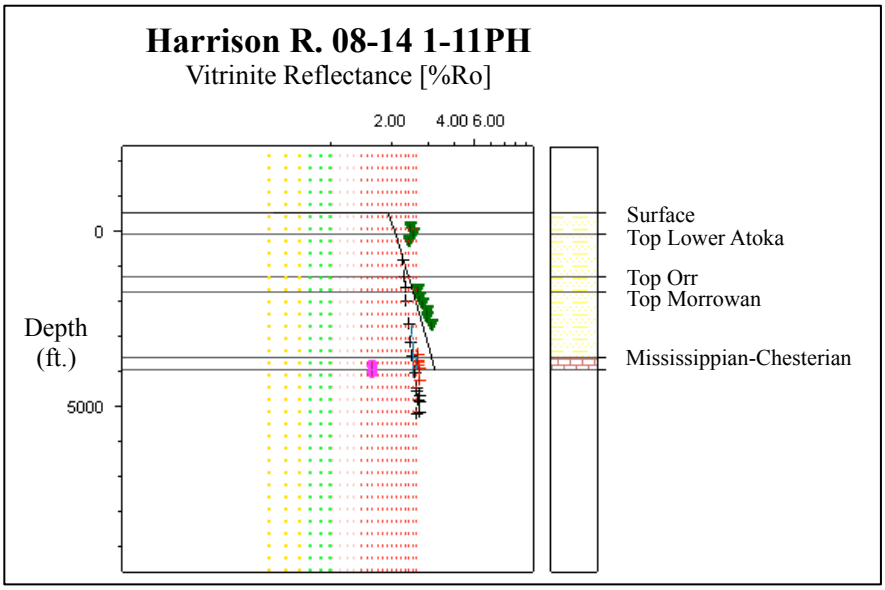

Wells in the surrounding area are displayed in the output model. Harrison R 08-14 1-11: green triangles and pink circles, Billiot A: blue crosses, Dancer No. 1: red crosses, Glenn Wright No. 1: black crosses

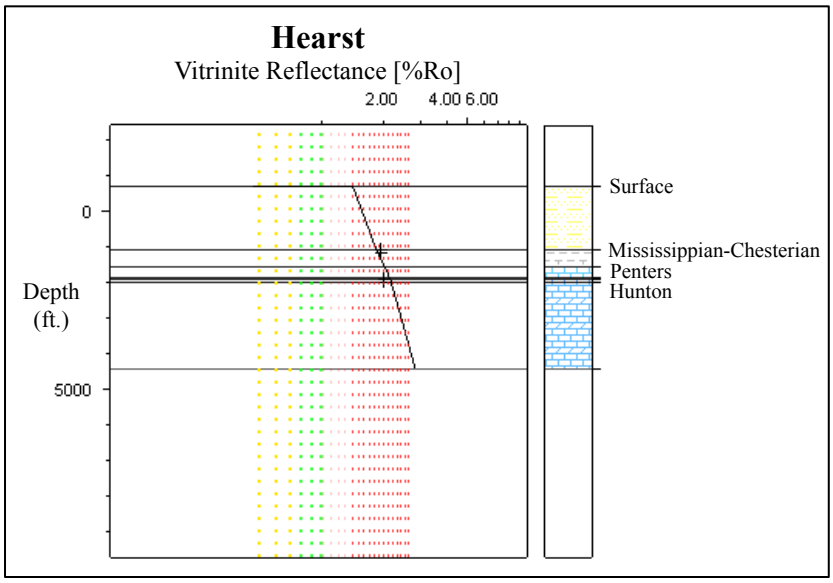
Hearst
Vitrinite Reflectance [%Ro]
2.00
4.00 6.00
0
5000
Depth
(ft.)
Surface
Mississippian-Chesterian
Penters
Hunton

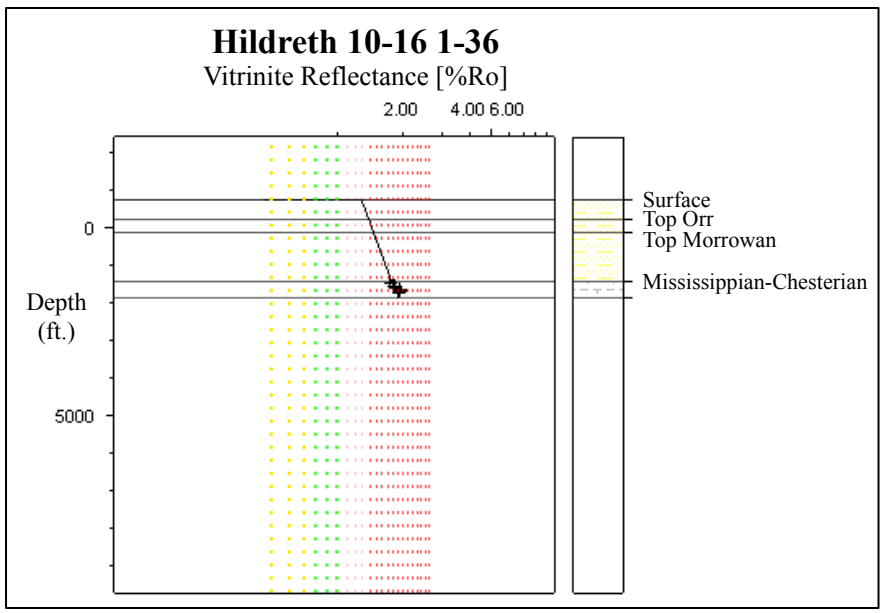
Hildreth 10-16 1-36
Vitrinite Reflectance [%Ro]
2.00
4.00 6.00
0
5000
Depth
(ft.)
Surface
Top Orr
Top Morrowan
Mississippian-Chesterian

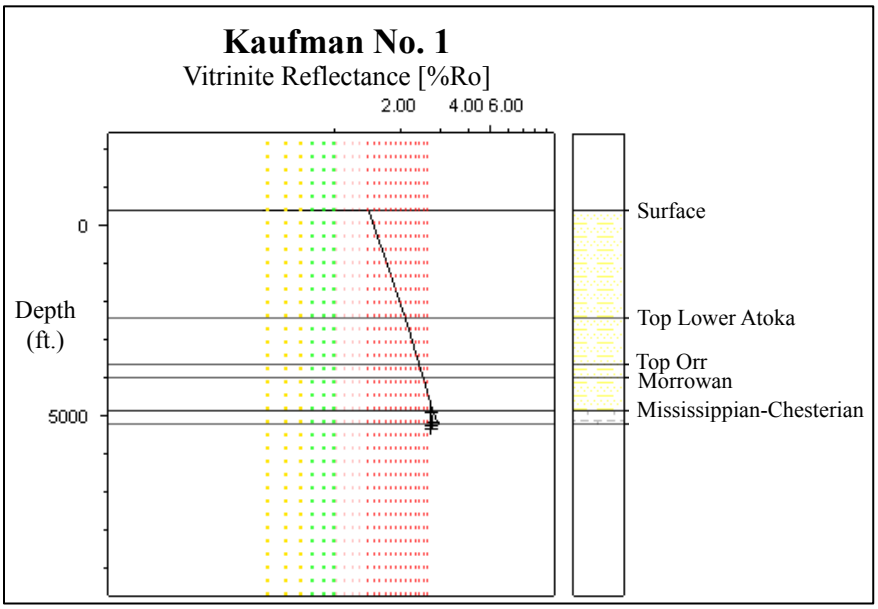
Kaufman No. 1
Vitrinite Reflectance [%Ro]
2.00
4.00 6.00
0
Depth
(ft.)
5000
Surface
Top Lower Atoka
Top Orr
Morrowan
Mississippian-Chesterian

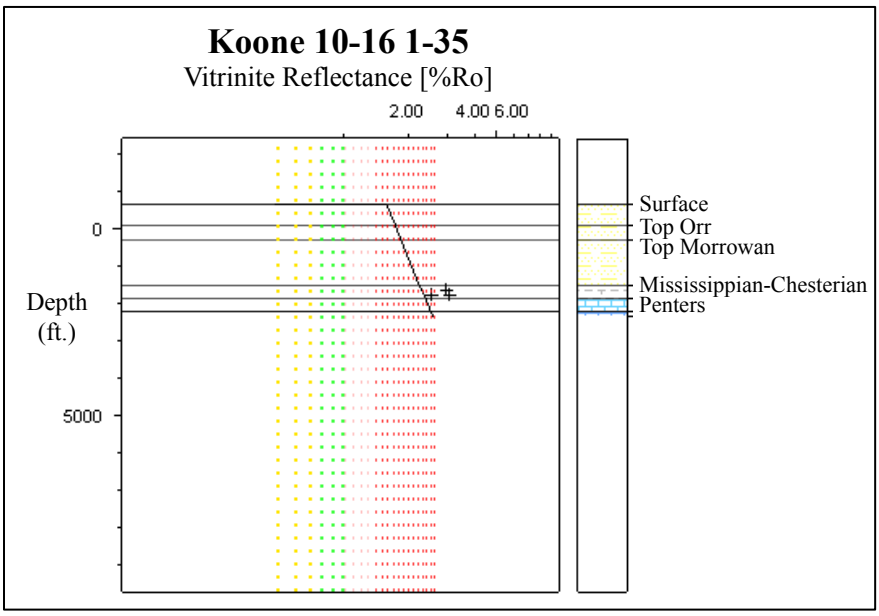
Koone 10-16 1-35
Vitrinite Reflectance [%Ro]
2.00
4.00 6.00
0
Depth
(ft.)
5000
Surface
Top Orr
Top Morrowan
Mississippian-Chesterian
Penters

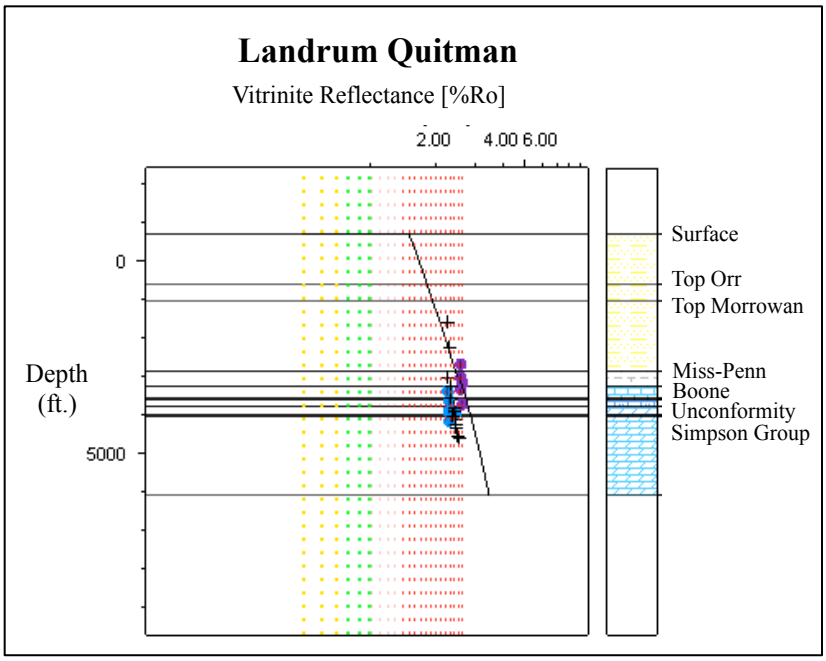

Wells in the surrounding area are displayed in the output model. Landrum Quitman: purple circles, Landrum T: blue circles, McNew 1-26: black crosses

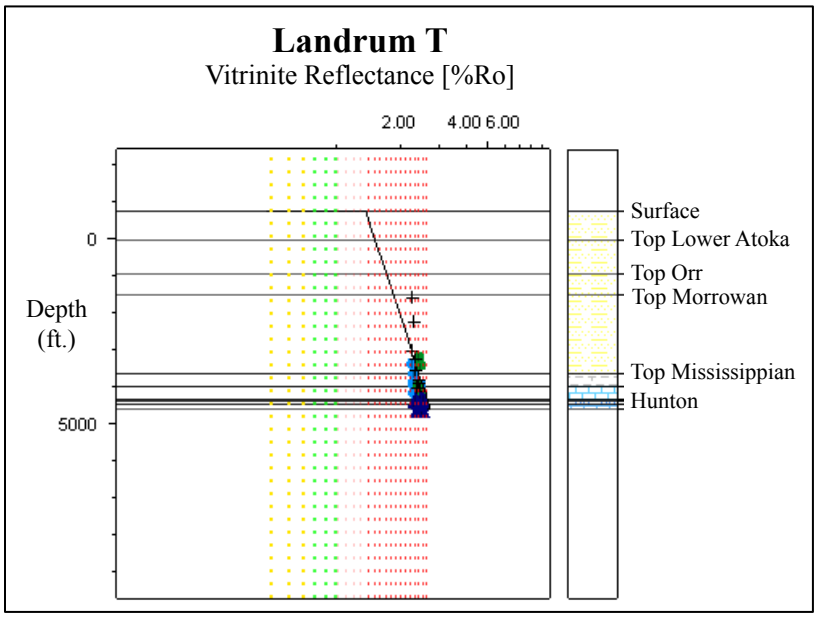

Wells in the surrounding area are displayed in the output model. Landrum T: blue circles, Liles: green circles, McNew 1-26: black crosses, Sneed 08-11 1-06: purple triangles

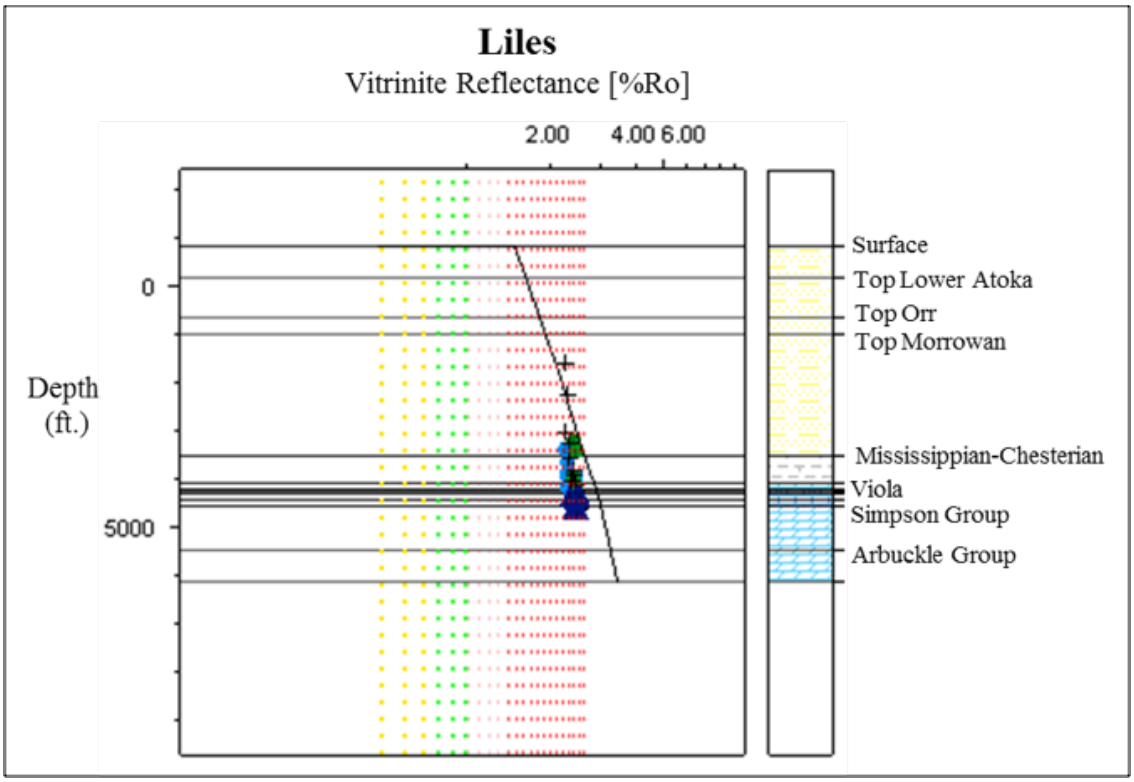

Wells in the surrounding area are displayed in the output model. Liles: green circles, Landrum T: blue circles, McNew 1-26: black crosses, Sneed 08-11 1-06: purple triangles

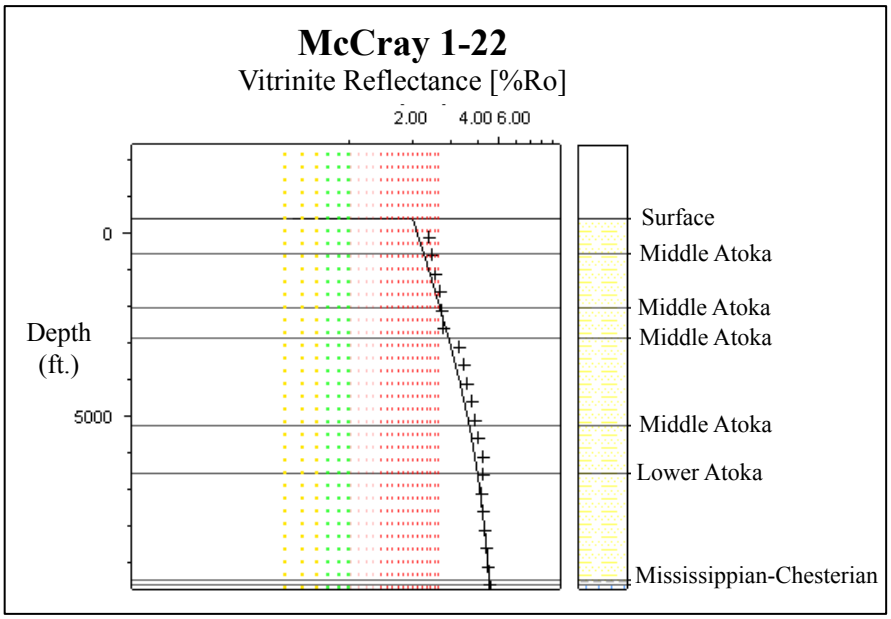

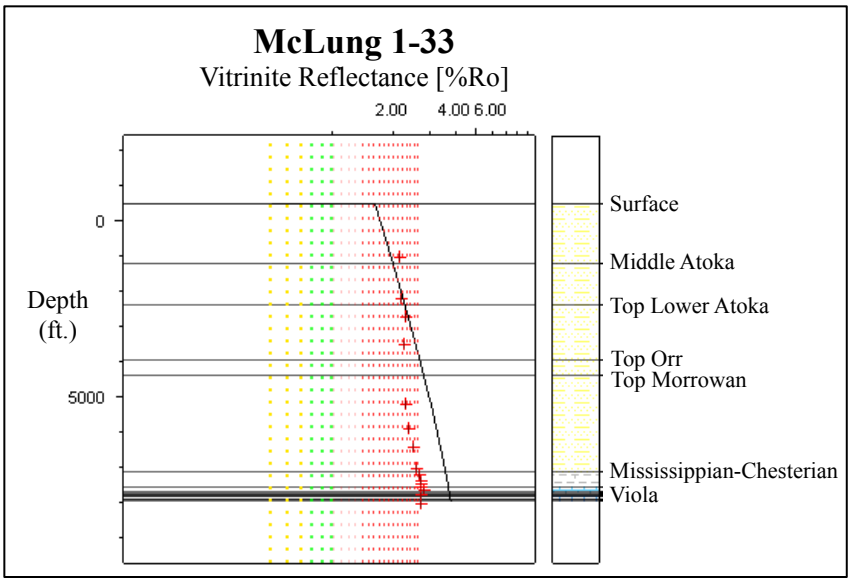

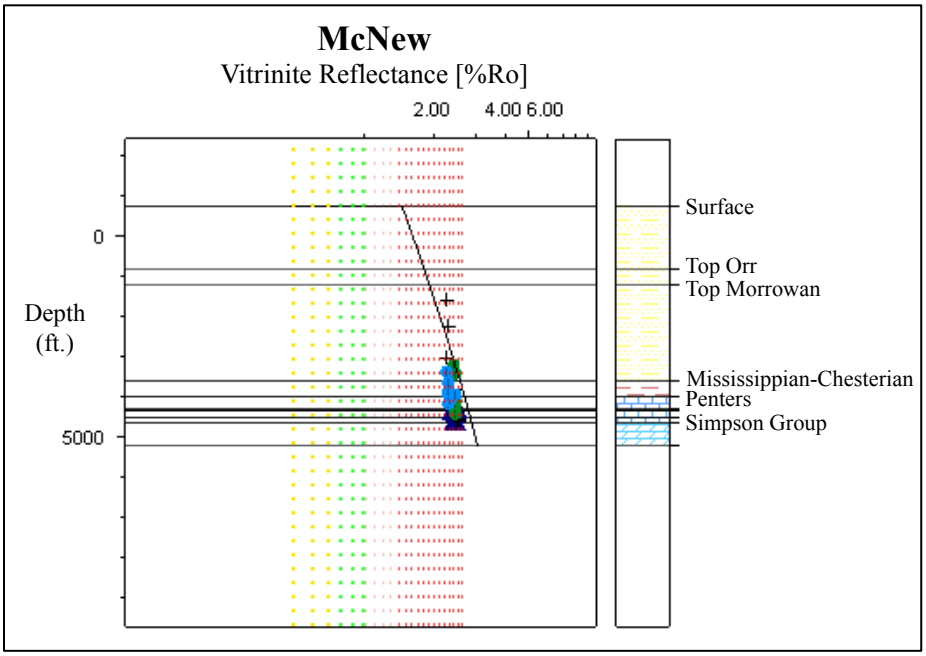

Wells in the surrounding area are displayed in the output model. McNew: black crosses, Landrum T: blue circles, Liles: green circles, Sneed 08-11 1-06: purple triangles

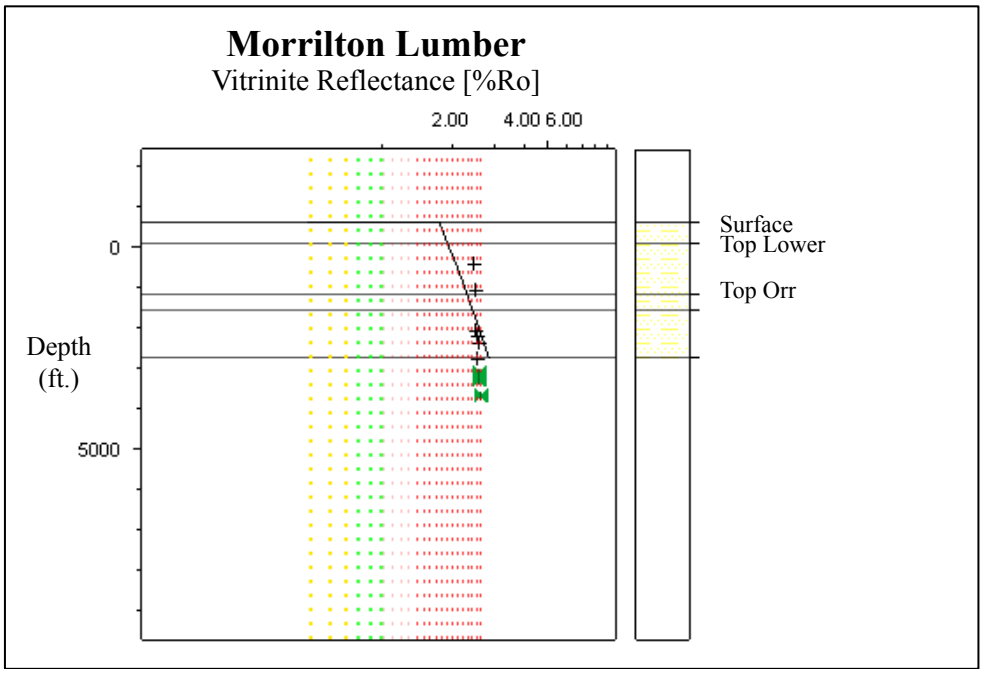

Wells in the surrounding area are displayed in the output model. Morrilton Lumber: black crosses, CS Ramsey No. 1: green bow ties

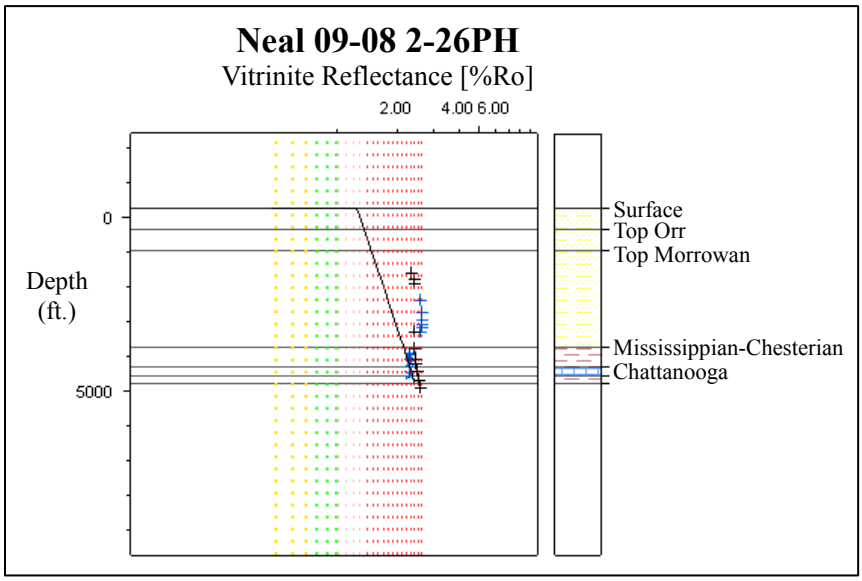

Wells in the surrounding area are displayed in the output model. Neal 09-08 2-26: blue stars, Albert Est. blue crosses, Rocka No. 1: black crosses

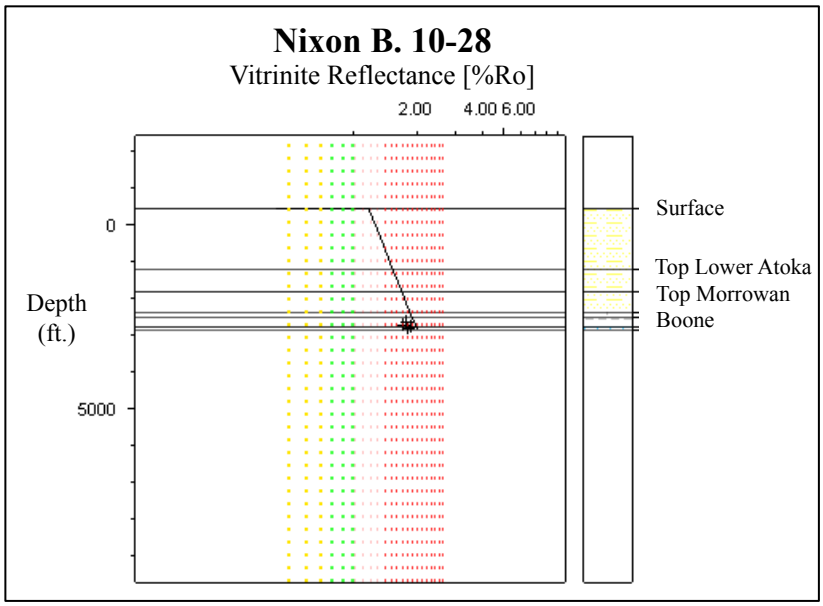
Nixon B. 10-28
Vitrinite Reflectance [%Ro]
2.00
4.00 6.00
0
5000
Depth
(ft.)
Surface
Top Lower Atoka
Top Morrowan
Boone

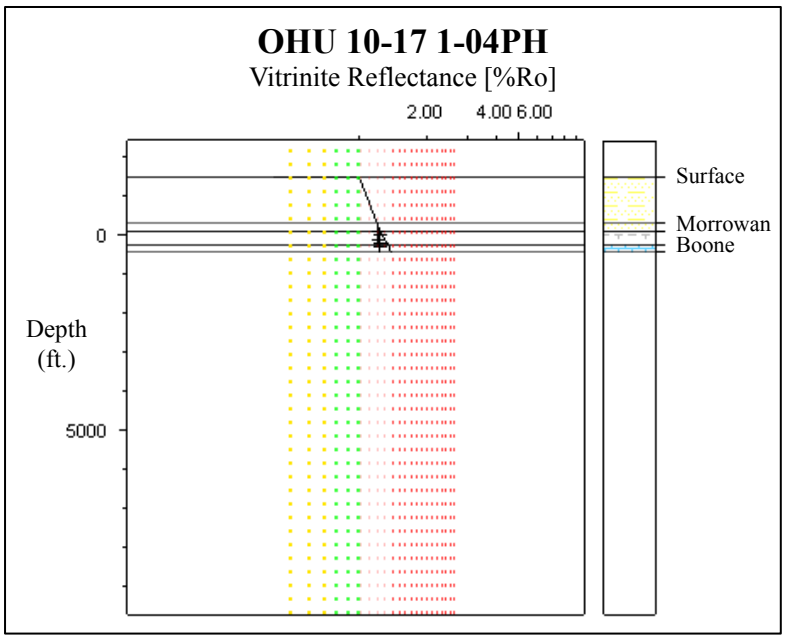
OHU 10-17 1-04PH
Vitrinite Reflectance [%Ro]
2.00
4.00 6.00
0
5000
Depth
(ft.)
Surface
Morrowan
Boone

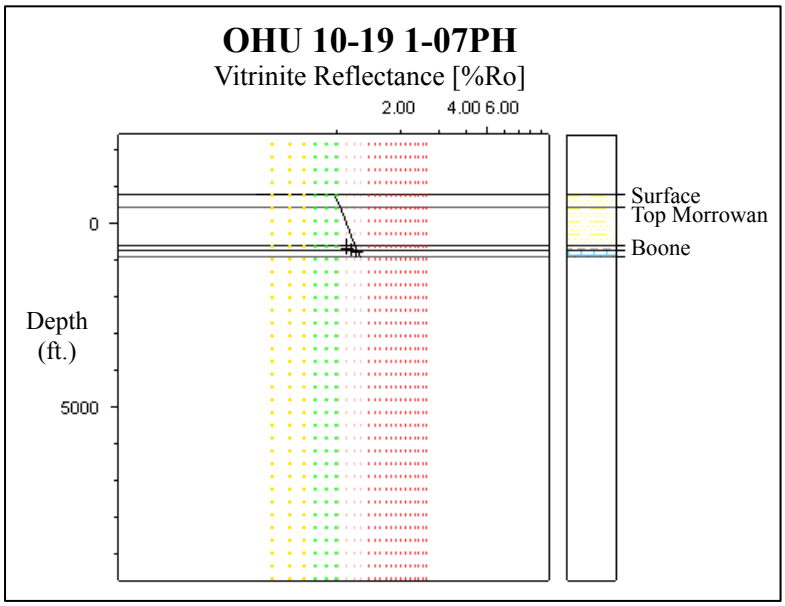
OHU 10-19 1-07PH
Vitrinite Reflectance [%Ro]
2.00
4.00 6.00
0
5000
Depth
(ft.)
Surface
Top Morrowan
Boone

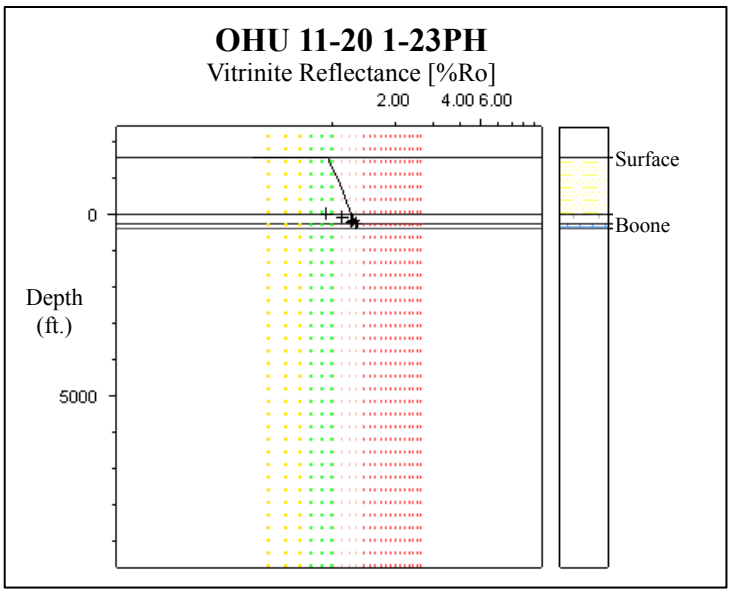
OHU 11-20 1-23PH
Vitrinite Reflectance [%Ro]
2.00
4.00 6.00
0
5000
Depth
(ft.)
Surface
Boone

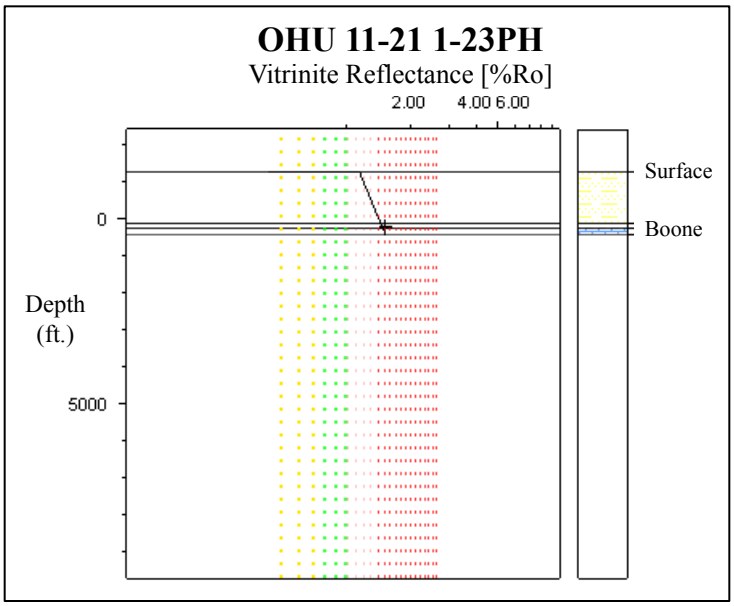
OHU 11-21 1-23PH
Vitrinite Reflectance [%Ro]
2.00
4.00 6.00
Surface
Boone
0
Depth
(ft.)
5000

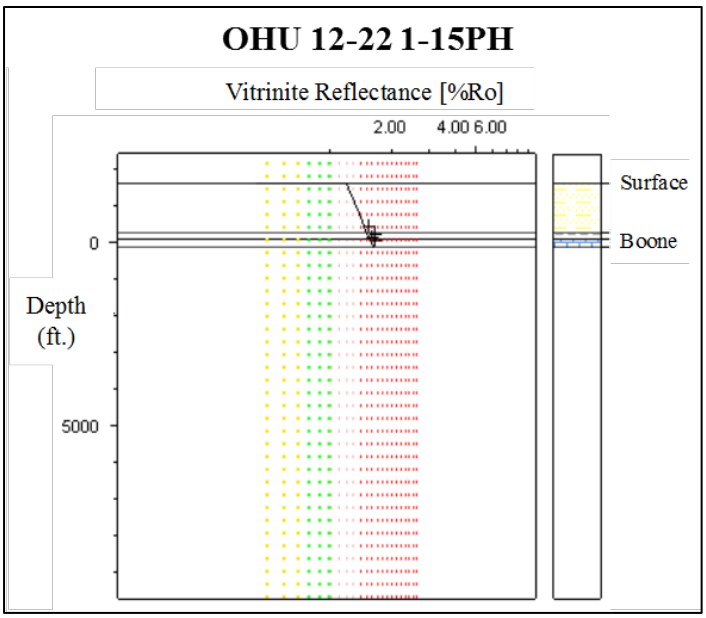
OHU 12-22 1-15PH
Vitrinite Reflectance [%Ro]
2.00
4.00 6.00
Surface
Boone
0
Depth
(ft.)
5000

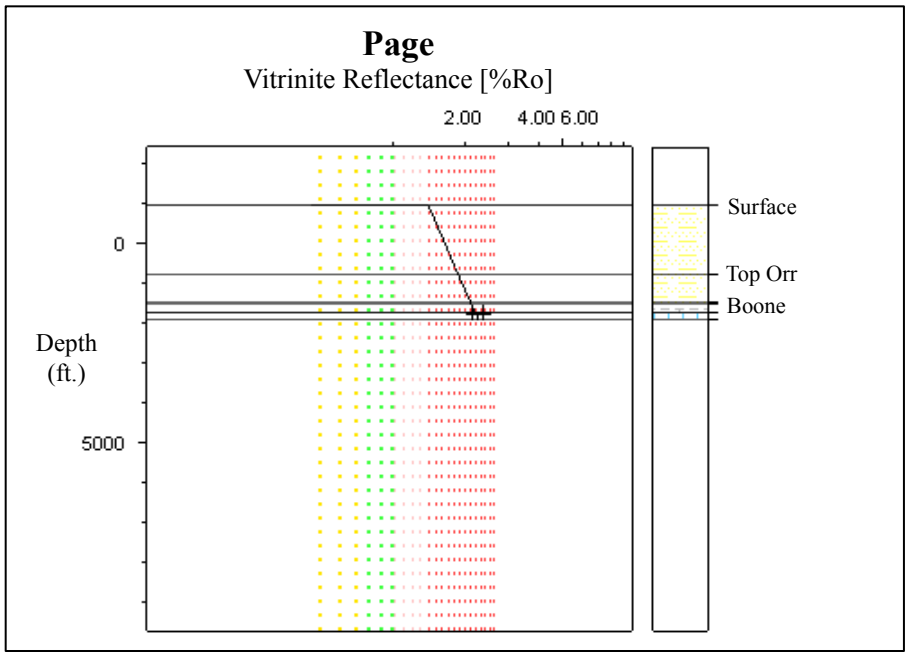

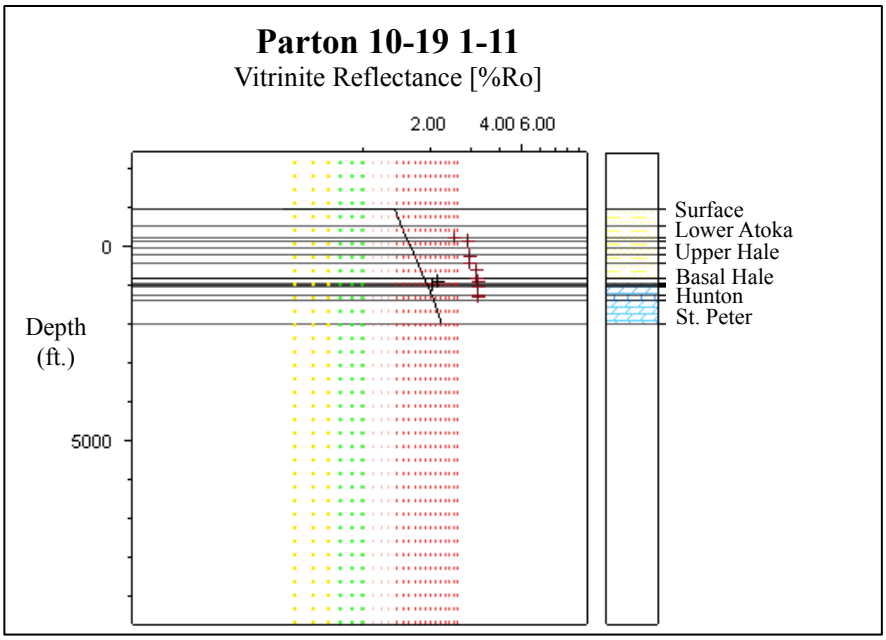

Wells in the surrounding area are displayed in the output model. Parton 10-19 1-11: black and red crosses. Red crosses are Rmax data; therefore, they were not used for calibration. Black crosses represent Parton 10-19 1-11 Ro data.

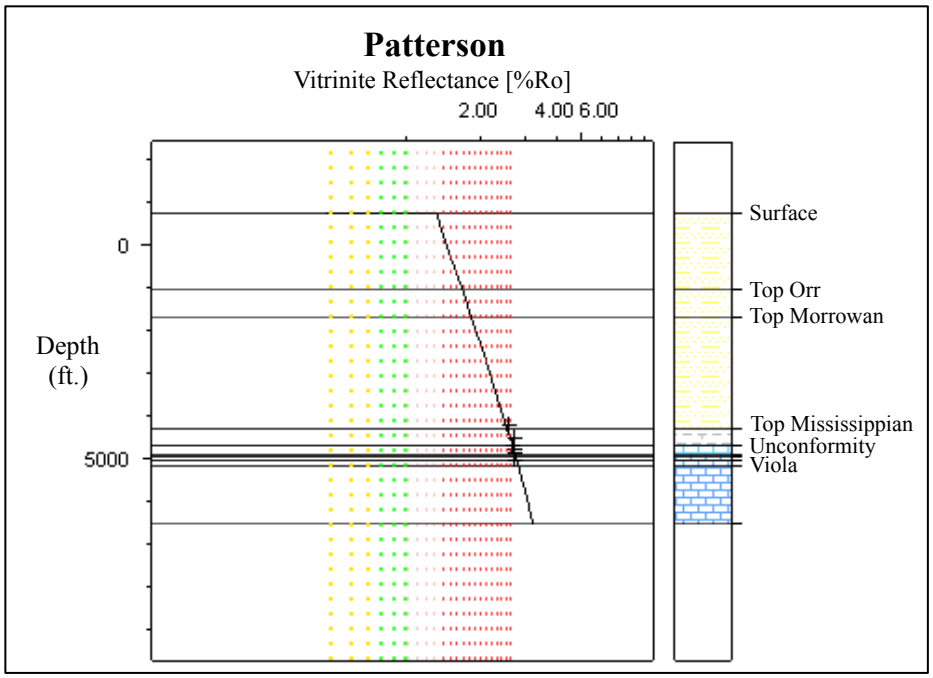
Patterson
Vitrinite Reflectance [%Ro]
2.00
4.00 6.00
0
5000
Depth
(ft.)
Surface
Top Orr
Top Morrowan
Top Mississippian
Unconformity
Viola

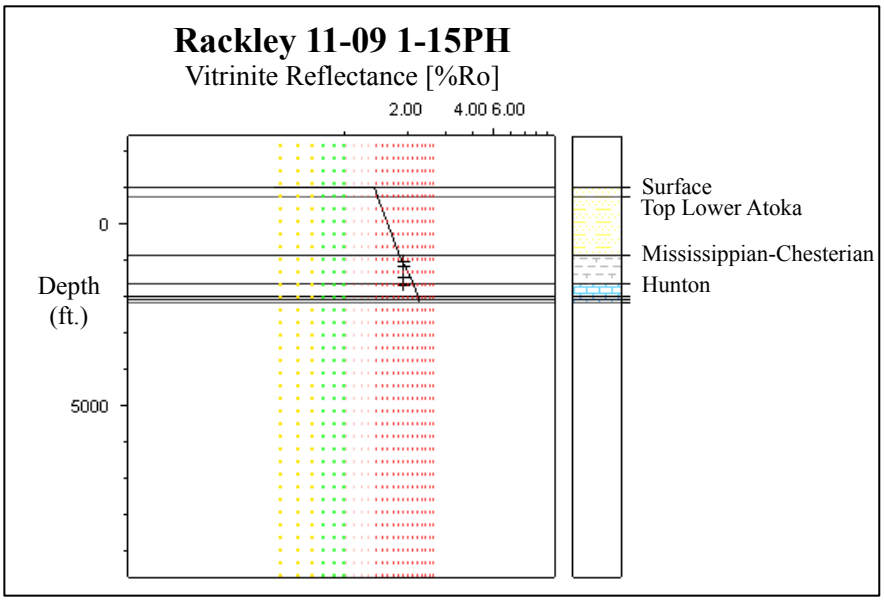
Rackley 11-09 1-15PH
Vitrinite Reflectance [%Ro]
2.00
4.00 6.00
0
5000
Depth
(ft.)
Surface
Top Lower Atoka
Mississippian-Chesterian
Hunton

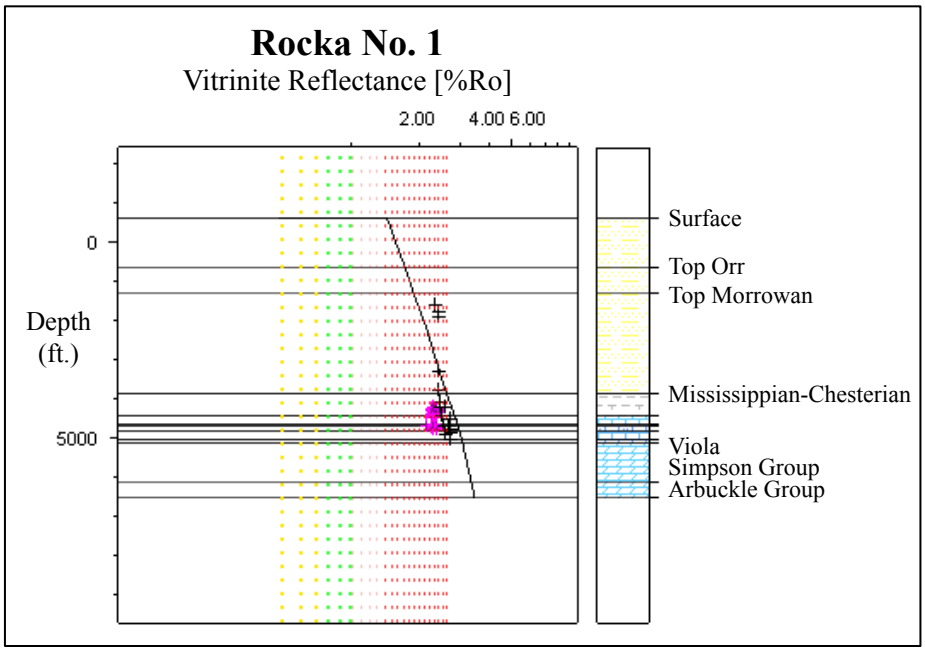

Wells in the surrounding area are displayed in the output model. Rocka No. 1: black crosses at 1,500'-4,900', Patterson No. 1: black crosses at 4,200'-5,000', Snyder 09-10 1-35: pink crosses

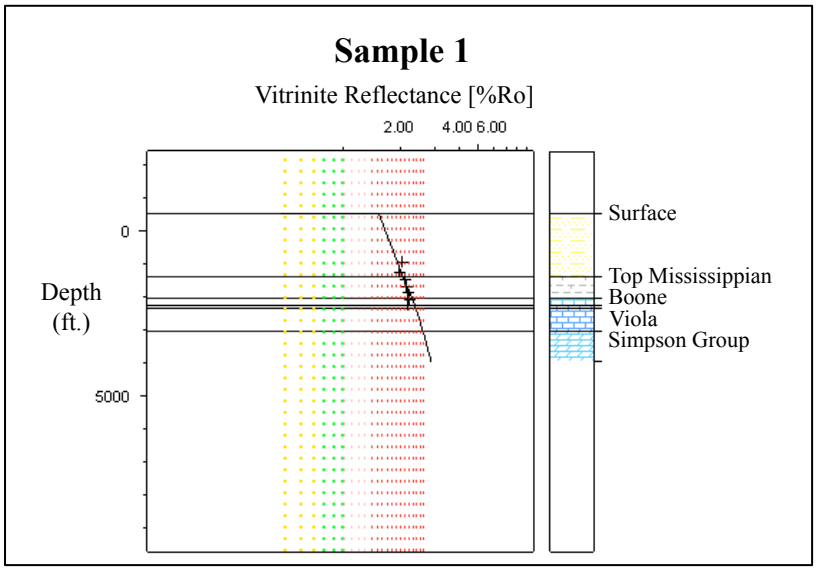

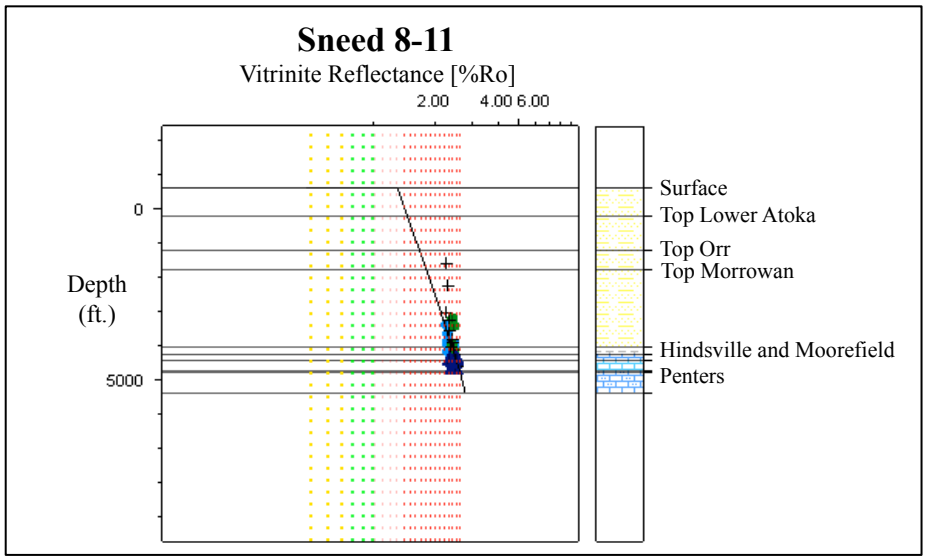

Wells in the surrounding area are displayed in the output model. Sneed 8-11: purple triangles, Liles: green circles, Landrum T: blue circles, McNew 1-26: black crosses

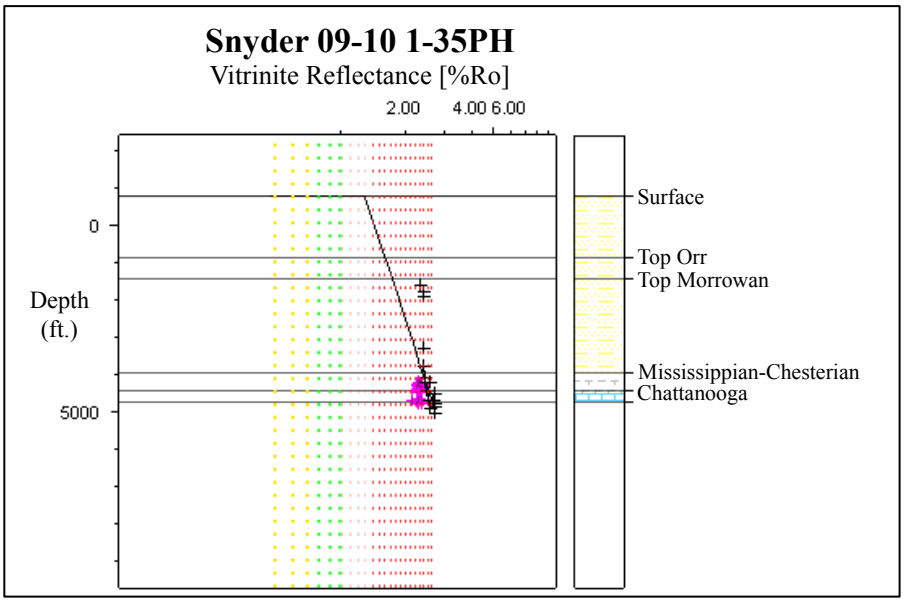

Wells in the surrounding area are displayed in the output model. Snyder 09-10 1-35: pink crosses, Patterson No. 1: black crosses at 4,200'-5,000', Rocka No. 1: black crosses at 1,500'-4,900'

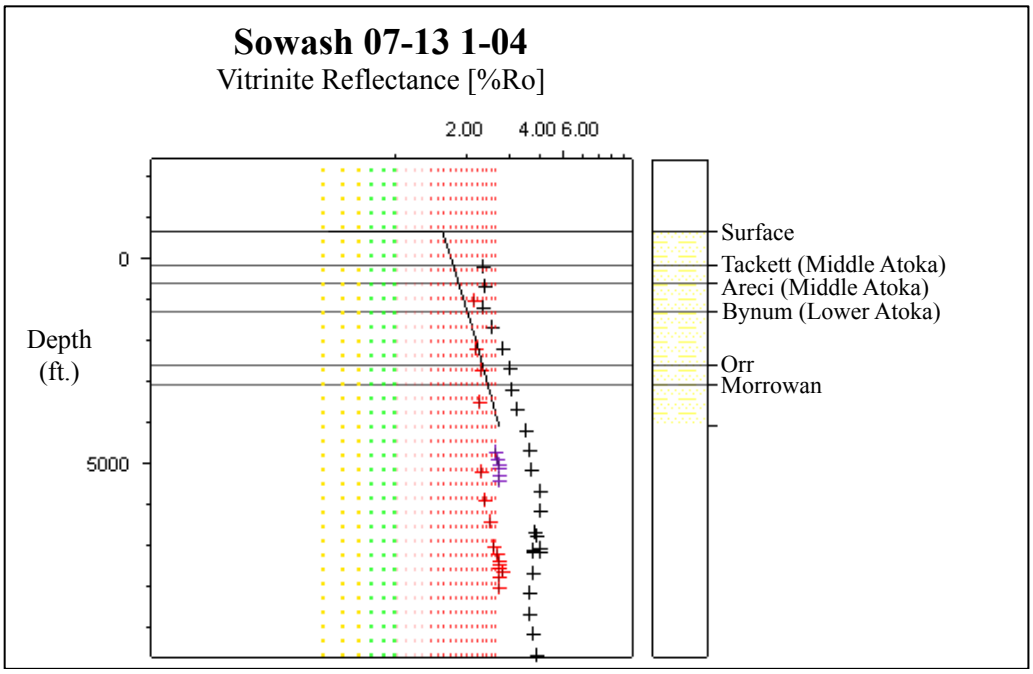

Wells in the surrounding area are displayed in the output model. Sowash 07-13 1-04: Ro data not available, EW Moore Est. 1: black crosses, McLung 1-33: red crosses, Zuber South No. 1: purple crosses

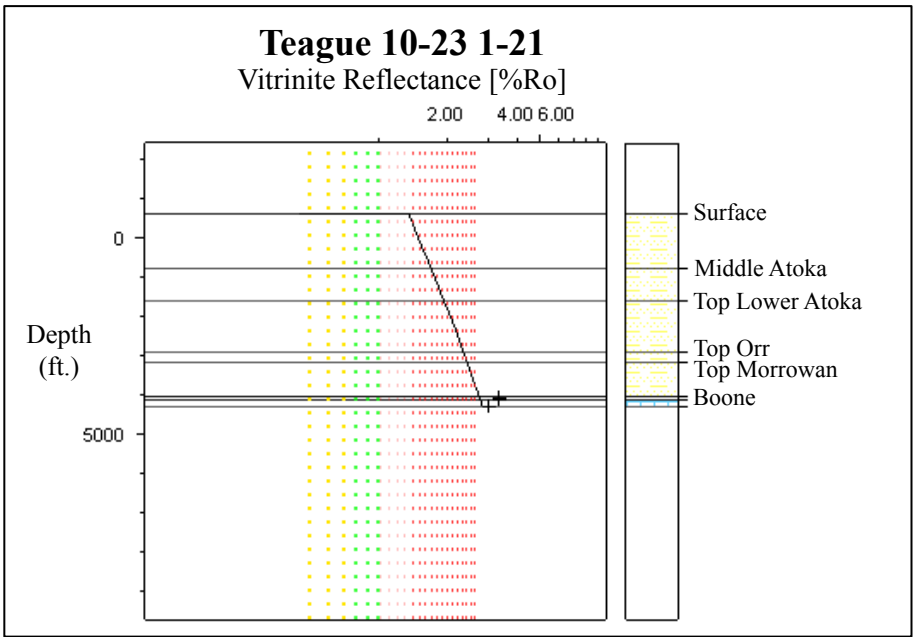

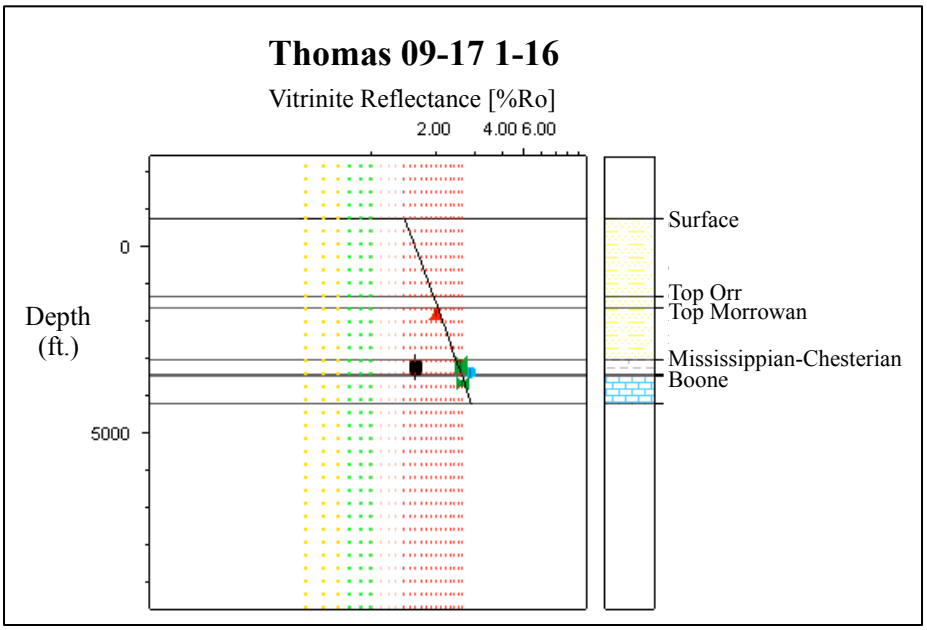

Wells in the surrounding area are displayed in the output model. Thomas 09-17 1-16: blue circles, Brown 1-17: black crosses, CS Ramsey No. 1: green bow ties, Halbrook 09-16 4-18: red triangle

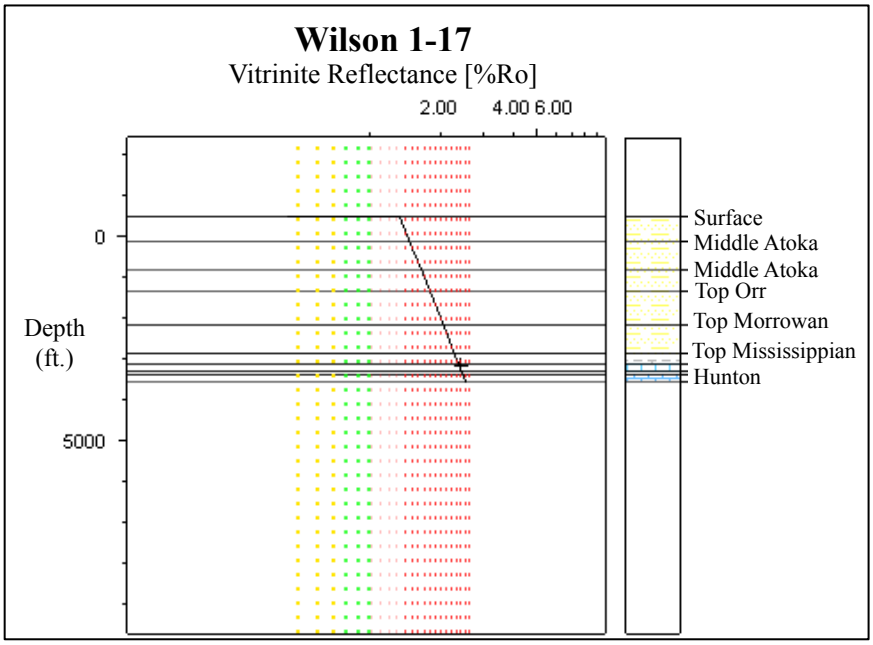

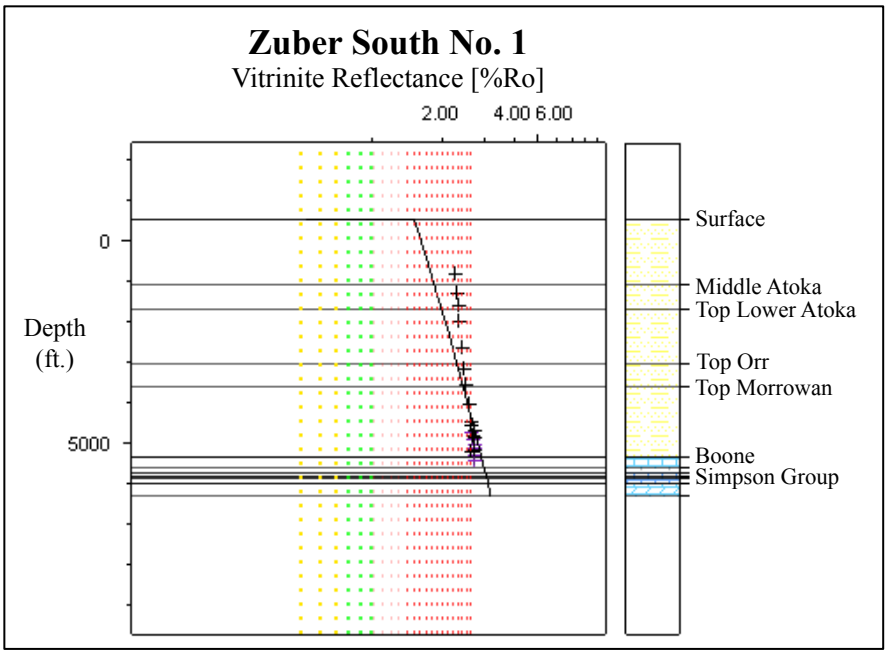

Wells in the surrounding area are displayed in the output model. Zuber South No. 1: purple crosses, Glenn Wright No. 1: black crosses